12-2014

Helical Models of the Bidirectional Vortex in a Conical Geometry

Timothy Andrew Barber
University of Tennessee - Knoxville, tbarber@utsi.edu

To the Graduate Council:

I am submitting herewith a dissertation written by Timothy Andrew Barber entitled "Helical Models of the Bidirectional Vortex in a Conical Geometry." I have examined the final electronic copy of this dissertation for form and content and recommend that it be accepted in partial fulfillment of the requirements for the degree of Doctor of Philosophy, with a major in Aerospace Engineering.

Joseph Majdalani, Major Professor

We have read this dissertation and recommend its acceptance:

Christian G. Parigger, Phuriwat Anusonti-Inthra, Roy J. Schulz

Accepted for the Council:
Carolyn R. Hodges

Vice Provost and Dean of the Graduate School

(Original signatures are on file with official student records.)

12-2014

Helical Models of the Bidirectional Vortex in a Conical Geometry

Timothy Andrew Barber
University of Tennessee - Knoxville, tbarber@utsi.edu

To the Graduate Council:

I am submitting herewith a dissertation written by Timothy Andrew Barber entitled "Helical Models of the Bidirectional Vortex in a Conical Geometry." I have examined the final electronic copy of this dissertation for form and content and recommend that it be accepted in partial fulfillment of the requirements for the degree of Doctor of Philosophy, with a major in Aerospace Engineering.

Joseph Majdalani, Major Professor

We have read this dissertation and recommend its acceptance:

Christian G. Parigger, Phuriwat Anusonti-Inthra, Roy J. Schulz

Accepted for the Council:
Carolyn R. Hodges

Vice Provost and Dean of the Graduate School

(Original signatures are on file with official student records.)

Helical Models of the Bidirectional Vortex in a Conical Geometry

A Dissertation Presented for the

Doctor of Philosophy

Degree

The University of Tennessee, Knoxville

Timothy Andrew Barber

December 2014

Dedication

I dedicate the toils of my labor to my exceptional parents, Jerry Dean Barber and Linda Ann Barber. Their guidance, patience, and unconditional love have made this dream possible, and for that I am eternally grateful.

This is also dedicated to those who have committed their lives to the advancement of scientific and mathematical research. The success of one's studies is never achieved without unrelenting effort and sacrifice. I extend my abounding admiration to all that are part of this inexorable yet rewarding pursuit of knowledge.

Acknowledgments

I would like to first start by thanking Dr. Majdalani for presenting this project. His unveiling guidance has provided me with exceptional mentorship over the years. This has been no easy feat, and I am grateful for his diligence, professional awareness, and academic excellence. He has taught many inspirational classes such as perturbation techniques, rocket propulsion, and aeroacoustics. These courses served as my primary inspiration for the completion of this dissertation and a life-long commitment to the field of theoretical science.

Much appreciation and gratitude is extended to Dr. Parigger, Dr. Anusonti-Inthra, and Dr. Schulz. As committee members for this dissertation, your time and thoughtful insight has been a tremendous support that I cannot begin to illustrate. Thank you for your service.

I must thank my parents, Jerry Dean Barber and Linda Ann (Lack) Barber for raising me in an incredible, loving environment. Their support of my studies and tolerance of my shenanigans demonstrate the true meaning of unconditional love. I am forever grateful to the most understanding, patient, and unsurpassed family I know.

My most gracious thanks go to the UTSI librarian, Brenda Brooks. Brenda, your professionalism and warmhearted kindness has always been inspirational. Your assistance has been unyielding through references, research, and many overdue library books. This dissertation would be incomplete without all of your help and your kind smile.

Charlene Hane, Charlotte Henley, Betsy Harbin, and Kathy Hice cannot go unrecognized. They have been wonderful to work with through the completion of this degree. Your dedication to the students at the university is appreciated beyond comprehension, and I

am very thankful for everything you have done and continue to do to make the UTSI an outstanding academic institution.

Last but not least, I must thank all of the friends I have made along this journey: Tony Saad, Michel Akiki, Anne Alford, Dimitri Kavelakis, Brian Maicke, Nick Perry, Nadim Zgheib, Josh Batterson, Erin Halpenny, Paula Sanematsu, Eric Jacobs, Lutz Blatte, Georges Akiki, Jacques Abboud, Charles Haddad, Tonya Battles, Dana Hale, Amy Glasgow, and Joe Hane. You have all been more than just friends. You have been mentors, scholars, and so much in between. I thank you with my deepest affection for your support, kind words, and unbelievable compassion over the years.

Abstract

This dissertation represents the descriptive and analytical breakdown of two new fluid dynamics solutions for vortex motion. Both solutions model the bidirectional vortex within a conical geometry. The first explored solution satisfies a simple Beltramian characteristic, where the Lamb vector is identically zero. The second solution is of the generalized Beltramian type, which fulfills the condition that the curl of the Lamb vector is equal to zero. The two Beltramian solutions describe the axisymmetric, double helical motion often found in industrial cyclone separators. Other applications include cone-shaped, vortex-driven combustion chambers and the swirling flow through conical devices. Both solutions are derived from first principles and Euler's equations of motion which showcase the stream function-vorticity relation and ultimately transforms into the Bragg-Hawthorne formulation. The Bragg-Hawthorne equation allows for various implementations of the Bernoulli and swirl functions. The angular momentum equation includes the source term for the Beltramian solution. On the other hand, the Bernoulli relation drives the generalized Beltramian model. Appropriate boundary conditions and assumptions reduce the governing partial differential equation to an ordinary differential equation which is then solved by a separation of variables approach. Resulting velocity, vorticity, and pressure variables are discussed and graphed. The tangential and axial velocities are compared to two experimental and numerical cyclone separator cases. Other features of the conical flow field such as the conical swirl number and dual mantle locations are also explored. The inviscid, incompressible, and rotational models ultimately lay the framework for complementary solutions derived from the Bragg-Hawthorne equation or similar formulations.

Table of Contents

List of Tables

List of Figures

Nomenclature

Abbreviations

BC	Boundary conditions
BDV or BV	Bidirectional vortex
BHE	Bragg-Hawthorne equation
GB	Generalized Beltramian
CPC	Cylindrical polar coordinates
CS	Cyclone separator
NSE	Navier-Stokes equations
ODE	Ordinary differential equation
PDE	Partial differential equations
SBR	Solid body rotation
SPC	Spherical polar coordinates
TC	Taylor-Culick

Symbols

A	Arbitrary area
$\mathcal{A}$	Constant, $\tan(\alpha/2)$
a	Maximum radius of conical BDV, radius of cylindrical BDV
B	Swirl function or angular momentum, $u_\theta R \sin\phi$ or $u_\theta r$
b	Outlet radius of conical and cylindrical BDV
b_R	Radius of the spherical polar radial velocity mantle at that axial location

b_z	Radius of the axial velocity mantle at that axial location
F	Separation variable as function of R
G	Separation variable as function of ϕ
H	Bernoulli function/equation, $\frac{1}{2}u^2 + p/\rho$
ℓ	Lamb vector ($\boldsymbol{\ell}$) component
l	Aspect ratio, L/a
p	Pressure
Q	Volumetric flowrate
Re	Reynolds number
R	Spherical radial coordinate, $\sqrt{r^2 + z^2}$
r	Cylindrical radial coordinate, $R\sin\phi$
S	Spherical radial coordinate, $\sqrt{r^2 + z^2}$
t	Time
U	An average tangential velocity
u_ϕ	Colatitudinal or zenith velocity
u_R	Spherical radial velocity
u_r	Cylindrical radial velocity
u_θ	Tangential or azimuthal velocity
u_z	Axial velocity
W	Average axial velocity
X	Ratio of mantle radius per maximum chamber width, b/a
z	Axial coordinate, $R\cos\phi$
$\bar{}$	Overbar, denotes a nondimensional variable unless otherwise indicated

Greek

α	Cone divergence half-angle
$\hat{\beta}$	Ratio of mantle radius per maximum chamber width, $X = b/a$
β_R	Angle of mantle for $u_R = 0$

β_z	Angle of mantle for $u_z = 0$
κ	Geometric swirl parameter
ω	Vorticity
ρ	Density
λ	Constant dependent upon divergence half-angle, α
μ	Dynamic viscosity
ν	Kinematic viscosity
Φ	$\tan(\phi/2)$
ϕ	Colatitudinal or zenith coordinate, $\tan^{-1}(r/z)$
ψ	Stream function
θ	Tangential or azimuthal coordinate
σ	Modified cylindrical swirl parameter
σ_c	Modified conical swirl parameter
ζ	Ratio of cylindrical coordinates z/r

Chapter 1

Introduction and Background

This dissertation investigates the bidirectional flow of the cyclone within a conical geometry. The analysis stems from the Journal of Fluid Mechanics article entitled, "Flow in Industrial Cyclones," written by M. I. G. Bloor and D. B. Ingham (BI) in 1987. The investigation reconstructs the Bloor and Ingham problem, corrects apparent errors, and extends the study to obtain additional results which has lead to several new solutions. The reconstructed Bloor and Ingham solution proves to be an exact Beltramian solution, while the original Bloor and Ingham investigation relies on a small-angle approximation. The presented Beltramian model in Chapters 2 and 3 derives a very straightforward solution and results. Likewise, a similar solution emerges from the governing equation of several inviscid flow models, usually called the Bragg-Hawthorne or Long-Squire equation. The second solution presented in Chapters 4 and 5 is of the generalized Beltramian (GB) type, which is a more universal constraint of Beltramian flows producing a wider class of possible models. The GB solution, similar to the Beltramian solution reconstruction, re-derives a conference paper entitled, "The Flow in Conical Cyclones," written by J. Q. Bloor and J. Abrahamson in 1999. Again, the reconstruction provides an exact generalized Beltramian model with an unambiguous solution and results.

Chapter 1 administers an introduction to necessary topics and background information. Since the models conferred in the dissertation emerge from strict analytical techniques, a

case is made for the pros and cons of theoretical methods in contrast to experimental and CFD/numerical efforts. The governing fluid equations of motion are then presented with brief discussion on related analytical solutions. Next, a section over vorticity, vortices, and rotational flow is explored since the GB and Beltramian models are swirling flows that rely heavily on rotation and prescribed vorticity. An investigation on various, yet related, topics follow in the adjoining sections. The myriad of topics include the vorticity transport equation, GB, Beltramian and Trkalian flows, the Beltrami-Gromeka-Lamb equation, and the Lamb vector. Directly on the heels of these topics, the development, background, and relevance of the Bragg-Hawthorne equation (BHE) is visited. Chapters 2 and 3 derive the Beltramian solution and present and discuss the results, respectively. Chapter 2 begins with the BHE in spherical coordinates. The following sections contain geometry, boundary conditions (BC), and discussion of inlet conditions. The inlet conditions set up the representation of the Bernoulli and swirl functions in the BHE. Next, the method of separation of variables solves the PDE and reduced ODE from the BHE. Finally in Chapter 2, the stream function materializes where the important flow characteristics, velocities, vorticity, pressure, and swirl number engender. Chapter 3 opens with a detailed discussion of the mantle and its historical nature followed by results of the mantle and streamlines from the Beltramian model. Next, the outcome of the graphs of the velocities is reviewed along with validation and comparison to experimental and numerical data by Hsieh and Rajamani (1988) and Monredon et al. (1992). Chapters 4 and 5 follow similar outlines to Chapters 2 and 3 except for the GB model. The GB model consists of a Gegenbauer equation so the Gegenbauer and related Lengendre and hypergeometric functions and background are examined briefly. Lastly, Chapter 6 reviews the dissertation in an abridged manner, succinctly citing theory, method, results, and future/recommended work.

1.1 Approaches to Fluid Dynamics Modeling

Analytical fluid dynamics attempts to solve the fluid dynamics equations using general applied mathematics. Many techniques and studies date back several decades and even centuries (Stokes 1842; Helmholtz 1858; Meissel 1873; Lamb 1877; Thomson (Kelvin) 1880; Berker 1936; Batchelor 1951; Truesdell 1954; Wang 1991). Many mathematically intense fluid dynamics studies occurred early on since computational capabilities were either nonexistent or inaccessible for the times. Even in the middle 20th century, analytical equations proved far more valuable than time consuming numerical calculations. However, as technology has progressed into the 21st century, computational power has become very robust for highly complex fluid dynamics flow situations. While computational methods have become more popular and widespread, analytical solutions provide the invaluable third pillar in the checks and balances system of theoretical, experimental, and computational fluid dynamics.

1.2 Fluid Motion - Incompressible Flow

The canonical governing equations consist of classes separating various types of flows into categories such as incompressible, inviscid, compressible, viscous, rotational, irrotational, etc. Additional types of flows and equations include the boundary layer equations, the vorticity transport equation, complex lamellar flow, potential flow, etc. Furthermore, various equation names are given to these equations and flows such as Navier-Stokes, Euler, Gromeka-Lamb, Crocco-Vazsonyi, Navier-Stokes-Fourier, Bragg-Hawthorne, Oseen, Helmholtz, Beltrami, Trkalian, etc.

Incompressible flow provides simplified cases of the fluid dynamics equations to be solved. Compressible flow allows more complex flows to be calculated where density changes are significant. Incompressible flow assumptions reduce the number of unknowns dramatically giving researchers and engineers quick, yet relatively reliable results. The primary ubiquitous equation for incompressible flow is known as the divergence field, or

continuity equation. All solutions presented in this dissertation assume incompressible flow conditions.

1.2.1 Viscous Incompressible Flows & the Navier-Stokes Equations

While the generalized Beltramian and Beltramian models presented in this dissertation are inviscid solutions, it remains important to understand how the inviscid Euler equations are a subgroup of the Navier-Stokes equations (NSE). Important relations, which, unfortunately, cannot be discussed in detail for this dissertation, exist between Euler solutions and the more refined exact Navier-Stokes solutions. According to Donaldson (1957), some of the earliest work in fluid dynamics involving the study of viscosity and viscous forces dates back to a period of scientific enlightenment in the 17th century, when Mariotte published a study in 1686 regarding the motion of water and its forces. Soon after in 1687, Newton published his study on the what is now known as plane Couette flow where he determined a definition for shear stress, $\tau = \mu\,(\mathrm{d}u/\mathrm{d}y)$. A 150 year drought passed before any progress was made in the field of theoretical fluid dynamics. In 1822, a French mathematician and engineer, Claude-Louie Navier, recited his findings and proposed a set of general equations for viscous motions of a fluid before the Acad'emie des Sciences. Navier attempted to postulate a reigning problem: incorporating frictional effects into the fluid dynamics equations developed by Euler and others (Zeytounian 2006).

In 1991, Wang writes a profound summary for the *Annual Review of Fluid Mechanics* on some of the exact solutions of the NSE. Chang-Yi Wang contributes to the fluid dynamics community with several articles on solutions he has formed in the past, including a class of exact solutions of the NSE (1966), a review of the exact solutions to the unsteady NSE (1989), and a review of the exact solutions of the NSE of the generalized Beltrami form (1990). Wang (1991) defines the NSE as a set of nonlinear partial differential equations (PDE) that govern fluid mechanics. In general, no universal solution exists for the NSE. Only a few exact solutions prevail. Wang, a proponent of analytical solutions, touts the importance of exact solutions of the NSE. Wang lists two points as:

1. The known exact solutions define the fundamentals of fluid dynamics and allow for a deeper insight to the NSE and flow phenomena.

2. Exact solutions provide a measuring stick for validating numerical, asymptotic, and empirical results, which are all approximate solutions. Even though the endlessly increasing computer power yields solutions for the NSE, only the exact solutions gauge the numerical accuracy.

Wang (1966, 1989, 1991) denotes exact solutions of the NSE as those which satisfy the conservation of mass and momentum. In vector form, the continuity and constant property (density, viscosity) NSE appear as

$$\nabla \cdot \mathbf{u} = 0$$

$$\frac{\partial \mathbf{u}}{\partial t} + (\mathbf{u} \cdot \nabla)\,\mathbf{u} = \mathbf{F} - \frac{1}{\rho}\nabla p + \nu \nabla^2 \mathbf{u} \tag{1.2.1}$$

or

$$\frac{\mathrm{D}\mathbf{u}}{\mathrm{D}t} = \mathbf{F} - \frac{1}{\rho}\nabla p + \nu \nabla^2 \mathbf{u} \tag{1.2.2}$$

where $\mathbf{u}\,(\mathbf{x}, t)$ is the velocity vector as a function of space $\mathbf{x}$ and time t, $p\,(\mathbf{x}, t)$ is the pressure, and ρ and μ remain constant and are the density and dynamic viscosity, respectively. Since the density and dynamic viscosity remain constant, the kinematic viscosity, a combination of density and dynamic viscosity, also remains constant where $\nu = \mu/\rho$.

The steady form of the NSE for momentum is

$$(\mathbf{u} \cdot \nabla)\,\mathbf{u} = \mathbf{F} - \frac{1}{\rho}\nabla p + \nu \nabla^2 \mathbf{u} \tag{1.2.3}$$

the no gravity form of the NSE for momentum is

$$\frac{\partial \mathbf{u}}{\partial t} + (\mathbf{u} \cdot \nabla)\,\mathbf{u} = -\frac{1}{\rho}\nabla p + \nu \nabla^2 \mathbf{u} \tag{1.2.4}$$

and the steady with no gravity form of the NSE for momentum is

$$(\mathbf{u} \cdot \nabla)\,\mathbf{u} = -\frac{1}{\rho}\nabla p + \nu\nabla^2\mathbf{u} \tag{1.2.5}$$

While the curl of the momentum equation eliminates the pressure term (see Section 1.3.2), the kinematic viscosity, ν, (or nondimensionally, the Reynolds number, Re), remains an important parameter (Richardson and Cornish 1977; Wang 1989, 1991; Kee et al. 2003). Thus, Wang (1989, 1991) gives the bearing of an exact solution as one that satisfies Eq. (1.2.1) and Eq. (1.2.28) and is valid for all velocity and viscosity values. All closed form solutions satisfy the requirements and are clear exact solutions. However, direct numerical solutions of the PDEs remain as approximations, regardless of accuracy, because the routine requires that an initial value for ν be given. In contrast, a similarity solution combines ν into a parameter which yield universal graphs of the flow characteristics, giving similarity solutions the title of, in accordance with Wang (1989, 1991), an exact solution. Wang (1991) does not consider, although some may dispute, infinite series solutions extracted from expansions or separation of variables (SOV) as exact solutions since, as the name implies, the solutions sum to infinity. Potential flow solutions, obviously, do not count towards exact solutions either since they are degenerate cases of the NSEs (Wang 1989). However, potential flows (and other constrained flows) satisfy the NSE constraints exactly. Wang (1989) also does not review other approximations of the NSEs such as the solutions of the boundary layer equations or Stokes' equations.

Exact solutions to the NSE bridge a century or so and grace a variety of journal publications. Usually, exact solutions narrow down the fluid problem to specific cases which, according to Wang (1991), limits cross-referencing. Thus, difficulty arises for fluid dynamics researchers to realize whether a solution has been solved and published already similar to the dual nature of early math and fluid dynamics discoveries. Wang divulges an example of multiple publications of an exact solution. Wang notes that the solution for oblique stagnation flow on a plate was published three times by different researchers over a period of 27 years. However, in today's internet-based world culture and society, it has

become ten times easier to find relevant material to research topics. On the other hand, this produces ten times as much material to digest. Advances have been made to unprecedented capability to access information, and in turn allows many researchers to contribute to this vast vat of knowledge. Thus, the problem of cross-referencing remains the same as in the year of Wang's publication, 1991, and in the early days of fluid dynamics evolution.

Only a few publications review the solutions to the NSE at the time of Wang's article, 1991. For a complete review of exact solutions of the NSE, Wang (1991) recommends Berker (1963) which is based on an earlier publication of Berker (1936) and a publication by Dryden et al. (1932). Other sources cited by Wang (1991) only refer to a partial set or class of NSE according to topic such as Schlitching's classic *Boundary Layer Theory* editions 1979 and 2000. Additional references published after Wang (1991) include Drazin and Riley (2006) and their book entitled *The Navier-Stokes Equation: A Classification of Flows and Exact Solutions* published by Cambridge University Press.

Classification of exact solutions of the NSE describe a myriad of flows types. Wang begins his 1966 article with three types:

1. "Those which show certain invariances along a direction in space."

2. "Those which possess certain properties such that a set of ordinary differential equations can be obtained from the original partial differential equations."

3. "Those whose nonlinear terms are not identically zero individually but as a whole they cancel each other out."

Type (1) flows contain parallel flows where the nonlinear terms vanish identically (Wang 1966). Couette and Poiseuille flows (steady flow between planes Drazin and Riley 2006, unsteady motion of infinite plates, etc. Type (2) classes contain two-dimensional and axisymmetric stagnation-point flows and similarity solutions such as flow near an infinite rotating disk, round jets, etc. Usually, according to Wang (1966), Type (2) yields a set of nonlinear ordinary equations which, known at that time (other techniques may be viable since Wang's paper dates back to 1966), need numerical integration.

1.2.1.1 General NSE in Cartesian Coordinates

From Drazin and Riley (2006), a general Cartesian coordinate expansion into three components of the NSE yields

Continuity:

$$\frac{\partial u_x}{\partial x} + \frac{\partial u_y}{\partial y} + \frac{\partial u_z}{\partial z} = 0 \tag{1.2.6}$$

x-direction:

$$\frac{\partial u_x}{\partial t} + u_x\frac{\partial u_x}{\partial x} + u_y\frac{\partial u_x}{\partial y} + u_z\frac{\partial u_x}{\partial z} = -\frac{1}{\rho}\frac{\partial p}{\partial x} + X + \nu\nabla^2 u_x \tag{1.2.7}$$

y-direction:

$$\frac{\partial u_y}{\partial t} + u_x\frac{\partial u_y}{\partial x} + u_y\frac{\partial u_y}{\partial y} + u_z\frac{\partial u_y}{\partial z} = -\frac{1}{\rho}\frac{\partial p}{\partial y} + Y + \nu\nabla^2 u_y \tag{1.2.8}$$

z-direction:

$$\frac{\partial u_z}{\partial t} + u_x\frac{\partial u_z}{\partial x} + u_y\frac{\partial u_z}{\partial y} + u_z\frac{\partial u_z}{\partial z} = -\frac{1}{\rho}\frac{\partial p}{\partial z} + Z + \nu\nabla^2 u_z \tag{1.2.9}$$

where the Laplacian in Cartesian coordinates, ∇^2, is equal to

$$\nabla^2 f = \frac{\partial^2 f}{\partial x^2} + \frac{\partial^2 f}{\partial y^2} + \frac{\partial^2 f}{\partial z^2} \tag{1.2.10}$$

The Laplace operator has also been called the Laplace-Beltrami operator (Kimura and Okamoto 1987).

1.2.1.2 General NSE in Cylindrical Polar Coordinates

From Drazin and Riley (2006), a general cylindrical polar coordinate expansion into three components of the NSE yields:

Continuity:

$$\frac{1}{r}\frac{\partial\left(ru_r\right)}{\partial r}+\frac{1}{r}\frac{\partial u_\theta}{\partial\theta}+\frac{\partial u_z}{\partial z}=0 \tag{1.2.11}$$

Cylindrical Polar Radial:

$$\begin{aligned}&\frac{\partial u_r}{\partial t}+u_r\frac{\partial u_r}{\partial r}+\frac{u_\theta}{r}\frac{\partial u_r}{\partial\theta}+u_z\frac{\partial u_r}{\partial z}-\frac{u_\theta^2}{r}\\&\quad=-\frac{1}{\rho}\frac{\partial p}{\partial r}+F_r+\nu\left(\nabla^2u_r-\frac{u_r}{r^2}-\frac{2}{r^2}\frac{\partial u_\theta}{\partial\theta}\right)\end{aligned} \tag{1.2.12}$$

Azimuthal:

$$\begin{aligned}&\frac{\partial u_\theta}{\partial t}+u_r\frac{\partial u_\theta}{\partial r}+\frac{u_\theta}{r}\frac{\partial u_\theta}{\partial\theta}+u_z\frac{\partial u_\theta}{\partial z}+\frac{u_ru_\theta}{r}\\&\quad=-\frac{1}{\rho r}\frac{\partial p}{\partial\theta}+F_{u_\theta}+\nu\left(\nabla^2u_r+\frac{2}{r^2}\frac{\partial u_r}{\partial\theta}-\frac{u\theta}{r^2}\right)\end{aligned} \tag{1.2.13}$$

Axial:

$$\frac{\partial u_z}{\partial t}+u_r\frac{\partial u_z}{\partial r}+\frac{u_\theta}{r}\frac{\partial u_z}{\partial\theta}+u_z\frac{\partial u_z}{\partial z}=-\frac{1}{\rho}\frac{\partial p}{\partial z}+F_z+\nu\nabla^2u_z \tag{1.2.14}$$

where the Laplacian in cylindrical polar coordinates, ∇^2, is equal to

$$\nabla^2f=\frac{1}{r}\frac{\partial}{\partial r}\left(r\frac{\partial f}{\partial r}\right)+\frac{1}{r^2}\frac{\partial^2f}{\partial\theta^2}+\frac{\partial^2f}{\partial z^2} \tag{1.2.15}$$

or

$$\nabla^2f=\frac{\partial^2f}{\partial r^2}+\frac{1}{r}\frac{\partial f}{\partial r}+\frac{1}{r^2}\frac{\partial^2f}{\partial\theta^2}+\frac{\partial^2f}{\partial z^2} \tag{1.2.16}$$

1.2.1.3 General NSE in Spherical Polar Coordinates

From Drazin and Riley (2006), a general spherical polar coordinate expansion into three components of the NSE yields:

Continuity:

$$\frac{1}{R^2}\frac{\partial}{\partial R}\left(R^2 u_R\right) + \frac{1}{R\sin\phi}\frac{\partial}{\partial\phi}\left(u_\phi \sin\phi\right) + \frac{1}{R\sin\phi}\frac{\partial u_\theta}{\partial\theta} = 0 \tag{1.2.17}$$

Spherical Polar Radial:

$$\begin{aligned}\frac{\partial u_R}{\partial t} + u_R\frac{\partial u_R}{\partial R} + \frac{u_\theta}{R}\frac{\partial u_R}{\partial\phi} + \frac{u_\theta}{R\sin\phi}\frac{\partial u_R}{\partial\theta} - \frac{u_\phi^2 + u_\theta^2}{R} \\ = -\frac{1}{\rho}\frac{\partial p}{\partial R} + F_R + \nu\left(\nabla^2 u_R - \frac{2u_R}{R^2} - \frac{2}{R^2}\frac{\partial u_\phi}{\partial\phi}\right. \\ \left. -\frac{2u_\theta\cos\theta}{R^2} - \frac{2}{R^2\sin\phi}\frac{\partial u_\theta}{\partial\theta}\right)\end{aligned} \tag{1.2.18}$$

Zenith:

$$u_r\frac{\partial u_\theta}{\partial r} + \frac{u_\theta}{r}\frac{\partial u_\theta}{\partial\theta} + u_z\frac{\partial u_\theta}{\partial z} + \frac{u_r u_\theta}{r} = -\frac{1}{\rho r}\frac{\partial p}{\partial\theta} \tag{1.2.19}$$

Azimuthal:

$$u_r\frac{\partial u_z}{\partial r} + \frac{u_\theta}{r}\frac{\partial u_z}{\partial\theta} + u_z\frac{\partial u_z}{\partial z} = -\frac{1}{\rho}\frac{\partial p}{\partial z} \tag{1.2.20}$$

where the Laplacian in spherical polar coordinates, ∇^2, is equal to

$$\nabla^2 f = \frac{1}{R^2}\frac{\partial}{\partial R}\left(R^2\frac{\partial f}{\partial R}\right) + \frac{1}{R^2\sin\phi}\frac{\partial}{\partial\phi}\left(\sin\phi\frac{\partial f}{\partial\phi}\right) + \frac{1}{R^2\sin^2\phi}\frac{\partial^2 f}{\partial\theta^2} \tag{1.2.21}$$

or

$$\nabla^2 f = \frac{\partial^2 f}{\partial R^2} + \frac{2}{R}\frac{\partial f}{\partial R} + \frac{1}{R^2}\frac{\partial^2 f}{\partial\phi^2} + \frac{\cot\phi}{R^2}\frac{\partial f}{\partial\phi} + \frac{1}{R^2\sin^2\phi}\frac{\partial^2 f}{\partial\theta^2} \tag{1.2.22}$$

1.2.2 Inviscid, Incompressible Flows & the Euler Equations

The basis for this dissertation also assumes inviscid flow properties. Again, similar to incompressible flow, compared to compressible flow, inviscid models versus viscous models reduce the complexity of equations to solve analytically. However, with more elementary solutions, some real physics predictions are lost such as the no-slip condition. Although, some areas of practical fluid flow mimic inviscid conditions. These areas are usually away from boundaries where friction is negligible. Just like numerical tools and caveats, as long as the user is aware of pitfalls and strengths, very useful information can be obtained in an effective manner.

The inviscid, incompressible flow equations are sometimes referred to as Euler's momentum equations. The full viscous momentum equations in vector form appear as (Kee et al. 2003; Drazin and Riley 2006)

$$\frac{1}{\rho}\frac{\mathrm{D}\rho}{\mathrm{D}t} + \nabla \cdot \mathbf{u} = 0 \tag{1.2.23}$$

$$\rho\frac{\mathrm{D}\mathbf{u}}{\mathrm{D}t} = \mathbf{F} - \nabla p - \mu\nabla \times (\nabla \times \mathbf{u}) + (\kappa + 2\mu)\,\nabla\,(\nabla \cdot \mathbf{u}) \tag{1.2.24}$$

or

$$\frac{1}{\rho}\left(\frac{\partial\rho}{\partial t} + \mathbf{u} \cdot \nabla\rho\right) + \nabla \cdot \mathbf{u} = 0 \tag{1.2.25}$$

$$\rho\left(\frac{\partial\mathbf{u}}{\partial t} + (\mathbf{u} \cdot \nabla)\,\mathbf{u}\right) = \mathbf{F} - \nabla p - \mu\nabla \times (\nabla \times \mathbf{u}) + (\kappa + 2\mu)\,\nabla\,(\nabla \cdot \mathbf{u}) \tag{1.2.26}$$

where the material (also called convective) derivative equals (Drazin and Riley 2006)

$$\frac{\mathrm{D}}{\mathrm{D}t} = \frac{\partial}{\partial t} + \mathbf{u} \cdot \nabla \tag{1.2.27}$$

For incompressible, inviscid flow, we have

$$\nabla \cdot \mathbf{u} = 0 \tag{1.2.28}$$

$$\mu = 0 \tag{1.2.29}$$

which reduces the equations to

$$\frac{\mathrm{D}\mathbf{u}}{\mathrm{D}t} = \mathbf{F} - \frac{1}{\rho}\nabla p \tag{1.2.30}$$

or

$$\frac{\partial \mathbf{u}}{\partial t} + (\mathbf{u} \cdot \nabla)\,\mathbf{u} = \mathbf{F} - \frac{1}{\rho}\nabla p \tag{1.2.31}$$

The momentum set without gravity effects, unsteady effects, and both, respectively, is as follows

$$\frac{\partial \mathbf{u}}{\partial t} + (\mathbf{u} \cdot \nabla)\,\mathbf{u} = -\frac{1}{\rho}\nabla p \tag{1.2.32}$$

$$(\mathbf{u} \cdot \nabla)\,\mathbf{u} = \mathbf{F} - \frac{1}{\rho}\nabla p \tag{1.2.33}$$

$$(\mathbf{u} \cdot \nabla)\,\mathbf{u} = -\frac{1}{\rho}\nabla p \tag{1.2.34}$$

where the divergence of the velocity field in the continuity equation, Eq. (1.2.28), is known as a solenoidal field (Wang 1991). Equation 1.2.34 is the fundamental basis for this dissertation.

1.3 Vorticity, Vortices, and Rotational Flow

According to Alkemade (1993) and his survey of vorticity and vortices, the mathematical and physical basis for rotating flows, only emerged in the second half of the 18th and first

half of the 19th century. The emergence of vorticity became a well established branch of fluid dynamics and mechanics when the German scientist, Herman L. F. von Helmholtz (1858; 1867) published his treatise on vortex motion. While the study of the motion of fluids dates back to the ancient Greeks, the theory behind fluid motion only becomes a serious science when Newton publishes his *Principia* in the 17th century. After his publication, the area of fluid dynamics and mechanics surged as scientist intricately and intensely study the physical and mathematical aspects of fluid motion.

Before Helmholtz (1858), Thomson (Kelvin) (1880), or Newton, the ancient Greeks often discussed fluid motion, vortices, and laws of their world (Alkemade 1993). For Anaxagoras' (499-428 BC) theory of an expanding universe, the vortex represented a base phenomena in his model (Vatistas 2008). Democritus (460-370 BC) utilized vortices for his hypothesis of a world of atoms (Alkemade 1993; Vatistas 2008). Diogenes Laertius records Democritus philosophy as

> "All things come into being by necessity, the cause of the coming into being of all things being the vortex, which he [Democritus] calls necessity."

Alkemade (1993) mentions that Democritus is more associated with theorizing about matter and atoms; nevertheless, his philosophy about the vortex remains ambiguous. However, Democritus may have been on to something according to present day theoretical and astrophysics theories and hypothesis.

Vorticity and vortices are two separate, yet connected concepts, wherein confusion can emerge deciphering between the two definitions. Therefore, this introductory section attempts to explain the two entities together, yet at the same time do so independently, since vorticity and vortices are generally connected even with having two different meanings. In Guyon et al. (2001), the authors depict vorticity as the tool that enables us to characterize the local rotation within a fluid. Vorticity usually appears minutely throughout the flow field but greatly influences the flow pattern as defined by Wu et al. (2006). However, a counterpart to vorticity, the vortex, as Lugt (1996) specifies, does not have a single written-in-stone definition like the clear mathematical interpretation of vorticity. Simply, Lugt

(1996) calls a vortex the rotating motion of a multitude of material particles around a common center. In other words, vortices comprise of a fluid spinning around a point or axis and physically exist as smoke rings, cyclones, turbulent eddies and more. Accordingly, vorticity and vortices are further explored, while also simultaneously revealing their purpose within the study of fluid motion.

Additional investigation into vorticity and vortices uncovers additional information to assist in clarification and importance to fluid dynamics. Wu et al. (2006) describe a vortex as a special form of fluid motion with an origin in the rotation of fluid elements. Wu et al. (2006) disseminate further and portray vorticity as delineating the rotationality of the fluid. Panton (2005) divides the two by stating that the vorticity is a local property of the flow field and that a vortex is a rotating fluid structure.

Since the vortex appears as an important flow structure throughout fluid dynamics and the physical world, scientists and engineers want to know how a vortex behaves. Thus, modeling the vortical entities through fluid dynamics and laws of mathematics is important in order to reveal velocity, pressure, and even temperature fields. In fluid dynamics, the velocities of fluids play a necessary role in determining flow characteristics and aid in the understanding fluid motions. Thus, the velocity field of a fluid $\mathbf{u}(\mathbf{x}, t)$ directs the actions of the flow as denoted by Saffman (1992). In Cartesian summation notation vorticity emanates as $\boldsymbol{\omega}(\mathbf{x}, t) = \omega_i = \epsilon_{ijk}\left(\partial u_k/\partial x_j\right)$, as seen in Saffman (1992), Green (1995), and Panton (2005). Therefore, as Green emphasizes, the mathematical definition of the vorticity vector *is proportional to the rate of rotation of a small fluid element about its own axes*. In other words, vorticity is directly connected to velocities and the change in velocity. Understanding vorticity gives fluid dynamicists another useful tool in evaluating fluid phenomena. Vorticity provides an additional eye into fluid dynamics problems.

Mathematically, the vorticity is defined as the curl of the velocity, expressed as

$$\boldsymbol{\omega} = \nabla \times \mathbf{u} \tag{1.3.1}$$

Many real world flows cannot be accurately described by flow potentials because most flows contain rotational components. Alkemade (1993) even states that for flows that are nearly irrotational the small amount of rotationality may be important to the flow behavior. Even though the direct mathematical concept of vorticity was not explicitly present in 18th century research, the writers hinted at the roationality in flows by showing that the vector field, $\nabla \times \mathbf{u}$, was not equal to zero, $\boldsymbol{\omega} \neq 0$. Both D'Alembert and Euler touted many scientific discoveries of fluid mechanics in the 18th century including the infamous theory of the D'Alembert-Euler vorticity equation written as

$$\frac{\mathrm{D}\boldsymbol{\omega}}{\mathrm{D}t} = (\boldsymbol{\omega} \cdot \nabla)\,\mathbf{u} - \boldsymbol{\omega}\,(\nabla \cdot \mathbf{u}) \tag{1.3.2}$$

Fundamentally, vorticity of a fluid originates due to the fluid shear deformation. A fluid element rotates and deforms due to differences in velocities acting upon the element as stated in pedagogical fluid dynamics books by Munson et al. (2002), White (2003), and Panton (2005). A difference in velocity vector speeds arises in viscous flows due to the internal fluid friction or in inviscid flows due to geometrical path changes, various injection points, etc. More specifically, the velocity gradients determine whether rotation and vorticity occur in fluid motion. Recall the vector calculus definition of vorticity as the curl of the velocity vector. In Cartesian coordinates, $\mathbf{d} = \mathbf{d}(x, y, z)$; $\mathbf{u} = \mathbf{u}(u, v, w)$, the vorticity vector equals

$$\boldsymbol{\omega} = \nabla \times \mathbf{u} = \begin{vmatrix} \mathbf{e}_x & \mathbf{e}_y & \mathbf{e}_z \\ \dfrac{\partial}{\partial x} & \dfrac{\partial}{\partial y} & \dfrac{\partial}{\partial z} \\ u & v & w \end{vmatrix} \tag{1.3.3}$$

$$\boldsymbol{\omega} = \left(\frac{\partial w}{\partial y} - \frac{\partial v}{\partial z}\right)\mathbf{e}_x + \left(\frac{\partial u}{\partial z} - \frac{\partial w}{\partial x}\right)\mathbf{e}_y + \left(\frac{\partial v}{\partial x} - \frac{\partial u}{\partial y}\right)\mathbf{e}_z \tag{1.3.4}$$

$$\omega_x = \left(\frac{\partial w}{\partial y} - \frac{\partial v}{\partial z}\right) \tag{1.3.5}$$

$$\omega_y = \left(\frac{\partial u}{\partial z} - \frac{\partial w}{\partial x}\right) \tag{1.3.6}$$

$$\omega_z = \left(\frac{\partial v}{\partial x} - \frac{\partial u}{\partial y}\right) \tag{1.3.7}$$

where, upon inspection, it is apparent that the velocity gradients determine the vorticity of the fluid.

Munson et al. (2002) and White (2003) break down the natural process using a square fluid element to assist in demonstrating angular deformation and fluid rotation. The fluid element rotates clockwise with an angular velocity of ω_{OB} if $\partial u/\partial y$ is positive and counterclockwise with an angular velocity of ω_{OA} if $\partial v/\partial x$ is positive. Notice, however, that the rotation will only be rigid (solid body rotation, $\omega_{OB} = -\omega_{OA}$) when $\partial u/\partial y = -\partial v/\partial x$ else, angular deformation occurs.

Vorticity or rotation may not always be apparent in fluid flow, especially when explicit vortices do not visually appear. However, rotational effects often occur in many situations. One mechanism of high vorticity generation engenders from the no-slip condition at boundaries such as solid walls. The laminar flow of a fluid in a pipe demonstrates several fundamental aspects of rotation and vorticity. A uniform velocity profile transforms (develops) over the distance of the pipe, eventually into a parabolic profile.

Important works in the 18th century also occurred due to the explosion and influence of institutions such as the École Polytechnique in Paris France where other fluid dynamics leaders, Laplace (1749-1827) and Poisson (1781-1840), developed techniques, the physique mathématique, to model various physical fluid motions. The simplification of mathematical equations, such as Laplace's algebraic approaches, to describe fluid phenomena were important as the solutions became more workable. However, much mathematical thought and effort were still required to understand the physical-mathematical connections such as Fourier's (1768-1830) improvement in models of heat theory utilizing rational mechanics. The first, according to Alkemade (1993), to utilize the symbolic notation for vorticity and its components were Cauchy (1789-1857) and Lagrange (1736-1813).

Green (1995) points out that the vorticity has the dimension of $1/s$, a frequency. This frequency characteristic implies a rotation thus confirming vorticity's relation to the rotation of a fluid element. The vorticity field by definition is solenoidal due to the mathematics of vector calculus which demonstrates that the divergence of the curl of a vector is equal to zero, $\nabla \cdot (\nabla \times \mathbf{x}) = 0$. Thus as confirmed by Donnelly (1991) and Green (1995), the divergence of the vorticity vector is zero, $\nabla \cdot \boldsymbol{\omega} = 0$, which is analogous to the velocity of an incompressible flow, $\nabla \cdot \mathbf{u} = 0$, Eq. (1.2.28), also a solenoidal field (Wang 1991). The vorticity vector can be expressed in cylindrical polar coordinates as

$$\boldsymbol{\omega} = \nabla \times \mathbf{u} = \frac{1}{r}\begin{vmatrix} \mathbf{e}_r & r\mathbf{e}_\theta & \mathbf{e}_z \\ \dfrac{\partial}{\partial r} & \dfrac{\partial}{\partial \theta} & \dfrac{\partial}{\partial z} \\ u_r & ru_\theta & u_z \end{vmatrix} \tag{1.3.8}$$

$$\boldsymbol{\omega} = \frac{1}{r}\left[\frac{\partial u_z}{\partial \theta} - \frac{\partial}{\partial z}(u_\theta r)\right]\mathbf{e}_r + \left(\frac{\partial u_r}{\partial z} - \frac{\partial u_z}{\partial r}\right)\mathbf{e}_\theta + \frac{1}{r}\left[\frac{\partial}{\partial r}(u_\theta r) - \frac{\partial u_r}{\partial \theta}\right]\mathbf{e}_z \tag{1.3.9}$$

$$\omega_r = \frac{1}{r}\left[\frac{\partial u_z}{\partial \theta} - \frac{\partial}{\partial z}(u_\theta r)\right] = \frac{1}{r}\frac{\partial u_z}{\partial \theta} - \frac{\partial u_\theta}{\partial z} \tag{1.3.10}$$

$$\omega_\theta = \frac{\partial u_r}{\partial z} - \frac{\partial u_z}{\partial r} \tag{1.3.11}$$

$$\omega_z = \frac{1}{r}\left[\frac{\partial}{\partial r}(u_\theta r) - \frac{\partial u_r}{\partial \theta}\right] = \frac{\partial u_\theta}{\partial r} + \frac{u_\theta}{r} - \frac{1}{r}\frac{\partial u_r}{\partial \theta} \tag{1.3.12}$$

In spherical polar coordinates, the vorticity expansion is (see page 128 in Karamcheti 1966)

$$\boldsymbol{\omega} = \nabla \times \mathbf{u} = \frac{1}{R^2 \sin\phi}\begin{vmatrix} \mathbf{e}_R & R\mathbf{e}_\phi & R\sin\phi\mathbf{e}_\theta \\ \dfrac{\partial}{\partial R} & \dfrac{\partial}{\partial \phi} & \dfrac{\partial}{\partial \theta} \\ u_R & Ru_\phi & R\sin\phi u_\theta \end{vmatrix} \tag{1.3.13}$$

$$\boldsymbol{\omega} = \frac{1}{R^2 \sin\phi}\left(\frac{\partial R \sin\phi u_\theta}{\partial \phi} - \frac{\partial R u_\phi}{\partial \theta}\right)\mathbf{e}_R - \frac{1}{R\sin\phi}\left(\frac{\partial R \sin\phi u_\theta}{\partial R} - \frac{\partial u_R}{\partial \theta}\right)\mathbf{e}_\phi + \frac{1}{R}\left(\frac{\partial R u_\phi}{\partial R} - \frac{\partial u_R}{\partial \phi}\right)\mathbf{e}_\theta \tag{1.3.14}$$

$$\omega_R = \frac{1}{R^2\sin\phi}\left(\frac{\partial R\sin\phi u_\theta}{\partial\phi} - \frac{\partial u_\phi}{\partial\theta}\right) = \frac{1}{R^2\sin\phi}\left[\frac{\partial}{\partial\phi}\left(u_\theta R\sin\phi\right) - \frac{\partial u_\phi}{\partial\theta}\right] = \frac{1}{R}\frac{\partial u_\theta}{\partial\phi} + \frac{u_\theta\cot\phi}{R} - \frac{1}{R^2\sin\phi}\frac{\partial u_\phi}{\partial\theta} \tag{1.3.15}$$

$$\omega_\phi = \frac{1}{R\sin\phi}\left(\frac{\partial u_R}{\partial\theta} - \frac{\partial R\sin\phi u_\theta}{\partial R}\right) = \frac{1}{R\sin\phi}\left[\frac{\partial u_R}{\partial\theta} - \frac{\partial}{\partial R}\left(u_\theta R\sin\phi\right)\right] = \frac{1}{R\sin\phi}\frac{\partial u_R}{\partial\theta} - \frac{\partial u_\theta}{\partial R} - \frac{u_\theta}{R} \tag{1.3.16}$$

$$\omega_\theta = \frac{1}{R}\left(\frac{\partial R u_\phi}{\partial R} - \frac{\partial u_R}{\partial\phi}\right) = \frac{1}{R}\left[\frac{\partial}{\partial R}\left(u_\phi R\right) - \frac{\partial u_R}{\partial\phi}\right] = \frac{\partial u_\phi}{\partial R} + \frac{u_\phi}{R} - \frac{\partial u_R}{\partial\phi} \tag{1.3.17}$$

As mentioned earlier, the vortex occurs naturally throughout the universe and dominates a myriad of fluid phenomena. Vortices appear at a range of scales from the atomic superfluid helium structures (Koplik and Levine 1993; Vatistas 2008), to the meso-scale bathtub vortex (Vatistas 2008), tornados (Rotunno 1979; Gupta et al. 1984; Vatistas 2008), tidal whirlpools (Gupta et al. 1984; Vatistas 2008), tropical cyclones, and atmospheric dynamics on Earth and other planets (Morton 1966), to finally, the infinitesimal large spiral galaxies and black holes in the universe (Vatistas 2008).

Turbulent flows materialize in most fluid situations, which are governed by eddies of swirling fluid. The vortex, as stated by Vatistas (2008), contains the best method, which occurs naturally in the world and utilized in technology, to effectively transport mass, momentum, and energy. Gupta et al. (1984) disseminate that swirling flows occur in vortex amplifiers and reactors, cyclone separators, Ranque-Hilsch tubes, agriculture spraying machines, heat exchangers, jet pumps, and the motions of frisbees and boomerangs. As noted before, swirling motion imparts a vortex or a spiral-type of flow giving an azimuthal or tangential component of velocity. To generate such swirling flows many types of techniques exist including swirl vanes, axial-tangential entry, or strictly tangential entry into a chamber. Other types of swirl generation encases vortex shedding which is produced by solid-fluid friction interactions. During vortex shedding an internal fluid friction (viscous flows) emerges as fluid passes around an object if conditions are right (usually depicted by the Reynolds number which relates the fluid viscosity (ν), speed (U), and a geometric parameter such as pipe diameter or sphere diameter (d), displayed as $Re = U\,d/\nu$). The production of vortices flowing past a solid occurs in situations such as backward facing steps (which are found in many combustion chamber systems), semi-trucks, airplane wings, and the von Kármán vortex street engendered by cylinders in cross flow and even island which is shown from satellite photographs in the cloud formations (Gupta et al. 1984; Spalart 1998). In reactive flows, the vortex or swirling motion appears as combustion enhancements such as mixing and stability (Lilley 1977; Bucher et al. 2003). Swirling flows assist gasoline and diesel engines, gas turbines, industrial furnaces, utility boilers, and many other mechanical apparatuses that utilize heat. Thus, vortex structures compose an important part of physical interactions throughout the world.

1.3.1 The Beltrami-Gromeka-Lamb Equation

This section covers discussion of a transformation of the NSEs which brings vorticity to the forefront as an important flow variable, explicitly linked to the velocity and stream function. Following Kee et al. (2003), we begin with the full NSEs from Eq. (1.2.26)

$$\rho\left(\frac{\partial \mathbf{u}}{\partial t} + (\mathbf{u}\cdot\nabla)\,\mathbf{u}\right) = \mathbf{F} - \nabla p - \mu\nabla\times(\nabla\times\mathbf{u}) + (\kappa + 2\mu)\,\nabla\,(\nabla\cdot\mathbf{u})$$

Next, a vector identity is applied and the resulting equations is known as the Gromeka-Lamb equation, named in honor of Ippolit Stepanovich Gromeka and Horace Lamb for their contributions (Lamb 1877, 1879, 1975) to the fluid dynamics community (Truesdell 1954). The Gromeka-Lamb equation can also be attributed to Eugenio Beltrami (Gostintsev et al. 1971; Lakhtakia 1994; Alekseenko et al. 2007) and Beltrami's work (Beltrami 1889). The vector momentum equation transforms to its Beltrami-Gromeka-Lamb equivalent (Granger 1995; Kiselev et al. 1999; Alekseenko et al. 2007; Luniev 2009) by utilizing Lamb's vector identity

$$(\mathbf{u}\cdot\nabla)\mathbf{u} = \tfrac{1}{2}\nabla u^2 - \mathbf{u}\times\boldsymbol{\omega} \tag{1.3.18}$$

Thus, 1.2.30 and 1.2.3 become the inviscid and viscous Beltrami-Gromeka-Lamb equation

$$\nabla\left(\frac{p}{\rho} + \frac{u^2}{2}\right) - \mathbf{u}\times\boldsymbol{\omega} = 0 \tag{1.3.19}$$

$$\nabla\left(\frac{p}{\rho} + \frac{u^2}{2}\right) - \mathbf{u}\times\boldsymbol{\omega} = \nu\nabla^2\mathbf{u} \tag{1.3.20}$$

This equation in turn morphs after combining terms into

$$\nabla \mathrm{H} - \mathbf{u}\times\boldsymbol{\omega} = 0 \tag{1.3.21}$$

or using the vector identity $-\mathbf{u}\times\boldsymbol{\omega} = \boldsymbol{\omega}\times\mathbf{u}$ the momentum equation becomes

$$\nabla \mathrm{H} + \boldsymbol{\omega}\times\mathbf{u} = 0 \tag{1.3.22}$$

or

$$\nabla \mathrm{H} = \mathbf{u}\times\boldsymbol{\omega} \tag{1.3.23}$$

1.3.2 The Vorticity Transport Equation and Beltramian Flows

According to Wang (1990, 1991), the NSEs can be written in terms of the vorticity by taking the curl to get

$$\frac{\partial \boldsymbol{\omega}}{\partial t} + \nu\left(\nabla \times \nabla \times \boldsymbol{\omega}\right) + \nabla \times \left(\boldsymbol{\omega} \times \mathbf{u}\right) = 0 \tag{1.3.24}$$

for the momentum and

$$\nabla \cdot \mathbf{u} = 0$$

for continuity. For steady-state cases (Wang 1991), Equation 1.3.24 becomes

$$\nabla \times \left(\boldsymbol{\omega} \times \mathbf{u}\right) = -\nu\left(\nabla \times \nabla \times \boldsymbol{\omega}\right) \tag{1.3.25}$$

For ***parallel*** and ***concentric*** flows, the nonlinear convection terms of Eq. (1.3.25) become zero. ***Beltrami flows***, also called ***screw fields*** (Wang 1991) or helical flows Wu et al. (2006); Alekseenko et al. (2007), satisfy

$$\mathbf{u} \times \boldsymbol{\omega} = 0 \tag{1.3.26}$$

The ***generalized Beltrami flows*** encompass a larger range of solutions by relaxing the limitations to

$$\nabla \times \mathbf{u} \times \boldsymbol{\omega} = 0 \tag{1.3.27}$$

A ***Trkalian field*** meets the requirement of

$$\boldsymbol{\omega} = c\mathbf{u} \tag{1.3.28}$$

where c is a constant. The ***complex lamellar*** classification of flows are grouped by the relation

$$\boldsymbol{\omega} \cdot \mathbf{u} = 0 \tag{1.3.29}$$

For more on Beltrami and related flows the reader is referred to Truesdell (1954), Vasil'ev (Vasilyev) (1958), Wang (1990), Wang (1991), Lakhtakia (1994), Sposito (1997), Wu et al. (2006), Alekseenko et al. (2007), and Truesdell and Rajagopal (2009).

1.3.3 The Lamb Vector

Equation 1.3.23 is the steady, inviscid, incompressible, and negligible body force form of the Beltrami-Gromeka-Lamb equation also known as Crocco's equation (Crocco 1937) without the entropy term (Granger 1995; Cooper and Peake 2001; Batchelor 2000) or the Crocco-Vazsony equation (Warsi 1999) which can be reduced further by implementing the Lamb vector (Lugt 1996; Sposito 1997; Hamman et al. 2008), $\boldsymbol{\ell} = -\mathbf{u} \times (\nabla \times \mathbf{u}) = -\mathbf{u} \times \boldsymbol{\omega}$, (also called the swirl vector, see Scofield and Huq 2010) to get

$$\nabla \mathrm{H} + \boldsymbol{\ell} = 0 \tag{1.3.30}$$

or

$$\nabla \mathrm{H} = -\boldsymbol{\ell} \tag{1.3.31}$$

For axisymmetric inviscid Beltrami flows in SPC the EOM become

$$\frac{\partial}{\partial R}\left(u_R R^2 \sin\phi\right) + \frac{\partial}{\partial \phi}\left(u_\phi R \sin\phi\right) = 0 \quad \text{(continuity)} \tag{1.3.32}$$

$$u_R \frac{\partial u_R}{\partial R} + \frac{u_\phi}{R}\frac{\partial u_R}{\partial \phi} = -\frac{1}{\rho}\frac{\partial p}{\partial R} \quad \text{(radial)} \tag{1.3.33}$$

$$u_R \frac{\partial u_\phi}{\partial R} + \frac{u_\phi}{R}\frac{\partial u_\phi}{\partial \phi} + \frac{u_R u_\phi}{R} - \frac{u_\theta^2 \cot\phi}{R} = -\frac{1}{\rho R}\frac{\partial p}{\partial \phi} \quad \text{(latitudinal)} \tag{1.3.34}$$

$$u_R \frac{\partial u_\theta}{\partial R} + \frac{u_\phi}{R}\frac{\partial u_\theta}{\partial \phi} + \frac{u_R u_\theta}{R} + \frac{u_\phi u_\theta}{R}\cot\phi = 0 \quad \text{(azimuthal)} \tag{1.3.35}$$

with vorticity being expressible by

$$\boldsymbol{\omega} = \frac{1}{R^2\sin\phi}\frac{\partial}{\partial\phi}\left(u_\theta R\sin\phi\right)\mathbf{e}_R - \frac{1}{R\sin\phi}\frac{\partial}{\partial R}\left(u_\theta R\sin\phi\right)\mathbf{e}_\phi + \frac{1}{R}\left[\frac{\partial}{\partial R}\left(Ru_\phi\right) - \frac{\partial u_R}{\partial\phi}\right]\mathbf{e}_\theta \tag{1.3.36}$$

and the Lamb vector as

$$\begin{aligned}\boldsymbol{\ell} = &\left\{\frac{u_\phi}{R}\left[\frac{\partial u_R}{\partial\phi} - \frac{\partial}{\partial R}\left(u_\phi R\right)\right] - \frac{u_\theta}{R\sin\phi}\frac{\partial}{\partial R}\left(u_\theta R\sin\phi\right)\right\}\mathbf{e}_R \\ &+ \left\{\frac{u_R}{R}\left[\frac{\partial}{\partial R}\left(u_\phi R\right) - \frac{\partial u_R}{\partial\phi}\right] - \frac{u_\theta}{R\sin\phi}\frac{\partial}{\partial\phi}\left(u_\theta R\sin\phi\right)\right\}\mathbf{e}_\phi \\ &+ \left[\frac{u_\phi}{R^2\sin\phi}\frac{\partial}{\partial\phi}\left(u_\theta R\sin\phi\right) + \frac{u_R}{R\sin\phi}\frac{\partial}{\partial R}\left(u_\theta R\sin\phi\right)\right]\mathbf{e}_\theta\end{aligned} \tag{1.3.37}$$

The vorticity components become

$$\omega_R = \frac{1}{R^2\sin\phi}\frac{\partial}{\partial\phi}\left(u_\theta R\sin\phi\right) = \frac{1}{R}\frac{\partial u_\theta}{\partial\phi} + \frac{u_\theta\cot\phi}{R} \tag{1.3.38}$$

$$\omega_\phi = -\frac{1}{R\sin\phi}\frac{\partial}{\partial R}\left(u_\theta R\sin\phi\right) = -\frac{1}{R}\frac{\partial}{\partial R}\left(u_\theta R\right) = -\frac{\partial u_\theta}{\partial R} - \frac{u_\theta}{R} \tag{1.3.39}$$

$$\omega_\theta = \frac{1}{R}\left[\frac{\partial}{\partial R}\left(Ru_\phi\right) - \frac{\partial u_R}{\partial\phi}\right] = \frac{\partial u_\phi}{\partial R} + \frac{u_\phi}{R} - \frac{1}{R}\frac{\partial u_R}{\partial\phi} \tag{1.3.40}$$

and likewise, the Lamb vector components transform into

$$\ell_R = u_\phi\frac{\partial u_R}{\partial\phi} - u_\phi\frac{\partial u_\phi}{\partial R} - u_\theta\frac{\partial u_\theta}{\partial R} - \frac{u_\phi^2 + u_\theta^2}{R} \tag{1.3.41}$$

$$\ell_\phi = u_R\frac{\partial u_\phi}{\partial R} - u_R\frac{\partial u_R}{\partial\phi} - \frac{u_\theta}{R}\frac{\partial u_\theta}{\partial\phi} + \frac{u_R u_\phi}{R} - \frac{u_\theta^2\cot\phi}{R} \tag{1.3.42}$$

$$\ell_\theta = u_R \frac{\partial u_\theta}{\partial R} + \frac{u_\phi}{R}\frac{\partial u_\theta}{\partial \phi} + \frac{u_R u_\theta}{R} + u_\phi u_\theta \frac{\cot\phi}{R} \tag{1.3.43}$$

where the axisymmetric Lamb vector before expansion is

$$\ell_R = \frac{u_\phi}{R}\left[\frac{\partial u_R}{\partial \phi} - \frac{\partial}{\partial R}\left(u_\phi R\right)\right] - \frac{u_\theta}{R\sin\phi}\frac{\partial}{\partial R}\left(u_\theta R \sin\phi\right) \tag{1.3.44}$$

$$\ell_\phi = \frac{u_R}{R}\left[\frac{\partial}{\partial R}\left(u_\phi R\right) - \frac{\partial u_R}{\partial \phi}\right] - \frac{u_\theta}{R\sin\phi}\frac{\partial}{\partial \phi}\left(u_\theta R \sin\phi\right) \tag{1.3.45}$$

$$\ell_\theta = \frac{u_R}{R\sin\phi}\frac{\partial}{\partial R}\left(u_\theta R \sin\phi\right) + \frac{u_\phi}{R^2\sin\phi}\frac{\partial}{\partial \phi}\left(u_\theta R \sin\phi\right) \tag{1.3.46}$$

Cylindrical polar coordinates for axisymmetric flows produces

$$\frac{1}{r}\frac{\partial\left(r u_r\right)}{\partial r} + \frac{\partial u_z}{\partial z} = 0 \quad \text{(continuity)} \tag{1.3.47}$$

$$u_r\frac{\partial u_r}{\partial r} + u_z\frac{\partial u_r}{\partial z} - \frac{u_\theta^2}{r} = -\frac{1}{\rho}\frac{\partial p}{\partial r} \quad \text{(radial)} \tag{1.3.48}$$

$$u_r\frac{\partial u_\theta}{\partial r} + u_z\frac{\partial u_\theta}{\partial z} + \frac{u_r u_\theta}{r} = 0 \quad \text{(azimuthal)} \tag{1.3.49}$$

$$u_r\frac{\partial u_z}{\partial r} + u_z\frac{\partial u_z}{\partial z} = -\frac{1}{\rho}\frac{\partial p}{\partial z} \quad \text{(axial)} \tag{1.3.50}$$

$$\boldsymbol{\omega} = -\frac{1}{r}\left(\frac{\partial r u_\theta}{\partial z}\right)\mathbf{e}_r - \left(\frac{\partial u_z}{\partial r} - \frac{\partial u_r}{\partial z}\right)\mathbf{e}_\theta + \frac{1}{r}\left(\frac{\partial r u_\theta}{\partial r}\right)\mathbf{e}_z \tag{1.3.51}$$

$$\omega_r = -\frac{1}{r}\left[\frac{\partial}{\partial z}\left(u_\theta r\right)\right] = -\frac{\partial u_\theta}{\partial z} \tag{1.3.52}$$

$$\omega_\theta = \frac{\partial u_r}{\partial z} - \frac{\partial u_z}{\partial r} \tag{1.3.53}$$

$$\omega_z = \frac{1}{r}\left[\frac{\partial}{\partial r}\left(u_\theta r\right)\right] = \frac{\partial u_\theta}{\partial r} + \frac{u_\theta}{r} \tag{1.3.54}$$

$$\begin{aligned}\boldsymbol{\ell} = &\left\{u_z\left(\frac{\partial u_r}{\partial z} - \frac{\partial u_z}{\partial r}\right) - \frac{u_\theta}{r}\left[\frac{\partial}{\partial r}\left(u_\theta r\right)\right]\right\}\mathbf{e}_r \\ &+ \left\{\left[\frac{\partial}{\partial z}\left(u_\theta r\right)\right] + \frac{u_r}{r}\left[\frac{\partial}{\partial r}\left(u_\theta r\right)\right]\right\}\mathbf{e}_\theta \\ &+ \left\{u_r\left(\frac{\partial u_z}{\partial r} - \frac{\partial u_r}{\partial z}\right) - \frac{u_\theta}{r}\left[\frac{\partial}{\partial z}\left(u_\theta r\right)\right]\right\}\mathbf{e}_z\end{aligned} \tag{1.3.55}$$

$$\ell_r = u_z\left(\frac{\partial u_r}{\partial z} - \frac{\partial u_z}{\partial r}\right) - \frac{u_\theta}{r}\left[\frac{\partial}{\partial r}\left(u_\theta r\right)\right] \tag{1.3.56}$$

$$\ell_\theta = \frac{u_z}{r}\left[\frac{\partial}{\partial z}\left(u_\theta r\right)\right] + \frac{u_r}{r}\left[\frac{\partial}{\partial r}\left(u_\theta r\right)\right] \tag{1.3.57}$$

$$\ell_z = u_r\left(\frac{\partial u_z}{\partial r} - \frac{\partial u_r}{\partial z}\right) - \frac{u_\theta}{r}\left[\frac{\partial}{\partial z}\left(u_\theta r\right)\right] \tag{1.3.58}$$

Expansion gives

$$\begin{aligned}\boldsymbol{\ell} = &\left(u_z\frac{\partial u_r}{\partial z} - u_z\frac{\partial u_z}{\partial r} - u_\theta\frac{\partial u_\theta}{\partial r} + \frac{u_\theta^2}{r}\right)\mathbf{e}_r \\ &+ \left(u_r\frac{\partial u_\theta}{\partial r} + \frac{u_r u_\theta}{r} + u_z\frac{\partial u_\theta}{\partial z}\right)\mathbf{e}_\theta \\ &+ \left(u_r\frac{\partial u_z}{\partial r} - u_\theta\frac{\partial u_\theta}{\partial z} - u_r\frac{\partial u_r}{\partial z}\right)\mathbf{e}_z\end{aligned} \tag{1.3.59}$$

$$\ell_r = u_z\frac{\partial u_r}{\partial z} - u_z\frac{\partial u_z}{\partial r} - u_\theta\frac{\partial u_\theta}{\partial r} + \frac{u_\theta^2}{r} \tag{1.3.60}$$

$$\ell_\theta = u_r\frac{\partial u_\theta}{\partial r} + \frac{u_r u_\theta}{r} + u_z\frac{\partial u_\theta}{\partial z} \tag{1.3.61}$$

$$\ell_z = u_r \frac{\partial u_z}{\partial r} - u_\theta \frac{\partial u_\theta}{\partial z} - u_r \frac{\partial u_r}{\partial z} \tag{1.3.62}$$

1.4 Introduction to the Bragg-Hawthorne Equation

The Bragg-Hawthorne, Long-Squire or Squire-Long equation appears as a non-linear elliptical partial differential equation in terms of the stream function under steady axisymmetric flow conditions, spherical polar coordinates, as noted by Saffman (1992), Susan-Resiga et al (2005b; 2005a; 2006), and Cervantes and Gustavsson (2007). The origin of the equation is generally credited to S. L. Bragg and W. R. Hawthorne (Saffman 1992) in their paper in the Journal of Aerospace Science entitled "Some Exact Solutions of the Flow through Annular Cascade Actuator Discs" which appeared in 1950. However, the equation also appears separately in R. R. Long's paper titled "Steady Motion around a Symmetrical Obstacle Moving along the Axis of a Rotating Liquid," which was published June of 1953 in the Journal of Meteorology and in H. B. Squire's "Rotating Fluids" article found in *Surveys in Mechanics* edited by Batchelor and Davies in 1956. Thus, the equation is commonly referred to the Bragg-Hawthorne equation (Horlock 1978; Saffman 1992), Long-Squire equation, or Squire-Long equation (Saffman 1992; Rusak 1996, 1998; Rusak et al. 1998). Thus, as a side note, the equation throughout this thesis is referred to as the Bragg-Hawthorne equation abbreviated BHE.

However, the BHE has actually appeared and been derived before these authors' scientific articles. As noted by many (Gol'dshtik and Shtern 1990; Gol'dshtik and Hussain 1998; Shtern and Hussain 1999; Shtern et al. 2000; Susan-Resiga et al. 2005b,a, 2006) one of the earliest discovered publications to formulate the BHE dates back to Meissel in the year 1873 in his paper entitled "Uber den Ausfluss der Wasser aus Gefässen in zwei besonderen Fällen nach Eintritt des Beharrungszustandes" or roughly translated as "Two Special Cases of the Steady State Flow of Water from Vessels." Meissel derives the BHE in cylindrical coordinates, and in his terminology it appears as

$$\varphi(u)\varphi'(u) + \frac{\partial^2 u}{\partial x^2} + \frac{\partial^2 u}{\partial r^2} - \frac{1}{r}\frac{\partial u}{\partial r} = r^2 f'(u) \tag{1.4.1}$$

In the scientific community, especially in the past when the world was less connected than it is today, it is often the case that equations and analyses were published more than once without either author or authors aware of the others' work Lakhtakia (1994). Just very recently, the author stumbled across another name for the exact equation which has been termed the BHE! In the 20th century the had been unofficially split into what most would consider a West and East division. The Americas had close ties with Europe due to previous colonization which can be grouped as the West while the East compromised of areas such as Russian, China, Japan, India, etc. Thus, only recently has the "barrier" come down, especially in the "Information Age" of the internet and now "social media." Many "lost" papers and schools of thought are surfacing. Notably, in the fluid dynamics community and from a Western point of view, Russian texts are emerging with exceptional and surprising results. Thus, we have what many Russian and Russian influenced schools of thought call the English or Western version of the BHE, the Gromeka-Beltrami equation Gledzer and Makarov (1990).

Even so, looking even further back to 1842, one of the most infamous forefathers of fluid dynamics, George Gabriel Stokes derives an equation describing the steady, incompressible symmetrical motion about an axes where the motion exist in planes passing through the axis. In other words, Stokes describes what is now simple called axisymmetrical motion. The equation arises in the form of Stokes notation as

$$\frac{1}{r^2}\left(\frac{\partial^2 U}{\partial z^2} + \frac{\partial^2 U}{\partial r^2} - \frac{1}{r}\frac{\partial U}{\partial r}\right) = \psi(U) \tag{1.4.2}$$

Not long after Meissel publishes his paper, Lamb (1877) in turn publishes his own paper, "On the Conditions for Steady Motion of a Fluid," in which he formulates the same equation as Stokes and Meissel for axisymmetric flow to be

$$\frac{\partial^2 \psi}{\partial r^2} - \frac{1}{r}\frac{\partial \psi}{\partial r} + \frac{\partial^2 \psi}{\partial z^2} = r^2 F(\psi) \tag{1.4.3}$$

However, before the axisymmetric case, Lamb defines the two-dimensional case surfaces as

$$\frac{\partial^2 \psi}{\partial x^2} + \frac{\partial^2 \psi}{\partial y^2} = F(\psi) \tag{1.4.4}$$

which he refers to Stokes as well. Stokes presents the equation as

$$\frac{\partial^2 U}{\partial x^2} + \frac{\partial^2 U}{\partial y^2} = \chi(U) \tag{1.4.5}$$

The two-dimensional equation sheds further light on the BHE as it shows the dependency of the equation of the Laplacian and Stokesian of the stream function equal to some global function. The Laplace and Stokes operator of the stream function are discussed further in upcoming sections. Lamb (1879) also displays the same equations in his original book, *A Treatise on the Mathematical Theory of the Motion of Fluids*, and later revised editions entitled *Hydrodynamics* (1975) with a slightly different notation as

$$\frac{\partial^2 \psi}{\partial x^2} + \frac{\partial^2 \psi}{\partial y^2} = f(\psi) \tag{1.4.6}$$

$$\frac{\partial^2 \psi}{\partial \varpi^2} - \frac{1}{\varpi}\frac{\partial \psi}{\partial \varpi} + \frac{\partial^2 \psi}{\partial x^2} = \varpi^2 f(\psi) \tag{1.4.7}$$

Interestingly, Lamb (1975) also transforms the two-dimensional case into cylindrical polar coordinates which appears as

$$\frac{\partial^2 \psi}{\partial \varpi^2} + \frac{1}{\varpi}\frac{\partial \psi}{\partial \varpi} + \frac{\partial^2 \psi}{\partial \theta^2} = f(\psi) \tag{1.4.8}$$

and explicitly cites the global function as an example to be $f(\psi) = -k^2\psi$, which transforms into the Helmholtz equation

$$\frac{\partial^2 \psi}{\partial \varpi^2} + \frac{1}{\varpi}\frac{\partial \psi}{\partial \varpi} + \frac{\partial^2 \psi}{\partial \theta^2} + k^2\psi = 0 \tag{1.4.9}$$

It is additionally noted that Lamb discusses the vorticity and its relation to the stream function displayed as

$$-\left(\frac{\partial^2\psi}{\partial\varpi^2}-\frac{1}{\varpi}\frac{\partial\psi}{\partial\varpi}+\frac{\partial^2\psi}{\partial x^2}\right)\frac{1}{\varpi}=\omega \tag{1.4.10}$$

and

$$-\left(\frac{\partial^2\psi}{\partial r^2}-\frac{1}{r}\frac{\partial\psi}{\partial r}+\frac{\partial^2\psi}{\partial z^2}\right)\frac{1}{r}=\omega \tag{1.4.11}$$

which has importance and relevance that becomes more apparent in following sections. Thus, several possible forms of the stream function equations materialize which are later discussed with their involvement in the BHE.

It is interesting that in 1884 Hicks studied the motions of a steady hollow vortex and corresponding vibrations in which he solved the irrotational equation of motion. The stream function equation turns out to be

$$\frac{\partial^2\psi}{\partial z^2}+\frac{\partial^2\psi}{\partial\rho^2}-\frac{1}{\rho}\frac{\partial\psi}{\partial\rho}=0 \tag{1.4.12}$$

However, Hicks solves the irrotational equation by transformation of the variables into a complex set. The author of this dissertation points out this occurrence because the question that needs to be asked is "how is all of this related?"

The next visible occurrence appears in a paper by Hicks (1885) when he studies the motions of vortex rings. Since the analysis is rotational, the BHE originates in the form of the angular rotation, ω, in the terms of

$$\frac{\partial^2\psi}{\partial z^2}+\frac{\partial^2\psi}{\partial\rho^2}-\frac{1}{\rho}\frac{\partial\psi}{\partial\rho}=2\omega\rho \tag{1.4.13}$$

The angular rotation is related to the vorticity, γ, by $2\omega=\gamma$ and $2\omega/\rho=f(\psi)$.

$$\frac{\partial^2\psi}{\partial z^2}+\frac{\partial^2\psi}{\partial\rho^2}-\frac{1}{\rho}\frac{\partial\psi}{\partial\rho}=\rho^2 f(\psi) \tag{1.4.14}$$

Hicks then limits the case of study to constant vorticity where $f(\psi) = A$. This is the first time the BHE is solved for a specific flow as the previous articles only formulated the equation of motion. Thus, the equation reduces to a very solvable case of

$$\frac{\partial^2 \psi}{\partial z^2} + \frac{\partial^2 \psi}{\partial \rho^2} - \frac{1}{\rho}\frac{\partial \psi}{\partial \rho} = \rho^2 A \tag{1.4.15}$$

where the equation can be solved for a homogeneous separable solution and a particular solution.

In 1894 Hill produces his famous paper on a spherical vortex. He too utilizes the stream function equation or as it was called then, the current function. In Hill's case the form of the BHE emerges as

$$\frac{\partial^2 \psi}{\partial z^2} + \frac{\partial^2 \psi}{\partial r^2} - \frac{1}{r}\frac{\partial \psi}{\partial r} = r^2\left(\frac{8k}{a^2} + \frac{2k}{c^2}\right) \tag{1.4.16}$$

where $f(\psi) = \left(8k/a^2 + 2k/c^2\right)$ and k, c, and a.

Another utilization of the BHE comes from the deemed Taylor-Culick (TC) flow. The TC flow cites back to G. I. Taylor's 1956 paper entitled "Fluid Flow in Regions Bounded by Porous Surfaces" which appears in the *Proceedings of the Royal Society of London, A* and F. E. Culick's 1966 article named "Rotational Axisymmetric Mean Flow and Damping of Acoustic Waves in a Solid Propellant Rocket" and logged in the *AIAA Journal*. The TC flow models incompressible, inviscid, rotational flow of injection (sometimes called blowing in the literature) or suction at the walls of a 2D Cartesian channel (or a parallel plate configuration) and the quasi-3D case, an axisymmetric tube. Additional modeling cases include an injection "headwall," where the traditional TC flow remains inert.

1.5 The Formulation of the BHE in a Conical Geometry Utilizing Spherical Polar Coordinates

The formulation of the BHE can be done in one of two ways. Since this studied is intricately linked to that of Bloor and Ingham (1987), the first method follows the formulation by Bloor and Ingham (1987). First, the formulation begins with the Beltrami-Gromeka-Lamb vector form of the momentum equation

$$\nabla\left(\frac{p}{\rho}+\frac{u^2}{2}\right)-\mathbf{u}\times\boldsymbol{\omega}=\nabla H+\boldsymbol{\ell}=0 \tag{1.5.1}$$

Bloor and Ingham (1987) assume that the momentum is conserved along a streamline so that

$$\nabla\left(\frac{p}{\rho}+\frac{u^2}{2}\right)\cdot\mathrm{d}\mathbf{s}-\mathbf{u}\times\boldsymbol{\omega}\cdot\mathrm{d}\mathbf{s}=\nabla H\cdot\mathrm{d}\mathbf{s}+\boldsymbol{\ell}\cdot\mathrm{d}\mathbf{s}=0 \tag{1.5.2}$$

$$\mathrm{d}\left(\frac{p}{\rho}+\frac{u^2}{2}\right)-\mathbf{u}\times\boldsymbol{\omega}\cdot\mathrm{d}\mathbf{s}=\mathrm{d}H+\boldsymbol{\ell}\cdot\mathrm{d}\mathbf{s}=0 \tag{1.5.3}$$

Integrated, the first term produces the Bernoulli equation

$$\frac{p}{\rho}+\frac{u^2}{2}=H(\psi) \tag{1.5.4}$$

The second term produces a vector parallel to the streamline for both irrotational $\boldsymbol{\omega}=\nabla\times\mathbf{u}=0$ and rotational flows

$$\mathbf{u}\times\boldsymbol{\omega}\cdot\mathrm{d}\mathbf{s}=\mathbf{u}\times(\nabla\times\mathbf{u})\cdot\mathrm{d}\mathbf{s}=\boldsymbol{\ell}\cdot\mathrm{d}\mathbf{s}=0 \tag{1.5.5}$$

Examining the tangential component only the scalar equation emerges as

$$\frac{1}{R\sin\phi}\frac{\partial}{\partial\theta}\left(\frac{p}{\rho}+\frac{1}{2}u^2\right)+\ell_\theta=0 \tag{1.5.6}$$

where

$$\nabla\left(\frac{p}{\rho}+\frac{1}{2}u^2\right)=\left[\frac{\partial}{\partial R}\mathbf{e}_R+\frac{1}{R}\frac{\partial}{\partial\phi}\mathbf{e}_\phi+\frac{1}{R\sin\phi}\frac{\partial}{\partial\theta}\mathbf{e}_\theta\right]\left(\frac{p}{\rho}+\frac{1}{2}u^2\right) \tag{1.5.7}$$

Axisymmetric conditions enforce $\dfrac{\partial}{\partial\theta}=0$ so only the Lamb vector component remains (see Wu et al. (2006) pg. 256 for vorticity transport components)

$$\ell_\theta = 0 \tag{1.5.8}$$

Expanding the Lamb component gives

$$\ell_\theta = \frac{u_R}{R\sin\phi}\frac{\partial}{\partial R}\left(u_\theta R\sin\phi\right)+\frac{u_\phi}{R^2\sin\phi}\frac{\partial}{\partial\phi}\left(u_\theta R\sin\phi\right)=0 \tag{1.5.9}$$

which then simplifies to

$$u_R\frac{\partial}{\partial R}\left(u_\theta R\sin\phi\right)+\frac{u_\phi}{R}\frac{\partial}{\partial\phi}\left(u_\theta R\sin\phi\right)=0 \tag{1.5.10}$$

Next, arranging the equation into the form of

$$\left(u_R\frac{\partial}{\partial R}+\frac{u_\phi}{R}\frac{\partial}{\partial\phi}\right)\left(u_\theta R\sin\phi\right)=0 \tag{1.5.11}$$

This allows the equation to be condensed into what is known as the material derivative

$$\frac{\mathrm{D}}{\mathrm{D}t}=\frac{\partial}{\partial t}+u_R\frac{\partial}{\partial R}+\frac{u_\phi}{R}\frac{\partial}{\partial\phi} \tag{1.5.12}$$

The problem formulates steady conditions so that

$$\frac{\partial}{\partial t}=0 \tag{1.5.13}$$

and

$$\frac{\mathrm{D}}{\mathrm{D}t}=u_R\frac{\partial}{\partial R}+\frac{u_\phi}{R}\frac{\partial}{\partial\phi} \tag{1.5.14}$$

After integration, the product consists of the swirl momentum as a function along the streamline

$$u_\theta R \sin\phi = B(\psi) \tag{1.5.15}$$

Rearranging yields a formulation for the swirl velocity

$$u_\theta = \frac{B(\psi)}{R \sin\phi} \tag{1.5.16}$$

Next, the tangential momentum is substituted into the spherical radial vorticity equation to obtain

$$\omega_R = \frac{1}{R^2 \sin\phi} \frac{\partial B}{\partial \phi} \tag{1.5.17}$$

The circulation function can be split in the partial derivative since it is a function of the stream function, ψ, to produce

$$\omega_R = \frac{1}{R^2 \sin\phi} \frac{\partial \psi}{\partial \phi} \frac{\mathrm{d}B}{\mathrm{d}\psi} \tag{1.5.18}$$

Next, the momentum equation in the zenith angle direction, ϕ, is examined

$$\frac{1}{R} \frac{\partial}{\partial \phi} \left(\frac{p}{\rho} + \frac{1}{2} u^2 \right) + \ell_\phi = 0 \tag{1.5.19}$$

$$\frac{1}{R} \frac{\partial H}{\partial \phi} + u_R \omega_\theta - u_\theta \omega_R = 0 \tag{1.5.20}$$

where the Bernoulli function derivative can be separated as well similar to the circulation function to yield

$$\frac{1}{R} \frac{\partial \psi}{\partial \phi} \frac{\mathrm{d}H}{\mathrm{d}\psi} + u_R \omega_\theta - u_\theta \omega_R = 0 \tag{1.5.21}$$

Recalling and substituting ω_R, from Eq. (1.5.18), u_θ from Eq. (1.5.16), and u_R from the velocity-stream function relation, Eq. (1.5.23), into Eq. (1.5.21) results in

$$\frac{1}{R}\frac{\partial\psi}{\partial\phi}\frac{\mathrm{d}H}{\mathrm{d}\psi}+\frac{1}{R^2\sin\phi}\frac{\partial\psi}{\partial\phi}\omega_\theta-\frac{B(\psi)}{R\sin\phi}\left(\frac{1}{R^2\sin\phi}\frac{\partial\psi}{\partial\phi}\frac{\mathrm{d}B}{\mathrm{d}\psi}\right)=0 \tag{1.5.22}$$

where the velocity-stream function relation is

$$u_R=\frac{1}{R^2\sin\phi}\frac{\partial\psi}{\partial\phi};\quad u_\phi=-\frac{1}{R\sin\phi}\frac{\partial\psi}{\partial R} \tag{1.5.23}$$

Eliminating $\frac{1}{R}$ and $\frac{\partial\psi}{\partial\phi}$ reduces Eq. (1.5.22)

$$\frac{\mathrm{d}H}{\mathrm{d}\psi}+\frac{1}{R\sin\phi}\omega_\theta-\frac{B(\psi)}{R\sin\phi}\left(\frac{1}{R\sin\phi}\frac{\mathrm{d}B}{\mathrm{d}\psi}\right)=0 \tag{1.5.24}$$

Rearranging gives a form of the tangential vorticity as

$$\frac{\omega_\theta}{R\sin\phi}=\frac{B(\psi)}{R^2\sin^2\phi}\frac{\mathrm{d}B}{\mathrm{d}\psi}-\frac{\mathrm{d}H}{\mathrm{d}\psi} \tag{1.5.25}$$

One of the last steps before revealing the BHE is to substitute Eq. (1.3.40) into Eq. (1.5.25) to produce

$$\frac{1}{R^2\sin\phi}\left[\frac{\partial}{\partial R}\left(Ru_\phi\right)-\frac{\partial u_R}{\partial\phi}\right]=\frac{B(\psi)}{R^2\sin^2\phi}\frac{\mathrm{d}B}{\mathrm{d}\psi}-\frac{\mathrm{d}H}{\mathrm{d}\psi} \tag{1.5.26}$$

Next, the velocity-stream function relation is utilized again to collect the equation into a form of the stream function only as

$$\frac{1}{R^2\sin\phi}\left[\frac{\partial}{\partial R}\left(-\frac{1}{\sin\phi}\frac{\partial\psi}{\partial R}\right)-\frac{\partial}{\partial\phi}\left(\frac{1}{R^2\sin\phi}\frac{\partial\psi}{\partial\phi}\right)\right]=\frac{B(\psi)}{R^2\sin^2\phi}\frac{\mathrm{d}B}{\mathrm{d}\psi}-\frac{\mathrm{d}H}{\mathrm{d}\psi} \tag{1.5.27}$$

Divide through by $\frac{1}{R^2\sin\phi}$

$$\frac{\partial}{\partial R}\left(-\frac{1}{\sin\phi}\frac{\partial\psi}{\partial R}\right)-\frac{\partial}{\partial\phi}\left(\frac{1}{R^2\sin\phi}\frac{\partial\psi}{\partial\phi}\right)=\frac{B(\psi)}{\sin\phi}\frac{\mathrm{d}B}{\mathrm{d}\psi}-R^2\sin\phi\frac{\mathrm{d}H}{\mathrm{d}\psi} \tag{1.5.28}$$

Finally, divide through by $-\dfrac{1}{\sin\phi}$ and bring the $\dfrac{1}{R^2}$ out of the ϕ partial derivative to obtain the final form of the BHE in spherical coordinates as

$$\frac{\partial^2\psi}{\partial R^2} + \frac{\sin\phi}{R^2}\frac{\partial}{\partial\phi}\left(\frac{1}{\sin\phi}\frac{\partial\psi}{\partial\phi}\right) = R^2\sin^2\phi\frac{\mathrm{d}H}{\mathrm{d}\psi} - B\frac{\mathrm{d}B}{\mathrm{d}\psi} \tag{1.5.29}$$

1.6 Cyclone Separators

The motion in the conical BDV closely models the fluid dynamics within cyclone separators. The cyclone separator has been around for over two hundred years. An important device for the processing industry for separating solids from gases, liquids from gases, and solids from liquids, the first issued patent for a cyclone device occurred in 1885 by the United States to John M. Finch of the Knickerbocker Company according to Hoffmann and Stein (2008). Finch's invention takes advantage of the centripetal force acting on dust particles in a moving air stream. As noted by Hoffmann and Stein, Finch's outside the box thinking goes against the grain during that time as most thought the best method to separate dust from air was to leave the air stagnate and let gravity separate the gas-solid mixture. For a 10-micron dust particle diameter to become quiescence at a distance of 1 meter in a medium of air takes about 5 1/2 minutes. Finch's device consisted of a cylindrical chamber where "dust-laden" air was injected tangentially to impart angular momentum. The dust collects into a thin layer on the casing of the chamber where a strategically placed slot diverts the dust layer into another chamber. The air outside the dust layer continues through the device exiting much cleaner.

Advancing into and through the early 1900's, the cyclone separator evolved into models similar to more modern designs. Most of today's cyclone separators consist of a cylinder fitted to a cone where the cylinder is located above the cone. In 1905 O. M. Morse develops a dust collector for flour mills in order to abate deadly explosions from fine particulates. Hoffmann and Stein (2008) mention cyclone separator benefits which accelerated design improvements through the 1920's. Some of these benefits include that cyclone separators are easy and cheap to construct, compact, and contain little to no moving parts.

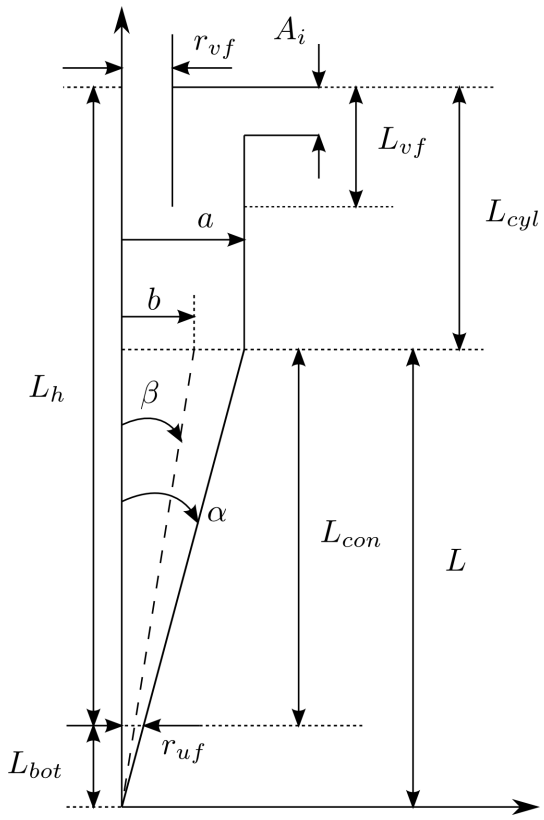

Figure 1.1: General dimensions of a cylindrical-conical cyclone separator.

Modern cyclone separators generally consist of a tangential inlet attached to a cylindrical chamber. The cylindrical chamber is contiguous to a conical chamber, which lies below the cylindrical section. Two outlets, one at the top and one at the bottom, allow particles to be separated according to density by the swirling motion generated by the cyclone separator. Figure 1.1 and Table 1.1 display a schematic and labels dimensions of a generic cyclone separator.

Table 1.1: Labels for general cylinder-cone cyclone separator

Label	Dimension
a	Conical maximum radius and cylindrical radius
b_z	axial velocity mantle radius $u_z\,(r = b_{ax}, z = b_z \cot\beta_z\,) = 0$
b_R	spherical radial velocity mantle radius $u_R\,(r = b_{sr}, z = b_R \cot\beta_R\,) = 0$
A_i	Area of inlet (circular or rectangular; r_i, $l \times w$)
α	Angle of cone
β_z	Angle of mantle (axial velocity) $u_z\,(\phi = \beta_z\,) = 0$
β_R	Angle of mantle (spherical radial velocity) $u_R\,(\phi = \beta_R\,) = 0$
L	Length of cone (to apex)
L_{con}	Length of cone (to underflow radius)
L_{cyl}	Length of cylinder
L_{vf}	Length of vortex finder (inside cyclone chamber)
L_h	Length of cyclone (from chamber top to underflow radius)
L_{bot}	Length from conical underflow radius to cone apex
r_{vf}	Radius of vortex finder
r_{uf}	Radius of conical underflow

Chapter 2

The Beltramian Conical Bidirectional Vortex (BDV): Analysis

2.1 Introduction

For a bidirectional flow in a conical geometry, an approach similar to Bloor and Ingham (1987) prescribes that the Bernoulli function remains constant w.r.t. the stream function, $H(\psi) = h(\psi) =$ constant; $\mathrm{d}H/\mathrm{d}\psi = n(\psi) = 0$, and that the swirl or circulation function (angular momentum) varies w.r.t. the stream function, $B = s(\psi)$; $\mathrm{d}B/\mathrm{d}\psi = q(\psi)$. The governing equation for the Beltramian model of the BDV in a cone is the inviscid, incompressible BHE in spherical coordinates derived in Section 1.5 from Eq. (1.5.29) shown as

$$\frac{\partial^2\psi}{\partial R^2} + \frac{\sin\phi}{R^2}\frac{\partial}{\partial\phi}\left(\frac{1}{\sin\phi}\frac{\partial\psi}{\partial\phi}\right) = R^2\sin^2\phi\frac{\mathrm{d}H}{\mathrm{d}\psi} - B\frac{\mathrm{d}B}{\mathrm{d}\psi} \tag{2.1.1}$$

2.2 Coordinate System & Geometry

The nomenclature of the spherical polar coordinate system (see Figure 2.1) lists as corresponding to the radial, latitudinal (colatitutde) or zenith direction, and tangential

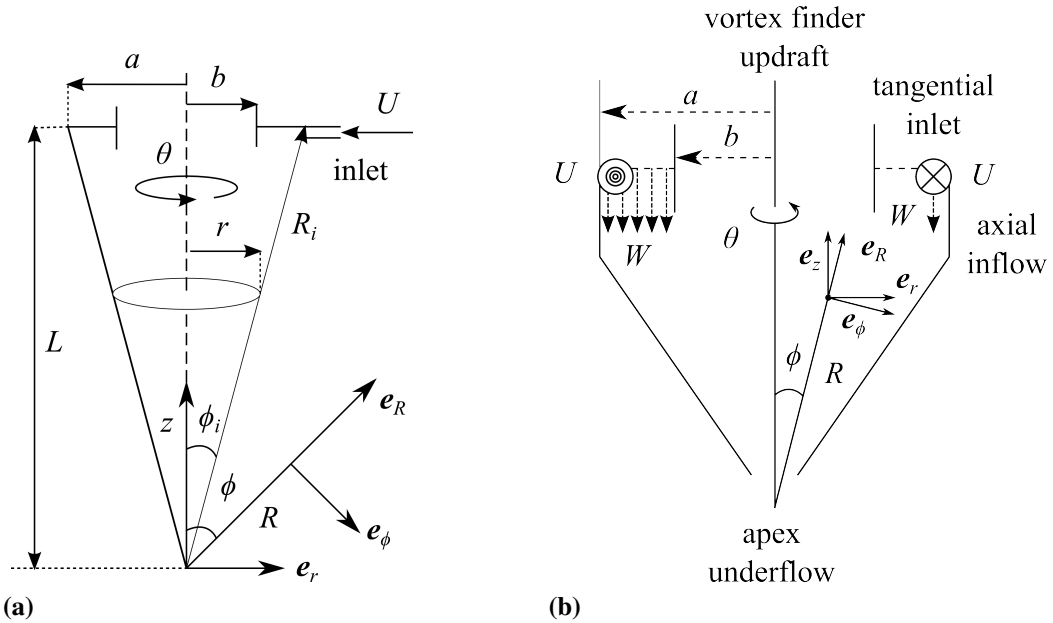

Figure 2.1: Diagrams of geometry and inlet conditions.

or azimuth directions. The dimensions of the structure dictate that the cone contains a divergence half-angle α with a length of L measured from the apex of the cone to its top. Table 2.1 displays the calculated length per conical half-angle for every five degrees beginning at $\alpha = 5°$. The maximum radius occurs the axial location of L and is denoted as a while the exit radius is b, at the same axial height. The length of the cone and maximum radius are linked by the divergence angle alpha, $\tan\alpha = a/L$.

2.3 Boundary Conditions

Due to the axisymmetric conditions enforced in the tangential direction, two boundary layers emerge for the conical geometry. The first ensures that the stream function, $\psi(R, \phi)$, at the centerline equals zero while the second applies the same condition at the sidewall, $\phi = \alpha$.

Table 2.1: Length of cone per α with $a = 1$.

α	$L = a\cot\alpha$	α	$L = a\cot\alpha$
5°	11.43	50°	0.893
10°	5.67	55°	0.700
15°	3.73	60°	0.577
20°	2.75	65°	0.466
25°	2.14	70°	0.364
30°	1.73	75°	0.268
35°	1.43	80°	0.176
40°	1.19	85°	0.088
45°	1.00	90°	0.000

$$\psi(R, 0) = 0 \tag{2.3.1}$$

$$\psi(R, \alpha) = 0 \tag{2.3.2}$$

The volumetric flow rate into the side of the cone equals the average tangential velocity, U, times the inlet area (see Figure 2.1a).

$$Q_i = u_\theta(R_i, \phi_i) = UA_i \tag{2.3.3}$$

At the same location (R_i, ϕ_i), the spherical radius and latitudinal angle can be expressed as

$$\phi_i = \alpha = \tan^{-1}(a/L); \quad R_i = \sqrt{L^2 + a^2} \tag{2.3.4}$$

Only the incoming tangential flow creates the mass addition into the outer annular cone region of the outer vortex. The axial velocity is created instantaneously as the fluid enters the cyclone since it is assumed in an actual cyclone a cylindrical portion generally attaches to the top of the cone and the velocity at this point has an axial component. The next

section, Section 2.4, reveals the relation between the tangential, U, and axial, W, boundary velocity components and the importance of that relation.

2.4 Inlet Conditions

The boundary condition at the cyclone inlet establishes a tangential flow which simultaneously develops an axial component and begins a descent towards the bottom of the cone. Physically, an axial velocity exist at this location in a true cyclone separator since in most cases a cylindrical portion connects above the conical portion. However, if for theoretical purposes the cylindrical portion does not exist, the axial velocity is either injected at this point similar to endwall injection conditions by Akiki and Majdalani (2010); Akiki (2011); Akiki and Majdalani (2012) or, as stated above, an axial velocity component is assumed to also exist at this location as a boundary condition for this analysis. An average axial velocity of W enters between the inner and outer radius, $b \geq r \geq a$, where b defines the outlet radius at the top of the cone. In this case the inlet axial velocity takes the uniform profile (see Figure 2.1b)

$$u_z(R_i, \phi_i = \alpha) = u_z(r_i, z_i) = u_z(a, L) = -W \tag{2.4.1}$$

The axisymmetric stream function relations in cylindrical polar coordinates and velocity components are

$$u_r = -\frac{1}{r}\frac{\partial \psi}{\partial z}; \quad u_z = \frac{1}{r}\frac{\partial \psi}{\partial r} \tag{2.4.2}$$

Likewise, the stream function-velocity relation for spherical polar coordinates from Eq. (1.5.23) is

$$u_R = \frac{1}{R^2 \sin\phi}\frac{\partial \psi}{\partial \phi}; \quad u_\phi = -\frac{1}{R \sin\phi}\frac{\partial \psi}{\partial R}$$

To find the stream function at the inlet we can set

$$u_z = -W = \frac{1}{r}\frac{\partial \psi}{\partial r} \tag{2.4.3}$$

Next, we separate variables

$$-Wr\mathrm{d}r = \mathrm{d}\psi \tag{2.4.4}$$

then integrate

$$-\int Wr\mathrm{d}r = \int \mathrm{d}\psi \tag{2.4.5}$$

which leaves us with

$$-\tfrac{1}{2}Wr^2 = \psi + \psi_0 \tag{2.4.6}$$

To find the constant the BC $\psi(R, \alpha) = \psi(a, L) = 0$

$$\psi_0 = -\tfrac{1}{2}Wa^2 \tag{2.4.7}$$

$$\psi = \tfrac{1}{2}W\left(a^2 - r^2\right) \tag{2.4.8}$$

which coincides with a stream function in spherical coordinates of the type

$$\psi = \tfrac{1}{2}W\left(a^2 - R^2\sin^2\phi\right) \tag{2.4.9}$$

and the derivative w.r.t. $(R\sin\phi)$

$$\frac{\mathrm{d}\psi}{\mathrm{d}(R\sin\phi)} = -WR\sin\phi \tag{2.4.10}$$

The tangential velocity injection at the inlet described by

$$u_\theta = (R_i, \phi_i = \alpha) = u_\theta = (r_i, z_i) = u_\theta = (a, L) = U \tag{2.4.11}$$

The volumetric flow rate relates to the stream function for axisymmetric flow by the integration over a surface of the velocity in the normal direction or in this case a line element in the r-direction which in this case turns out to be the axial velocity (hence, the stream function) difference between two points. For reference, see Happel and Brenner (1983) page 98, Bojarevičs et al. (1989) page 31, Graebel (2007) pages 8 and 9, Hoffmann and Stein (2008) page 73, and Pozrikidis (2011) on page 157.

$$Q_i = \int_S \mathbf{u} \cdot \mathbf{n} \, \mathrm{d}S = 2\pi \int_a^b \mathbf{u} \cdot \mathbf{n} r \, \mathrm{d}r = 2\pi \int_a^b u_z r \, \mathrm{d}r \tag{2.4.12}$$

$$Q_i = 2\pi \int_a^b \mathrm{d}\psi = 2\pi \left[\psi(a) - \psi(b)\right] = \pi W \left(a^2 - b^2\right) \tag{2.4.13}$$

Thus, the tangential and axial velocities relate by

(2.4.14)

which then produces

$$W = \frac{UA_i}{\pi \left(a^2 - b^2\right)} \tag{2.4.15}$$

where the term A_i is an arbitrary inlet area. Equation 2.4.15 later becomes a swirl parameter (see Section 2.10).

2.5 Relations for the Bernoulli & Circulation Functions

In order to determine the values of $B(\psi)$ and $H(\psi)$, the inlet conditions are again examined. Previously, it was shown that the circulation function is simply the angular momentum of the incoming fluid. Since the tangential velocity at the inlet is equal to the average velocity, the circulation function becomes

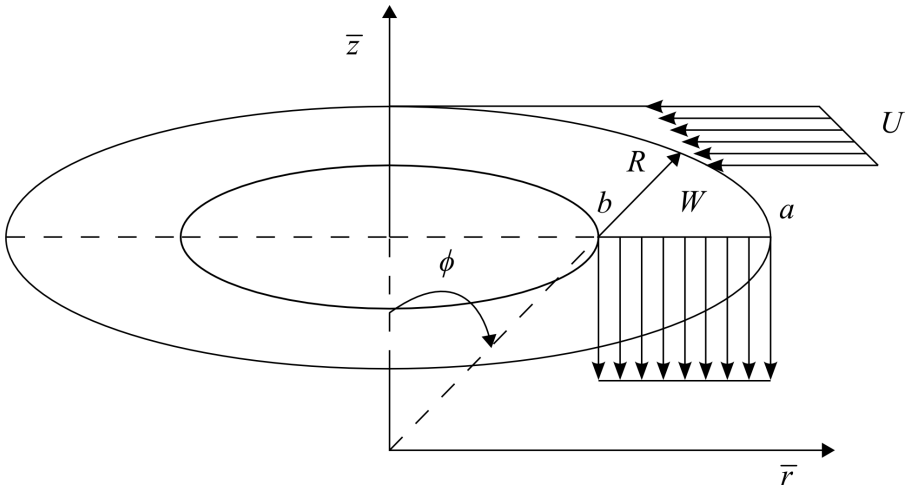

Figure 2.2: Inlet axial velocity.

$$B(\psi) = UR\sin\phi \tag{2.5.1}$$

where B is defined as remaining constant along a streamline. Also, the tangential velocity profile exists as a uniform injection at the inlet between $b \geq r \geq a$. Next, the equation is differentiated w.r.t. $R\sin\phi$ to find that

$$\frac{\mathrm{d}B}{\mathrm{d}\left(R\sin\phi\right)} = U \tag{2.5.2}$$

Thus, combining both the circulation function and its derivative divided by Eq. (2.4.10) we obtain

$$B\frac{\mathrm{d}B}{\mathrm{d}\psi} = \frac{UR\sin\phi}{-WR\sin\phi}U = -\frac{U^2}{W} = \text{constant} \tag{2.5.3}$$

As is shown later, this relation permits the tangential velocity to vary with the stream function throughout the cone. As with the case of Bloor and Ingham (1987), the entry cylindrical polar radial velocity is chosen so that the Bernoulli function remains a constant while its derivative is zero so that

$$H = \tfrac{1}{2}\left[u_r^2\left(R_i,\phi_i\right) + U^2 + W^2\right] + p_0/\rho = \text{constant} \quad \text{or} \quad \frac{\mathrm{d}H}{\mathrm{d}\psi} = 0 \tag{2.5.4}$$

Finally, inserting the values for 2.5.3 and 2.5.4 into the BHE to obtain

$$\frac{\partial^2\psi}{\partial R^2} + \frac{\sin\phi}{R^2}\frac{\partial}{\partial\phi}\left(\frac{1}{\sin\phi}\frac{\partial\psi}{\partial\phi}\right) = \frac{U^2}{W} \tag{2.5.5}$$

2.6 Stream Function Solution

The solution of the stream variables starts with a semi-separation of variables approach. The first separation function, by inspection, comes out to be $F(R) = R^2$ so that the stream function now represents

$$\psi(R,\phi) = R^2 G(\phi) \tag{2.6.1}$$

Now, substitution of Eq. (2.6.1) into the BHE (Eq. (2.5.5)) produces the equation

$$2G + \sin\phi\frac{\mathrm{d}}{\mathrm{d}\phi}\left(\frac{1}{\sin\phi}\frac{\mathrm{d}G}{\mathrm{d}\phi}\right) = \frac{U^2}{W} \tag{2.6.2}$$

or expanded

$$G'' - \frac{\cos\phi}{\sin\phi}G' + 2G = \frac{U^2}{W} \tag{2.6.3}$$

and

$$G'' - \cot\phi G' + 2G = \frac{U^2}{W} \tag{2.6.4}$$

This ODE is of second order and non-homogeneous so two complementary solutions to the homogeneous equation are needed along with the particular solution to satisfy the non-homogeneity. The first solution to satisfy the homogeneous equation is

$$G_1 = K_1 \sin^2\phi \tag{2.6.5}$$

and can be checked through inspection by simply inserting $\sin^2\phi$ into either Eq. (2.6.2) or Eq. (2.6.4). As an Ansatz, the second solution is sought of the form

$$G_2 = K_2\, g\,(\phi) \sin^2\phi \tag{2.6.6}$$

which is deduced from the first solution when it is known for an ODE with variable coefficients. Now this form may be substituted into either Eq. (2.6.2) or Eq. (2.6.4) to arrive at

$$g = \int \frac{1}{\sin^3\phi} \mathrm{d}\phi = \int \csc^3\phi \; \mathrm{d}\phi \tag{2.6.7}$$

In order to solve for g, the integral may be solved by the method of integration by parts. First, we designate our variables as

$$\mathrm{d}v = \csc^2\phi \; \mathrm{d}\phi \tag{2.6.8}$$

$$u = \csc\phi \tag{2.6.9}$$

$$v = -\cot\phi \tag{2.6.10}$$

$$\mathrm{d}u = -\csc\phi\cot\phi \; \mathrm{d}\phi \tag{2.6.11}$$

The formula for integration by parts is

$$uv - \int v\mathrm{d}u \tag{2.6.12}$$

Substituting in the correct values gives

$$-\csc\phi\cot\phi - \int \csc\phi\cot^2\phi \; \mathrm{d}\phi \tag{2.6.13}$$

Using the trigonometric identity $\cot^2\phi = \csc^2\phi - 1$ transforms the relation to

$$-\csc\phi\cot\phi - \int \csc\phi\left(\csc^2\phi - 1\right)\mathrm{d}\phi \tag{2.6.14}$$

Multiplying through we obtain

$$-\csc\phi\cot\phi - \int \csc^3\phi - \csc\phi\ \mathrm{d}\phi \tag{2.6.15}$$

Separating the RHS integrals produces

$$-\csc\phi\cot\phi - \int \csc^3\phi\ \mathrm{d}\phi + \int \csc\phi\ \mathrm{d}\phi \tag{2.6.16}$$

Recall that this whole relation is equal to $\int \csc^3\phi\mathrm{d}\phi$ which yields

$$\int \csc^3\phi\mathrm{d}\phi = -\csc\phi\cot\phi - \int \csc^3\phi\ \mathrm{d}\phi + \int \csc\phi\ \mathrm{d}\phi \tag{2.6.17}$$

At first this seems counter-intuitive and does not seem to help. However, if the integrals of $\csc^3\phi$ are collected, then the equation becomes clearer as where to go next. So collecting the $\csc^3\phi$ integrals to the LHS, we obtain

$$2\int \csc^3\phi\mathrm{d}\phi = -\csc\phi\cot\phi + \int \csc\phi\ \mathrm{d}\phi \tag{2.6.18}$$

Then we can divide by two and evaluate the left hand side which gives us

$$\int \csc^3\phi\ \mathrm{d}\phi = \frac{1}{2}\left[-\csc\phi\cot\phi + \int \csc\phi\ \mathrm{d}\phi\right] \tag{2.6.19}$$

$$g(\phi) = \frac{1}{2}\left[-\csc\phi\cot\phi - \ln|\csc\phi + \cot\phi|\right] \tag{2.6.20}$$

or

$$g(\phi) = -\frac{1}{2}\left[\csc\phi\cot\phi + \ln|\csc\phi + \cot\phi|\right] \tag{2.6.21}$$

Thus, integration by parts yields

$$g(\phi) = -\frac{1}{2}\left[\csc\phi\cot\phi - \ln|\csc\phi - \cot\phi|\right] \tag{2.6.22}$$

Therefore the second complementary equation becomes

$$G_2 = K_2\left[\cos\phi - \left(\sin^2\phi\right)\ln\Phi\right] \tag{2.6.23}$$

where a $-1/2$ is absorbed into the constant, K_2, and where

$$\Phi = \tan\frac{\phi}{2} \tag{2.6.24}$$

The tangent of the half-angle can be shown as

$$\tan\frac{\phi}{2} = \frac{\sin\phi}{1+\cos\phi} = \frac{1-\cos\phi}{\sin\phi} \tag{2.6.25}$$

To verify the tangent half-angle and a few logarithmic and trigonometric relations, the definition for the tangent half-angle is plugged back into the logarithm. Through the properties of the logarithm and trigonometry, it can be shown that

$$\begin{aligned} -\ln\left(\tan\frac{\phi}{2}\right) &= -\ln\left(\frac{\sin\phi}{1+\cos\phi}\right) = \ln\left(\frac{1+\cos\phi}{\sin\phi}\right) \\ &= \ln\left(\frac{1}{\sin\phi} + \frac{\cos\phi}{\sin\phi}\right) = \ln(\csc\phi + \cot\phi) \end{aligned} \tag{2.6.26}$$

Finally, the tangent half-angle can be expressed in the relation of

$$\ln\left(\tan\frac{\phi}{2}\right) = \ln\left(\frac{1-\cos\phi}{\sin\phi}\right) = \ln(\csc\phi - \cot\phi) \tag{2.6.27}$$

which finally brings us to the relation

$$\ln(\csc\phi - \cot\phi) = -\ln(\csc\phi + \cot\phi) \tag{2.6.28}$$

and

$$\tan\frac{\phi}{2} = \csc\phi - \cot\phi = \Phi \tag{2.6.29}$$

Thus, the full complementary part for G is

$$G_c = K_1 \sin^2\phi + K_2\left[\cos\phi - \left(\sin^2\phi\right)\ln\Phi\right] \tag{2.6.30}$$

Next, the particular solution is going to be of the form of a constant, $G_p = K_3$, since the non-homogeneous function is a constant (see . Therefore, by substituting G_p and its derivatives into either Eq. (2.6.2) or Eq. (2.6.4) the particular solution is revealed as

$$G_p = \frac{U^2}{2W} \tag{2.6.31}$$

Now by combining the complementary and particular forms, the solution for G is of the form

$$G = \frac{U^2}{2W} + K_1 \sin^2\phi + K_2\left[\cos\phi - \left(\sin^2\phi\right)\ln\Phi\right] \tag{2.6.32}$$

In order to solve for the constants of Eq. (2.6.32) the boundary conditions are needed. Thus, corresponding to 2.3.1 and 2.3.1 the boundary conditions become

$$G(0) = 0 \tag{2.6.33}$$

$$G(\alpha) = 0 \tag{2.6.34}$$

Substituting in the BC at the centerline produces

$$0 = \frac{U^2}{2W} + K_1 \sin^2(0) + K_2\left[\cos(0) - \sin^2(0)\ln(0)\right] \tag{2.6.35}$$

which reduces to

$$0 = \frac{U^2}{2W} + K_2 \tag{2.6.36}$$

and finally yields

$$K_2 = -\frac{U^2}{2W} \tag{2.6.37}$$

Substituting in the BC at the wall gives

$$0 = \frac{U^2}{2W} + K_1 \sin^2\alpha - \frac{U^2}{2W}\left[\cos\alpha - \left(\sin^2\alpha\right)\ln\mathcal{A}\right] \tag{2.6.38}$$

Rearranging the constant to one side of the equation

$$K_1 \sin^2\alpha = -\frac{U^2}{2W} + \frac{U^2}{2W}\left[\cos\alpha - \left(\sin^2\alpha\right)\ln\mathcal{A}\right] \tag{2.6.39}$$

Condensing the RHS of the equation

$$K_1 \sin^2\alpha = -\frac{U^2}{2W}\left[1 - \cos\alpha + \left(\sin^2\alpha\right)\ln\mathcal{A}\right] \tag{2.6.40}$$

Finally, results in the constant, K_1, after dividing both sides

$$K_1 = -\frac{U^2}{2W}\csc^2\alpha\left[1 - \cos\alpha + \left(\sin^2\alpha\right)\ln\mathcal{A}\right] \tag{2.6.41}$$

Next, applying 2.6.33 and 2.6.34 the constants emerge as

$$K_1 = -\frac{U^2}{2W}\left[\csc^2\alpha + \ln\mathcal{A} - \csc\alpha\cot\alpha\right] = -\frac{U^2}{2W}\left[\mathcal{A}\csc\alpha + \ln\mathcal{A}\right] \tag{2.6.42}$$

where

$$\mathcal{A} = \tan\frac{\alpha}{2} = \csc\alpha - \cot\alpha \tag{2.6.43}$$

To simplify the equation even further, a constant is brought in where

$$\lambda = -\frac{2W}{U^2}K_1 = \left[\csc^2\alpha + \ln\mathcal{A} - \csc\alpha\cot\alpha\right] = \left[\mathcal{A}\csc\alpha + \ln\mathcal{A}\right] \tag{2.6.44}$$

Now the solution for G is complete

$$G = \frac{U^2}{2W} - \frac{U^2}{2W}\lambda\sin^2\phi - \frac{U^2}{2W}\left[\cos\phi - \left(\sin^2\phi\right)\ln\Phi\right] \tag{2.6.45}$$

Bringing everything in the equation under the the velocity ratio constant (with a recovered negative sign) yields

$$G = \frac{U^2}{2W}\left[(\lambda - \ln\Phi)\sin^2\phi + \cos\phi - 1\right] \tag{2.6.46}$$

The recovered sign enforces that the constant on the RHS of the BHE is to be negative for this solution. The equation can also be expressed with the sin squared term upfront

$$G = \frac{U^2\sin^2\phi}{2W}\left(\lambda - \ln\Phi + \csc\phi\cot\phi - \csc^2\phi\right) \tag{2.6.47}$$

Now a co-secant term can be factored out for the last term

$$G = \frac{U^2\sin^2\phi}{2W}\left[\lambda - \ln\Phi + \csc\phi\left(\cot\phi - \csc\phi\right)\right] \tag{2.6.48}$$

Factoring out a negative term as well produces

$$G = \frac{U^2\sin^2\phi}{2W}\left[\lambda - \ln\Phi - \csc\phi\left(\csc\phi - \cot\phi\right)\right] \tag{2.6.49}$$

Which eventually results in the compact equation of

$$G = \frac{U^2\sin^2\phi}{2W}\left(\lambda - \ln\Phi - \Phi\csc\phi\right) \tag{2.6.50}$$

Finally, the stream function takes its form as

$$\psi = \frac{U^2R^2}{2W}\left[(\lambda - \ln\Phi)\sin^2\phi + \cos\phi - 1\right] \tag{2.6.51}$$

or

$$\psi = \frac{U^2 R^2 \sin^2\phi}{2W}\left(\lambda - \ln\Phi - \Phi\csc\phi\right) \tag{2.6.52}$$

2.7 Spherical Radial and Zenith Velocities

Now the spherical radial and latitudinal velocities come about from the Stokes stream function-velocity relation (Eq. (1.5.23))

$$u_R = \frac{1}{R^2\sin\phi}\frac{\partial\psi}{\partial\phi}$$

$$u_\phi = -\frac{1}{R\sin\phi}\frac{\partial\psi}{\partial R}$$

Utilizing Eq. (1.5.23), the derivatives of the stream function w.r.t. the spherical radius and latitudinal angle are sought. Beginning with the derivative w.r.t. the zenith angle

$$\frac{\partial\psi}{\partial\phi} = \frac{\partial}{\partial\phi}\left\{\frac{U^2R^2}{2W}\left[(\lambda - \ln\Phi)\sin^2\phi + \cos\phi - 1\right]\right\} \tag{2.7.1}$$

First, the constant is brought to the outside of the derivative

$$\frac{U^2R^2}{2W}\frac{\partial}{\partial\phi}\left\{\left[(\lambda - \ln\Phi)\sin^2\phi + \cos\phi - 1\right]\right\} \tag{2.7.2}$$

Next, the first term is separated and evaluated first

$$\frac{\partial}{\partial\phi}\left[(\lambda - \ln\Phi)\sin^2\phi\right] \tag{2.7.3}$$

The derivative is separated even further by applying the chain rule

$$\frac{\partial}{\partial\phi}\left[(\lambda - \ln\Phi)\sin^2\phi\right] = (\lambda - \ln\Phi)\frac{\partial}{\partial\phi}\left(\sin^2\phi\right) + \sin^2\phi\frac{\partial}{\partial\phi}(\lambda - \ln\Phi) \tag{2.7.4}$$

The first term in the previous equation is considered first

$$(\lambda - \ln \Phi) \frac{\partial}{\partial \phi} \left(\sin^2 \phi \right) = 2 (\lambda - \ln \Phi) \sin \phi \cos \phi \tag{2.7.5}$$

Then the second term

$$\sin^2 \phi \frac{\partial}{\partial \phi} (\lambda - \ln \Phi) \tag{2.7.6}$$

First, the tangent half-angle is expanded

$$- \frac{\partial}{\partial \phi} (\ln \Phi) = - \frac{\partial}{\partial \phi} \left[\ln \left(\tan \frac{\phi}{2} \right) \right] \tag{2.7.7}$$

The general derivative rule for the logarithm is

$$- \frac{\mathrm{d}}{\mathrm{d}x} (\ln u) = - \frac{u'}{u} \tag{2.7.8}$$

The general derivative rule for the tangent is

$$\frac{\mathrm{d}}{\mathrm{d}x} (\tan v) = v' \sec^2 v \tag{2.7.9}$$

where $u = \tan \phi/2$ and $v = \phi/2$.

$$\frac{\mathrm{d}}{\mathrm{d}x} \left(\tan \frac{\phi}{2} \right) = \frac{1}{2} \sec^2 \frac{\phi}{2} \tag{2.7.10}$$

Reclaiming the negative sign

$$- \frac{\mathrm{d}}{\mathrm{d}x} (\ln \Phi) = - \frac{\frac{1}{2} \sec^2 \frac{\phi}{2}}{\tan \frac{\phi}{2}} \tag{2.7.11}$$

Next, a simplification can begin by transforming the tangent into sines and cosines

$$= -\frac{\frac{1}{2}\cos\frac{\phi}{2}}{\cos^2\frac{\phi}{2}\sin\frac{\phi}{2}} \tag{2.7.12}$$

Canceling out cosine terms is the next step

$$= -\frac{\frac{1}{2}}{\cos\frac{\phi}{2}\sin\frac{\phi}{2}} \tag{2.7.13}$$

Recalling a trigonometric relation

$$\cos u \sin v = \frac{1}{2}\left[\sin(u+v) - \sin(u-v)\right] \tag{2.7.14}$$

The equation now reduces to

$$-\frac{\frac{1}{2}}{\frac{1}{2}\sin\phi} = -\csc\phi \tag{2.7.15}$$

So now the derivative is shown to be

$$\frac{\partial}{\partial\phi}(\lambda - \ln\Phi) = -\csc\phi \tag{2.7.16}$$

Multiplying the sine term back in gives

$$\sin^2\phi\frac{\partial}{\partial\phi}(\lambda - \ln\Phi) = -\sin\phi \tag{2.7.17}$$

Combining both terms from 2.7.5 and 2.7.17 yields

$$\frac{\partial}{\partial\phi}\left[(\lambda - \ln\Phi)\sin^2\phi\right] = 2(\lambda - \ln\Phi)\sin\phi\cos\phi - \sin\phi \tag{2.7.18}$$

Now taking the derivatives of the cosine and constant term provides

$$\frac{U^2R^2}{2W}\frac{\partial}{\partial\phi}\left\{\left[(\lambda-\ln\Phi)\sin^2\phi+\cos\phi-1\right]\right\}$$
$$=\frac{U^2R^2}{2W}\left[2\left(\lambda-\ln\Phi\right)\sin\phi\cos\phi-\sin\phi-\sin\phi\right] \tag{2.7.19}$$

Finally, the analysis of the derivative w.r.t. phi leaves

$$\frac{\partial\psi}{\partial\phi}=\frac{U^2R^2}{W}\left[(\lambda-\ln\Phi)\sin\phi\cos\phi-\sin\phi\right] \tag{2.7.20}$$

or

$$\frac{\partial\psi}{\partial\phi}=\frac{U^2R^2\sin\phi}{W}\left[(\lambda-\ln\Phi)\cos\phi-1\right] \tag{2.7.21}$$

The derivative in the spherical radial direction is a simple power term which gives

$$\frac{\partial\psi}{\partial R}=\frac{U^2R\sin^2\phi}{W}\left(\lambda-\ln\Phi-\Phi\csc\phi\right) \tag{2.7.22}$$

Thus, completing the stream function-velocity relation engenders the spherical radial and zenith velocities as

$$u_R=\frac{U^2}{W}\left[(\lambda-\ln\Phi)\cos\phi-1\right] \tag{2.7.23}$$

$$u_\phi=-\frac{2\psi}{R^2\sin\phi}=-\frac{U^2\sin\phi}{W}\left(\lambda-\ln\Phi-\Phi\csc\phi\right) \tag{2.7.24}$$

or

$$u_\phi=\frac{U^2}{W}\left[(\lambda-\ln\Phi)\sin\phi-\Phi\right] \tag{2.7.25}$$

2.8 Tangential Velocity: Slip Permitting

The tangential velocity evolves from the swirl function relation and can be shown to equal

$$u_{\theta,\text{slip}} = \frac{Ua}{R\sin\phi}\sqrt{1+\frac{2}{Wa^2}\left[\frac{U^2R^2\sin^2\phi}{2W}\left(\lambda-\ln\Phi-\Phi\csc\phi\right)\right]} \tag{2.8.1}$$

Eliminating some terms simplifies to

$$u_{\theta,\text{slip}} = \frac{Ua}{R\sin\phi}\sqrt{1+\frac{U^2R^2\sin^2\phi}{W^2a^2}\left(\lambda-\ln\Phi-\Phi\csc\phi\right)} \tag{2.8.2}$$

and combining simplifies even further to

$$u_{\theta,\text{slip}} = \frac{Ua}{R\sin\phi}\sqrt{1+\left(\frac{UR\sin\phi}{Wa}\right)^2\left(\lambda-\ln\Phi-\Phi\csc\phi\right)} \tag{2.8.3}$$

2.9 Tangential Velocity: No Slip

A second condition may be implied in order to obtain a slightly different result. Now the equation for the tangential velocity appears as

$$u_{\theta,\text{no slip}} = \frac{U}{R\sin\phi}\sqrt{\left(\frac{UR\sin\phi}{W}\right)^2\left(\lambda-\ln\Phi-\Phi\csc\phi\right)} \tag{2.9.1}$$

Finally, bringing out some terms from under the square root reduces the equation to

$$u_{\theta,\text{no slip}} = \frac{U^2}{W}\sqrt{\lambda-\ln\Phi-\Phi\csc\phi} \tag{2.9.2}$$

2.10 Conical BDV Inlet Swirl and Geometric Parameters

In order to simplify and reduce the stream function and velocity equations even further, a parameter is introduced which relates the average tangential inlet velocity to the average

axial inlet velocity also known as a swirl parameter (Greitzer et al. 2004). Retrieving Eq. (2.4.15) which relates the incoming volumetric flow rate establishes a relation of

$$W = \frac{UA_i}{\pi\left(a^2 - b^2\right)} = \frac{UA_i}{\pi a^2\left(1 - X_\beta^2\right)} \tag{2.10.1}$$

where $X_\beta = \hat{\beta} = b/a$. Now upon examination of the original BDV in a cylindrical geometry study by Vyas and Majdalani (2003a; 2006) the this swirl parameter is

$$S = \frac{\pi ab}{A_i} = \frac{\pi X_\beta a^2}{A_i} = \frac{\pi X_\beta}{Q_i} = \pi X_\beta \sigma \tag{2.10.2}$$

where $\sigma = Q_i^{-1}$ and is the modified swirl number. The swirl parameter, S, has been based upon a definition by Hoekstra et al and Derksen (1999) and Van den Akker (2000). Thus, following parameters are deduced

$$W = \frac{U}{\pi\sigma_c\left(1 - X_\beta^2\right)} = \frac{U}{\pi\sigma_c} \tag{2.10.3}$$

$$W^2 = \frac{U^2}{\pi^2\sigma^2\left(1 - X_\beta^2\right)^2} = \frac{U^2}{\pi^2\sigma_c^2} \tag{2.10.4}$$

where a type of modified swirl parameter is of the geometric type appears as

$$\sigma_c = \frac{a^2 - b^2}{A_i} = \frac{a^2\left(1 - X_\beta^2\right)}{A_i} = \frac{L^2}{A_i}\left(\tan^2\alpha - \tan^2\beta\right) \tag{2.10.5}$$

$$\sigma_c = \sigma\left(1 - X_\beta^2\right) \tag{2.10.6}$$

were β is the angle of the mantle throughout the cone, $X_\beta = b/a$ is the ratio of the mantle location to maximum radius, and $\sigma = a^2/A_i$ is the modified swirl parameter of a cylindrical BV as designated by Vyas et al (Vyas et al. 2003a; Vyas and Majdalani 2006). The mantle angle of the conical cyclone terminates at the axial location L and radial location b. The

modified swirl number also turns out to be defined by the tangential velocity and axial velocity ratio

$$\sigma_c = \frac{U}{\pi W} \tag{2.10.7}$$

verifying that σ_c is a swirl parameter. In terms of the swirl number, $S = \pi ab/A_i$, of a cyclone separator the simplified modified swirl parameter for the conical cyclone becomes

$$\sigma_c = 0.45S\left(1 - X_\beta^2\right) \tag{2.10.8}$$

if the theoretical location of $X_\beta \approx 0.707$ from Vyas and Majdalani (2006) is used for the cylindrical modified swirl parameter to get $\sigma \approx 0.45S$. The theoretical location of X_β for the conical swirl parameter is discussed in Section 3.1.2.

Thus, substituting in the swirl parameter reduces equations of the stream function and velocities due to elimination of the axial velocity, W, to

$$\psi = \tfrac{1}{2}\pi\sigma_c U R^2\left[(\lambda - \ln\Phi)\sin^2\phi + \cos\phi - 1\right] \tag{2.10.9}$$

or

$$\psi = \tfrac{1}{2}\pi\sigma_c U R^2 \sin^2\phi\,(\lambda - \ln\Phi - \Phi\csc\phi) \tag{2.10.10}$$

$$u_R = \pi\sigma_c U\left[(\lambda - \ln\Phi)\cos\phi - 1\right] \tag{2.10.11}$$

$$u_\phi = -\pi\sigma_c U\left[(\lambda - \ln\Phi)\sin\phi - \Phi\right] \tag{2.10.12}$$

$$u_{\theta,\text{slip}} = \frac{Ua}{R\sin\phi}\sqrt{1 + \left(\frac{\pi\sigma_c R\sin\phi}{a}\right)^2(\lambda - \ln\Phi - \Phi\csc\phi)} \tag{2.10.13}$$

$$u_{\theta,\text{no slip}} = U\pi\sigma_c\sqrt{\lambda - \ln\Phi - \Phi\csc\phi} \tag{2.10.14}$$

Another geometric parameter from Vyas et al (2003a; 2006) appears as well in this conical solution. The parameter from Vyas and Majdalani relates the modified swirl number, the constant pi, and the chamber aspect ratio shown as

$$\kappa = \frac{1}{2\pi\sigma l} \tag{2.10.15}$$

A similar parameter materializes for this conical solution as

$$\kappa_c = \pi\sigma_c = \frac{U}{W} \tag{2.10.16}$$

Relating the geometric inflow parameters gives

$$\kappa = \frac{1 - X_\beta^2}{2\pi\sigma_c l} = \frac{1 - X_\beta^2}{2\kappa_c l} \tag{2.10.17}$$

Since this model is solved with a different methodology and geometry, the aspect ratio, l, does not explicitly appear in the conical geometric parameter but is automatically satisfied through the coupled ratio based upon the half-angle α since $l = \tan^{-1}\alpha$. The stream function and velocities now become

$$\psi = \tfrac{1}{2}\kappa_c U R^2\left[(\lambda - \ln\Phi)\sin^2\phi + \cos\phi - 1\right] \tag{2.10.18}$$

or

$$\psi = \tfrac{1}{2}\kappa_c U R^2\sin^2\phi\,(\lambda - \ln\Phi - \Phi\csc\phi) \tag{2.10.19}$$

$$u_R = \kappa_c U\left[(\lambda - \ln\Phi)\cos\phi - 1\right] \tag{2.10.20}$$

$$u_\phi = -\kappa_c U \left[(\lambda - \ln \Phi) \sin \phi - \Phi \right] \tag{2.10.21}$$

$$u_{\theta,\text{slip}} = \frac{Ua}{R \sin \phi} \sqrt{1 + \left(\frac{\kappa_c R \sin \phi}{a} \right)^2 (\lambda - \ln \Phi - \Phi \csc \phi)} \tag{2.10.22}$$

$$u_{\theta,\text{no slip}} = U \kappa_c \sqrt{\lambda - \ln \Phi - \Phi \csc \phi} \tag{2.10.23}$$

2.11 Nondimensional Variables and Equations

Next, a simplification to elucidate the equations further comes about from prescribing nondimensional variables. For the sake of typesetting, the overbar, which generally denotes a dimensional variable, was purposely left out in this chapter beforehand. The normalization here follows previous studies such as those by Vyas and Majdalani (2006), Majdalani and Rienstra (2007), Majdalani and Saad (2007), Majdalani (2012)

$$R = \frac{\bar{R}}{a}; \quad \psi = \frac{\bar{\psi}}{Ua^2}; \quad u_R = \frac{\bar{u}_R}{U}; \quad u_\phi = \frac{\bar{u}_\phi}{U}; \quad u_\theta = \frac{\bar{u}_\theta}{U} \tag{2.11.1}$$

The stream function reduces to

$$\psi = \tfrac{1}{2} \kappa_c R^2 \left[(\lambda - \ln \Phi) \sin^2 \phi + \cos \phi - 1 \right] \tag{2.11.2}$$

or

$$\psi = \tfrac{1}{2} \kappa_c R^2 \sin^2 \phi \, (\lambda - \ln \Phi - \Phi \csc \phi) \tag{2.11.3}$$

The velocities transition to

$$u_R = \kappa_c \left[(\lambda - \ln \Phi) \cos \phi - 1 \right] \tag{2.11.4}$$

$$u_\phi = -\kappa_c \left[(\lambda - \ln \Phi) \sin \phi - \Phi \right] \tag{2.11.5}$$

$$u_{\theta,\text{slip}} = \frac{1}{R \sin \phi} \sqrt{1 + (\kappa_c R \sin \phi)^2 \left(\lambda - \ln \Phi - \Phi \csc \phi \right)} \tag{2.11.6}$$

$$u_{\theta,\text{no slip}} = \kappa_c \sqrt{\lambda - \ln \Phi - \Phi \csc \phi} \tag{2.11.7}$$

Where the angular momentum function appears as

$$B_{\text{slip}} = \sqrt{1 + (\kappa_c R \sin \phi)^2 \left(\lambda - \ln \Phi - \Phi \csc \phi \right)} \tag{2.11.8}$$

$$B_{\text{no slip}} = \kappa_c R \sin \phi \sqrt{\lambda - \ln \Phi - \Phi \csc \phi} \tag{2.11.9}$$

2.12 An Alternate Approach: Normalizing Upfront

An alternate approach may be considered in order to arrive at the same equations. This approach normalizes and applies the conical swirl number upfront. This also confirms the differences between this solution and the one posed by Bloor and Ingham (1987) (see Section 2.18 for more detail). This produces

$$\frac{\partial^2 \psi}{\partial R^2} + \frac{\sin \phi}{R^2} \frac{\partial}{\partial \phi} \left(\frac{1}{\sin \phi} \frac{\partial \psi}{\partial \phi} \right) = -\kappa_c \tag{2.12.1}$$

Thus where applicable, the equation within the derivation turns out to be opposite in sign since it is absorbed with the conical swirl number. First the swirl is normalized as

$$B = \frac{\bar{B}}{Ua} \tag{2.12.2}$$

Then the swirl term in the BHE becomes

$$B\mathrm{d}B = \frac{\kappa_c R \sin\phi}{R\sin\phi} = \kappa_c \tag{2.12.3}$$

Thus, transforming the non-homogeneous ODE into

$$G'' - \frac{\cos\phi}{\sin\phi}G' + 2G = -\kappa_c \tag{2.12.4}$$

with a particular solution of

$$G_p = -\tfrac{1}{2}\kappa_c \tag{2.12.5}$$

The general homogeneous solution is now

$$G = K_1 \sin^2\phi + K_2\left[\cos\phi - \left(\sin^2\phi\right)\ln\Phi\right] - \tfrac{1}{2}\kappa_c \tag{2.12.6}$$

Applying the BCs and solving for the constants produces

$$K_2 = \tfrac{1}{2}\kappa_c \tag{2.12.7}$$

$$K_1 = \tfrac{1}{2}\kappa_c \csc^2\alpha\left[1 - \cos\alpha + \left(\sin^2\alpha\right)\ln\mathcal{A}\right] \tag{2.12.8}$$

$$K_1 = \tfrac{1}{2}\kappa_c\left(\csc^2\alpha + \ln\mathcal{A} - \csc\alpha\cot\alpha\right) = \tfrac{1}{2}\kappa_c\left(A\csc\alpha + \ln\mathcal{A}\right) \tag{2.12.9}$$

$$\lambda = 2K_1\kappa_c^{-1} = \csc^2\alpha + \ln\mathcal{A} - \csc\alpha\cot\alpha = A\csc\alpha + \ln\mathcal{A} \tag{2.12.10}$$

Finally, the full solution to the ODE appears as

$$G = \tfrac{1}{2}\kappa_c\left[(\lambda - \ln\Phi)\sin^2\phi + \cos\phi - 1\right] \tag{2.12.11}$$

$$G = \tfrac{1}{2}\kappa_c \sin^2\phi\,(\lambda - \ln\Phi - \Phi\csc\phi) \tag{2.12.12}$$

2.13 Cylindrical Polar Velocities Conversion

Since many cyclone separator studies investigate and present the axial velocity, u_z, and cylindrical polar radial velocity, u_r, at this point a conversion from the spherical polar velocities (u_R, u_ϕ, u_θ) to the cylindrical polar velocities, (u_r, u_θ, u_z), is presented (where the tangential velocities in both cases remains the same as u_θ). A simple conversion is provided as

$$\begin{cases} u_r = u_R \sin\phi + u_\phi \cos\phi \\ u_z = u_R \cos\phi - u_\phi \sin\phi \end{cases} \tag{2.13.1}$$

The first term in the cylindrical radial velocity is examined as

$$u_R \sin\phi = \kappa_c \sin\phi \left[(\lambda - \ln\Phi)\cos\phi - 1\right] \tag{2.13.2}$$

While the second term in the cylindrical radial velocity is presented as

$$u_\phi \cos\phi = -\kappa_c \cos\phi \left[(\lambda - \ln\Phi)\sin\phi - \Phi\right] \tag{2.13.3}$$

Some terms cancel simplifying the equation as

$$u_r = -\kappa_c \left(\sin\phi - \Phi\cos\phi\right) \tag{2.13.4}$$

Expanding the Φ-term elucidates how to simplify the equation further.

$$u_r = -\kappa_c \left[\sin\phi - \cos\phi\left(\csc\phi - \cot\phi\right)\right] \tag{2.13.5}$$

Multiplying in terms yields

$$u_r = -\kappa_c \left(\sin\phi - \cot + \cos^2\phi \csc\phi\right) \tag{2.13.6}$$

Next, the cosine squared is converted to one minus sine squared

$$u_r = -\kappa_c \left(\sin\phi - \cot\phi + \left(1 - \sin^2\phi\right)\csc\phi\right) \tag{2.13.7}$$

Canceling out some of the terms produces

$$u_r = -\kappa_c \left(\csc\phi - \cot\phi\right) \tag{2.13.8}$$

Which then gives the straightforward equation of

$$u_r = -\kappa_c \Phi \tag{2.13.9}$$

Next, the axial velocity terms are multiplied through

$$u_R \cos\phi = \kappa_c \left[(\lambda - \ln\Phi)\cos^2\phi - \cos\phi\right] \tag{2.13.10}$$

$$-u_\phi \sin\phi = \kappa_c \left[(\lambda - \ln\Phi)\sin^2\phi - \Phi\sin\phi\right] \tag{2.13.11}$$

Reducing the cosine and sine squared terms contracts the equation to

$$u_z = \kappa_c \left(\lambda - \ln\Phi - \Phi\sin\phi - \cos\phi\right) \tag{2.13.12}$$

Again, expanding the Φ-term administers further abridgment to

$$u_z = \kappa_c \left[\lambda - \ln\Phi - \sin\phi\left(\csc\phi - \cot\phi\right) - \cos\phi\right] \tag{2.13.13}$$

Factoring in the sine term gives

$$u_z = \kappa_c \left(\lambda - \ln\Phi + \cos\phi - 1 - \cos\phi\right) \tag{2.13.14}$$

Which finally shortens the axial velocity equation to

$$u_z = \kappa_c \left(\lambda - \ln\Phi - 1\right) \tag{2.13.15}$$

Thus, after the cylindrical polar velocity conversion, the equations for the stream function and all velocities in spherical polar coordinates materialize as

$$\psi = \tfrac{1}{2}\kappa_c R^2 \sin^2\phi\,(\lambda - \ln\Phi - \Phi\csc\phi) \tag{2.13.16}$$

$$u_R = \kappa_c\left[(\lambda - \ln\Phi)\cos\phi - 1\right] \tag{2.13.17}$$

$$u_\phi = -\kappa_c\left[(\lambda - \ln\Phi)\sin\phi - \Phi\right] \tag{2.13.18}$$

$$u_{\theta,\text{slip}} = \frac{1}{R\sin\phi}\sqrt{1 + (\kappa_c R\sin\phi)^2\,(\lambda - \ln\Phi - \Phi\csc\phi)} \tag{2.13.19}$$

$$u_{\theta,\text{no slip}} = \kappa_c\sqrt{\lambda - \ln\Phi - \Phi\csc\phi} \tag{2.13.20}$$

$$u_r = -\kappa_c\Phi \tag{2.13.21}$$

$$u_z = \kappa_c\,(\lambda - \ln\Phi - 1) \tag{2.13.22}$$

or condensed into

$$\psi = \tfrac{1}{2}\kappa_c R^2 \sin^2\phi\,(\Phi_1 - \Phi_2) \tag{2.13.23}$$

$$u_R = \kappa_c\,(\Phi_1\cos\phi - 1) \tag{2.13.24}$$

$$u_\phi = -\kappa_c\,(\Phi_1\sin\phi - \Phi) \tag{2.13.25}$$

$$u_{\theta,\text{slip}} = \frac{1}{R\sin\phi}\sqrt{1 + (\kappa_c R\sin\phi)^2\,(\Phi_1 - \Phi_2)} \tag{2.13.26}$$

$$u_{\theta,\text{no slip}} = \sqrt{\Phi_1 - \Phi_2} \tag{2.13.27}$$

$$u_r = -\kappa_c\Phi \tag{2.13.28}$$

$$u_z = \kappa_c\,(\Phi_1 - 1) \tag{2.13.29}$$

where $\Phi_1 = \lambda - \ln\Phi$ and $\Phi_2 = \Phi\csc\phi$.

The total velocity for the spherical polar velocities in spherical polar coordinates can now be written as

$$\mathbf{u} = \kappa_c \left(\Phi_1 \cos\phi - 1\right) \mathbf{e}_R - \kappa_c \left(\Phi_1 \sin\phi - \Phi\right) \mathbf{e}_\phi + \left(\frac{1}{r}\sqrt{1 + 2\kappa_c \psi}\right) \mathbf{e}_\theta \qquad \text{(slip)} \qquad (2.13.30)$$

$$\mathbf{u} = \kappa_c \left(\Phi_1 \cos\phi - 1\right) \mathbf{e}_R - \kappa_c \left(\Phi_1 \sin\phi - \Phi\right) \mathbf{e}_\phi + \left(\frac{1}{r}\sqrt{2\kappa_c \psi}\right) \mathbf{e}_\theta \qquad \text{(no slip)} \qquad (2.13.31)$$

Next, the velocity magnitude can be calculated from the velocity components as

$$|u| = \sqrt{u_R^2 + u_\phi^2 + u_\theta^2} \qquad (2.13.32)$$

A symbolic mathematical software such as Mathematica can be used to render the result of the velocity magnitude. To check Mathematica, a mathematical derivation can be found in Appendix B. The outcome for the velocity magnitude ends up being

$$|u| = \frac{1}{R\sin\phi}\sqrt{1 + (\kappa_c R \sin\phi)^2 \left[(\lambda - \ln\Phi)^2 - (\lambda - \ln\Phi) + \Phi \csc\phi\right]} \qquad (2.13.33)$$

and in a condensed form of

$$|u| = \frac{1}{R\sin\phi}\sqrt{1 + (\kappa_c R \sin\phi)^2 \left(\Phi_1^2 - \Phi_1 + \Phi \csc\phi\right)} \qquad (2.13.34)$$

2.14 Cylindrical Polar Coordinates Conversion

Since cylindrical polar coordinates (CPC) are much easier to visualize than spherical polar coordinates (SPC), a transformation from SPC to CPC is undertaken by the following relations:

$$R = \sqrt{r^2 + z^2} = r\sqrt{1 + \zeta^2} = r\mathcal{Z}_1 \tag{2.14.1}$$

$$R^2 = r^2 + z^2 = r^2\left(1 + \zeta^2\right) = r^2\mathcal{Z}_1^2 \tag{2.14.2}$$

$$R\sin\phi = r \tag{2.14.3}$$

$$R\cos\phi = z \tag{2.14.4}$$

$$\sin\phi = \frac{r}{\sqrt{r^2 + z^2}} = \frac{1}{\sqrt{1 + \zeta^2}} = \mathcal{Z}_2 \tag{2.14.5}$$

$$\sin^2\phi = \frac{r^2}{r^2 + z^2} = \frac{1}{1 + \zeta^2} = \mathcal{Z}_2^2 \tag{2.14.6}$$

$$\cos\phi = \frac{z}{\sqrt{r^2 + z^2}} = \frac{\zeta}{\sqrt{1 + \zeta^2}} = \zeta\mathcal{Z}_2 \tag{2.14.7}$$

$$\cos^2\phi = \frac{z^2}{r^2 + z^2} = \frac{\zeta^2}{1 + \zeta^2} = \zeta^2\mathcal{Z}_2^2 \tag{2.14.8}$$

$$\tan\phi = \frac{r}{z} = \frac{1}{\zeta} = \eta \tag{2.14.9}$$

$$\tan^2\phi = \frac{r^2}{z^2} = \frac{1}{\zeta^2} = \eta^2 \tag{2.14.10}$$

$$\csc\phi = \frac{\sqrt{r^2 + z^2}}{r} = \sqrt{1 + \zeta^2} = \mathcal{Z}_1 \tag{2.14.11}$$

$$\csc^2\phi = \frac{r^2 + z^2}{r^2} = 1 + \zeta^2 = \mathcal{Z}_1^2 \tag{2.14.12}$$

$$\sec\phi = \frac{\sqrt{r^2 + z^2}}{z} = \frac{\sqrt{1 + \zeta^2}}{\zeta} = \eta\mathcal{Z}_1 \tag{2.14.13}$$

$$\sec^2\phi = \frac{r^2 + z^2}{z^2} = 1 + \zeta^{-2} = 1 + \eta^2 \tag{2.14.14}$$

$$\cot\phi = \frac{z}{r} = \zeta \tag{2.14.15}$$

$$\cot^2\phi = \frac{z^2}{r^2} = \zeta^2 \tag{2.14.16}$$

$$\Phi = \csc\phi - \cot\phi = \sqrt{1 + \zeta^2} - \zeta = \mathcal{Z} \tag{2.14.17}$$

$$\zeta = z/r \tag{2.14.18}$$

$$\eta = r/z \tag{2.14.19}$$

Thus, the stream function becomes

$$\psi = \frac{1}{2}\kappa_c r^2 \left[\lambda - \ln\left(\sqrt{1+\zeta^2} - \zeta\right) - \left(\sqrt{1+\zeta^2} - \zeta\right)\left(\sqrt{1+\zeta^2}\right)\right] \tag{2.14.20}$$

or with the last term factored

$$\psi = \frac{1}{2}\kappa_c r^2 \left[\lambda - \ln\left(\sqrt{1+\zeta^2} - \zeta\right) + \zeta\sqrt{1+\zeta^2} - \zeta^2 - 1\right] \tag{2.14.21}$$

The velocities result in a transformation of

$$u_R = \kappa_c \left\{\left[\lambda - \ln\left(\sqrt{1+\zeta^2} - \zeta\right)\right]\left(\zeta/\sqrt{1+\zeta^2}\right) - 1\right\} \tag{2.14.22}$$

$$u_\phi = -\kappa_c \left\{\left[\lambda - \ln\left(\sqrt{1+\zeta^2} - \zeta\right)\right]/\left(\sqrt{1+\zeta^2}\right) - \sqrt{1+\zeta^2} + \zeta\right\} \tag{2.14.23}$$

$$u_\theta = \frac{1}{r}\sqrt{1 + (\kappa_c r)^2\left[\lambda - \ln\left(\sqrt{1+\zeta^2} - \zeta\right) + \zeta\sqrt{1+\zeta^2} - \zeta^2 - 1\right]} \tag{2.14.24}$$

$$u_r = \kappa_c\left(\zeta - \sqrt{1+\zeta^2}\right) = -\kappa_c\left(\sqrt{1+\zeta^2} - \zeta\right) \tag{2.14.25}$$

$$u_z = \kappa_c\left[\lambda - \ln\left(\sqrt{1+\zeta^2} - \zeta\right) - 1\right] \tag{2.14.26}$$

The stream function and velocities can be condensed into the following forms

$$\psi = \frac{1}{2}\kappa_c r^2\left(\mathcal{Z}_3 + \zeta\mathcal{Z}_1 - \mathcal{Z}_1^2\right) \tag{2.14.27}$$

$$\psi = \frac{1}{2}\kappa_c r^2 \left(\mathcal{Z}_3 + \zeta\mathcal{Z} - 1\right) \tag{2.14.28}$$

$$\psi = \frac{1}{2}\kappa_c r^2 \left(\lambda - \ln\mathcal{Z} - \mathcal{Z}\mathcal{Z}_1\right) \tag{2.14.29}$$

$$\psi = \frac{1}{2}\kappa_c r^2 \left(\mathcal{Z}_3 - \mathcal{Z}_4\right) \tag{2.14.30}$$

where $\mathcal{Z}_3 = \lambda - \ln\mathcal{Z}$ and $\mathcal{Z}_4 = \mathcal{Z}\mathcal{Z}_1$

$$u_R = \kappa_c \left[\left(\lambda - \ln\mathcal{Z}\right)\zeta\mathcal{Z}_2 - 1\right] \tag{2.14.31}$$

$$u_R = \kappa_c \left[\left(\lambda - \ln\mathcal{Z}\right)\mathcal{Z}_5 - 1\right] \tag{2.14.32}$$

$$u_R = \kappa_c \left(\mathcal{Z}_3\mathcal{Z}_5 - 1\right) \tag{2.14.33}$$

$$u_R = \kappa_c \left(\mathcal{Z}_6 - 1\right) \tag{2.14.34}$$

where $\mathcal{Z}_5 = \zeta\mathcal{Z}_2$ and $\mathcal{Z}_6 = \mathcal{Z}_3\mathcal{Z}_5$.

$$u_\phi = -\kappa_c \left[\left(\lambda - \ln\mathcal{Z}\right)\mathcal{Z}_2 - \mathcal{Z}_1 + \zeta\right] \tag{2.14.35}$$

$$u_\phi = -\kappa_c \left(\mathcal{Z}_3\mathcal{Z}_2 - \mathcal{Z}\right) \tag{2.14.36}$$

$$u_\phi = -\kappa_c \left(\mathcal{Z}_7 - \mathcal{Z}\right) \tag{2.14.37}$$

where $\mathcal{Z}_7 = \zeta\mathcal{Z}_2\mathcal{Z}_3$.

$$u_{\theta,\text{slip}} = \frac{1}{r}\sqrt{1 + (r\kappa_c)^2\left(\lambda - \ln \mathcal{Z} + \zeta\mathcal{Z} - 1\right)} \tag{2.14.38}$$

$$u_{\theta,\text{slip}} = \frac{1}{r}\sqrt{1 + (r\kappa_c)^2\left(\lambda - \ln \mathcal{Z} + \zeta\mathcal{Z}_1 - \mathcal{Z}_1^2\right)} \tag{2.14.39}$$

$$u_{\theta,\text{slip}} = \frac{1}{r}\sqrt{1 + (r\kappa_c)^2\left(\lambda - \ln \mathcal{Z} - \mathcal{Z}\mathcal{Z}_1\right)} \tag{2.14.40}$$

$$u_{\theta,\text{slip}} = \frac{1}{r}\sqrt{1 + (r\kappa_c)^2\left(\mathcal{Z}_3 - \mathcal{Z}_4\right)} \tag{2.14.41}$$

$$u_r = -\kappa_c\mathcal{Z} \tag{2.14.42}$$

$$u_z = \kappa_c\left(\mathcal{Z}_3 - 1\right) \tag{2.14.43}$$

Thus, the stream function and velocities group as

$$\psi = \frac{1}{2}\kappa_c r^2\left[\lambda - \ln\left(\sqrt{1+\zeta^2} - \zeta\right) + \zeta\sqrt{1+\zeta^2} - \zeta^2 - 1\right] \tag{2.14.44}$$

$$u_R = \kappa_c\left\{\zeta\left(1+\zeta^2\right)^{-1/2}\left[\lambda - \ln\left(\sqrt{1+\zeta^2} - \zeta\right)\right] - 1\right\} \tag{2.14.45}$$

$$u_\phi = -\kappa_c\left\{\left(1+\zeta^2\right)^{-1/2}\left[\lambda - \ln\left(\sqrt{1+\zeta^2} - \zeta\right)\right] - \sqrt{1+\zeta^2} + \zeta\right\} \tag{2.14.46}$$

$$u_{\theta,\text{slip}} = \frac{1}{r}\sqrt{1 + (\kappa_c r)^2\left[\lambda - \ln\left(\sqrt{1+\zeta^2} - \zeta\right) + \zeta\sqrt{1+\zeta^2} - \zeta^2 - 1\right]} \tag{2.14.47}$$

$$u_{\theta,\text{no slip}} = \kappa_c\sqrt{\lambda - \ln\left(\sqrt{1+\zeta^2} - \zeta\right) + \zeta\sqrt{1+\zeta^2} - \zeta^2 - 1} \tag{2.14.48}$$

$$u_r = \kappa_c\left(\zeta - \sqrt{1+\zeta^2}\right) = -\kappa_c\left(\sqrt{1+\zeta^2} - \zeta\right) \tag{2.14.49}$$

$$u_z = \kappa_c\left[\lambda - \ln\left(\sqrt{1+\zeta^2} - \zeta\right) - 1\right] \tag{2.14.50}$$

or in an alternate form provided by Mathematica

$$\psi = \frac{1}{2}\kappa_c r^2 \left[\lambda + \sinh^{-1}(\zeta) + \zeta\sqrt{1+\zeta^2} - \zeta^2 - 1\right] \tag{2.14.51}$$

$$u_R = \kappa_c \left\{\zeta\left(1+\zeta^2\right)^{-1/2}\left[\lambda + \sinh^{-1}(\zeta)\right] - 1\right\} \tag{2.14.52}$$

$$u_\phi = -\kappa_c \left\{\left(1+\zeta^2\right)^{-1/2}\left[\lambda + \sinh^{-1}(\zeta)\right] - \sqrt{1+\zeta^2} + \zeta\right\} \tag{2.14.53}$$

$$u_{\theta,\text{slip}} = \frac{1}{r}\sqrt{1 + (\kappa_c r)^2\left[\lambda + \sinh^{-1}(\zeta) + \zeta\sqrt{1+\zeta^2} - \zeta^2 - 1\right]} \tag{2.14.54}$$

$$u_{\theta,\text{no slip}} = \kappa_c\sqrt{\lambda + \sinh^{-1}(\zeta) + \zeta\sqrt{1+\zeta^2} - \zeta^2 - 1} \tag{2.14.55}$$

$$u_r = \kappa_c\left(\zeta - \sqrt{1+\zeta^2}\right) = -\kappa_c\left(\sqrt{1+\zeta^2} - \zeta\right) \tag{2.14.56}$$

$$u_z = \kappa_c\left[\lambda + \sinh^{-1}(\zeta) - 1\right] \tag{2.14.57}$$

or in a more condensed form as

$$\psi = \frac{1}{2}\kappa_c r^2 (\mathcal{Z}_3 - \mathcal{Z}_4) \tag{2.14.58}$$

$$u_R = \kappa_c (\mathcal{Z}_6 - 1) \tag{2.14.59}$$

$$u_\phi = -\kappa_c (\mathcal{Z}_7 - \mathcal{Z}) \tag{2.14.60}$$

$$u_{\theta,\text{slip}} = \frac{1}{r}\sqrt{1 + (r\kappa_c)^2 (\mathcal{Z}_3 - \mathcal{Z}_4)} \tag{2.14.61}$$

$$u_{\theta,\text{no slip}} = \kappa_c\sqrt{\mathcal{Z}_3 - \mathcal{Z}_4} \tag{2.14.62}$$

$$u_r = -\kappa_c \mathcal{Z} \tag{2.14.63}$$

$$u_z = \kappa_c (\mathcal{Z}_3 - 1) \tag{2.14.64}$$

where $-\ln\left(\sqrt{1+\zeta^2} - \zeta\right) = \sinh^{-1}(\zeta)$.

$$\mathbf{u} = -\kappa_c \mathcal{Z}\mathbf{e}_r + \left(\frac{1}{r}\sqrt{1 + 2\kappa_c\psi}\right)\mathbf{e}_\theta + \kappa_c (\mathcal{Z}_3 - 1)\,\mathbf{e}_z \tag{2.14.65}$$

The velocity magnitude can be calculated

$$|u| = \sqrt{u_r^2 + u_\theta^2 + u_z^2} \tag{2.14.66}$$

$$|u| = \frac{1}{r}\sqrt{1+(\kappa_c r)^2\left\{1-\zeta\mathcal{Z}+\lambda^2-\lambda+\sinh^{-1}(\zeta)\left[2\lambda-1+\sinh^{-1}(\zeta)\right]\right\}} \tag{2.14.67}$$

or

$$|u| = \frac{1}{r}\sqrt{1+(\kappa_c r)^2\left\{1-\zeta\mathcal{Z}+\lambda^2-\lambda-\ln\mathcal{Z}\left[2\lambda-1-\ln\mathcal{Z}\right]\right\}} \tag{2.14.68}$$

The angular momentum in CPC becomes

$$B_{\text{slip}} = \sqrt{1+(\kappa_c r)^2\left[\lambda-\ln\left(\sqrt{1+\zeta^2}-\zeta\right)+\zeta\sqrt{1+\zeta^2}-\zeta^2-1\right]} \tag{2.14.69}$$

$$B_{\text{no slip}} = \kappa_c r\sqrt{\lambda-\ln\left(\sqrt{1+\zeta^2}-\zeta\right)+\zeta\sqrt{1+\zeta^2}-\zeta^2-1} \tag{2.14.70}$$

$$B_{\text{slip}} = \sqrt{1+(r\kappa_c)^2\left(\mathcal{Z}_3-\mathcal{Z}_4\right)} \tag{2.14.71}$$

$$B_{\text{no slip}} = \kappa_c r\sqrt{\mathcal{Z}_3-\mathcal{Z}_4} \tag{2.14.72}$$

2.15 Alternate Solution and Swirl Number

If we begin with the BHE and set the RHS to a simple unknown constant

$$\frac{\partial^2\psi}{\partial R^2}+\frac{\sin\phi}{R^2}\frac{\partial}{\partial\phi}\left(\frac{1}{\sin\phi}\frac{\partial\psi}{\partial\phi}\right) = -C \tag{2.15.1}$$

We arrive at the same form of stream function and velocities

$$\psi = \tfrac{1}{2}CR^2\sin^2\phi\left(\lambda-\ln\Phi+\csc\phi\cot\phi-\csc^2\phi\right) \tag{2.15.2}$$

$$u_R = C\left[(\lambda-\ln\Phi)\cos\phi-1\right] \tag{2.15.3}$$

$$u_\phi = C\left[(\ln\Phi-\lambda)\sin\phi+\Phi\right] \tag{2.15.4}$$

$$u_\theta = \frac{1}{R\sin\phi}\sqrt{1+(CR\sin\phi)^2\left(\lambda-\ln\Phi-\Phi\csc\phi\right)} \tag{2.15.5}$$

$$u_r = -C\Phi \tag{2.15.6}$$

$$u_z = C\left(\lambda-\ln\Phi-1\right) \tag{2.15.7}$$

$$\psi = \tfrac{1}{2}Cr^2\left(\lambda-\ln Z-Z\sqrt{1+\zeta^2}\right) \tag{2.15.8}$$

$$u_R = C\left[\left(\zeta/\sqrt{1+\zeta^2}\right)\left(\lambda-\ln\mathcal{Z}\right)-1\right] \tag{2.15.9}$$

$$u_\phi = -C\left[\left(\lambda-\ln\mathcal{Z}\right)/\sqrt{1+\zeta^2}-\mathcal{Z}\right] \tag{2.15.10}$$

$$u_\theta = \frac{1}{r}\sqrt{1+(rC)^2\left(\lambda-\ln\mathcal{Z}-\mathcal{Z}\sqrt{1+\zeta^2}\right)} \tag{2.15.11}$$

$$u_r = -C\mathcal{Z} \tag{2.15.12}$$

$$u_z = C\left(\lambda-\ln\mathcal{Z}-1\right) \tag{2.15.13}$$

In order to get the final constant a method from Vyas and Majdalani may be used which examines the incoming and outgoing flow rates.

$$Q_i = 2\pi\int_0^b u_z r\mathrm{d}r = UA_i \tag{2.15.14}$$

which produces

$$UA_i = \pi C r^2 \left(\lambda + \sqrt{1+\zeta^2} - \ln \mathcal{Z} - 1\right) \tag{2.15.15}$$

$$UA_i = \pi C b^2 \left[\lambda + \sqrt{1+\frac{L^2}{b^2}} - \ln\left(\sqrt{1+\frac{L^2}{b^2}} - \frac{L}{b}\right) - 1\right] \tag{2.15.16}$$

Partial normalization gives

$$UA_i = \pi C a^2 X_\beta^2 \left[\lambda + \sqrt{1+\frac{l^2}{X_\beta^2}} - \ln\left(\sqrt{1+\frac{l^2}{X_\beta^2}} - \frac{l}{X_\beta}\right) - 1\right] \tag{2.15.17}$$

$$C = \frac{UA_i}{\pi a^2 X_\beta^2 \left[\lambda + \sqrt{1+\cot^2\beta} - \ln\left(\sqrt{1+\cot^2\beta} - \cot\beta\right) - 1\right]} \tag{2.15.18}$$

The velocity U transfers to the stream function equation, which drops out due to normalization. The constant now becomes

$$C = \left\{\pi\sigma X_\beta^2 \left[\lambda + \csc\beta - \ln\left(\csc\beta - \cot\beta\right) - 1\right]\right\}^{-1} \tag{2.15.19}$$

$$C = \frac{1}{\pi \varsigma_c} \tag{2.15.20}$$

$$C = \varkappa_c \tag{2.15.21}$$

where

$$\varsigma_c = \sigma X_\beta^2 \left(\lambda + \csc\beta - \ln\Phi_\beta - 1\right) \tag{2.15.22}$$

The stream function and velocities in SPC now become

$$\psi = \tfrac{1}{2}\kappa_c R^2 \sin^2\phi\,(\lambda - \ln\Phi - \Phi\csc\phi) \tag{2.15.23}$$

$$u_R = \varkappa_c\left[(\lambda - \ln\Phi)\cos\phi - 1\right] \tag{2.15.24}$$

$$u_\phi = -\varkappa_c\left[(\ln\Phi - \lambda)\sin\phi + \Phi\right] \tag{2.15.25}$$

$$u_{\theta,\text{slip}} = \frac{1}{R\sin\phi}\sqrt{1 + (\varkappa_c R\sin\phi)^2\,(\lambda - \ln\Phi - \Phi\csc\phi)} \tag{2.15.26}$$

$$u_{\theta,\text{no slip}} = \varkappa_c\sqrt{\lambda - \ln\Phi - \Phi\csc\phi} \tag{2.15.27}$$

$$u_r = -\varkappa_c\Phi \tag{2.15.28}$$

$$u_z = \varkappa_c\,(\lambda - \ln\Phi - 1) \tag{2.15.29}$$

While the stream function and velocities in CPC emerge as

$$\psi = \tfrac{1}{2}\varkappa_c r^2\,(\mathcal{Z}_3 - \mathcal{Z}_4) \tag{2.15.30}$$

$$u_R = \varkappa_c\,(\mathcal{Z}_6 - 1) \tag{2.15.31}$$

$$u_\phi = -\varkappa_c\,(\mathcal{Z}_7 - \mathcal{Z}) \tag{2.15.32}$$

$$u_{\theta,\text{slip}} = \frac{1}{r}\sqrt{1 + (r\varkappa_c)^2\,(\mathcal{Z}_3 - \mathcal{Z}_4)} \tag{2.15.33}$$

$$u_{\theta,\text{no slip}} = \varkappa_c\sqrt{\mathcal{Z}_3 - \mathcal{Z}_4} \tag{2.15.34}$$

$$u_r = -\varkappa_c\mathcal{Z} \tag{2.15.35}$$

$$u_z = \varkappa_c\,(\mathcal{Z}_3 - 1) \tag{2.15.36}$$

This alternate swirl number allows for different theoretical calculations to be made in order to compare experimental and numerical data.

2.16 Vorticity

The vorticity is calculated from the previous equations in Section 1.3.3. Since the tangential velocity is required for several of the vorticity component equation calculations, two sets

of vorticity components are needed. One each for the slip and no slip cases. The vorticity components in SPC arise as

$$\omega_R = \frac{\kappa_c^2 \left(\Phi_1 \cos\phi - 1\right)}{\sqrt{1 + \left(\kappa_c R \sin\phi\right)^2 \left(\Phi_1 - \Phi_2\right)}} \tag{2.16.1}$$

$$\omega_\phi = -\frac{\kappa_c^2 \left(\Phi_1 \sin\phi - \Phi\right)}{\sqrt{1 + \left(\kappa_c R \sin\phi\right)^2 \left(\Phi_1 - \Phi_2\right)}} \tag{2.16.2}$$

$$\omega_\theta = \frac{\kappa_c}{R \sin\phi} \qquad \text{(slip)} \tag{2.16.3}$$

$$\omega_r = -\frac{\kappa_c^2 \Phi}{\sqrt{1 + \left(\kappa_c R \sin\phi\right)^2 \left(\Phi_1 - \Phi_2\right)}} \tag{2.16.4}$$

$$\omega_z = \frac{\kappa_c^2 \left(\Phi_1 - 1\right)}{\sqrt{1 + \left(\kappa_c R \sin\phi\right)^2 \left(\Phi_1 - \Phi_2\right)}} \tag{2.16.5}$$

$$\omega_R = \frac{\kappa_c \left(\Phi_1 \cos\phi - 1\right)}{\sqrt{\Phi_1 - \Phi_2}} \tag{2.16.6}$$

$$\omega_\phi = -\frac{\kappa_c \left(\Phi_1 \sin\phi - \Phi\right)}{\sqrt{\Phi_1 - \Phi_2}} \tag{2.16.7}$$

$$\omega_\theta = \frac{\kappa_c}{R \sin\phi} \qquad \text{(no slip)} \tag{2.16.8}$$

$$\omega_r = -\frac{\kappa_c \Phi}{\sqrt{\Phi_1 - \Phi_2}} \tag{2.16.9}$$

$$\omega_z = \frac{\kappa_c \left(\Phi_1 - 1\right)}{\sqrt{\Phi_1 - \Phi_2}} \tag{2.16.10}$$

In CPC, the vorticity components are written as

$$\omega_R = \frac{\kappa_c^2 (\mathcal{Z}_6 - 1)}{\sqrt{1 + (r\kappa_c)^2 (\mathcal{Z}_3 - \mathcal{Z}_4)}} \tag{2.16.11}$$

$$\omega_\phi = -\frac{\kappa_c^2 (\mathcal{Z}_7 - \mathcal{Z})}{\sqrt{1 + (r\kappa_c)^2 (\mathcal{Z}_3 - \mathcal{Z}_4)}} \tag{2.16.12}$$

$$\omega_\theta = \frac{\kappa_c}{r} \qquad \text{(slip)} \tag{2.16.13}$$

$$\omega_r = -\frac{\kappa_c^2 \mathcal{Z}}{\sqrt{1 + (r\kappa_c)^2 (\mathcal{Z}_3 - \mathcal{Z}_4)}} \tag{2.16.14}$$

$$\omega_z = \frac{\kappa_c^2 (\mathcal{Z}_3 - 1)}{\sqrt{1 + (r\kappa_c)^2 (\mathcal{Z}_3 - \mathcal{Z}_4)}} \tag{2.16.15}$$

$$\omega_R = \frac{\kappa_c (\mathcal{Z}_6 - 1)}{\sqrt{\mathcal{Z}_3 - \mathcal{Z}_4}} \tag{2.16.16}$$

$$\omega_\phi = -\frac{\kappa_c (\mathcal{Z}_7 - \mathcal{Z})}{\sqrt{\mathcal{Z}_3 - \mathcal{Z}_4}} \tag{2.16.17}$$

$$\omega_\theta = \frac{\kappa_c}{r} \qquad \text{(no slip)} \tag{2.16.18}$$

$$\omega_r = -\frac{\kappa_c \mathcal{Z}}{\sqrt{\mathcal{Z}_3 - \mathcal{Z}_4}} \tag{2.16.19}$$

$$\omega_z = \frac{\kappa_c (\mathcal{Z}_3 - 1)}{\sqrt{\mathcal{Z}_3 - \mathcal{Z}_4}} \tag{2.16.20}$$

After examination, a relation between the velocity and vorticity components is recognized. The components of velocity and vorticity amalgamate into the following properties for both slip and no slip tangential velocities:

$$\omega_R = \frac{\kappa_c}{r}\frac{u_R}{u_\theta} = \frac{\kappa_c}{R\sin\phi}\frac{u_R}{u_\theta} = \omega_\theta\frac{u_R}{u_\theta} = u_R\frac{\omega_\theta}{u_\theta} \tag{2.16.21}$$

$$\omega_\phi = \frac{\kappa_c}{r}\frac{u_\phi}{u_\theta} = \frac{\kappa_c}{R\sin\phi}\frac{u_\phi}{u_\theta} = \omega_\theta\frac{u_\phi}{u_\theta} = u_\phi\frac{\omega_\theta}{u_\theta} \tag{2.16.22}$$

$$\omega_r = \frac{\kappa_c}{r}\frac{u_r}{u_\theta} = \frac{\kappa_c}{R\sin\phi}\frac{u_r}{u_\theta} = \omega_\theta\frac{u_r}{u_\theta} = u_r\frac{\omega_\theta}{u_\theta} \tag{2.16.23}$$

$$\omega_z = \frac{\kappa_c}{r}\frac{u_z}{u_\theta} = \frac{\kappa_c}{R\sin\phi}\frac{u_z}{u_\theta} = \omega_\theta\frac{u_z}{u_\theta} = u_z\frac{\omega_\theta}{u_\theta} \tag{2.16.24}$$

The ratio of the vorticity components to the corresponding velocity are shown to be equal. The vorticity-velocity ratio also reduces to a simple relation between the swirl parameter and swirl function.

$$\frac{\omega_R}{u_R} = \frac{\omega_\phi}{u_\phi} = \frac{\omega_\theta}{u_\theta} = \frac{\omega_r}{u_r} = \frac{\omega_z}{u_z} \tag{2.16.25}$$

$$\frac{\omega_j}{u_j} = \frac{\kappa_c}{u_\theta r} = \frac{\kappa_c}{u_\theta R\sin\phi} = \frac{\kappa_c}{B(\psi)} \tag{2.16.26}$$

$$\omega_R = \kappa_c\frac{u_R}{B(\psi)} = \frac{\kappa_c}{B(\psi)}u_R \tag{2.16.27}$$

$$\omega_\phi = \kappa_c\frac{u_\phi}{B(\psi)} = \frac{\kappa_c}{B(\psi)}u_\phi \tag{2.16.28}$$

$$\omega_r = \kappa_c\frac{u_r}{B(\psi)} = \frac{\kappa_c}{B(\psi)}u_r \tag{2.16.29}$$

$$\omega_z = \kappa_c\frac{u_z}{B(\psi)} = \frac{\kappa_c}{B(\psi)}u_z \tag{2.16.30}$$

$$\omega_j = \frac{\kappa_c}{B(\psi)}u_j \tag{2.16.31}$$

The vorticity vector emerges as

$$\boldsymbol{\omega} = \frac{\kappa_c}{R\sin\phi}\frac{u_R}{u_\theta}\mathbf{e}_R + \frac{\kappa_c}{R\sin\phi}\frac{u_\phi}{u_\theta}\mathbf{e}_\phi + \frac{\kappa_c}{R\sin\phi}\mathbf{e}_\theta \tag{2.16.32}$$

$$\boldsymbol{\omega} = \frac{\kappa_c}{r}\frac{u_r}{u_\theta}\mathbf{e}_r + \frac{\kappa_c}{r}\mathbf{e}_\theta + \frac{\kappa_c}{r}\frac{u_z}{u_\theta}\mathbf{e}_z \tag{2.16.33}$$

The ratio between the vorticity vector and velocity vector differs by an eigenvalue. Thus, the flow field type is confirmed to be of the Beltramian or helical flow type (Wu et al. 2006). The vorticity-velocity vector ratio appears as

$$\boldsymbol{\omega} = \frac{\kappa_c}{B(\psi)}\mathbf{u} \tag{2.16.34}$$

The vorticity magnitude in SPC calculates as

$$|\omega| = \frac{\kappa_c}{R\sin\phi}\sqrt{1 + \left[\frac{\kappa_c}{B(\psi)}\right]^2 \left[(\lambda - 2 - \log\Phi)(\lambda - \log\Phi) + 2\Phi\csc\Phi\right]} \tag{2.16.35}$$

or in condensed forms

$$|\omega| = \frac{\kappa_c}{R\sin\phi}\sqrt{1 + \left[\frac{\kappa_c}{B(\psi)}\right]^2 \left[\Phi_1^2 - 2(\Phi_2 - \Phi_1)\right]} \tag{2.16.36}$$

The vorticity magnitude in CPC becomes as

$$|\omega| = \frac{\kappa_c}{r}\sqrt{1 + \left[\frac{\kappa_c}{B(\psi)}\right]^2 \left[\mathcal{Z}_3^2 - 2(\mathcal{Z}_4 - \mathcal{Z}_3)\right]} \tag{2.16.37}$$

2.17 Pressure

From the equations in Section 1.3.3, the pressure differentials are calculated (see Appendix D for more detailed mathematics).

$$\frac{\partial p}{\partial R} = \frac{\kappa_c^2}{R}\{(\lambda - \ln\Phi) + \Phi\cot\phi - (\lambda - \ln\Phi)^2 + [(\lambda - \ln\Phi)\cos\phi - 1]^2 - 1\} \tag{2.17.1}$$

$$\frac{\partial p}{\partial \phi} = \frac{1}{R^2\sin^2\phi}\left\{\cot\phi + (\kappa_c R\sin\phi)^2\left[(\lambda - \ln\Phi)\csc\phi - \Phi\csc^2\phi\right]\right\} \tag{2.17.2}$$

$$\frac{\partial p}{\partial r} = \frac{r\sqrt{1+\frac{z^2}{r^2}} + \kappa_c^2\left\{z^2 r\sqrt{1+\frac{z^2}{r^2}} - z^3 + \frac{zr^2\left[\lambda - \ln\left(\sqrt{1+\frac{z^2}{r^2}} - \frac{z}{r}\right) - 1\right]}{r^4\sqrt{1+\frac{z^2}{r^2}}}\right\}}{r^4\sqrt{1+\frac{z^2}{r^2}}} \tag{2.17.3}$$

$$\frac{\partial p}{\partial z} = \kappa_c^2\left\{\frac{z^2 - zr\sqrt{1+\frac{z^2}{r^2}} - r^2\left[\lambda - \ln\left(\sqrt{1+\frac{z^2}{r^2}} - \frac{z}{r}\right) - 1\right]}{r^3\sqrt{1+\frac{z^2}{r^2}}}\right\} \tag{2.17.4}$$

$$\frac{\partial p}{\partial R} = \frac{\kappa_c^2}{R}\left[\Phi_1 + \Phi\cot\phi - \Phi_1^2 + (\Phi_1\cos\phi - 1)^2 - 1\right] \tag{2.17.5}$$

$$\frac{\partial p}{\partial \phi} = \frac{1}{R^2\sin^2\phi}\left[\cot\phi + (\kappa_c R\sin\phi)^2(\Phi_1\csc\phi - \Phi_2\csc\phi)\right] \tag{2.17.6}$$

$$\frac{\partial p}{\partial r} = \frac{\mathcal{Z}_2}{r^3} + \kappa_c^2\frac{\mathcal{Z}_2}{r}\left[\zeta^2\mathcal{Z}_1 - \zeta^3 + \zeta\mathcal{Z}_2(\mathcal{Z}_3 - 1)\right] \tag{2.17.7}$$

$$\frac{\partial p}{\partial z} = \kappa_c^2\frac{\mathcal{Z}_2}{r}\left(\zeta^2 - \zeta\mathcal{Z}_1 - \mathcal{Z}_3 + 1\right) \tag{2.17.8}$$

Taking the normalized p_0 as our baseline at the inlet of the cone where $(r, z) = (1, \cot\alpha)$, Eq. (2.17.3) and Eq. (2.17.4) may be partially integrated to yield, $\Delta p(\alpha) = p(\alpha) - p_0(\alpha)$, where p_0 may be correlated to the cone geometry according to Table 2.2. One deduces

$$p(r,z) = -\frac{1}{2r^2} + \frac{1}{2}\kappa_c^2\left[\left(\zeta + \zeta^3\right)/\sqrt{1+\zeta^2} - \zeta^2 - \ln^2 \mathcal{Z} - (2\lambda - 1)\ln\left(\mathcal{Z} + 2\zeta\right)\right] \quad (2.17.9)$$

Table 2.2: Pressure constant p_0 versus α with $\sigma_c = 1$.

α	p_0	α	p_0
5°	50.32	50°	3.48
10°	31.15	55°	2.53
15°	22.04	60°	1.73
20°	16.49	65°	1.07
25°	12.68	70°	0.522
30°	9.88	75°	0.091
35°	7.73	80°	0.226
40°	6.02	85°	-0.429
45°	4.63	90°	-0.500

Likewise, the same procedure concludes that the no slip tangential velocity pressure terms appear as

$$p(r,z)_{\text{no slip}} = \frac{1}{2}\kappa_c^2\left[\left(\zeta + \zeta^3\right)/\sqrt{1+\zeta^2} - \zeta^2 - \ln^2 \mathcal{Z} - (2\lambda - 1)\ln\left(\mathcal{Z} + 2\zeta\right)\right] \quad (2.17.10)$$

2.18 Reconstruction of Bloor and Ingham's Analysis (1987)

The basis of this dissertation is inspired by two original analyses for the fluid dynamic flow of a BDV in a conical geometry, one by Bloor and Ingham (1987) and the other by Zhao and Abrahamson (1999). The findings of this dissertation improve the solutions of Bloor and Ingham (1987) and Zhao and Abrahamson (1999) by demonstrating *concise* and

straightforward analysis which advances the understanding of the fluid dynamics regarding BHE flows and expands the family of solutions by Majdalani et al (Saad et al. 2006; Vyas and Majdalani 2006; Maicke and Majdalani 2008b; Majdalani 2012) and others (Hill 1894; Hicks 1899; Fraenkel 1956; Yih 1959; O'Brien 1961; Moffatt 1969; Gostintsev et al. 1971; Duda and Vrentas 1972; Yarmitskii 1992). Thus, distinguishing between previous studies and the current one is imperative.

Again, the formulation and method to obtain the full solution for the stream function remain similar. However, it is at this juncture that an obvious difference appears between the solution of presented in Section 2.11 and the solution by Bloor and Ingham (1987). Within the publication by Bloor and Ingham (1987), the stream function solution appears as

$$\psi = \sigma_{BI} R^2 \left\{ \left[\lambda_{BI} - \ln\left(\frac{1}{2}\tan\phi\right) \right] \sin^2\phi + \cos\phi - 1 \right\} \tag{2.18.1}$$

The discrepancy manifests as the difference between $\tan(\phi/2)$ and $(1/2)\tan\phi$. At first glance, this looks like it could simply be a typographical error. However, the typo propagates throughout the paper from this point forward. The typo also appears in the constant, $\lambda_{BI} = \ln\left[\left(\frac{1}{2}\right)\tan\alpha\right]\sin^2 - \csc\alpha\cot\alpha$, where the discrepancy is between $\tan(\alpha/2)$ and $(1/2)\tan\alpha$. This is even more confusing as what exactly happened at this point in the analysis by Bloor and Ingham (1987). Another possibility (and most probable) arises in an approximation where for small angles it is assumed that $\tan(\phi/2) \approx \phi/2$. Back substitution allows for $\phi \approx \tan\phi$ and thus $\tan(\phi/2) \approx (1/2)\tan\phi$. A residual between the two stream functions is calculated as

$$\frac{1}{2}\pi\sigma_c\left(2\cos\phi - \sec^2\phi - 3\right) = -\pi\sigma_c \tag{2.18.2}$$

Next Bloor and Ingham (1987) determine the constant, σ_{BI} by assuming that $\psi = \psi_f = 1$ at the vortex finder of the cyclone at the coordinates $R = R_f$ and $\phi = \phi_f$. The reason for this approximation is because W is not known beforehand. Bloor and Ingham (1987) give the approximation of $\phi_f \approx \frac{1}{5}\alpha$ claiming that this is typical the location in practice (no

reference is given to back this up). The equation of the vortex finder streamline given by Bloor and Ingham (1987) appears as

$$1 = \sigma_{BI} R_f^2 \left\{ K_1 \sin^2 \phi_f - \sin^2 \phi_f \left[\ln \left(\tfrac{1}{2} \tan \phi_f \right) \right] + \cos \phi_f - 1 \right\} \tag{2.18.3}$$

Several typos appear within the vortex finder equation in the investigation by Bloor and Ingham (1987). One is the possible misplaced 1/2 of unknown origin within the logarithmic-tan function, and another involves the placement of the constant K_1. In the previous equation by Bloor and Ingham (1987), the general stream function, the constant σ_{BI} appears outside the braces as in the vortex finder stream function equation. However, the typographical differences consist of the comparison of the general stream function where $K_1/\sigma_{BI} = \lambda$ appears inside the braces and the vortex finder streamline whereas only σ_{BI} appears inside of the braces and only on one term. Thus, the equation in correct form is

$$1 = \sigma_{BI} R_f^2 \left\{ \lambda_{BI} \sin^2 \phi_f - \sin^2 \phi_f \left[\ln \left(\tfrac{1}{2} \tan \phi_f \right) \right] + \cos \phi_f - 1 \right\} \tag{2.18.4}$$

Bloor and Ingham (1987) go on to derive the velocities as

$$\bar{u}_\theta / U = u_\theta = \frac{1}{R \sin \phi} \sqrt{1 - \frac{Q^2 \sigma_{BI} \psi}{(\pi a U)^2}} \tag{2.18.5}$$

$$u_R = 2 \cos \phi - 2\sigma_{BI} \left[\cos \phi \ln \left(\tfrac{1}{2} \tan \phi \right) \right] \tag{2.18.6}$$

$$u_\phi = \frac{2\psi}{\sin 2\phi} \tag{2.18.7}$$

In order to verify the analysis by Bloor and Ingham (1987), an attempt is made to reproduce the results in the next chapter. However, the looming possible typos mentioned earlier put the velocities in question. The tangential velocity is noted as the velocity most in question since there exist a negative sign under the square root. Again, a simple negative sign and

orientation of the axis could be the answer to clear the confusion. However, Bloor and Ingham (1987) leave out much detail in their analysis making verification difficult.

Chapter 3

The Beltramian Conical Bidirectional Vortex (BDV): Results and Discussion

3.1 Mantle Location & Streamlines

3.1.1 Mantle Location Background & History

The mantle location denotes the locus in the swirling flow field where there exists a changeover in direction in the downward-upward velocities. Mantle identifications occur in devices and setups such as the cylindrical BDV (Batterson et al. 2007; Majdalani 2007; Maicke and Majdalani 2008a; Saad and Majdalani 2008; Akiki and Majdalani 2010), cyclone separators Bhattacharyya (1980a), swirling nozzle flow (Binnie and Teare 1956), and swirling pipe flow (Nuttall 1953; Gore and Ranz 1964; Escudier et al. 1980). According to Bradley and Pulling (1959) (see also Bradley 1965) one of the earliest mentions of the term "mantle" dates back to Binnie and Teare (1956). The flow reversal and cylindrical mantle experienced by Binnie and Teare (1956) and Bradley and Pulling (1959) relates closely to vortex breakdown for swirling flow in a diverging tube (Leibovich 1978) and cylindrical tube (Bottaro et al. 1991). Recirculating zones in swirling free jets (Gore and Ranz 1964) and general swirling pipe flows (Nissan and Bresan 1961; King et al. 1969; Lavan et al. 1969; Escudier et al. 1980; Vakili et al. 1996) also experience flow reversals

(all discussed later). Discrepancy and similarity between the mantle description by Binnie and Teare (1956) and Bradley and Pulling (1959) and cyclone separators location of zero vertical velocity (Bradley 1965; Bhattacharyya 1980a) are also reviewed.

First, the study of an experiment on the swirling flow in a circular tube and unexpected axial flow reversal is revisited. In 1953 Nuttall wrote a brief article in *Nature* entitled "Axial Flow in a Vortex." Nuttall (1953) reported how an unexpected flow reversal appeared around the long axis of the pipe for some cases of swirl and discharge rates. The experimental apparatus consisted of 2 and $^{7}/_{8}$ inch inside diameter of Perspex pipe. The pipe was mounted vertically topped by a cylindrical tank. Swirl was induced through a ring of guide vanes. Discharge rates were governed by a throttle at the end of the 56 inch long tube and inflow into the tank to retain a constant free surface level. The throttling devices utilized ranged from a circular orifice, a divergent cone which ended attached to a flat plate with an orifice, an annular orifice, and more. The intent for the experiment generated an average axial velocity of $1.5\,m/s$ and $Re = 3 \times 10^4$. Nuttall (1953) did not record any velocity measurements. Nuttall, instead, injected dye to highlight the fluid trajectories. Nuttall (1953) made the following observations about the flow structure for various flow conditions utilizing the dye injection for visualization. Low swirl produced lower than maximum axial velocity at the center of the pipe as demonstrated in Nuttall (1953) by curve **a**. An increase in swirl caused the axial velocity to become negative around the centerline of the tube as shown in curve **b**. Finally, for even higher swirl rates the axial velocity profile transformed into a positive direction near the centerline while a positive region existed in an annular fashion between the centerline and pipe wall, curve **c**. The annular region noted by Nuttall (1953) is a possible first, if not, very early indication of an annular mantle region similar to the observations of Binnie and Teare (1956) and Bradley and Pulling (1959). Some notes made by Nuttall (1953) included that only the annular and circular exit orifices (no details given) reproduced curve **c** while the transfer from **b** and **c** took place with the circular orifice at lower swirl rates. Nuttall (1953) concluded that

> "So far no satisfactory explanation of this phenomenon has been found. It seems to be related to the reverse flow at the centre of a Ranque-Hilsch vortex tube, although no thermal effects are present in this case."

Binnie (1957) later labeled curves, **a**, **b**, and **c**, as "Regime I", "Regime II", and "Regime III," respectively. The experimental method of a rotating portion of the pipe utilized by Binnie (1957) differed from the tangential feed injection of Nuttall (1953).

The Ranque-Hilsch vortex tube explains the flow reversal much more naturally since an upper exit port exists which allows for the gas or liquid that does not exit at the bottom to reverse direction and emerge from the top outlet. The Ranque-Hilsch tube is a form of the BDV as seen in cyclone separators (Barth 1956; Bloor and Ingham 1973a; Boysan et al. 1982; Bloor and Ingham 1983; Bhattacharyya 1985; Dabir and Petty 1986; Brayshaw 1990; Castro et al. 1996; Chiné and Concha 2000; Bergström and Vomhoff 2007) and the BDV rocket engines (Majdalani 2007, 2009; Saad 2010; Akiki 2011; Maicke 2012). However, for the case of "unidirectional" vortex flow through a tube or nozzle, the flow reversal stumped early researchers as to why the axial velocity sometimes became negative in direction to the outlet. Additional studies have also examined and experienced flow reversal for unidirectional swirling pipe flow including those by Binnie (1957), Nissan and Bresan (1961), King et al. (1969), Bottaro et al. (1991). Flow reversal also occurred for studies with unidirectional swirling flows in diverging and/or converging pipes or nozzles (Binnie and Teare 1956; Binnie et al. 1957; Gore and Ranz 1964; So 1967; Chow 1969). Vortex breakdown also plays a large role related to swirling flows and recirculation zones (flow reversal) (see Harvey (1962), Sarpkaya (1971), Syred et al. (1975), Faler and Leibovich (1977), Faler and Leibovich (1978), Brücker and Althaus (1992), Delery (1994), Brücker (2002)). The key to flow reversal in the axial velocity profile depends upon swirl rates (Nissan and Bresan 1961; Lavan et al. 1969).

Next the experiment and observations (especially flow reversal and mantle recordings) by Binnie and Teare are discussed swirling flow of water in a pressure nozzle and "open trumpet." In 1956, Binnie and Teare publish a paper over the hydrodynamic examination

of a pressure nozzle by Binnie and Teare (1956) which is motivated by the relation to the applications of swirl atomizers (see Taylor 1950; Binnie and Harris 1950; Som and Mukherjee 1980b,a). Swirl atomizers find relevance in dispersing oil in furnaces and combustion chambers of gas turbines. One occurrence of swirl atomizers is the generation within the liquid medium of a gaseous core which engenders from atmospheric or exit boundary conditions (usually air).

Binnie and Teare (1956) undertake the hydraulic investigation at the Engineering Laboratory in Cambridge, England. The objective aims to effectively measure the pressure and velocity distributions with a converging nozzle as water exits under pressurized conditions. A second experiment analyzed the flow field under gravity as it flows from a reservoir into a vertical pipe with an open trumpet entrance. Since the nozzle was large in scale compared to typical swirl atomizers, Binnie and Teare (1956) were able to utilize devices to examine the flow field. For the pressurized nozzle flow, water entered the nozzle from a cylindrical tank 4 feet in diameter and 4 feet 6 inches high. The nozzle connected to the bottom of the center of the tank. Binnie and Teare (1956) introduced water into the tank in one of two ways. The first consisted of a swirl-free feed of water which was introduced into the the top-center of the tank from a vertical pipe. As the water entered the tank a horizontal baffle plate redirected the water away from the middle of the tank. The second method for water to be supplied to the tank included two horizontal pipes symmetrically attached tangentially near the top of the reservoir. The amalgamation of the tangential pipes and baffle plate allowed Binnie and Teare (1956) to control a range of swirl and pressure parameters for the experiment. A bleed system was devised in order to increase the flow through the reservoir and, in turn, increase the upper limit of swirl produced at the inlet of the nozzle. The bleed system was made by securing a brass volute chamber in between the nozzle and bottom of the cylindrical chamber.

Binnie and Teare (1956) noted that,

> "In the course of the experiments it was discovered that a boundary layer of forced vortex motion existed on the free surface at the core, and that when

> the swirl was sufficiently great compared with the supply pressure, **the axial component of velocity was reversed in the upper part of the nozzle**."

Figures from Binnie and Teare (1956) show both flow properties experienced. One photo in particular reveals a highly helical flow structure near the air core as highlighted by the dye injection. The inked helical filament winds tightly around the core with a nearly constant pitch and remains visible for a distinct distance with little diffusion into the surround flow structure. Binnie and Teare (1956) note that the naked eye distinguished a longer, more visible helical filament than the photograph shows. The definition of the helical filament implies that there exists solid-body rotation (SBR) near the air core boundary, a departure from inviscid theory. If the tangential velocity experienced rates which varied inversely with the radius, the high shear stresses would have disintegrated the dye particles more quickly.

Binnie and Teare (1956) expounded that in order to achieve flow reversal the device required full bleed, strong swirl, and steady pressure heads less than 7 feet. The flow reversal recessed as the head increased. Binnie and Teare (1956) comment that

> "...the largest zone of reverse flow that was seen when the supply was kept constant constant and the interior of the nozzle was fully explored; under other conditions the zones did not extend so far down the nozzle and their outer diameters were less."

However, Binnie and Teare (1956) additionally explain that further experiments confirmed that device setup does not always determine flow reversal conditions. Binnie and Teare (1956) described in their own words how different apparatus arrangements produced flow reversal as

> "At first it was found impossible to obtain reverse flow without the bleed in operations, but the reservoir was connected to a pump giving five times the normal maximum supply pressure, and a very strong vortex was obtained with full bleed. After the supply and bleed had been cut off, the head fell to 6 feet

> and the swirl was sufficiently powerful for reverse for to appear. It persisted even when the level in the reservoir fell below the baffle plate, the uncovering which was accompanied by a change in the wave pattern on the core. Under some conditions the existence of inward radial motion within the reservoir was detected. A large injection of permanganate solution into the zone of reverse flow was carried up into the reservoir, whence it reappeared moving uniformly downwards in the forced vortex region close to the core; and after the last injected fluid had vanished upwards, the colour near the core gradually decreased in intensity but was still visible 20s later. ”

Next, curious of the unusual and unexpected axial flow reversal, Binnie and Teare (1956) expanded the experiment to consist of an open circular tank where water could flow out of a central vertical pipe under the influence of gravity (generally called an open trumpet; see Binnie and Hookings 1948). The reasoning behind the additional apparatus by Binnie and Teare (1956) was due to the more perceptible flow properties near the core. The water tank for the open trumpet measured 5 feet in diameter and 3 feet tall. Four tangential inlets fed water into the reservoir where the swirling water exited through a 1 inch vertical pipe. A conical Perspex trumpet measuring 8.4 inches high and 5.9 inches in maximum width attached to the opening of the vertical pipe. An annular area around the pipe at the bottom of the experimental chamber let water escape which crafted the boundary layer bleed system for the open trumpet experiment.

Again, the axial reversion occurred within the tank. Figures, as described by Binnie and Teare (1956), capture the flow reversal and the mantle. Binnie and Teare (1956) mentioned that the same flow reversal has been recorded by Nuttall (1953) for swirling water flow in a pipe under certain circumstances (previously discussed). Binnie and Teare (1956) remarked that reverse flow even occurred under weak swirl conditions for the open trumpet setup. For low swirl conditions, the “feebile” vortices were seen when there was no bleed and with a throttled outlet pipe, which restricted the throat of the open trumpet to dictate

the flow dynamics. A "free outlet" allowed for increased vortex strength where reverse flow consistently appeared indubitably.

However, another mysterious phenomena occurred in which Binnie and Teare (1956) described the motion as

> "The two effects, mentioned above, were seen again; and, in addition, it was found that the slow downward movement in the tank outside the forced vortex was sometimes concentrated into thin **cylindrical mantles** round the core."

Within these regions of observation by Binnie and Teare (1956), permanganate, introduced into the flow for visualization, gradually transversed downwards and formed a marked cylinder form. Binnie and Teare (1956), hence, called the cylindrical image a "mantle." Binnie and Teare (1956) commented their observations on the mantle as,

> "The cylinder faded very slowly and usually remained visible for several minutes. With a feeble vortex the edge of the mantle was indistinct, but at large swirls not only was the edge sharply defined but several mantles at different radii were formed."

Furthermore, Binnie and Teare (1956) cited that the mantles were "remarkably stable" and formed to the wave shapes mimicking the sinuous pattern of the air core. In one case, once the mantle appeared, Binnie and Teare (1956) ramped up the bleed causing the swirl to increase which resulted in a denser and larger mantle diameter.

Finally, the results of a dye visualization experiment with a hydrocyclone by Bradley and Pulling (1959) (also see the book by Bradley (1965) entitled *Hydrocyclones* for details on the experiment and much more) are discussed, especially flow reversal and mantle observations. The experiment consisted of transparent Perspex cyclones of 3 inch and $1^1/_2$ inch diameters. Existing pressure taps allowed for a methylene blue concoction to be injected through the walls of the cyclone apparatus. The experiment also recorded dye injection from the inlet feed. Bradley and Pulling (1959) designed the cyclone to be versatile with swappable feed, overflow, underflow, cone, and cylinder sections. The

overall flow feed remained at 30 liters per minute unless noted by Bradley and Pulling (1959).

One photo by Bradley and Pulling (1959) demonstrates the outer downward flow from dye injection in the feed. The dye fills most of the outer spiral but has not reached the inner upward spiral. A second photo highlights clearing of ink from outer flow as fresh feed displaces the previously injected dye. Some of the solution travels to the inner flow which elevates to the overflow at the top of the cyclone. An annular clear region also appear in photos by Bradley and Pulling (1959) where little to no inward radial flow exist leaving a dye free zone. Bradley and Pulling (1959) note that the annulus remains visible for 5 to 10 seconds after appearance. In contrast, another photo shows the stationary layer highlighted by the dye. Additionally, Bradley and Pulling (1959) demonstrate direct injection of dye penetrating the mantle zone, which remains very stable. At this point Bradley and Pulling (1959) call the annular "stationary layer" the "mantle," first attributed to Binnie and Teare (1956).

At this point, the author discusses in more detail the mantle and flow reversal regions for swirling pipe, nozzle, and fully BDV flow in order relieve any confusion. Binnie and Teare (1956) and Bradley and Pulling (1959) coined the term mantle which describes an annular cylindrical region with little or no crossflow in swirling flows. However, for clarity, the mantle and reverse flow regions vary a bit with different geometries. As has been discussed and demonstrated by many, (Nuttall 1953; Binnie 1957; Nissan and Bresan 1961; Gore and Ranz 1964; Escudier et al. 1980; Vakili et al. 1996; Mattner et al. 2002), for unidirectional (at least initially) swirling pipe flow several possibilities exist. At low swirl, Regime I dictates uniform and unidirectional swirling pipe flow. As the swirl increases, Regime II sees a reverse flow region where part of the axial flow reverses direction to the normal flow, usually occurring near the centerline. Finally, at certain swirl and flow parameters Regime III appears which profiles a second axial reversal so that the velocity near the centerline and wall reverts to a "positive" value while the annular region in between is in the opposite or "negative" direction. For "unidirectional" swirling cylindrical pipe and nozzle flows, the annular region in Regime III usually does not extend through the entire length of the device.

Instead the reversal zone is an "eddy" type flow which occupies a small section of the length of the pipe or nozzle (see Binnie and Teare (1956)). The eddy type flow can also be seen in the fully BDV flow as demonstrated by the results from Bradley and Pulling (1959). By a "fully BDV flow," the author is referring to such devices as the cyclone separator, BDV propulsion chamber, and the reverse vortex chamber by Mateveev et al (Matveev 2006) at Applied Plasma Technologies. An ideal fully BDV flow sees full flow reversal through the entire length of the device. Bradley and Pulling (1959) also confirm full flow reversal in their experiments. In one photo, Bradley and Pulling (1959) capture dye injection near the bottom of the outer vortex. The dye then diffuses into the reversed inner vortex, heading towards to top of the hydrocyclone. Another photo displays a direct dye injection into the inner vortex where a dark region of dye swirls upwards. Similarly in Majdalani (2012), streamline plots display how the outer and inner vortex reside in the entire chamber. The full length inner and outer vortices also enforces flow reversal throughout the cylinder. The streamlines convey an outer downward movement until the bottom wall restricts downward motion and forces the fluid back upwards into the middle of the chamber where it eventually exits at the outlet located at the top of the chamber. The same motion occurs in conical cyclones (setup similar to the cylinder BDV) which will be confirmed in Section 3.1.2. An actual cyclone separator usually contains an additional outlet at the bottom of the chamber. Thus, the outlet at the top of the chambers seems to promote the full BDV flow. Majdalani et al recently discuss the mantle location regarding BDV research (see (Vyas and Majdalani 2006; Majdalani 2007; Maicke and Majdalani 2008a; Saad and Majdalani 2008; Batterson et al. 2007; Akiki and Majdalani 2010, 2012; Maicke and Majdalani 2012a,b)). For the theoretical cases cited, the mantle pinpoints the locus of zero vertical velocity (LZVV), otherwise the location of axial velocity flow reversal. Again, for the Beltramian conical BDV, the mantle location acts in the same way as the cylindrical BDV, as shown in Section 3.1.2. The mantle in the cylindrical BDV by Majdalani et al extends to the bottom of the chamber forming a full double vortex. The closest image to this experimentally is in the open trumpet gravity driven hydraulic flow by Binnie and Teare (1956). Thus, a fully reversed flow, in order to see a fully developed annular mantle cylinder, does not always

require an "upper" outlet. Additionally, unidirectional vortices usually traverse longer lengths than a "forced" double vortex like the BDV chamber flow models of Majdalani et al. In turn, the unidirectional vortices undergo possible stability conditions which eventually evolve into vortex breakdown. Vortex breakdowns also produce recirculation zones which is a possible candidate for observations by Binnie and Teare (1956) and other researchers. The recirculation zones Binnie and Teare (1956) and others have discovered could also be related to flow separation such as forward and backward step configurations Thus, a wide range of geometry and flow conditions gives a wide range of results which makes swirling flow so enticing to analyze by researchers, regardless of the complexity of possible outcomes.

However, "secondary" flows can develop for actual cyclone separator devices, which seems to promote and eddy "mantle" flow and a conical "mantle" of LZVV. For the case of Bradley and Pulling (1959), the dye injections only highlighted a small cylindrical mantle region in the upper portion of the cyclone (which is very similar to Binnie and Teare (1956) swirling nozzle flow and thus Bradley and Pulling (1959) utilize the term mantle). Thus, from the findings by Bradley and Pulling (1959), the initial mantle zone only consisted of an eddy region. Diagrams in Bradley and Pulling (1959) show a completely circular eddy which occupies the upper portion of the hydrocyclone. The upper portion of the apparatus includes the cylindrical "cap" and part of the uppermost conical section. The eddy or mantle remains in a annular cylinder even as the lower part of the mantle extends into the conical section of the hydrocyclone. Other schematics in Bradley and Pulling (1959) and Bradley (1965) clearly illustrate the "short circuit" phenomena where part of the immediate inlet flow seeps around the vortex finder and exits before cycling through the cyclone. The defined eddy regions could be influenced by the usual vortex finder, which extends into a portion of the cylindrical section of the cyclone separator. The meridional recirculation zone near the vortex finder is similar to those found for flow separation from sudden expansions (or constrictions) and swirl burners. Theoretical models for BDV flows do not account for possible secondary flows such as corner eddies. However, some researchers do attempt to model recirculation zones (Yih 1959; Duda and Vrentas 1972).

Remarkably, certain flow conditions engender the formation of more than one mantle layer in swirling vortex flows, creating multiple mantles. Bradley and Pulling (1959) created multiple mantles in their hydrocyclone experiment. Multiple mantles were present for both the 9 degree and 20 degree conical section angles. However, according to Bradley and Pulling (1959), the multiple mantles appeared less intense in the 9 degree section compared to the distinct double mantle formation in the 20 degree conical section. Thus, multiple eddy circulations zones occupy the upper part of the hydrocyclone. Even before Bradley and Pulling (1959), evidence of multiple mantles came from comments made by Binnie and Teare (1956) suggesting multiple mantles forming during the open trumpet water experiment. Documentation of the evidence of multiple mantles emerged from hybrid vortex rocket tests by ORBITEC which exhibit concentric grooves etched in the solid fuel grain in a photo taken after a firing test Vyas et al. (2003c). The grooves are believed to be the result from several vortex flow reversals. Theoretical models also corroborate the existence of multiple mantles including the multi-cellular model of Sullivan (1959), Donaldson and Sullivan (1960), Kuo (1966), Bellamy-Knights (1970), Bellamy-Knights (1971), Kendall (1978), Vyas et al. (2003c), and Batterson and Majdalani (2010a). Other studies confirm multi-celled vortices such as meteorological studies by Ward (1972) and Mitsuta et al. (1987), a theoretical and numerical thesis investigation over the Donaldson-Sullivan vortex by Mickel (2000), an experiment of hydraulic swirling flow through a pipe by Vakili et al. (1996), and an experimental flow visualization of rotating fluid by Huang et al. (2008). Streamline plots by Vyas et al. (2003c) for the cylindrical complex lamellar BDV show flows with two, three, and four vortex cells, respectively.

Even though the mantle remains in cylindrical form and penetrates into the conical section (according to Bradley and Pulling 1959 from resulting photos), Bradley and Pulling (1959) and Bradley (1965) assume at some point that the mantle does eventually conform to a conical geometry to mimic the cone-shaped walls. Bradley and Pulling (1959) and Bradley (1965) denote that the turnover from a cylindrical geometric surface to a conical surface occurs at an axial location where the conical radius becomes 70% of the cylindrical (or maximum) diameter of the apparatus. Bradley and Pulling (1959) and Bradley (1965)

also determine the location of the annular mantle resides at the radial distance from the centerline of approximately 43% of the maximum diameter. In addition, an illustration by Bradley and Pulling (1959) names the cone-shaped limit as the "conical classification surface." Bradley (1965) also terms the ***conical classification surface*** as the "locus of zero vertical velocity" or "***LZVV***" (probably the first mention of the term, the LZVV, in the literature). Essentially, it will be shown that the mantle in the theoretical analysis of the Beltramian conical BDV is also at an angle originating from the apex similar to the cone wall.

Thus, figures by Bradley and Pulling (1959) and Kelsall (1952) appear to fuel confusion and discrepancy as to what the mantle consist of (cylindrical and/or conical) and where the mantle is located (all cylindrical and/or conical). The culprit to the foggy understanding of the mantle remains with conflicting evidence. A diagram by Bhattacharyya (1980a) of the flowfield of a hydrocyclone also conceives that the LZVV remains cylindrical and very close to the core throughout the entirety of the device. However, while the drawing by Bhattacharyya (1980a) may conflict with the drawing and analysis by Bradley and Pulling (1959), the photo by Bradley and Pulling (1959) shows similar flow physics, where it seems that the inner vortex is a thin cylindrical column as it is separated from the outer vortex. Others, such as Rietema (1961), Dietz (1981), Pericleous and Rhodes (1986), and Pericleous (1987), also depict the LZVV as cylindrical and very close to the core. On the contrary, many more, such as Kelsall (1952), Mikhaylov and Romenskiy (1974), Pervov (1974), Mothes and Löffler (1985), Luo et al. (1989), Zhou and Soo (1990), Griffiths and Boysan (1996), Peng et al. (2002), Derksen (2003) portray a zone of zero axial velocity as following a conical shape similar to the angled wall.

3.1.2 Mantle Location & Streamlines for the Beltramian BDV Conical Solution

The mantle location arises from the angle where either the spherical radial or axial velocity goes to zero. That is, the locations where only crossflow velocities, the colatitudinal and

radial velocities, exist. Two mantle locations appear in the conical geometry as a function of the colatitudinal angle ϕ. One mantle angle, β_R, corresponds to the location where the spherical radial velocity, u_R, equals zero and the other matches with the angle, β_z, where the axial velocity, u_z, goes to zero. The equations for the mantles engender from when the u_R and u_z are equated to zero and the angles are solved as the roots of the characteristic equation.

$$[\lambda - \ln(\tan\beta_R/2)]\cos\beta_R - 1 = 0 \tag{3.1.1}$$

$$\lambda - \ln(\tan\beta_z/2) - 1 = 0 \tag{3.1.2}$$

Tables 3.1–3.3 display information about each mantle location per half-angle of the conical wall. Table 3.1 lists the mantle angles for both β_R and β_z, the percentage of the mantle angles per the divergence half-angle, and the differences between the mantles in degrees and percentage. A few distinguishing items emerge from the data in Table 3.1. First, the percentage of β_R of the chamber wall angle remains close to constant at 60% over an α range of $5^\circ - 85^\circ$ while β_z varies from 60% to almost 95% of α over its range. The difference between β_R and β_z begins with very minute values of 0.01° and 0% for $\alpha = 5^\circ$ but grows to a difference of about 29° and 35% for $\alpha = 85^\circ$. The mantle differences become evident with Figure 3.1 and Figure 3.2. However, for small divergence half-angles (the conventional range for most practical cyclone separators seems to be $< 10^\circ$), both mantle angle percentages remain near 60%. Second, the importance for divulging both mantles arises from experimental and CFD studies of BV conical cyclones measuring u_z and not u_R, thus the LZVV term. The conical mantle in the spherical radial velocity gives a more natural "angle" since the spherical radial velocity equals zero along the direction of β_R while the axial velocity equals zero at its own mantle angle "pointing" in vertically downward" direction.

The second table, Table 3.2, displays the radial distance from the vertical axis of the inflection point of the spherical radial velocity mantle, β_R, for four axial ratios of z/L in

quarter lengths. Table 3.3 shows the same information as Table 3.2, except for the axial velocity mantle, β_z. Both Tables 3.2 and 3.3 also cover the range of divergence half-angles, α, from $5° - 85°$. Interestingly, the radial distance percentage ratio of the mantle in reference to the conical wall exhibits the opposite characteristics when comparing to the angle ratio percentages. The radial distance ratio percentage for b_R varies from 60.6% for $\alpha = 5°$ to 10.7% for $\alpha = 85°$. In contrast, radial distance ratio percentage for b_z only varies from 60.6% for $\alpha = 5°$ to 52.0% for $\alpha = 85°$.

Finally, Figure 3.3 plots the stream lines for the Beltramian conical BDV and the small half-angle approximation of Bloor and Ingham (1987). Note that the approximation by Bloor and Ingham (1987) does not capture the flow field of higher divergence half-angles.

3.2 Velocities

Figure 3.4 displays the spherical coordinate velocities of the spherical radial, u_R, and zenith, u_ϕ, components. Figure 3.4a plots the spherical radial component in cylindrical polar coordinates for a divergence half-angle of $\alpha = 45°$ and a modified conical swirl number of $\sigma_c = 1$ over four axial locations ($z/L = 1.00$, 0.75, 0.50, and 0.25) at quarter section lengths of the cone. Figure 3.4a plots the spherical radial component in cylindrical polar coordinates for an axial location of $z/L = 1.00$ and a modified conical swirl number of $\sigma_c = 1$ over divergence half-angles of $\alpha = 15°$, $30°$, $45°$, $60°$, and $75°$. Similarly, Figure 3.4c plots the spherical radial component in spherical polar coordinates for a modified conical swirl number of $\sigma_c = 1$ over divergence half-angles of $\alpha = 15°$, $30°$, $45°$, $60°$, and $75°$. Note from 2.13.17 and 2.13.18 that the spherical polar radial velocity and zenith velocity are both independent of the coordinate R and dependent only on the zenith angle variable, ϕ. For both a variation in four axial locations and a variation over five divergence half-angles, the spherical radial velocity component exhibits similarity everywhere, even in SPC. The general curve for the spherical radial velocity component begins at the highest axial magnitude in the downward direction and lowers in a somewhat linear fashion until the velocity reaches zero at the mantle inflection point of approximately

Table 3.1: Mantle angle location dependence on conical half-angle.

Conical Half-Angle, α	**Mantle Angle** β_R	**Mantle Position** $\beta_R/\alpha\,(\%)$	**Mantle Angle** β_z	**Mantle Position** $\beta_z/\alpha\,(\%)$	**Difference** (°) $\lvert\beta_R-\beta_z\rvert$	**Difference** (%) $\lvert\beta_R-\beta_z\rvert$
5°	3.03°	60.7	3.04°	60.7	0.01°	0.0
10°	6.06°	60.6	6.10°	61.0	0.04°	0.4
15°	9.09°	60.6	9.21°	61.4	0.13°	0.8
20°	12.12°	60.6	12.40°	62.0	0.28°	1.4
25°	15.15°	60.6	15.70°	62.8	0.55°	2.2
30°	18.16°	60.5	19.14°	63.8	0.98°	3.3
35°	21.18°	60.5	22.73°	64.9	1.55°	4.4
40°	24.18°	60.5	26.54°	66.4	2.39°	5.9
45°	27.18°	60.4	30.62°	68.0	3.44°	7.6
50°	30.17°	60.3	35.00°	70.0	4.83°	9.7
55°	33.15°	60.3	39.76°	72.3	6.61°	12.0
60°	36.12°	60.2	44.95°	74.9	8.83°	14.7
65°	39.07°	60.1	50.66°	77.9	11.59°	17.8
70°	42.01°	60.0	56.98°	81.4	14.97°	21.4
75°	44.93°	59.9	66.99°	85.3	22.06°	25.4
80°	47.83°	59.8	71.79°	89.7	24.15°	29.9
85°	50.71°	59.7	80.44°	94.6	29.73°	34.9

Table 3.2: Mantle radius location b_R dependence on conical half-angle with $a = 1$.

Conical Half-Angle	**Mantle Radius** $l_z = 0.25$	**Mantle Radius** $l_z = 0.50$	**Mantle Radius** $l_z = 0.75$	**Mantle Radius** $l_z = 1.00$	**Mantle Radius** %
α	b_R	b_R	b_R	b_R	b_R/r_{l_z}
5°	0.151	0.302	0.454	0.606	60.6
10°	0.151	0.301	0.452	0.602	60.2
15°	0.149	0.299	0.448	0.597	59.7
20°	0.148	0.295	0.443	0.590	59.0
25°	0.145	0.290	0.435	0.580	58.0
30°	0.142	0.284	0.426	0.568	56.8
35°	0.138	0.277	0.415	0.553	55.3
40°	0.134	0.268	0.401	0.535	53.5
45°	0.128	0.257	0.385	0.514	51.4
50°	0.122	0.244	0.366	0.488	48.8
55°	0.114	0.229	0.343	0.457	45.7
60°	0.105	0.211	0.316	0.421	42.1
65°	0.095	0.189	0.284	0.379	37.9
70°	0.082	0.164	0.246	0.328	32.8
75°	0.067	0.134	0.200	0.267	26.7
80°	0.049	0.097	0.146	0.195	19.5
85°	0.027	0.053	0.080	0.107	10.7

Table 3.3: Mantle radius location b_z dependence on conical half-angle with $a = 1$.

Conical Half-Angle	**Mantle Radius** $l_z = 0.25$	**Mantle Radius** $l_z = 0.50$	**Mantle Radius** $l_z = 0.75$	**Mantle Radius** $l_z = 1.00$	**Mantle Radius** %
α	b_z	b_z	b_z	b_z	b_z/r_{l_z}
5°	0.151	0.303	0.455	0.606	60.6
10°	0.151	0.303	0.454	0.606	60.6
15°	0.151	0.303	0.454	0.605	60.5
20°	0.151	0.302	0.453	0.604	60.4
25°	0.151	0.301	0.452	0.603	60.3
30°	0.150	0.300	0.451	0.601	60.1
35°	0.150	0.299	0.449	0.598	59.8
40°	0.149	0.298	0.447	0.595	59.5
45°	0.148	0.296	0.444	0.592	59.2
50°	0.147	0.294	0.441	0.588	58.8
55°	0.146	0.291	0.437	0.582	58.2
60°	0.144	0.288	0.432	0.576	57.6
65°	0.142	0.284	0.427	0.569	56.9
70°	0.140	0.280	0.420	0.560	56.0
75°	0.137	0.275	0.412	0.549	54.9
80°	0.134	0.268	0.402	0.534	53.4
85°	0.130	0.260	0.390	0.520	52.0

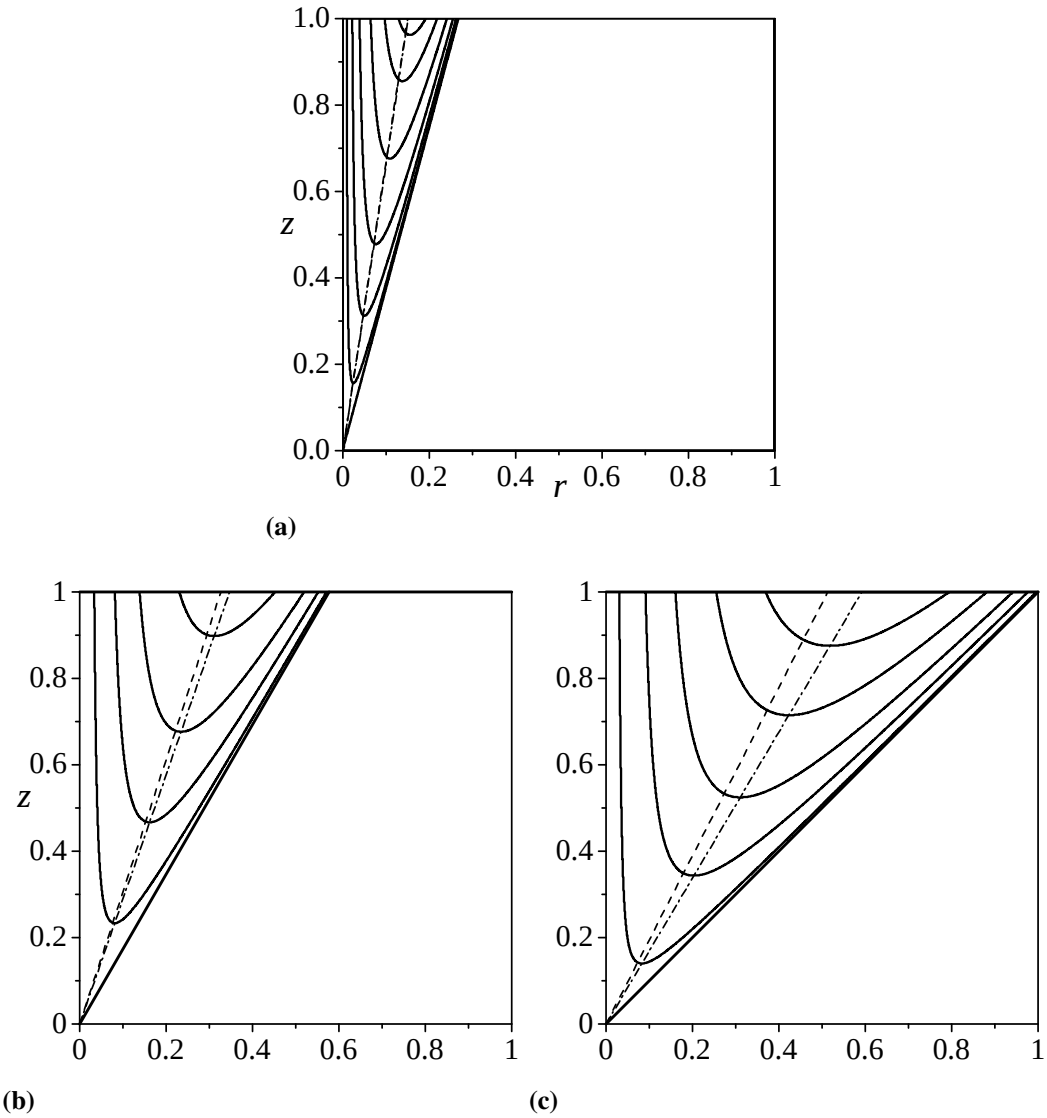

Figure 3.1: Streamlines of the Beltramian model for $\sigma_c = 1$ with the spherical radial velocity mantle, β_R, as $(- - -)$ and the axial velocity mantle, β_z, as $(- \cdot -)$. Plot (a) displays the divergence half-angle of $\alpha = 15°$ with values of $\beta_R = 9.09°$, $\beta_z = 9.21°$ and at the axial location of $z/L = 1$, $b_r = 0.597$ and $b_z = 0.605$. Plot (b) displays the divergence half-angle of $\alpha = 30°$ with values of $\beta_R = 18.16°$, $\beta_z = 19.14°$ and at the axial location of $z/L = 1$, $b_r = 0.568$ and $b_z = 0.601$. Plot (c) displays the divergence half-angle of $\alpha = 45°$ with values of $\beta_R = 27.18°$, $\beta_z = 30.62°$ and at the axial location of $z/L = 1$, $b_r = 0.514$ and $b_z = 0.592$.

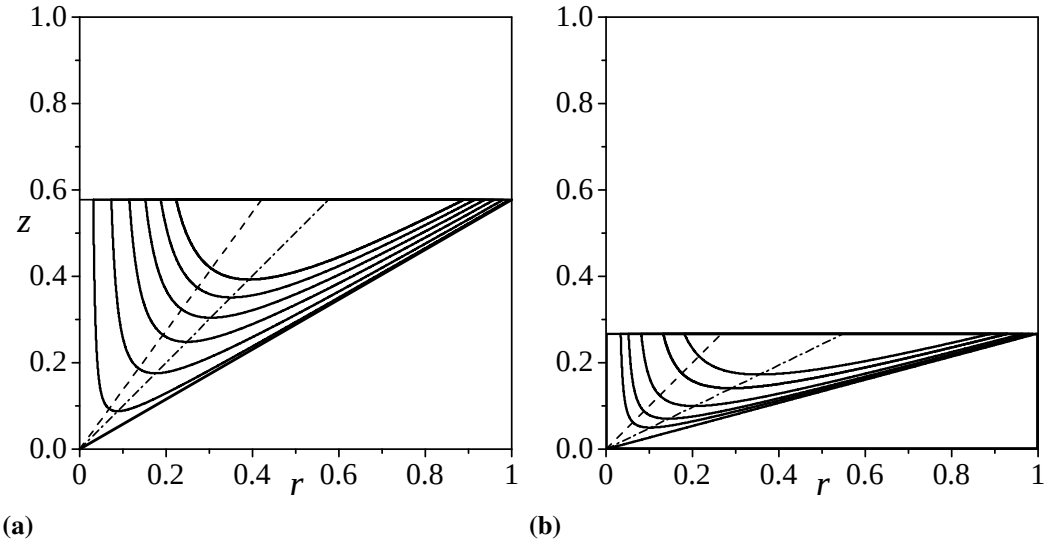

Figure 3.2: Streamlines of the Beltramian model for $\sigma_c = 1$ with the spherical radial velocity mantle, β_R, as $(- - -)$ and the axial velocity mantle, β_z, as $(- \cdot -)$. Plot (a) displays the divergence half-angle of $\alpha = 60°$ with values of $\beta_R = 36.12°$, $\beta_z = 44.95°$ and at the axial location of $z/L = 1$, $b_r = 0.421$ and $b_z = 0.576$. Plot (b) displays the divergence half-angle of $\alpha = 75°$ with values of $\beta_R = 44.93°$, $\beta_z = 66.99°$ and at the axial location of $z/L = 1$, $b_r = 0.267$ and $b_z = 0.549$.

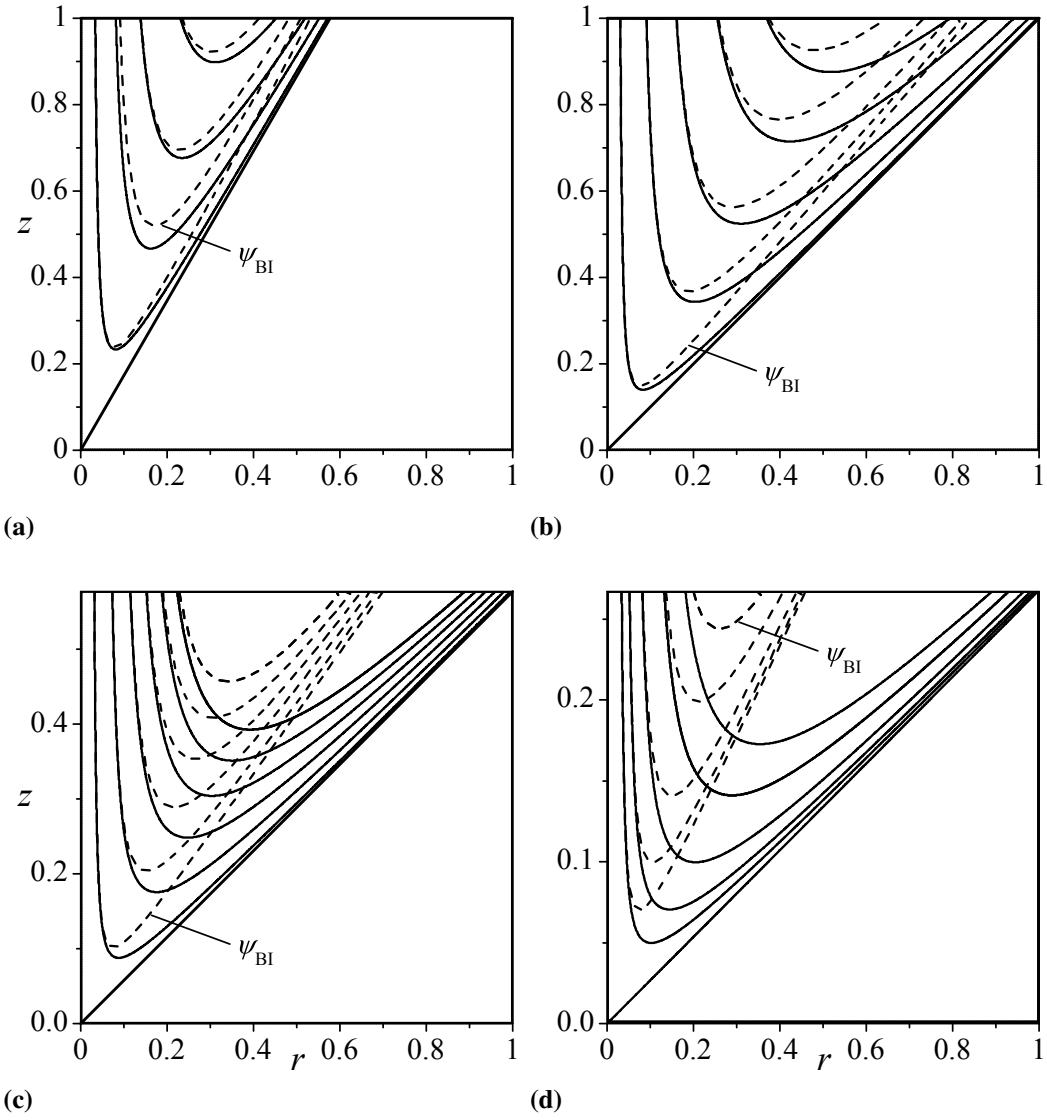

Figure 3.3: Streamlines of the Beltramian model, (——), as they compare with the small angle approximation model of Bloor and Ingham (1987), (– – –) for $\sigma_c = 1$. Plots are for the divergence half-angles of (a) $\alpha = 30°$, (b) 45°, (c) 60°, and (d) 75°, respectively.

60% of the chamber half-angle. The spherical radial velocity then curves drastically upwards in an inverse fashion as the radius approaches zero. Since the Beltramian model assumes an inviscid flow, the spherical radial velocity goes to infinity at $r = 0$. A viscous model similar to previous studies is expected to overcome the infinite spherical radial velocity at the core (Vyas et al. 2003b). An analysis of the sidewall viscous corrections is needed as well (Batterson and Majdalani 2010b).

Figure 3.4d portrays the zenith velocity graph counterpart as Figure 3.4a while Figure 3.4e mimics Figure 3.4b and Figure 3.4f mimics Figure 3.4c. Again, similarity is seen amongst the curves of each figure. For Figure 3.4d, the curves exhibit an asymmetric parabola. The negative magnitude indicates an inward direction. As the velocity component traverses the chamber radius at a set axial location, the magnitude increases from zero until it reaches a plateau. After reaching the maximum, the zenith velocity magnitude curves back, decreasing in magnitude, until the velocity reaches zero again at the centerline. Another curve characteristic for the zenith velocity in Figure 3.4d reveals that the maximum magnitude at each axial location remains the same for the given divergence half-angle.

Next, the radial, tangential, and axial velocities are plotted against experimental and numerical data. The experiments and numerical calculations derive from papers by Hsieh and Rajamani (1988) and Monredon et al. (1992). Both the data and cyclone separator configurations by Hsieh and Rajamani (1988) and Monredon et al. (1992) influenced the choices of the two studies. Another factor in choosing the articles by Hsieh and Rajamani (1988) and Monredon et al. (1992) is due to the fact that the experiments came from the same group at the University of Utah. Many cyclone separator articles in the literature do not provide very clear data relating to the velocities, especially in the conical section (Hoekstra et al. 1999). Most analyses focus on separation efficiency while the general fluid dynamics of the flow field goes uninvestigated (Leith and Licht 1972; Leith and Mehta 1973; Kessler and Leith 1991; Xiang et al. 2001; Peng et al. 2004). Some of the CS compositions make comparing the Beltramian model to corresponding data difficult (see

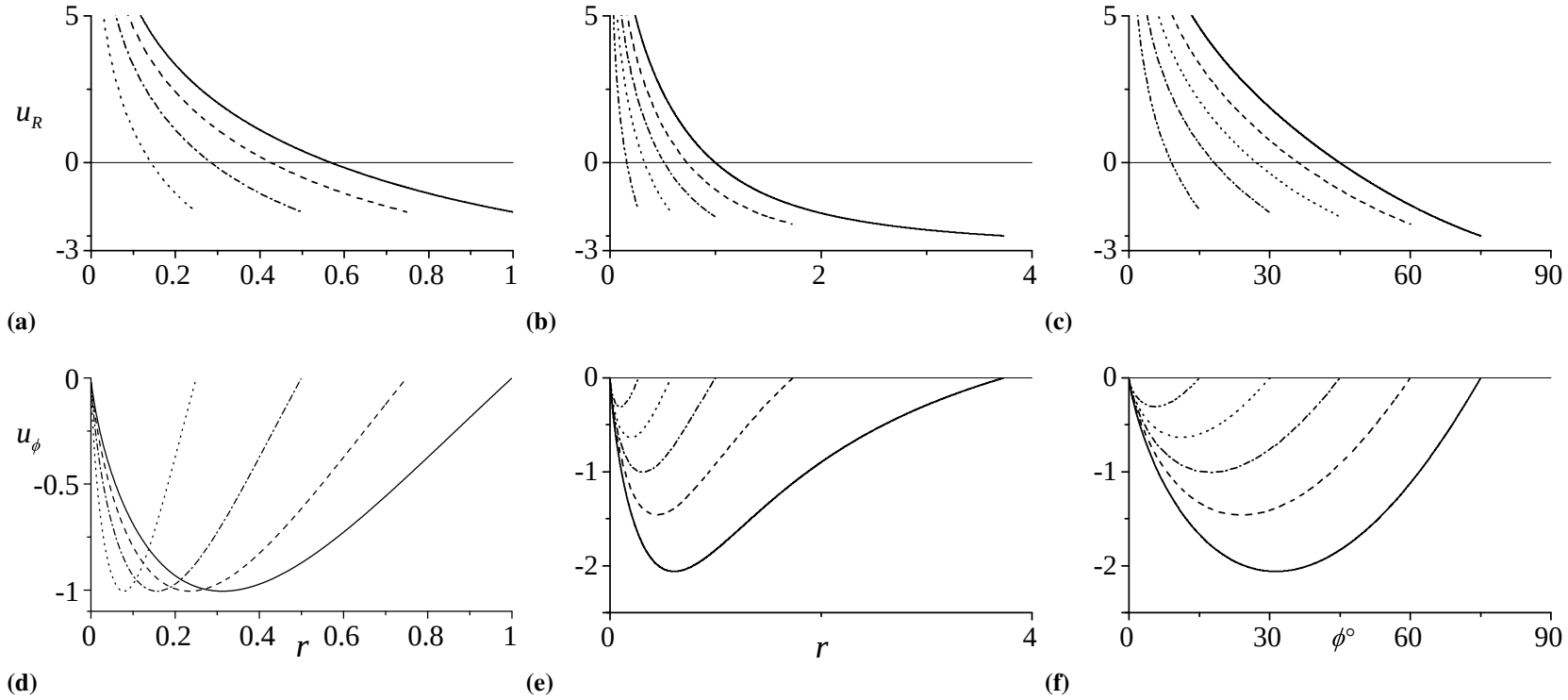

Figure 3.4: Graphs of the (a)-(c) spherical radial velocity, u_R, and (d)-(f) zenith velocity, u_ϕ, for $\sigma_c = 1$. Plots (a) and (d) consist of a divergence half-angle of $\alpha = 45°$ at four axial locations of $z/L = 1$ (——), 0.75 (– – –), 0.5 (– · –), and 0.25 (· · · ·). Figures (b) and (e) plot the velocities at an axial location of $z/L = 1$ (——) for five divergence half-angles of $\alpha = 75°$ (——), 60° (– – –), 45° (– · –), 30° (· · · ·), and 15° (· · –) while (c) and (f) graph over the same angles as (b) and (e) except over the variable ϕ instead of r. Note that (b) and (e) do not contain an "axial" location (the variable R in this case) since the velocities are dependent on ϕ only when in SPC.

Kelsall 1952 and Knowles et al. 1973). Other theoretical models do exist (Bhattacharyya 1980a; Concha 2007). However, it is not in the scope of this dissertation to review them all. Thus, in the future, a survey is in need as well as generic CFD and numerical testing of a simple cone geometry in order to elucidate the findings here even more.

Two figures provide comparison of data to show similar characteristics between the Beltramian model and experimental and numerical tests. The experimental test in Hsieh and Rajamani (1988) utilized a single-channel 35 mW He-Ne laser Doppler velocimeter (LDV) system to gauge the velocity in the flow field. The hydrocyclone consisted of glass encased by a water jacket in order to reduce optical refraction. Table 3.4 provides the dimensions of the hydrocyclone for the experiment. The difference between the hydrocyclone experiments by Hsieh and Rajamani (1988) and Monredon et al. (1992) is that Monredon et al. (1992) studied the flow for various inlet and outlet conditions.

Figure 3.5 shows the cylindrical radial velocity, u_r, for the Beltramian model and the experimental measurements and numerical calculations of Hsieh and Rajamani (1988). Actually, Hsieh and Rajamani (1988) reported that the velcocity in the radial direction could not be calculated. Hence, Hsieh and Rajamani (1988) were forced to use the continuity equation to compute the radial velocity from the measured tangtial and axial velocities. Nonetheless, the Beltramian model and the method by Hsieh and Rajamani (1988) are both linear in nature. The negative magnitudes indicates an inward motion towards the center of the cyclone. The highest velocities are near the wall and linearly dissipate to zero as the radius goes to zero. However, in order to match magnitudes the Beltramian model was scaled down by approximately 90.5%. A viscous analysis may be needed in the future to model the boundary layer at the sidewall. The viscous model requires the velocity to go to zero in order to satisfy no slip and overcome the inviscid model limitations.

Figure 3.6 plots the tangential and axial velocities for the Beltramian model and the experimental measurements and numerical calculations of Hsieh and Rajamani (1988) and Monredon et al. (1992). Figure 3.6a shows the tangential velocity at an axial position of $z = 167.67$ from Hsieh and Rajamani (1988). The Beltramian model is graphed for

Table 3.4: Dimensions of hydrocyclone in the experiment by Hsieh and Rajamani (1988).

Label	Description	Value and Dimension
a	Conical maximum radius and cylindrical radius	37.5 mm
b_z	axial velocity mantle radius $u_z\,(r = b_{ax}, z = b_z \cot\beta_z\,) = 0$	0.602×37.5mm = 22.725 mm (Theoretical)
b_R	spherical radial velocity mantle radius $u_R\,(r = b_{sr}, z = b_R \cot\beta_R\,) = 0$	0.602×37.5mm = 22.575 mm (Theoretical)
A_i	Area of inlet (circular or rectangular; r_i, $l \times w$)	$\pi \times (11.5\text{mm})^2$ = 415.475mm^2
α	Half-angle of cone	10°
β_z	Angle of mantle (axial velocity) $u_z\,(\phi = \beta_z\,) = 0$	6.06° (Theoretical)
β_R	Angle of mantle (spherical radial velocity) $u_R\,(\phi = \beta_R\,) = 0$	6.10° (Theoretical)
L	Length of cone (to apex)	5.67×37.5 mm = 212.625 mm
L_{con}	Length of cone (to underflow radius)	255 mm - 75 mm = 180 mm
L_{cyl}	Length of cylinder	75 mm
L_{vf}	Length of vortex finder (inside cyclone chamber)	50 mm
L_h	Length of cyclone (from chamber top to underflow radius)	255 mm
L_{bot}	Length from conical underflow radius to cone apex	212.67 mm - 180 mm 32.67 mm
L_{tot}	Length from chamber top to cone apex	212.67 mm + 75 mm 287.67 mm
r_{vf}	Radius of vortex finder	11.5 mm
r_{uf}	Radius of conical underflow	5.5 mm

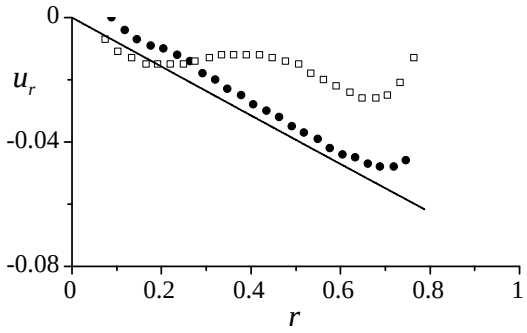

Figure 3.5: The theoretical Beltramian model (——) plotted against experimental (•) and numerical (□) results by Hsieh and Rajamani (1988) at an axial location of $z = 167.67$.

$U = 7.98$ m/s for scaling purposes. Likewise, Figure 3.6b shows the tangential velocity at an axial position of $z = 181.67$ from Monredon et al. (1992). Again, the Beltramian model must be scaled to match, similarly to the tangential and axial velocities, (where in Figure 3.6b $U = 6.26$ m/s). The scaling corrections could be a result of the limitations of the inviscid Beltramian model. However, the characteristics of the curves match reasonably well away from the core and sidewall where inviscid conditions are usually expected for theory. In the same manner, Figure 3.6c and Figure 3.6d show the axial velocity curves measured and calculated from Hsieh and Rajamani (1988) and Monredon et al. (1992), respectively. The Beltramian models displayed in Figure 3.6c and Figure 3.6d are depicted for the modified conical swirl numbers of $\sigma_c = 0.2$ and $\sigma_c = 0.305$, respectively.

3.3 Vorticity & Pressure

Figure 3.7 represents the graphs depicting characteristics of the pressure and vorticity of the Beltramian BDV cone solution. The pressure drop for $\sigma_c = 1$ at four axial locations of $z/L = 1$, 0.75, 0.5, and 0.25 appears in Figure 3.7a. The nature of the pressure change follows the leading order term of $-\frac{1}{2}r^{-2}$ which is congruent with the BDV solutions in a cylinder (Vyas and Majdalani 2006; Majdalani 2012). The singularity near the core can be aligned with a viscous study. Figure 3.7b demonstrate the attributes of the vorticity of the Beltramian model and plots the curves at four axial locations of $z/L = 1$, 0.75,

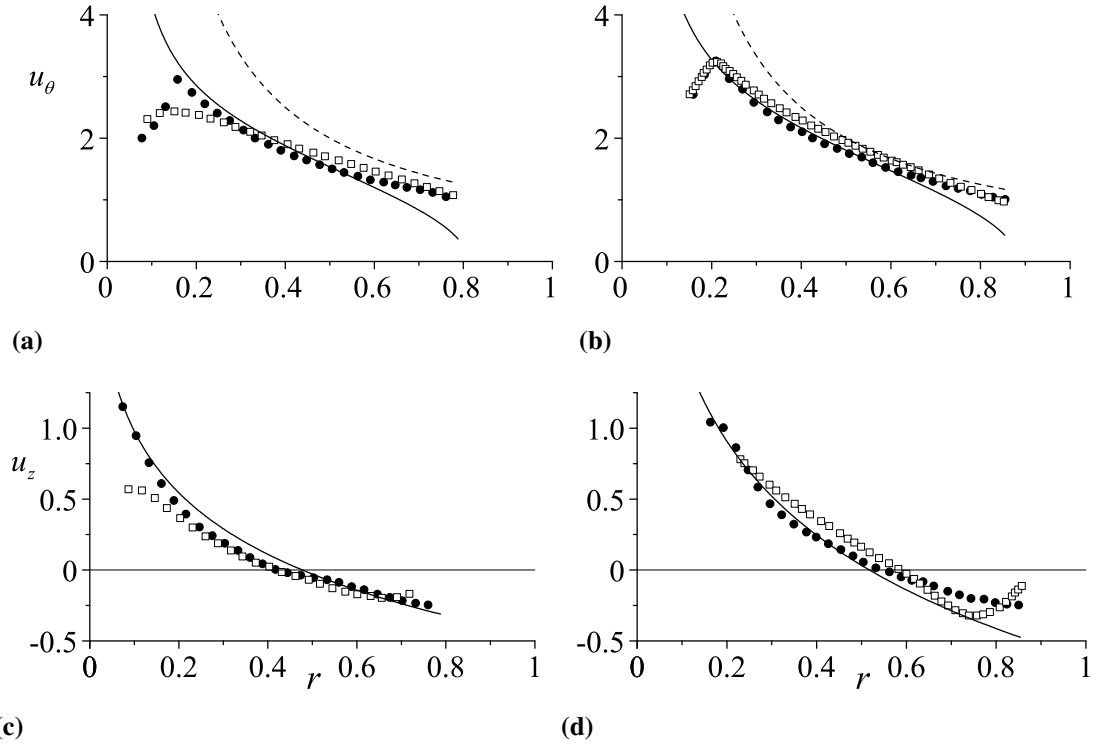

Figure 3.6: The theoretical Beltramian model (——) and free vortex ($1/r$) model (– – –) plotted against experimental (•) and numerical (□) results by (a) and (c) Hsieh and Rajamani (1988) at an axial location of $z = 167.67$ and (b) and (d) Monredon et al. (1992) at an axial location of $z = 181.67$. The tangential velocity, u_θ, scales with (a) $U = 7.98$ m/s and (b) $U = 6.26$ m/s while the axial velocity, u_z, scales with (c) $\sigma_c = 0.2$ and (e) $\sigma_c = 0.305$.

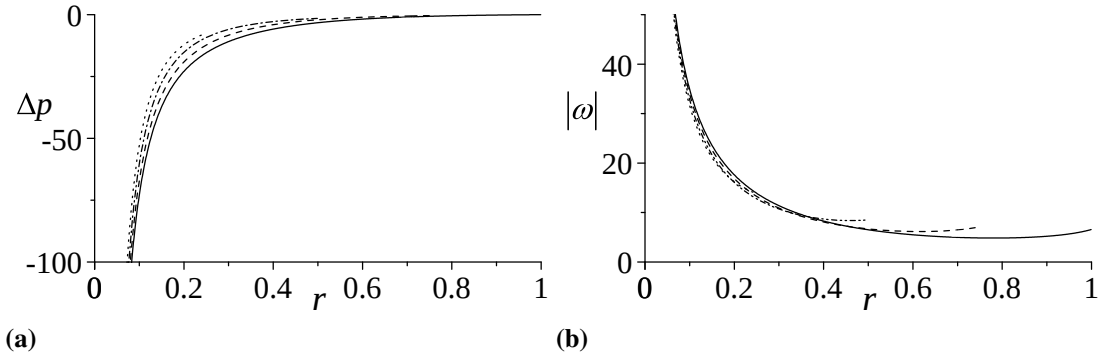

Figure 3.7: The (a) pressure difference and (b) vorticity magnitude for $\sigma_c = 1$ and divergence angle $\alpha = 45°$ at four axial locations of $z/L = 1$ (——), 0.75 (– – –), 0.5 (– · –), and 0.25 (· · · ·).

0.5, and 0.25 for $\sigma_c = 1$ of the vorticity magnitude. The magnitude remains fairly constant until the radius reaches about 50% of the chamber width per axial location. As the radius approaches zero the vorticity magnitude rapidly increases towards infinity. Again, a boundary layer investigation should resolve the core singularities. Note that the highest vorticity magnitudes occur near the centerline and wall where viscous effects are responsible for high vorticity regions Marshall (2001).

Chapter 4

The Generalized Beltramian Conical Bidirectional Vortex (BDV)

4.1 Introduction

This chapter examines the solution of the BDV in a conical geometry which is of the generalized Beltramian type Wu et al. (2006). Again, the generalized Beltramian solution (from Eq. (1.3.27)) satisfies the relation

$$\nabla \times \mathbf{u} \times \boldsymbol{\omega} = 0$$

The generalized Beltramian conditions (recall Eq. (1.3.26)) are more relaxed than the traditional Beltramian constrictions of

$$\mathbf{u} \times \boldsymbol{\omega} = 0$$

As seen from the relations, the Beltramian solution is a subclass of the generalized Beltramian (GB) class. The GB solution, similar to the Bletramian solution, re-examines a previous study. An investigation by Zhao and Abrahamson (1999) attempt to model the flow in a hydrocylone complementary to Bloor and Ingham (1987). However, the article

by Zhao and Abrahamson (1999), akin to Bloor and Ingham (1987), presents an unclear analysis and leaves room for improvement. The main difference between the Bletramian solution and generalized Beltramian solution is that the terms in the BHE for the Bernoulli equation and angular momentum equation are switched. That is, the Bernoulli term in the BHE for the generalized Beltramian formulation remains constant while the angular momentum combination equals zero. Recall, that the opposite occurred for the Beltramian investigation in Chapters 2 and 3.

4.2 Boundary Conditions

Along the same lines of the Beltramian solution, the boundary conditions enforce a stream function equal to zero, $\psi = 0$ along the two main boundaries of the cone, the centerline and outer wall. This translates into

$$\psi\left(R, \phi = 0\right) = 0 \tag{4.2.1}$$

$$\psi\left(R, \phi = \alpha\right) = 0 \tag{4.2.2}$$

Additionally, the conditions at the inlet provide information regarding the behavior of the incoming fluid. Previously, for the Beltramian solution, the inlet conditions assume that there is a simultaneous axial inflow described by a uniform axial injection as demonstrated by the value of the stream function at the inlet

$$u_z\left(R_i, \phi_i = \alpha\right) = u_z\left(r_i, z_i\right) = u_z\left(a, L\right) = -W$$

$$\psi = \tfrac{1}{2} W\left(a^2 - R^2 \sin^2 \phi\right)$$

and a tangential velocity injection at the inlet described by

$$u_\theta = (R_i, \phi_i = \alpha) = u_\theta = (r_i, z_i) = u_\theta = (a, L) = U$$

where the average tangential velocity is U and the average axial velocity is W. Additionally in the Beltramian analysis, the tangential and axial velocities are related by the volumetric flow rate formulated as

$$Q_i = W\pi\left(a^2 - b^2\right) = UA_i$$

$$W = \frac{UA_i}{\pi\left(a^2 - b^2\right)}$$

Also, interestingly Zhao and Abrahamson (1999) note that the inlet stream function can be written as

$$\psi = \tfrac{1}{2}W\left[\left(a^2 - \frac{\mathrm{B}}{U}\right)^2\right] \tag{4.2.3}$$

In their notation, they have substituted $r = B/u_\theta$ transforming the variable at the inlet. However, for the generalized Beltramian study, the axial velocity profile adopts a half-parabola shape in the radial direction according to Zhao and Abrahamson (1999) so that

$$u_z = C_2 r^2 + C_0 \tag{4.2.4}$$

where a full parabola equals $u_z = C_2 r^2 + C_1 r + C_0$, so in 4.2.4 $C_1 = 0$ (see Figure 4.1). The use of cylindrical polar coordinates here to describe the inlet conditions is valid since usually in real world conditions a cylinder sits on top of the cone in a conical cyclone separator. It also logically makes sense to use these coordinates instead of spherical polar coordinates because they are mathematically easily interchangeable and it is visually easier to picture cylindrical polar coordinates as is seen later in the physically velocity profile graphs and such. For instance, the axial velocity can be displayed in spherical coordinates, but at that instance at the inlet it is cemented to the axial location of the height of the cone,

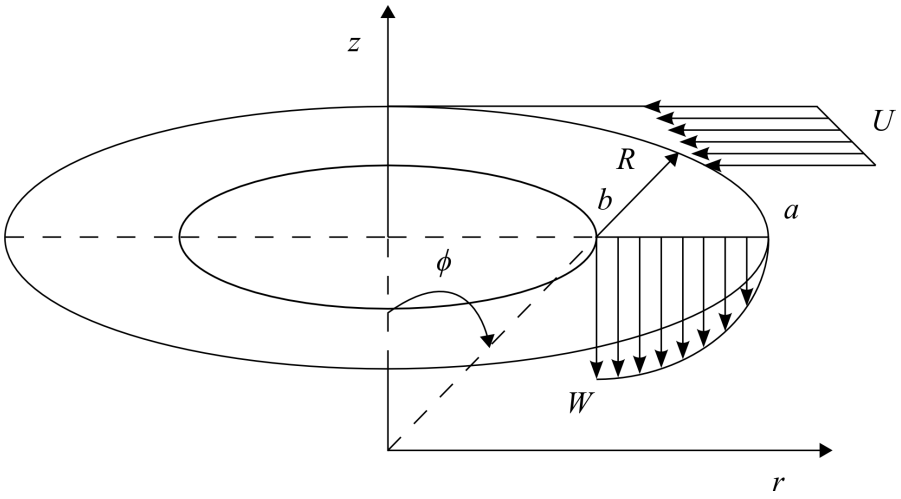

Figure 4.1: The generalized Beltramian analysis inlet axial velocity profile as a half-parabola shape.

L, and it theoretically only possess variations in the radial direction. The same also applies to other axial locations as the velocity is held at the location and varied radially.

Two locations are needed to resolve the constants in the inlet axial velocity. The inner and outer boundaries

$$u_z\,(r = b, z = L) = -W \tag{4.2.5}$$

$$u_z\,(r = a, z = L) = 0 \tag{4.2.6}$$

which produces

$$u_z = C_2 b^2 + C_0 = -W \tag{4.2.7}$$

$$u_z = C_2 a^2 + C_0 = 0 \tag{4.2.8}$$

Applying the first BC from Eq. (4.2.7) gives C_0 as

$$C_0 = -W - C_2 b^2 \tag{4.2.9}$$

which gives

$$u_z = C_2 r^2 - W - C_2 b^2 \tag{4.2.10}$$

$$u_z = C_2 \left(r^2 - b^2\right) - W \tag{4.2.11}$$

Now utlizing the second BC in Eq. (4.2.8), the equation becomes

$$C_2 a^2 - W - C_2 b^2 = 0 \tag{4.2.12}$$

$$C_2 a^2 - C_2 b^2 = W \tag{4.2.13}$$

$$C_2 \left(a^2 - b^2\right) = W \tag{4.2.14}$$

$$C_2 = \frac{W}{a^2 - b^2} \tag{4.2.15}$$

Backwards substitution produces the final form of C_0 as

$$C_0 = -W - \frac{W b^2}{a^2 - b^2} = -\frac{W a^2}{a^2 - b^2} \tag{4.2.16}$$

$$u_z = \frac{W}{(a^2 - b^2)} \left(r^2 - b^2\right) - W \tag{4.2.17}$$

which rearranged delivers the axial velocity as

$$u_z = \frac{W}{(a^2 - b^2)} \left(r^2 - b^2 - a^2 + b^2\right) \tag{4.2.18}$$

reducing further to

$$u_z = \frac{W}{(a^2 - b^2)}\left(r^2 - a^2\right) \tag{4.2.19}$$

or

$$u_z = W\frac{r^2 - a^2}{a^2 - b^2} \tag{4.2.20}$$

The stream function at the inlet can now be evaluated which comes out to be

$$\psi = \int u_z r dr = \int W\frac{r^2 - a^2}{a^2 - b^2} r dr \tag{4.2.21}$$

$$\psi = \frac{W\left(r^4 - 2a^2r^2\right)}{4\left(a^2 - b^2\right)} + \psi_0 \tag{4.2.22}$$

The constant ψ_0 can be determined by ensuring that the BC for the stream function is zero at the wall, $\psi\left(r = a\right) = 0$, so that we get

$$0 = \frac{W\left(a^4 - 2a^2a^2\right)}{4\left(a^2 - b^2\right)} + \psi_0 \tag{4.2.23}$$

$$\psi_0 = \frac{Wa^4}{4\left(a^2 - b^2\right)} \tag{4.2.24}$$

$$\psi = \frac{W\left(r^4 - 2a^2r^2 + a^4\right)}{4\left(a^2 - b^2\right)} \tag{4.2.25}$$

4.3 Bernoulli and Swirl Functions for the BHE

The BHE equation in spherical polar coordinates appears as

$$\frac{\partial^2\psi}{\partial R^2} + \frac{\sin\phi}{R^2}\frac{\partial}{\partial\phi}\left(\frac{1}{\sin\phi}\frac{\partial\psi}{\partial\phi}\right) = R^2\sin^2\phi\frac{\mathrm{dH}}{\mathrm{d}\psi} - \mathrm{B}\frac{\mathrm{dB}}{\mathrm{d}\psi}$$

Similar to Zhao and Abrahamson (1999, 2003), the right-hand side (RHS) of the BHE can be expressed as a polynomial in terms of the stream function, ψ. The BHE becomes

$$\frac{\partial^2\psi}{\partial R^2} + \frac{\sin\phi}{R^2}\frac{\partial}{\partial\phi}\left(\frac{1}{\sin\phi}\frac{\partial\psi}{\partial\phi}\right) = R^2\sin^2\phi\left(a_0 + a_1\psi + a_2\psi^2 + \ldots\right) + b_0 + b_1\psi + b_2\psi^2 + \ldots \tag{4.3.1}$$

Summation constricts the functions on the RHS to

$$\frac{\mathrm{dH}}{\mathrm{d}\psi} = \sum_{n=0}^{i} a_i\psi^i; \qquad \mathrm{B}\frac{\mathrm{dB}}{\mathrm{d}\psi} = \sum_{n=0}^{i} a_i\psi^i \tag{4.3.2}$$

The argument is made, according to Zhao and Abrahamson (1999) (also mentioned in Bloor and Ingham 1987), that the stream function can be made to be less than one so that the higher order terms can be neglected. Therefore, the only terms that remain in the stream function polynomial are the leading order constants and reduce the BHE to

$$\frac{\partial^2\psi}{\partial R^2} + \frac{\sin\phi}{R^2}\frac{\partial}{\partial\phi}\left(\frac{1}{\sin\phi}\frac{\partial\psi}{\partial\phi}\right) = a_0R^2\sin^2\phi + b_0 \tag{4.3.3}$$

Notice that the equation containing only the second constant is the same as the one solved by Bloor and Ingham (1987) and Barber and Majdalani (2009) (see Chapters 2 and 3)

$$\frac{\partial^2\psi}{\partial R^2} + \frac{\sin\phi}{R^2}\frac{\partial}{\partial\phi}\left(\frac{1}{\sin\phi}\frac{\partial\psi}{\partial\phi}\right) = b_0 = \frac{U}{W}$$

This equation assumes that the Bernoulli function is constant along a streamline, thus eliminating the first term, and a variable swirl function. However, for this chapter a new solution is examined which only contains the first constant in the BHE which modifies the equation to

$$\frac{\partial^2\psi}{\partial R^2} + \frac{\sin\phi}{R^2}\frac{\partial}{\partial\phi}\left(\frac{1}{\sin\phi}\frac{\partial\psi}{\partial\phi}\right) = a_0R^2\sin^2\phi \tag{4.3.4}$$

where a_0 is to be determined by new inlet flow assumptions. The inlet conditions enforce constant angular momentum and a variable head as shown by

$$\mathrm{H}(\psi) = \frac{1}{2}u^2 + \frac{p}{\rho} \approx H_0\psi + H_1 \tag{4.3.5}$$

$$\mathrm{B}(\psi) = u_\theta R \sin\phi = \text{constant} \tag{4.3.6}$$

$$\frac{\mathrm{dH}}{\mathrm{d}\psi} = \text{constant} = a_0 \tag{4.3.7}$$

$$-\mathrm{B}\frac{\mathrm{dB}}{\mathrm{d}\psi} = 0 = b_0 \tag{4.3.8}$$

In order to determine the value of the constant a_0, an approach similar to the steps of Zhao and Abrahamson (1999) is presented. The equation of motion for steady, inviscid flow in the cylindrical polar radial direction is presented so that it is unambiguous how the Bernoulli function appears. Using cylindrical polar coordinates at this juncture is for the same reasons as stated earlier.

$$u_r\frac{\partial u_r}{\partial r}\frac{u_\theta^2}{r} - \frac{u_\theta}{r} + u_z\frac{\partial u_r}{\partial z} = -\frac{1}{\rho}\frac{\partial p}{\partial r} \tag{4.3.9}$$

At the inlet, an assumption that the cylindrical polar radial velocity equals zero, $u_r(a, L) = 0$, shortens the equation of motion in the cylindrical polar radial direction to

$$\rho\frac{u_\theta^2}{r} = \frac{\partial p}{\partial r} \tag{4.3.10}$$

Replacing the definition of the tangential velocity with the swirl function divided by the cylindrical polar radius transforms the equation into

$$\rho\frac{B^2}{r^3} = \frac{\partial p}{\partial r} \tag{4.3.11}$$

A definition for the pressure emerges after separating and integrating

$$p = -\frac{\rho \mathrm{B}^2}{2r^2} + C_3 \tag{4.3.12}$$

The Bernoulli function in cylindrical polar coordinates is

$$\mathrm{H} = \tfrac{1}{2}\left(u_r^2 + u_\theta^2 + u_z^2\right) + p/\rho \tag{4.3.13}$$

At the inlet the Bernoulli function truncates to

$$\mathrm{H} = \frac{1}{2}\left(\frac{\mathrm{B}}{r}^2 + u_z^2\right) + \frac{p}{\rho} \tag{4.3.14}$$

Subsituting in the pressure from Eq. (4.3.12) gives

$$\mathrm{H} = \frac{1}{2}\left(\frac{\mathrm{B}}{r}^2 + u_z^2\right) - \frac{\mathrm{B}^2}{2r^2} + C_3 \tag{4.3.15}$$

where the density, ρ, is a constant and absorbed into C_3. Thus, the Bernoulli function finally comes about after simplification to be

$$\mathrm{H} = \tfrac{1}{2}u_z^2 + C_3 \tag{4.3.16}$$

The next step bringing the Bernoulli function closer to a function of the stream function begins with now substituting in the axial velocity arriving at

$$\mathrm{H} = \tfrac{1}{2}\left(C_2 r^2 + C_0\right)^2 + C_3 \tag{4.3.17}$$

The constants are left for the time being in order for clarity. Expanding the square in the parenthesis delivers

$$\mathrm{H} = \tfrac{1}{2}\left(C_2^2 r^4 + 2C_2 C_0 r^2 + C_0^2\right) + C_3 \tag{4.3.18}$$

The stream function at the inlet is examined in order for a comparison to the Bernoulli function

$$\psi = \int u_z r dr = \int \left(C_2 r^3 + C_0 r\right) dr \tag{4.3.19}$$

Integrating, the stream function appears as

$$\psi = \frac{C_2}{4} r^4 + \frac{C_0}{2} r^2 + C_4 \tag{4.3.20}$$

The stream function and Bernoulli function resemble each other so that

$$\frac{\mathrm{H}}{2C_2} = \frac{C_2 r^4}{4} + \frac{C_0}{2} r^2 + \frac{C_0^2 + C_3}{2C_2} \tag{4.3.21}$$

and thus

$$\frac{\mathrm{H}}{2C_2} - \frac{C_0^2 + C_3}{2C_2} = \frac{C_2}{4} r^4 + \frac{C_0}{2} r^2 \tag{4.3.22}$$

Now the relation between the Bernoulli and stream functions is elucidated to get

$$\psi = \frac{\mathrm{H}}{2C_2} \tag{4.3.23}$$

where $-\dfrac{C_0^2 + C_3}{2C_2} = C_4$. Finally, taking the derivative and rearranging gives

$$\frac{\mathrm{dH}}{\mathrm{d}\psi} = 2C_2 = a_0 \tag{4.3.24}$$

This relation can also be verified if the derivative of Eq. 4.3.18 is taken wrt r

$$\frac{\mathrm{d}H}{\mathrm{d}r} = 2C_2^2 r^3 + 2C_2 C_0 r \tag{4.3.25}$$

and by taking the derivative of the stream function of Eq. 4.3.20 wrt to r as well

$$\frac{\mathrm{d}\psi}{\mathrm{d}r} = C_2 r^3 + C_0 r \tag{4.3.26}$$

Next, $\mathrm{d}H/\mathrm{d}\psi$ emerges if Eq. 4.3.25 is divided by Eq. 4.3.26

$$\frac{\frac{\mathrm{d}H}{\mathrm{d}r}}{\frac{\mathrm{d}\psi}{\mathrm{d}r}} = \frac{\mathrm{dH}}{\mathrm{d}\psi} = \frac{2C_2^2 r^3 + 2C_2 C_0 r}{C_2 r^3 + C_0 r} \tag{4.3.27}$$

The equation simplifies by separating $2C_2$ from the numerator

$$\frac{\mathrm{dH}}{\mathrm{d}\psi} = \frac{2C_2\left(C_2 r^3 + C_0 r\right)}{C_2 r^3 + C_0 r} \tag{4.3.28}$$

which reduces to the same in Eq. 4.3.24

$$\frac{\mathrm{dH}}{\mathrm{d}\psi} = 2C_2$$

Next, the stream function at the inlet appears from integration and substitution. First, the Bernoulli function and stream function are separated

$$\mathrm{d}H = 2C_2 \mathrm{d}\psi \tag{4.3.29}$$

is integrated to show that

$$\int \mathrm{d}H = 2C_2 \int \mathrm{d}\psi \implies H = 2C_2\psi + \psi_0 \tag{4.3.30}$$

Substituting in the Bernoulli function at the inlet transforms the stream function equation into a relation with the axial velocity

$$\tfrac{1}{2}\left(C_2^2 r^4 + 2C_2 C_0 r^2 + C_2^0\right) + C_3 = 2C_2\psi + \psi_0 \tag{4.3.31}$$

which simplifies further to

$$\frac{1}{4}\left(C_2 r^4 + 2C_0 r^2 + \frac{C_0^2}{C_2}\right) = \psi \tag{4.3.32}$$

where

$$C_3 = \psi_0 \tag{4.3.33}$$

Substituting in the values for C_2 and C_0 from 4.2.15 and 4.2.16 recovers Eq. (4.2.25) as

$$\psi = \frac{W}{4\left(a^2 - b^2\right)}\left(r^4 - 2a^2r^2 + a^4\right) \tag{4.3.34}$$

The same equation for the stream function can also be derived by utilizing Eq. 4.3.20 and the boundary condition $\psi\left(r = a, z = L\right) = 0$

$$\psi = 0 = \frac{C_2}{4}a^4 + \frac{C_0}{2}a^2 + C_4 \tag{4.3.35}$$

which produces the constant C_4 as

$$C_4 = -\frac{C_2}{4}a^4 - \frac{C_0}{2}a^2 \tag{4.3.36}$$

and the stream function becomes

$$\psi = \frac{C_2}{4}r^4 + \frac{C_0}{2}r^2 - \frac{C_2}{4}a^4 - \frac{C_0}{2}a^2 \tag{4.3.37}$$

$$\psi = \frac{C_2}{4}\left(r^4 - a^4\right) + \frac{C_0}{2}\left(r^2 - a^2\right) \tag{4.3.38}$$

Substituting the constants C_2 and C_0 gives

$$\psi = \frac{W}{4\left(a^2 - b^2\right)}\left(r^4 - a^4\right) - \frac{Wa^2}{2\left(a^2 - b^2\right)}\left(r^2 - a^2\right) \tag{4.3.39}$$

which simplifies to

$$\psi = \frac{W}{4\left(a^2 - b^2\right)}\left(r^4 - a^4 - 2a^2r^2 + 2a^4\right) \tag{4.3.40}$$

and finally recovers Eq. (4.2.25)

$$\psi = \frac{W}{4\left(a^2 - b^2\right)}\left(r^4 - 2a^2r^2 + a^4\right)$$

4.4 Equation Reduction

The BHE to be solved now obtains the format of

$$\frac{\partial^2\psi}{\partial R^2} + \frac{\sin\phi}{R^2}\frac{\partial}{\partial\phi}\left(\frac{1}{\sin\phi}\frac{\partial\psi}{\partial\phi}\right) = 2C_2R^2\sin^2\phi = \frac{2W}{\left(a^2 - b^2\right)}R^2\sin^2\phi \tag{4.4.1}$$

The first step to breakdown the PDE into a more manageable ODE is applying the assumption that the solution is separable in the co-latitudinal angle and spherical polar radius and is, thus, of the form $\psi(R,\phi) = F(R)\,G(\phi)$. Upon inspection it is demonstrated that the spherical polar radial function F is $F(R) = R^4$ so that the stream function becomes $\psi(R,\phi) = R^4G(\phi)$. Substituting into the BHE retrieves

$$12R^2G + R^2\sin\phi\frac{\mathrm{d}}{\mathrm{d}\phi}\left(\frac{1}{\sin\phi}G'\right) = \frac{2W}{\left(a^2 - b^2\right)}R^2\sin^2\phi \tag{4.4.2}$$

The spherical polar radius drops out of the PDE and simplifies the governing equation into an ODE in the colatitudinal angle variable

$$12G + \sin\phi\frac{\mathrm{d}}{\mathrm{d}\phi}\left(\frac{1}{\sin\phi}G'\right) = \frac{2W}{\left(a^2 - b^2\right)}\sin^2\phi \tag{4.4.3}$$

The equation reduces further by expanding and combining terms to result in the following forms of the ODE

$$12G + G'' + \sin\phi G'\left(-\csc\phi\cot\phi\right) = \frac{2W}{\left(a^2 - b^2\right)}\sin^2\phi \tag{4.4.4}$$

$$12G + G'' - G'\cot\phi = \frac{2W}{\left(a^2 - b^2\right)}\sin^2\phi \tag{4.4.5}$$

$$G'' - G' \cot\phi + 12G = \frac{2W}{(a^2 - b^2)} \sin^2\phi \tag{4.4.6}$$

4.5 Separation of Variables - the Homogeneous Solution and the Gegenbauer Equation

The complimentary function is first pursued in revealing the general solution. Therefore, the ODE is expressed in its homogeneous form as

$$12G + \sin\phi \frac{\mathrm{d}}{\mathrm{d}\phi}\left(\frac{1}{\sin\phi} G'\right) = 0 \tag{4.5.1}$$

$$G'' - G' \cot\phi + 12G = 0 \tag{4.5.2}$$

Thus, this equation can be transformed by using the substitution $x = \cos\phi$ which can be confirmed by a myriad of mathematical texts(O'Neil 1995; Wylie and Barrett 1995; Kreyszig 1999; Zill 2000; Zill and Cullen 2000; Riley et al. 2002; Polyanin and Zaitsev 2003; Arfken and Weber 2005).

$$\frac{\mathrm{d}}{\mathrm{d}\phi} = \frac{\mathrm{d}}{\mathrm{d}x}\frac{\mathrm{d}x}{\mathrm{d}\phi} = -\sin\phi \frac{\mathrm{d}}{\mathrm{d}x} \tag{4.5.3}$$

$$12G_x - \sin^2\phi \frac{\mathrm{d}}{\mathrm{d}x}\left(-G'_x\right) = 0 \tag{4.5.4}$$

$$\left(1 - x^2\right) G''_x + 12G_x = 0 \tag{4.5.5}$$

Expanding Eq. (4.5.5) produces the following form (Bojarevičs et al. 1989; Dassios and Vafeas 2006; Dassios 2008; Dassios and Vafeas 2008)

$$\left(1 - x^2\right) G''_x + n\,(n-1)\, G_x = 0; \qquad n = 4 \tag{4.5.6}$$

A more general form also known as the ultraspherical differential equation (Weisstein 2003) is called the Gegenbauer's differential equation (Happel and Brenner 1983; Bojarevičs et al. 1989; Weisstein 2003) where Eq. (4.5.6) is a special case of

$$\left(1-x^2\right)G_x''-2\left(2\mu+1\right)xG_x'+\nu\left(\nu+2\mu\right)G_x=0;\quad \mu=-\tfrac{1}{2},\ \ \nu=4 \tag{4.5.7}$$

The differential equation is named for a 19th century Austrian mathematician, Leopold Bernhard Gegenbauer, who worked immensely with the polynomials that are solutions of the ODE. The solutions to Eq. (4.5.7) emerge as

$$G_x=\left(x^2-1\right)^{(1-2\mu)/4}\left[C_5P^{1/2-\mu}_{-1/2+\mu-\nu}\left(x\right)+C_6Q^{1/2-\mu}_{-1/2+\mu-\nu}\left(x\right)\right] \tag{4.5.8}$$

$$G_x=\left(x^2-1\right)^{1/2}\left[C_5P^{1}_{3}\left(x\right)+C_6Q^{1}_{3}\left(x\right)\right] \tag{4.5.9}$$

where $P^m_n\left(x\right)$ and $Q^m_n\left(x\right)$ are the associated Legendre functions of the first and second kind of order μ which are named in honor of French mathematician Adrien Marie Legendre for his work in this area. When $m=0$ the associated Legendre differential equations and polynomials are equal to the more commonly known regular Legendre differential equation and polynomials. The Gegenbauer differential equation derives from the hyperspherical differential equation

$$\left(1-x^2\right)G_x''-2\left(2\mu+1\right)xG_x'+\left(\nu-\mu\right)\left(\nu+\mu+1\right)G_x=0 \tag{4.5.10}$$

which has a solution of the form

$$G_x=\left(x^2-1\right)^{-\mu/2}\left[C_7P^{\mu}_{\nu}\left(x\right)+C_8Q^{\mu}_{\nu}\left(x\right)\right] \tag{4.5.11}$$

which in turn recovers the differential equation and the solution found in Eq. (4.5.6) and Eq. (4.5.9), respectively, with $\mu=-1$ and $\nu=3$. The equation is recovered even though

$\mu = -1$ since $P_n^{-m}(x) = P_n^m(x)$. The associated Legendre polynomial relates to the Legendre polynomial by

$$\begin{cases} P_\nu^\mu(x) = \left(1 - x^2\right)^{|\mu|/2} \dfrac{\mathrm{d}^{|\mu|}}{\mathrm{d}x^{|\mu|}} P_\nu(x) \\ \\ Q_\nu^\mu(x) = \left(1 - x^2\right)^{|\mu|/2} \dfrac{\mathrm{d}^{|\mu|}}{\mathrm{d}x^{|\mu|}} Q_\nu(x) \end{cases} \tag{4.5.12}$$

Now the complimentary equation evolves into

$$G_x = \left(x^2 - 1\right)^{1/2} \left[\left(1 - x^2\right)^{1/2} C_7 \frac{\mathrm{d}}{\mathrm{d}x} P_3(x) + \left(1 - x^2\right)^{1/2} C_8 \frac{\mathrm{d}}{\mathrm{d}x} Q_3(x) \right] \tag{4.5.13}$$

since $m = 1$ from Eq. (4.5.9). Further simplification reduces the equation to

$$G_x = -\left(1 - x^2\right) \left[C_7 \frac{\mathrm{d}}{\mathrm{d}x} P_3(x) + C_8 \frac{\mathrm{d}}{\mathrm{d}x} Q_3(x) \right] \tag{4.5.14}$$

$$G_x = \left(1 - x^2\right) \left[C_7 P_3'(x) + C_8 Q_3'(x) \right] \tag{4.5.15}$$

Note that the negative sign resulting from Eq. (4.5.13) has been absorbed into the constants C_7 and C_8. The relation of the derivative of a Legendre function relates the equations in terms of regular Legendre function of the first and second kind

$$\left(1 - x^2\right) P_\nu'(x) = \nu P_{\nu-1}(x) - \nu x P_\nu(x) \tag{4.5.16}$$

$$\left(1 - x^2\right) Q_\nu'(x) = \nu Q_{\nu-1}(x) - \nu x P_\nu(x) \tag{4.5.17}$$

Implementing the derivative transform, the general solution converts to

$$G_x = 3C_7 \left[x P_3(x) - P_2(x) \right] + 3C_8 \left[x Q_3(x) - Q_2(x) \right] \tag{4.5.18}$$

However, when $n \geq 2$, then the solution to Eq. (4.5.6) is expressed as

$$G_x = C_9 \mathcal{J}_n^{-1/2}(x) + C_{10} \mathcal{H}_n^{-1/2}(x) \tag{4.5.19}$$

or

$$G_x = C_9 \mathcal{J}_n(x) + C_{10} \mathcal{H}_n(x) \tag{4.5.20}$$

where $J_n^{\mu}(x)$ and $H_n^{\mu}(x)$ are sometimes called the ultraspherical or Gegenbauer functions/polynomials of the first and second kind. Note that the superscript $^{-1/2}$ has been omitted in Eq. (4.5.20) for aesthetics and inherently is implied on the Gegenbauer functions. The omitted superscript constitutes the degree of the function while n represents the order. Also, note that function/polynomial are interchangeable when n is an integer.

The families of orthogonal polynomials, Jacobi, Gegenbauer, Chebyshev, Legendre, Laguerre, and Hermite, are also known as the classical orthogonal polynomials. The classes of polynomials remain different yet closely linked. The relation between Legendre and Gegenbauer is anticipated since Legendre's equation commonly Laplace's partial differential equation and the similarity between the Laplace and Stokes operators. The Legendre differential equation is a special case of the Gegenbauer differential equation since when $\mu = 1/2$ in Eq. (4.5.9) the Legendre differential equation is recovered and the Gegenbauer polynomials translate directly to Legendre polynomials as $\mathcal{J}_n^{-1/2}(x) = P_n(x)$ and when n is an positive integer and when $n \geq 2$ for in Eq. (4.5.6). However, when μ is an integer in Eq. (4.5.8) then the solutions remain Gegenbauer polynomials and cannot be reduced to Legendre polynomials. Thus, the Legendre functions are special cases of Gegenbauer functions.

Both the Legendre functions/polynomial and Gegenbauer functions/polynomial derive from Jacobi functions/polynomial family. The Gegenbauer special case is true for Jacobi polynomials when $\alpha = \beta = \nu = -1$ and thus $P_n^{(\alpha,\beta)}(x) = \mathcal{J}_n(x)$. Likewise, when $\alpha = \beta = 0$ the Legendre polynomial special case is demonstrated from the Jacobi polynomial. Gegenbauer functions are commonly experienced in fluid dynamics or

electrodynamics involving axisymmetric flows such as Stokes/creeping flow, droplet and bubble fluid dynamics, astrophysics, and bio-fluid dynamics (Happel and Brenner 1983; Bojarevičs et al. 1989; Dassios and Vafeas 2006; Dassios 2008; Dassios and Vafeas 2008). The common linkage is the use of spherical polar coordinates and the need to transform the variable by employing $x = \cos\phi$.

The solution from after inserting the corresponding n constant Eq. (4.5.20) becomes

$$G_x = C_9 \mathcal{J}_4(x) + C_{10} \mathcal{H}_4(x) \tag{4.5.21}$$

The Gegenbauer functions can be transformed directly into Legendre functions as given by

$$\left(1 - x^2\right) \frac{\mathrm{d}}{\mathrm{d}x} P_{n-1}(x) = n(n-1) \mathcal{J}_n(x) \tag{4.5.22}$$

$$\left(1 - x^2\right) \frac{\mathrm{d}}{\mathrm{d}x} Q_{n-1}(x) = n(n-1) \mathcal{H}_n(x) \tag{4.5.23}$$

or

$$\mathcal{J}_n(x) = \frac{P_{n-2}(x) - P_n(x)}{2n-1} \tag{4.5.24}$$

$$\mathcal{H}_n(x) = \frac{Q_{n-2}(x) - Q_n(x)}{2n-1} \tag{4.5.25}$$

The solution converts to

$$G_x = C_9 \frac{1}{12} \left(1 - x^2\right) \frac{\mathrm{d}}{\mathrm{d}x} P_3(x) + C_{10} \frac{1}{12} \left(1 - x^2\right) \frac{\mathrm{d}}{\mathrm{d}x} Q_3(x) \tag{4.5.26}$$

$$G_x = C_9 \left(1 - x^2\right) \frac{\mathrm{d}}{\mathrm{d}x} P_3(x) + C_{10} \left(1 - x^2\right) \frac{\mathrm{d}}{\mathrm{d}x} Q_3(x) \tag{4.5.27}$$

Recalling Eq. (4.5.16) and Eq. (4.5.17), the solution is modified

$$G_x = 3C_9 \left[P_2(x) - xP_3(x)\right] + 3C_{10}\left[Q_2(x) - xQ_3(x)\right] \tag{4.5.28}$$

Thus, recovering the general solution previously found where $C_9 = -C_7$ and $C_{10} = -C_8$. The same result appears using the other Gegenbauer-Legendre relation in Eq. (4.5.24) and Eq. (4.5.25) which validates that the solution is correct. The expanded Legendre functions are

$$P_2(x) = \frac{1}{2}\left(3x^2 - 1\right) \tag{4.5.29}$$

$$P_3(x) = \frac{1}{2}\left(5x^3 - 3x\right) \tag{4.5.30}$$

$$Q_2(x) = \frac{1}{4}\left(3x^2 - 1\right)\ln\left(\frac{1+x}{1-x}\right) - \frac{3}{2}x \tag{4.5.31}$$

$$Q_3(x) = \frac{1}{4}\left(5x^3 - 3x\right)\ln\left(\frac{1+x}{1-x}\right) - \frac{5}{2}x^2 + \frac{3}{2} \tag{4.5.32}$$

Looking more closely at Eq. (4.5.31) and Eq. (4.5.32) ensures that C_8 is zero in Eq. (4.5.18)

$$C_8 = 0 \tag{4.5.33}$$

because the properties of the Legendre functions of the second kind, $Q_i(x)$ demonstrate that both equations, $Q_2(x)$ and $Q_3(x)$, blow up as $x \to 1$ or as $\phi \to 0$.

Thus, substituting (and recovering a negative sign) the Legendre expanded polynomials into the solution of Eq. (4.5.18) produces

$$G_x = -3C_7\left[\frac{1}{2}x\left(5x^3 - 3x\right) - \frac{1}{2}\left(3x^2 - 1\right)\right] \tag{4.5.34}$$

Multiplying through provides a better view of the final complementary solution

$$G_x = -C_7\left(\frac{15}{2}x^4 - \frac{9}{2}x^2 - \frac{9}{2}x^2 + \frac{3}{2}\right) \tag{4.5.35}$$

The homogeneous solution equation abridges when combing like terms to

$$G_x = C_7\left(9x^2 - \frac{15}{2}x^4 - \frac{3}{2}\right) \tag{4.5.36}$$

The equation finally converts back to the original variable by substitution of $x = \cos\phi$ producing the complementary function of

$$G_c = C_7\left(9\cos^2\phi - \frac{15}{2}\cos^4\phi - \frac{3}{2}\right) \tag{4.5.37}$$

4.6 Particular Solution

The solution corresponding to the nonhomogeneity of the ODE is needed before the last step of applying the boundary conditions. The particular solution is solved by standard ODE methods. The solution consists of powers of cosine and the nonhomogeneous term contains the square of sine. Therefore, upon inspection the next logical solution contains the particular form of

$$G_p = C_p\sin^2\phi \tag{4.6.1}$$

The first and second derivatives of G_p are executed, back substituted, and then condensed. First, perform the derivative operation on Eq. (4.6.1) twice to obtain

$$G_p' = 2C_p\sin\phi\cos\phi \tag{4.6.2}$$

$$G_p'' = -2C_p\sin^2\phi + 2C_p\cos^2\phi \tag{4.6.3}$$

Next, substitute Eq. (4.6.1), Eq. (4.6.2), and Eq. (4.6.3) into Eq. (4.5.2)

$$-2C_p \sin^2\phi + 2C_p \cos^2\phi - \cot\phi\left(2C_p \sin\phi\cos\phi\right) + 12C_p \sin^2\phi = 2C_0 \sin^2\phi \tag{4.6.4}$$

The constant develops straightforwardly as

$$C_p = C_0/5 \tag{4.6.5}$$

Thus, the exact form for the particular solution which satisfies the nonhomogeneity is

$$G_p = \frac{W}{5\left(a^2 - b^2\right)} \sin^2\phi \tag{4.6.6}$$

4.7 General Solution of the ODE and PDE

Therefore, the general solution satisfying the function $G(\phi)$ matures to the linear superposition of the complimentary and particular solutions, $G(\phi) = G_c + G_p$

$$G = C_7\left(9\cos^2\phi - \frac{15}{2}\cos^4\phi - \frac{3}{2}\right) + \frac{W}{5\left(a^2 - b^2\right)} \sin^2\phi \tag{4.7.1}$$

The stream function comes to fruition as

$$\psi = R^4\left[C_7\left(9\cos^2\phi - \frac{15}{2}\cos^4\phi - \frac{3}{2}\right) + \frac{W}{5\left(a^2 - b^2\right)} \sin^2\phi\right] \tag{4.7.2}$$

by exercising the relation of $\psi(R,\phi) = F(R)\,G(\phi) = R^4 G(\phi)$.

4.8 The Boundary Conditions and the Stream Function Solution

The natural progression moves to administer the appropriate boundary conditions in order to solve for the constant, C_7. The boundary condition at the centerline, $\psi(R,0) = 0$ or

$$G(0) = 0 \tag{4.8.1}$$

for the colatitudinal function, has been used previously to eliminate the Legendre function of the second kind, $Q(x)$. Therefore, the boundary conditions at the wall, $\psi(R, \alpha) = 0$ or

$$G(\alpha) = 0 \tag{4.8.2}$$

is used to find the constant, C_7, which appears as

$$G(\alpha) = 0 = C_7\left(9\cos^2\alpha - \frac{15}{2}\cos^4\alpha - \frac{3}{2}\right) + \frac{W}{5(a^2 - b^2)}\sin^2\alpha \tag{4.8.3}$$

$$C_7\left(9\cos^2\phi - \frac{15}{2}\cos^4\phi - \frac{3}{2}\right) = -\frac{W}{5(a^2 - b^2)}\sin^2\alpha \tag{4.8.4}$$

$$C_7 = \frac{W\left(\sin^2\alpha\right)}{5(a^2 - b^2)\left(\frac{15}{2}\cos^4\phi - 9\cos^2\phi + \frac{3}{2}\right)} \tag{4.8.5}$$

$$C_7 = \frac{2W\left(\sin^2\alpha\right)}{5(a^2 - b^2)(15\cos^4\alpha - 18\cos^2\alpha + 3)} \tag{4.8.6}$$

$$C_7 = \frac{2W}{5(a^2 - b^2)}\lambda \tag{4.8.7}$$

where

$$\lambda = \frac{\sin^2\alpha}{(15\cos^4\alpha - 18\cos^2\alpha + 3)} \tag{4.8.8}$$

So the colatitudinal and stream functions become

$$G = \frac{2W}{5(a^2 - b^2)}\lambda\left(\frac{15}{2}\cos^4\phi - 9\cos^2\phi + \frac{3}{2}\right) - \frac{W}{5(a^2 - b^2)}\sin^2\phi \tag{4.8.9}$$

$$\psi = R^4\left[\frac{2W}{5\left(a^2-b^2\right)}\lambda\left(\frac{15}{2}\cos^4\phi - 9\cos^2\phi + \frac{3}{2}\right) - \frac{W}{5\left(a^2-b^2\right)}\sin^2\phi\right] \tag{4.8.10}$$

and simplified

$$G = \frac{W}{5\left(a^2-b^2\right)}\left[\lambda\left(15\cos^4\phi - 18\cos^2\phi + 3\right) - \sin^2\phi\right] \tag{4.8.11}$$

$$\psi = \frac{W}{5\left(a^2-b^2\right)}R^4\left[\lambda\left(15\cos^4\phi - 18\cos^2\phi + 3\right) - \sin^2\phi\right] \tag{4.8.12}$$

4.9 Dimensional Velocities

Again, once the stream function is at hand, the spherical polar radial and co-latitudinal velocities egress from the velocity-stream function relation

$$u_R = \frac{1}{R^2\sin\phi}\frac{\partial\psi}{\partial\phi}$$

$$u_\phi = -\frac{1}{R\sin\phi}\frac{\partial\psi}{\partial R}$$

The derivatives become,

$$\frac{\partial\psi}{\partial\phi} = \frac{W}{5\left(a^2-b^2\right)}R^4\left[\lambda\left(-60\cos^3\phi\sin\phi + 36\cos\phi\sin\phi\right) - 2\sin\phi\cos\phi\right] \tag{4.9.1}$$

$$\frac{\partial\psi}{\partial\phi} = \frac{W\sin\phi}{5\left(a^2-b^2\right)}R^4\left[\lambda\left(36\cos\phi - 60\cos^3\phi\right) - 2\cos\phi\right] \tag{4.9.2}$$

$$\frac{\partial\psi}{\partial R} = \frac{4W}{5\left(a^2-b^2\right)}R^3\left[\lambda\left(15\cos^4\phi - 9\cos^2\phi + 3\right) - \sin^2\phi\right] \tag{4.9.3}$$

and the complementary velocities amend as

$$u_R = \frac{2W}{5\left(a^2 - b^2\right)} R^2 \left[\lambda\left(18\cos\phi - 30\cos^3\phi\right) - \cos\phi\right] \tag{4.9.4}$$

$$u_\phi = -\frac{4W}{5\left(a^2 - b^2\right)} R^2 \left[\lambda \csc\phi\left(15\cos^4\phi - 18\cos^2\phi + 3\right) - \sin\phi\right] \tag{4.9.5}$$

The tangential velocity remains the same as the assumption at the beginning of the investigation which requires

$$u_\theta = \frac{\mathrm{B}}{R\sin\phi} \tag{4.9.6}$$

The swirl function is based upon the set inlet conditions

$$\mathrm{B} = u_\theta R\sin\phi = Ua \tag{4.9.7}$$

and

$$u_\theta = \frac{Ua}{R\sin\phi} \tag{4.9.8}$$

4.10 Conical Modified Swirl Number

Before proceeding into the normalization of the solution equations, a conical modified swirl number is introduced for better resolution. Utilizing Eq. (4.2.25) the inlet stream function emerges

$$\psi_a = 0 \tag{4.10.1}$$

$$\psi_b = \frac{W}{4\left(a^2 - b^2\right)}\left(b^4 - 2a^2b^2 + a^4\right) \tag{4.10.2}$$

where the stream function simplifies to

$$\psi_b = \frac{W\left(a^2 - b^2\right)^2}{4\left(a^2 - b^2\right)} = \frac{W}{4}\left(a^2 - b^2\right) \tag{4.10.3}$$

for the boundary conditions of

$$\psi\left(r = a, z = L\right) \tag{4.10.4}$$

$$\psi\left(r = b, z = L\right) \tag{4.10.5}$$

The volumetric inlet flow rate derives from Eq. (2.4.13) in Chapter 2

$$Q_i = 2\pi \int_b^a d\psi = 2\pi\left(\psi_a - \psi_b\right) \tag{4.10.6}$$

Thus, the volumetric flow rate at the inlet surfaces into the form of

$$Q_i = \frac{\pi}{2} W\left(a^2 - b^2\right) \tag{4.10.7}$$

In a similar form as Eq. (2.4.14) in Chapter 2, the volumetric flow rate relates the average tangential and axial inlet velocities by

$$Q_i = \frac{\pi}{2} W\left(a^2 - b^2\right) = UA_i \tag{4.10.8}$$

Thus, the average axial and tangential velocities associate as

$$W = \frac{2UA_i}{\pi\left(a^2 - b^2\right)} \tag{4.10.9}$$

Next, a modified conical swirl number condenses the ratio further as

$$\sigma_c = \frac{a^2 - b^2}{A_i} \tag{4.10.10}$$

and the corresponding average axial velocity relation is written as

$$W = \frac{2U}{\pi\sigma_c} \tag{4.10.11}$$

Thus, the corresponding stream function and velocities are

$$\psi = \frac{2U}{5\left(a^2-b^2\right)\pi\sigma_c}R^4\left[\lambda\left(15\cos^4\phi - 18\cos^2\phi + 3\right) - \sin^2\phi\right] \tag{4.10.12}$$

$$u_R = \frac{2U}{5\left(a^2-b^2\right)\pi\sigma_c}R^2\left[\lambda\left(18\cos\phi - 30\cos^3\phi\right) - \cos\phi\right] \tag{4.10.13}$$

$$u_\phi = -\frac{4U}{5\left(a^2-b^2\right)\pi\sigma_c}R^2\left[\lambda\csc\phi\left(15\cos^4\phi - 18\cos^2\phi + 3\right) - \sin\phi\right] \tag{4.10.14}$$

4.11 Nondimensionalization

Following the same normalization from Chapter 2, the variables reform to

$$R = \frac{\bar{R}}{a}; \quad \psi = \frac{\bar{\psi}}{Ua^2}; \quad u_R = \frac{\bar{u}_R}{U}; \quad u_\phi = \frac{\bar{u}_\phi}{U}; \quad u_\theta = \frac{\bar{u}_\theta}{U} \tag{4.11.1}$$

In turn, the stream function and velocities materialize as

$$\psi = \tfrac{2}{5}\kappa_c R^4\sin^4\phi\left[\lambda\left(15 - 12\csc^2\phi\right) - \csc^2\phi\right] \tag{4.11.2}$$

$$u_R = \tfrac{4}{5}\kappa_c R^2\sin^2\phi\left[\lambda\cos\phi\left(30 - 12\csc^2\phi\right) - \csc^2\phi\cos\phi\right] \tag{4.11.3}$$

$$u_\phi = -\tfrac{8}{5}\kappa_c R^2\sin^2\phi\left[\lambda\left(15\sin\phi - 12\csc\phi\right) - \csc\phi\right] \tag{4.11.4}$$

where

$$\kappa_c = \frac{1}{\left(1-\hat{\beta}^2\right)\pi\sigma_c} = \frac{\sigma}{\pi\sigma_c^2} \tag{4.11.5}$$

4.12 Cylindrical Polar Velocities & Coordinates Conversions

Visually, spherical polar coordinates are difficult to interpret. Therefore, a conversion from spherical polar coordinates to cylindrical polar coordinates as done previously in Section 2.14 is undertaken in order to illuminate the equations. First, the velocities are

converted from spherical polar velocities to cylindrical polar counterparts by exercising Eq. (2.13.1) in Section 2.13. The cylindrical polar radial and axial velocities appear as

$$u_r = \tfrac{2}{5}R^2\kappa_c\left[(1+12\lambda)\sin 2\phi\right] \tag{4.12.1}$$

$$u_z = \tfrac{2}{5}R^2\kappa_c\left[(1-18\lambda)\cos 2\phi - 3 - 6\lambda\right] \tag{4.12.2}$$

The stream function and velocities in CPC become

$$\psi = \tfrac{2}{5}\kappa_c r^4\left[\lambda\left(15-12\mathcal{Z}_1^2\right)-\mathcal{Z}_1^2\right] \tag{4.12.3}$$

$$u_R = \tfrac{4}{5}\kappa_c r^2\zeta\mathcal{Z}_2\left[\lambda\left(30-12\mathcal{Z}_1^2\right)-\mathcal{Z}_1^2\right] \tag{4.12.4}$$

$$u_\phi = -\tfrac{8}{5}\kappa_c r^2\left[\lambda\left(15\mathcal{Z}_2-12\mathcal{Z}_1\right)-\mathcal{Z}_1\right] \tag{4.12.5}$$

$$u_\theta = \frac{1}{r} \tag{4.12.6}$$

$$u_r = \tfrac{2}{5}rz\kappa_c\left(1+12\lambda\right) \tag{4.12.7}$$

$$u_z = \tfrac{2}{5}\kappa_c\left[(6\lambda-2)\,r^2-(1+12\lambda)\,z^2\right] \tag{4.12.8}$$

4.13 Vorticity & Pressure

In the same vein as Sections 2.16 and 2.17 in Chapter 2, the vorticity components and pressure can be derived for the generalized Beltramian solution. Tables 4.1–4.4 showcase the Beltramian and generalized Beltramian solutions in parallel.

Table 4.1: Generalized Beltramian and Beltramian cases compared.

Variable	Generalized Beltramian ($\nabla \times \mathbf{u} \times \boldsymbol{\omega} = 0$)	Beltramian ($\mathbf{u} \times \boldsymbol{\omega} = 0$)
$\psi_i\,(R, \phi, \theta)$	$\dfrac{W\left(R^4 \sin^4\phi - 2a^2R^2\sin^2\phi + a^4\right)}{4\left(a^2 - b^2\right)}$	$\frac{1}{2}W\left(a^2 - R^2\sin^2\phi\right)$
$\psi_i\,(r, \theta, z)$	$\dfrac{W\left(r^4 - 2a^2r^2 + a^4\right)}{4\left(a^2 - b^2\right)}$	$\frac{1}{2}W\left(a^2 - r^2\right)$
$\dfrac{\mathrm{d}H}{\mathrm{d}\psi}$	$\dfrac{2W}{\left(a^2 - b^2\right)}$	0
$B\dfrac{\mathrm{d}B}{\mathrm{d}\psi}$	0	$-\dfrac{U^2}{W}$
$F(R)\,G(\phi)$	$R^4G(\phi)$	$R^2G(\phi)$
$\psi\,(R, \phi, \theta)$	$\frac{2}{5}\kappa_c R^4\sin^4\phi\left[\lambda\left(15 - 12\csc^2\phi\right) - \csc^2\phi\right]$	$\frac{1}{2}\kappa_c R^2\sin^2\phi\left(\lambda - \ln\Phi + \csc\phi\cot\phi - \csc^2\phi\right)$
$\psi\,(r, \theta, z)$	$\frac{2}{5}\kappa_c r^4\left[\lambda\left(15 - 12\mathcal{Z}_1^2\right) - \mathcal{Z}_1^2\right]$	$\frac{1}{2}\kappa_c r^2\left(\lambda - \ln\mathcal{Z} - \mathcal{Z}\sqrt{1+\zeta^2}\right)$
λ	$\csc^2\alpha\left(15\cos^4\alpha - 18\cos^2\alpha + 3\right)^{-1}$	$\Phi_\alpha\csc\alpha + \ln\Phi_\alpha$
κ_c	$\left[\left(1 - \hat{\beta}^2\right)\pi\sigma_c\right]^{-1}$	$\pi\sigma_c$

Table 4.2: Generalized Beltramian and Beltramian cases velocity comparison.

Variable	Generalized Beltramian ($\nabla \times \mathbf{u} \times \boldsymbol{\omega} = 0$)	Beltramian ($\mathbf{u} \times \boldsymbol{\omega} = 0$)
$u_R(R,\phi,\theta)$	$\frac{4}{5}\kappa_c R^2\left[\lambda\left(18\cos\phi - 30\cos^3\phi\right) - \cos\phi\right]$	$\kappa_c\left[(\lambda - \ln\Phi)\cos\phi - 1\right]$
$u_R(r,\theta,z)$	$\frac{4}{5}\kappa_c r^2\zeta\mathcal{Z}_2\left[\lambda\left(30 - 12\mathcal{Z}_1^2\right) - \mathcal{Z}_1^2\right]$	$\kappa_c\left[\zeta\left(\lambda - \ln\mathcal{Z}\right)\left(1+\zeta^2\right)^{-1/2} - 1\right]$
$u_\phi(R,\phi,\theta)$	$-\frac{8}{5}\kappa_c R^2\left[\lambda\left(15\sin^3\phi - 12\sin\phi\right) - \sin\phi\right]$	$\kappa_c\left[(\ln\Phi - \lambda)\sin\phi + \Phi\right]$
$u_\phi(r,\theta,z)$	$-\frac{8}{5}\kappa_c r^2\left[\lambda\left(15\mathcal{Z}_2 - 12\mathcal{Z}_1\right) - \mathcal{Z}_1\right]$	$-\kappa_c\left[\left(\lambda - \ln\mathcal{Z}\right)\left(1+\zeta^2\right)^{-1/2} - \mathcal{Z}\right]$
$u_\theta(R,\phi,\theta)$	$\dfrac{1}{R\sin\phi}$	$\dfrac{1}{R\sin\phi}\left[1 + (\kappa_c R\sin\phi)^2\left(\lambda - \ln\Phi - \Phi\csc\phi\right)\right]^{1/2}$
$u_\theta(r,\theta,z)$	$\dfrac{1}{r}$	$\dfrac{1}{r}\left[1 + (r\kappa_c)^2\left(\lambda - \ln\mathcal{Z} - \mathcal{Z}\sqrt{1+\zeta^2}\right)\right]^{1/2}$
$u_r(R,\phi,\theta)$	$\frac{2}{5}R^2\kappa_c\left[(1+12\lambda)\sin 2\phi\right]$	$-\kappa_c\Phi$
$u_r(r,\theta,z)$	$\frac{2}{5}rz\kappa_c\left(1+12\lambda\right)$	$-\kappa_c\mathcal{Z}$
$u_z(R,\phi,\theta)$	$\frac{2}{5}R^2\kappa_c\left[(1-18\lambda)\cos 2\phi - 3 - 6\lambda\right]$	$\kappa_c\left(\lambda - \ln\Phi - 1\right)$
$u_z(r,\theta,z)$	$\frac{2}{5}\kappa_c\left[(6\lambda - 2)\,r^2 - (1+12\lambda)\,z^2\right]$	$\kappa_c\left(\lambda - \ln\mathcal{Z} - 1\right)$

Table 4.3: Generalized Beltramian and Beltramian cases vorticity comparison.

Variable	Generalized Beltramian ($\nabla \times \mathbf{u} \times \boldsymbol{\omega} = 0$)	Beltramian ($\mathbf{u} \times \boldsymbol{\omega} = 0$)
$\omega_R\,(R, \phi, \theta)$	0	$\kappa_c \dfrac{u_R}{B}$
$\omega_R\,(r, \theta, z)$	0	$\kappa_c \dfrac{u_R}{B}$
$\omega_\phi\,(R, \phi, \theta)$	0	$\kappa_c \dfrac{u_\phi}{B}$
$\omega_\phi\,(r, \theta, z)$	0	$\kappa_c \dfrac{u_\phi}{B}$
$\omega_\theta\,(R, \phi, \theta)$	$4\kappa_c R \sin\phi$	$\kappa_c \dfrac{u_\theta}{B}$
$\omega_\theta\,(r, \theta, z)$	$4\kappa_c r$	$\kappa_c \dfrac{u_\theta}{B}$
$\omega_r\,(R, \phi, \theta)$	0	$\kappa_c \dfrac{u_r}{B}$
$\omega_r\,(r, \theta, z)$	0	$\kappa_c \dfrac{u_r}{B}$
$\omega_z\,(R, \phi, \theta)$	0	$\kappa_c \dfrac{u_z}{B}$
$\omega_z\,(r, \theta, z)$	0	$\kappa_c \dfrac{u_z}{B}$

Table 4.4: Generalized Beltramian and Beltramian cases pressure comparison.

Variable	Generalized Beltramian ($\nabla \times \mathbf{u} \times \boldsymbol{\omega} = 0$)	Beltramian ($\mathbf{u} \times \boldsymbol{\omega} = 0$)
$\frac{\partial p}{\partial r}$	$\frac{1}{r^3} + \frac{32}{25}\kappa_c^2 r^3 \left(36\lambda^2 - 9\lambda - 1\right)$	$\frac{\mathcal{Z}_2}{r^3} + \frac{\kappa_c^2 \mathcal{Z}_2}{r}\left[\zeta^2 \mathcal{Z}_1 - \zeta^3 + \zeta \mathcal{Z}_2 \left(\lambda - \ln \mathcal{Z} - 1\right)\right]$
$\frac{\partial p}{\partial z}$	$-\frac{32}{25}\kappa_c^2 z^3 \left(1 + 12\lambda\right)$	$\frac{\kappa_c^2 \mathcal{Z}_2}{r}\left(\zeta^2 - \zeta \mathcal{Z}_1 - \lambda + \ln \mathcal{Z} + 1\right)$
$p\left(r, z\right)$	$-\frac{1}{2r^2} - \frac{8}{25}\kappa_c^2 \tau$	$-\frac{1}{2r^2} + \frac{1}{2}\kappa_c^2 \tau$
$\tau\left(r, z\right)$	$\left(36\lambda^2 - 9\lambda - 1\right) r^4 + \left(144\lambda^2 + 24\lambda + 1\right) z^4$	$\left(\zeta + \zeta^3\right) \mathcal{Z}_2 - \zeta^2 - \ln^2 \mathcal{Z} - \left(2\lambda - 1\right) \ln\left(\mathcal{Z} + 2\zeta\right)$

Chapter 5

The Generalized Beltramian Conical Bidirectional Vortex (BDV): Results and Discussion

5.1 Mantle Location & Streamlines

The generalized Beltramian (GB) mantle formulation appears exactly as the Beltramian case, except the equations are different to the respective solutions. Again, the BG analysis engenders two mantle locations, one each for the spherical radial velocity and axial velocity. The velocity equations are solved for the roots and appear as

$$\lambda\left(18\cos\phi - 30\cos^3\phi\right) - \cos\phi = 0 \tag{5.1.1}$$

$$(1 - 18\lambda)\cos 2\phi - 3 - 6\lambda = 0 \tag{5.1.2}$$

Tables 5.1–5.3 display the characteristics of the GB solution and the comparison to the values for the original Beltramian solution. Tables 5.1 and 5.2 provide information on the constant lambda, λ, the angle of the spherical radial velocity mantle, β_R, the ratio in

Table 5.1: Comparison of mantle inclinations versus conical divergence angle.

	Generalized Beltramian ($\nabla \times \mathbf{u} \times \boldsymbol{\omega} = 0$)			Beltramian ($\mathbf{u} \times \boldsymbol{\omega} = 0$)		
α	λ	β_R	β_z	λ	β_R	β_z
5°	-0.084	3.5°	3.5°	-2.63	3.0°	3.0°
10°	-0.087	7.1°	7.1°	-1.92	6.1°	6.1°
15°	-0.091	10.5°	10.7°	-1.52	9.1°	9.2°
20°	-0.098	13.1°	14.4°	-1.22	12.1°	12.6°
25°	-0.107	17.4°	18.2°	-0.982	15.2°	15.7°
30°	-0.121	20.7°	22.2°	-0.781	18.2°	19.1°
35°	-0.142	23.9°	26.3°	-0.605	21.2°	22.7°
40°	-0.172	27.0°	30.7°	-0.445	24.2°	26.5°
45°	-0.222	30.0°	35.3°	-0.296	27.2°	30.6°

percentage of the spherical radial velocity mantle to the divergence half-angle, β_R/α, the angle of the axial velocity mantle, β_z, and the ratio in percentage of the axial velocity mantle to the divergence half-angle, β_z/α. Table 5.3 shows the ratio of the mantle radius at the top of the cone, $(a = 1, z/L = 1)$, for both the spherical radial velocity mantle and the axial velocity mantle, X_{β_R}, and X_{β_z}, respectively. Additionally, Table 5.3 compares the difference between the spherical radial velocity mantle and the axial velocity mantle in degrees and percentage for both the GB and Beltramian solution.

Examining Tables 5.1–5.3 reveal the characteristics about the GB solution and the differences between the behavior of the GB model compared to the Beltramian model. One characteristic for both solutions shows that the differences between the spherical radial velocity mantle and axial velocity mantle begin at or near zero and remain small for low divergence half-angles. When the divergence half-angle reaches 45°, there only exist a difference of approximately 5° and 3° for the GB model and Beltramian model, respectively. In both cases, the axial velocity mantle becomes larger than the spherical radial velocity mantle. A second characteristic involves the ratio in percentage of the

Table 5.2: Comparison of mantle inclination ratios versus conical divergence angle.

	Generalized Beltramian ($\nabla \times \mathbf{u} \times \boldsymbol{\omega} = 0$)			Beltramian ($\mathbf{u} \times \boldsymbol{\omega} = 0$)		
α	λ	β_R/α (%)	β_z/α (%)	λ	β_R/α (%)	β_z/α (%)
5°	-0.084	70.7	70.7	-2.63	60.7	60.6
10°	-0.087	70.5	71.1	-1.92	60.6	61.0
15°	-0.091	70.3	71.5	-1.52	60.6	61.4
20°	-0.098	70.0	72.2	-1.22	60.6	62.0
25°	-0.107	69.6	73.0	-0.982	60.6	62.8
30°	-0.121	69.0	74.0	-0.781	60.5	63.8
35°	-0.142	68.4	75.3	-0.605	60.5	64.9
40°	-0.172	67.6	76.7	-0.445	60.5	66.4
45°	-0.222	66.7	78.4	-0.296	60.4	68.0

Table 5.3: Mantle inclination versus conical divergence angle.

	Generalized Beltramian ($\nabla \times \mathbf{u} \times \boldsymbol{\omega} = 0$)				Beltramian ($\mathbf{u} \times \boldsymbol{\omega} = 0$)			
α	X_{β_R}	X_{β_z}	$\lvert\beta_R - \beta_z\rvert$ (%)	$\lvert\beta_R - \beta_z\rvert^\circ$	X_{β_R}	X_{β_z}	$\lvert\beta_R - \beta_z\rvert$ (%)	$\lvert\beta_R - \beta_z\rvert^\circ$
5°	0.706	0.707	0.0	0°	0.606	0.606	0.1	0.0°
10°	0.702	0.707	0.6	0°	0.602	0.606	0.4	0.0°
15°	0.694	0.707	1.2	0.2°	0.597	0.605	0.8	0.1°
20°	0.685	0.707	2.2	1.3°	0.590	0.604	1.4	0.5°
25°	0.672	0.707	3.4	0.8°	0.580	0.603	2.2	0.5°
30°	0.655	0.707	5.0	1.5°	0.568	0.601	3.3	0.9°
35°	0.634	0.707	6.9	2.4°	0.553	0.598	4.4	1.5°
40°	0.608	0.707	9.1	3.7°	0.535	0.595	5.9	2.3°
45°	0.577	0.707	11.7	5.3°	0.514	0.592	7.6	3.4°

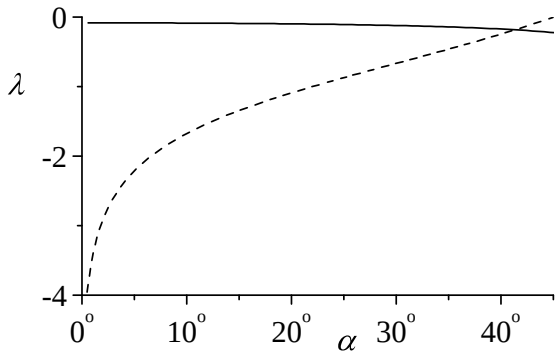

Figure 5.1: The constant, λ, which derives from the divergence half-angle wall BC, as it varies with divergence half-angle, α. Here the present model (——) is compared to the Beltramian model (– – –).

spherical radial velocity mantle to the divergence half-angle. The ratio in percentage of the spherical radial velocity mantle to the divergence half-angle begins at 70.7% for a divergence half-angle of 5° and slowly reduces to 66.7% as the divergence half-angle increases to 45°. The 70.7% remarkably pinpoints the same theoretical mantle location as the complex lamellar type BDV in a cylinder (Vyas et al. 2003a; Vyas and Majdalani 2006). The spherical radial velocity for the Beltramian solution exhibits a similar behavior as it remains close to 60.7% as the divergence half-angle increases. A third characteristic illustrates that while the spherical radial velocity mantle decreases for the ratio in percentage of the spherical radial velocity mantle to the divergence half-angle, the axial velocity mantle increases. However, the radial distance of the spherical radial velocity mantle at $z/L = 1$ decreases with successive increases in divergence half-angles while the axial velocity mantle radial distance remains exactly the same at 0.707 of the maximum radius when $a = 1$. Finally, graphs for the model comparisons of the constant, λ, and both mantles are shown in Figure 5.1 and Figure 5.2, respectively.

Figure 5.3 plots the streamlines for both the GB model and the Beltramian model. Solid lines plot the streamline paths for the GB model in the $r - z$ plane while dashed lines trace the Beltramian model. Figures 5.3a–5.3c show the conical BDV at divergence half-angles of $\alpha = 15°$, 30°, and 45°, respectively. The spherical velocity mantle angles appear on Figure 5.3 where the larger angle denotes the GB solution and the smaller angle

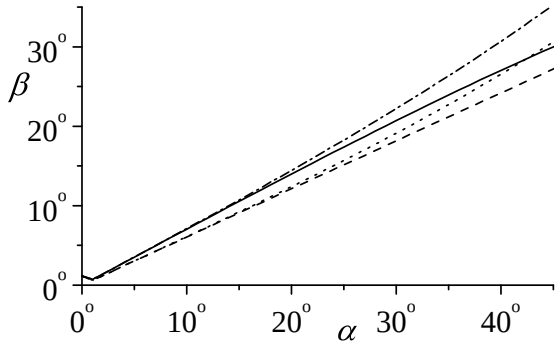

Figure 5.2: The mantle delineation angles, β, vs. the divergence half-angle, α. Here the present GB models for β_R (——) and β_z $(- \cdot -)$ compared to the Beltramian models β_R $(- - -)$ and β_z $(\cdots)$, respectively.

the Beltramian solution. Both Figure 5.3a and Figure 5.3b show a deeper convection of streamlines for the uppermost curve for the GB solution compared to the Beltramian solution. However, the following lower curves display the opposite effect with a deeper convection by the Beltramian solution over the GB solution. Figure 5.3a presents the same effects except that the second streamline curves remain about even at the deepest maximum for both solutions. The deeper convection for the Beltramian solution in the lower portion of the cyclones and vice versa for the GB solution can be contributed to the mantle shift predicted by the models.

5.2 Velocities

Figure 5.4 depicts the spherical radial, u_R, zenith, u_ϕ, axial, u_z, and cylindrical radial velocities, u_r, for a divergence half-angle of $\alpha = 45°$, $\kappa_c = 1$, and four axial locations of $z/L = 0.25$, 0.5, 0.75, and 1. A general characteristic of all the velocities corroborates the streamlines in Figure 5.3. In the higher axial locations, the magnitudes of the velocities of the GB model are greater than those of the Beltramian model. However, the opposite effect occurs at the lowest axial locations. The spherical radial velocity and axial velocity contain very similar curves for the GB model, as well as the Beltramian. However, the GB model includes a R^2 term in SPC for both the spherical radial velocity and axial velocity

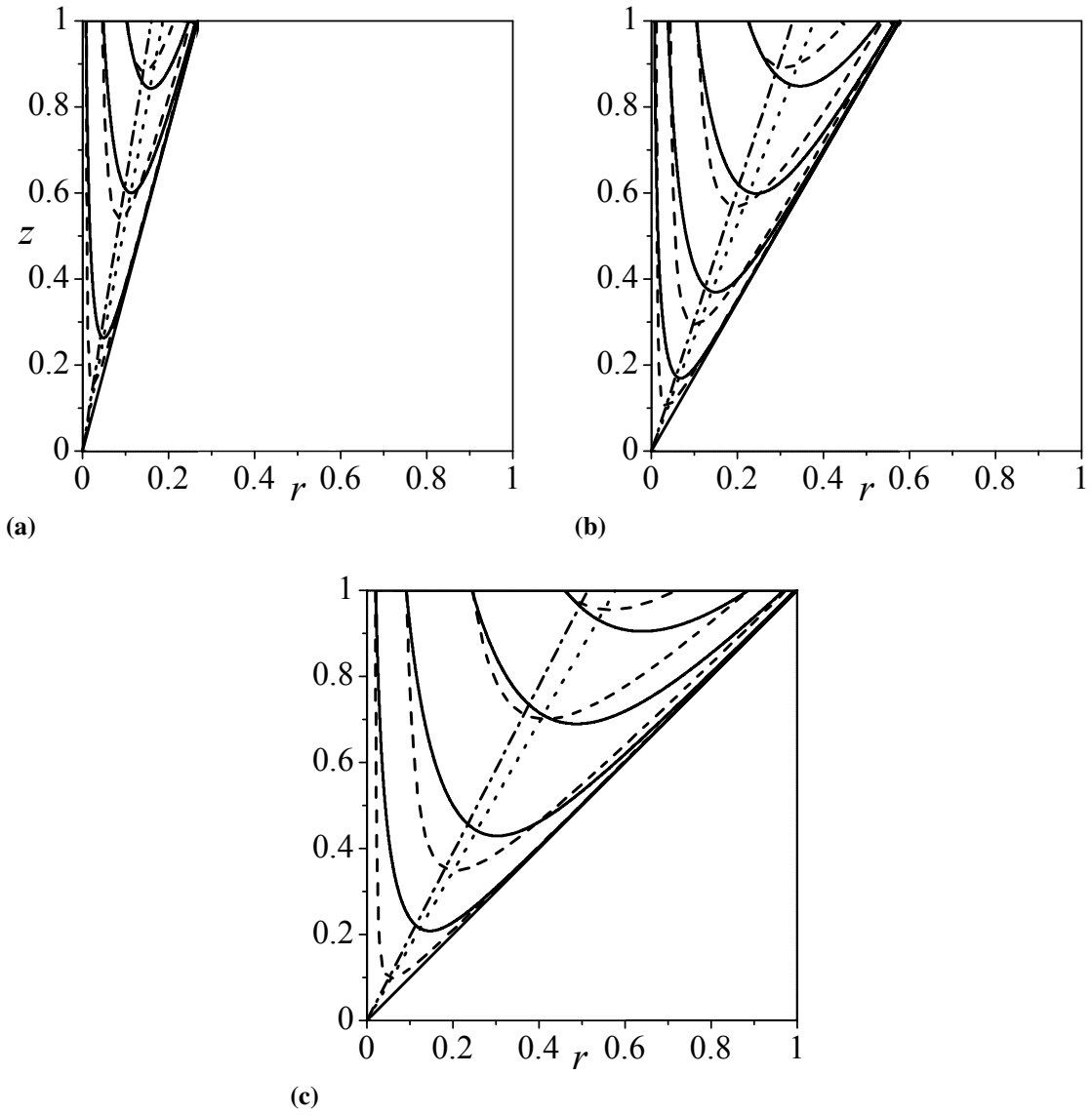

Figure 5.3: Flow streamlines for $\sigma_c = 1$ and cone half-angles of α = (a) 15°, (b) 30°, and (c) 45°. Here the present model (——) is compared to the Beltramian model (– – –).

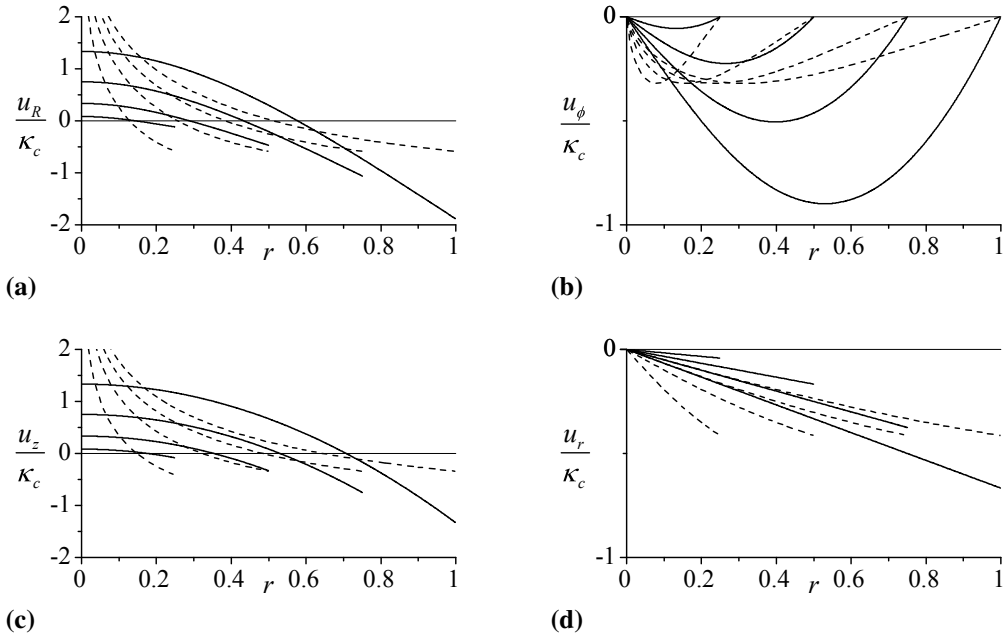

Figure 5.4: The (a) spherical radial velocity, u_R, (b) zenith velocity, u_ϕ, (c) axial velocity, u_z, and (d) cylindrical radial velocities, u_r, at four axial locations $z/L = 0.25$, 0.50, 0.75, and 1 for $\alpha = 45°$. Here the present model (——) is compared to the Beltramian model (– – –).

while the Beltramian model only depends upon the zenith angle, ϕ, for both the spherical radial velocity and axial velocity (see Table 4.2). The influence of the R^2 term causes the the spherical radial velocity and axial velocity to remain finite as the radius approaches the core, a much more favorable quality for an inviscid model. The zenith velocity preserves a parabolic form for the GB model while the radial velocity preserves a linear form. Both the zenith velocity and the radial velocity of the GB model indicate an inward flow, the same as the Beltramian case.

Figure 5.5 plots the GB solution tangential velocity and axial velocity against the Beltramian model and experimental and numerical data from Hsieh and Rajamani (1988) and Monredon et al. (1992). Unfortunately, the tangential velocity from the GB solution does not add any information since the tangential velocity takes the form of a free vortex. The axial velocity provides promising results since the velocity remains finite at the centerline and matches relatively well in the less viscous regions away from the axis and

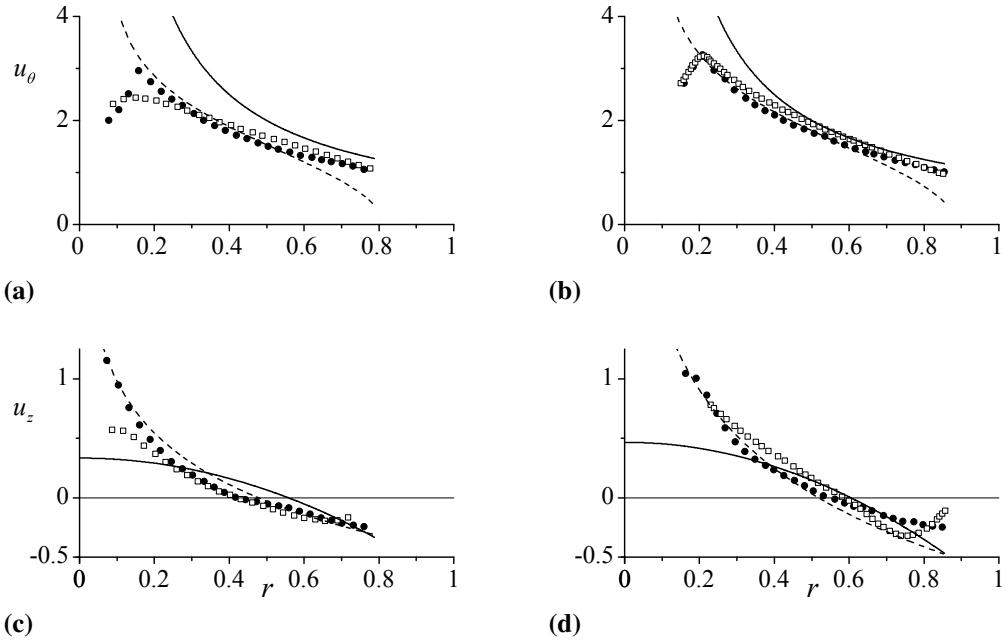

Figure 5.5: Present theoretical velocity (——) and the Beltramian model (− − −) compared to experimental (•) and numerical (□) data by (a) and (c) Hsieh and Rajamani (1988), and (b) and (d) Monredon et al. (1992).

wall. The axial velocity data from Hsieh and Rajamani (1988) and Monredon et al. (1992) shows a sharp rise near the centerline. However, an air core is present in the hydrocyclone analysis conducted by Hsieh and Rajamani (1988) and Monredon et al. (1992) which restricts the data collection capabilities. Likewise, the axial velocity profile could also be useful for other BCs or flow conditions. Thus, the data gathered from the GB and Beltramian solutions provide two additional models for vortex flows.

5.3 Vorticity & Pressure

Lastly, Figure 5.6 exhibits the pressure difference and vorticity magnitude plots for the GB model in contrast to the Beltramian model for four axial locations of $z/L = 0.25, 0.5, 0.75,$ and 1, $\kappa_c = 1$, and a divergence half-angle of $\alpha = 30°$. Figure 5.6a results in a pressure drop for the GB model similar to Beltramian model. Again, the dominating term, $\frac{1}{2}r^{-2}$, defines the slope of the curve. Figure 5.6b shows the graph of the vorticity magnitude. The

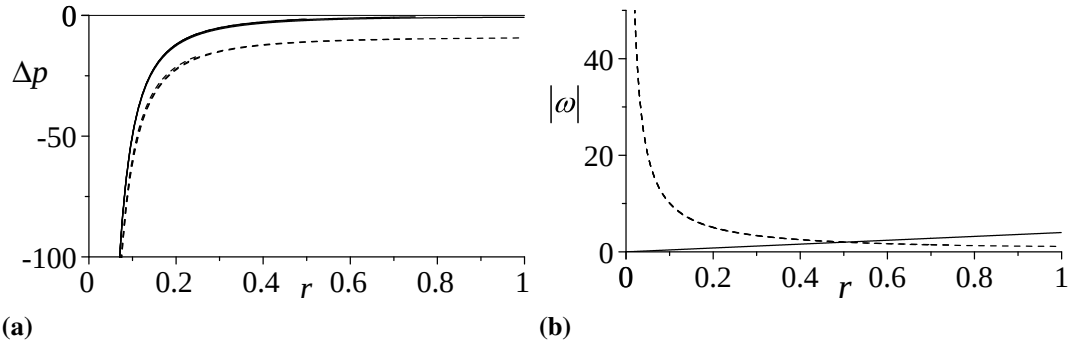

Figure 5.6: Distribution of (a) pressure and (b) vorticity magnitude at four axial locations z/L = 0.25, 0.5, 0.75, and 1 for α = 30°. Here the present model (——) is compared to the Beltramian model (– – –).

vorticity magnitude for the GB model remains highest near the conical wall and linearly decreases to zero as the radius decreases to zero. The vorticity magnitude varies linearly in r since the GB model only contains one vorticity component, the tangential vorticity.

Chapter 6

Conclusions

The analysis of this dissertation engenders two new solutions, one of the generalized Beltramian (GB) type [$\nabla \times \mathbf{u} \times \boldsymbol{\omega} = 0$] and the other of the Beltramian type [$\mathbf{u} \times \boldsymbol{\omega} = 0$]. The solutions presented here provide clear and exact derivations and results, specifically, two additional models are introduced to classify bidirectional vortex flows for a conical geometry. The GB and Beltramian solutions mimic the physical flow field of a cyclone separator or conical combustion chamber. Both solutions engender from the Bragg-Hawthorne equation with appropriate boundary conditions which provide the double helix motion within a cone. Values are obtained for the stream functions, velocities, pressure distributions, and vorticity. Additional properties, such as the dual mantle locations and conical swirl parameters, are also found which determine important characteristics of the models and effects on flow fields.

The Beltramian solution is based upon inviscid, incompressible assumptions resulting in the Bragg-Hawthorne equation (BHE). A vorticity distribution formulation conditional to a uniform inlet axial velocity allows for the swirl velocity to vary axially rather than the traditional free vortex model. The BHE is then solved utilizing a straightforward separation of variables technique with proper boundary condition to bring forth the stream function solution. Once the stream function is at hand, the spherical polar velocities and cylindrical polar velocities are obtained in both spherical polar coordinates and cylindrical

polar coordinates. Following the velocity derivations, the pressure distribution and vorticity are found from fluid dynamics principles. A modified conical swirl number relates the axial and tangential inlet velocities and provides a controlling parameter to vary the flow field characteristics. Two mantle locations are verified by setting the spherical radial velocity and axial velocity equal to zero. Streamlines and velocities are produced for a range of conical divergent half-angles. The tangential and axial velocities are then compared to two hydrocyclone experimental and numerical cases with favorable agreement.

A similar approach is taken for the GB model. However, a half-parabolic axial profile at the inlet is imposed instead of the Beltramian uniform profile assumption. The vorticity distribution for the GB model is based upon the Bernoulli equation as opposed to the Beltramian model and the angular momentum condition. The resulting separation of variables produces an ordinary differential equation of the Gegenbauer type, a generalization of the Legendre type. Resulting flow properties such as the stream function, velocities, pressure, and vorticity are then derived and compared to the Beltramian counterparts. Most importantly, the spherical polar and axial velocities of the GB type model do not exhibit the singular behavior at the centerline, unlike the Beltramian solution. Viscous models are suggested for future studies in order to model friction effects near the centerline and conical walls.

Swirling flow and vortices make up many fluid phenomena including meteorological events (tornadoes, hurricanes, dust devils, fire whirls, weather systems), astronomical events (spiral galaxies, star and planet magnetic fields, black holes), combustion events (swirl injectors, combustors, furnaces), and power production (gas turbines, solar vortex towers, hydroelectric turbines, propulsion systems). On a mesoscale, swirling pipe and convergent or divergent nozzle flow encompass copious flow conditions and devices, including heat transfer enhancement, combustion mixing enhancement and lengthened entrainment, particle separation and entrainment, contactless suction, and electro-/magneto-hydrodynamics, for example. Thus, the developed models contribute to an understanding of the swirling flow and vortex dynamics scientific communities in a general sense.

This dissertation addresses several important fluid dynamic and related fundamentals. However, the area of vortex dynamics encompass a myriad of topics that should be investigated. These topics include the Bragg-Hawthorne or Squire-Long (also Beltrami-Gromeka) equation, Beltrami and related flows and conditions, and mathematical fluid aspects. Work is recommended to develop generalized solutions and explore their symmetry and topology. It is further desirable to address variational Hamiltonian principles in order to develop a generalized, perhaps unified theory of numerous vortex and swirl related phenomena. Most importantly, the dissertation has laid the groundwork for a myriad of other investigations including, viscous solutions, compressible solutions, and solutions for other geometries and boundary conditions.

Bibliography

Abrahamson, J., Martin, C. G., and Wong, K. K. (1978). The physical mechanisms of dust collection in a cyclone. *Transactions of the Institution of Chemical Engineers - Chemical Engineering Research and Design*, 56a:168–177.

Akiki, G. (2011). *On the bidirectional vortex engine flowfield with arbitrary endwall injection*. PhD thesis, University of Tennessee. 41, 87

Akiki, G. and Majdalani, J. (2010). On the bidirectional vortex with arbitrary endwall velocity. In *46th AIAA/ASME/SAE/ASEE Joint Propulsion Conference & Exhibit*. AIAA Paper No. 2010-6652. 41, 85, 93

Akiki, G. and Majdalani, J. (2012). New framework for modeling the bidirectional vortex engine flowfield with arbitrary injection. In *50th AIAA Aerospace Sciences Meeting including the New Horizons Forum and Aerospace Exposition*. AIAA Paper No. 2012-0138. 41, 93

Alekseenko, S. V., Kuĭbin, P. A., and Okulov, V. L. (2007). *Theory of Concentrated Vortices*. Springer, Berlin, Germany. 20, 21, 22

Alkemade, A. J. Q. (1993). *On vortex atoms and vortons*. PhD thesis, Delft University of Technology. 12, 13, 15, 16

Arfken, G. B. and Weber, H.-J. (2005). *Mathematical Methods for Physicists*. Academic Press, San Diego, 6 edition. 125

Avci, A. and Karagoz, I. (2003). Effects of flow and geometrical parameters on the collection efficiency in cyclone separators. *Journal of Aerosol Science*, 34(7):937–955.

Barber, T. A. and Majdalani, J. (2009). Exact Eulerian solution of the conical bidirectional vortex. In *45th AIAA/ASME/SAE/ASEE Joint Propulsion Conference & Exhibit*. 118

Barth, W. (1956). Berechnung und auslegung von zyklonabscheiden auf grund neuerer untersuchungen (Design and layout of the cyclone separator on the basis of new investigations). *Brennstoff-Warme-Kraft*, 8(1):1–9. 87

Batchelor, G. K. (1951). Note on a class of solutions of the Navier-Stokes equations representing steady rotationally-symmetric flow. *The Quarterly Journal of Mechanics and Applied Mathematics*, 4(1):29–41. 3

Batchelor, G. K. (2000). *An Introduction to Fluid Dynamics*. Cambridge University Press, New York. 22

Batterson, J. W., Maicke, B. A., and Majdalani, J. (2007). Advancements in theoretical models of confined vortex flowfields. In *JANNAF 54th Propulsion Meeting/3rd Liquid Propulsion Subcommittee/2nd Spacecraft Propulsion Subcommittee/5th Modelingand Simulation Subcommittee Joint Meeting, Denver, CO, 14-17 May 2007*. 85, 93

Batterson, J. W. and Majdalani, J. (2010a). On the viscous bidirectional vortex. part 3: multiple mantles. In *46th AIAA/ASME/SAE/ASEE Joint Propulsion Conference & Exhibit*. AIAA Paper No. 2010-6765. 95

Batterson, J. W. and Majdalani, J. (2010b). Sidewall boundary layers of the bidirectional vortex. *Journal of Propulsion and Power*, 26(1):102–112. 105

Bellamy-Knights, P. G. (1970). An unsteady two-cell vortex solution of the Navier-Stokes equations. *Journal of Fluid Mechanics*, 41(03):673–687. 95

Bellamy-Knights, P. G. (1971). Unsteady multicellular viscous vortices. *Journal of Fluid Mechanics*, 50(01):1–16. 95

Beltrami, E. (1889). Considerazioni idrodinamiche (Considerations on hydrodynamics). *Rendiconti del Reale Istituto Lombardo di Scienze Lettere (Proceedings of the Royal Lombard Institute of Sciences, Letters)*, 22(2):122–131. 20

Bergström, J. and Vomhoff, H. (2007). Experimental hydrocyclone flow field studies. *Separation and Purification Technology*, 53(1):8–20. 87

Berker, A. R. (1936). *Sur Quelques Cas d'Integration des Equations du Mouvement d'un Fluide Visqueux Incompressible*. Imprimerie A. Taffin-Lefort, Paris-Lille. 3, 7

Berker, A. R. (1963). Integration des equations du mouvement d'un fluide visqueux incompressible. In Flügge, S., editor, *Handbuch der Physik VIII/2*, volume 8/2, pages 1–384. Springer-Verlag, Berlin. 7

Berman, A. S. (1953). Laminar flow in channels with porous walls. *Journal of Applied Physics*, 24(9):1232–1235.

Bhattacharyya, P. (1980a). Theoretical study of the flow field inside a hydrocyclone with vortex finder diameter greater than that of apex opening-I. laminar case. *Applied Scientific Research*, 36(3):197–212. 85, 86, 96, 107

Bhattacharyya, P. (1980b). Theoretical study of the flow field inside a hydrocyclone with vortex finder diameter greater than that of apex opening-II. turbulent case. *Applied Scientific Research*, 36(3):213–225.

Bhattacharyya, P. (1985). Theoretical study of the flowfield inside a hydrocyclone for higher Reynolds numbers. *Applied Scientific Research*, 42(1):3–13. 87

Binnie, A. M. (1957). Experiments on the slow swirling flow of a viscous liquid through a tube. *The Quarterly Journal of Mechanics and Applied Mathematics*, 10(3):276–290. 87, 92

Binnie, A. M. and Harris, D. P. (1950). The application of boundary-layer theory to swirling liquid flow through a nozzle. *The Quarterly Journal of Mechanics and Applied Mathematics*, 3(1):89–106. 88

Binnie, A. M. and Hookings, G. A. (1948). Laboratory experiments on whirlpools. *Proceedings of the Royal Society of London. Series A, Mathematical and Physical Sciences*, 194(1038 (September 2)):398–415. 90

Binnie, A. M., Hookings, G. A., and Kamel, M. Y. M. (1957). The flow of swirling water through a convergent-divergent nozzle. *Journal of Fluid Mechanics*, 3(03):261–274. 87

Binnie, A. M. and Teare, J. D. (1956). Experiments on the flow of swirling water through a pressure nozzle and an open trumpet. *Proceedings of the Royal Society of London. Series A, Mathematical and Physical Sciences*, 235(1200 (April 10)):78–89. 85, 86, 87, 88, 89, 90, 91, 92, 93, 94, 95

Bloor, M. I. G. and Ingham, D. (1984a). The Influence of Vorticity on the Efficiency of the Hydrocyclone. In *2nd International Conference on Hydrocyclones, BHRA, Bath, England, paper B*, volume 2, pages 41–50.

Bloor, M. I. G. and Ingham, D. B. (1973a). On the efficiency of the industrial cyclone. *Transactions of the Institution of Chemical Engineering: Chemical Engineering Research and Design*, 51a:173–176. 87

Bloor, M. I. G. and Ingham, D. B. (1973b). Theoretical investigation of the flow in a conical hydrocyclone. *Chemical Engineering Research and Design*, 51a:36–41.

Bloor, M. I. G. and Ingham, D. B. (1975). Turbulent spin in a hydrocyclone. *Transactions of the Institution of Chemical Engineers*, 53:1–6.

Bloor, M. I. G. and Ingham, D. B. (1976). Boundary layer flows on the side walls of conical cyclones. *Transactions of the Institution of Chemical Engineering: Chemical Engineering Research and Design*, 54(a):276–280.

Bloor, M. I. G. and Ingham, D. B. (1983). *Theoretical aspects of hydrocyclone flows*, volume 3. 87

Bloor, M. I. G. and Ingham, D. B. (1984b). A theoretical investigation of the fluid mechanics of the hydrocyclone. *Filtration & separation*, 21(4):266–269.

Bloor, M. I. G. and Ingham, D. B. (1987). The flow in industrial cyclones. *Journal of Fluid Mechanics*, 178:507–519. xii, 1, 31, 38, 44, 61, 81, 82, 83, 84, 98, 104, 112, 113, 118

Bojarevičs, V., Freibergs, Y., Shilova, E. I., and Shcherbinin, E. V. (1989). *Electrically Induced Vortical Flows*. Mechanics of Fluids and Transport Processes. Kluwer Academic Publishers, Dordrecht; Boston. 43, 125, 126, 129

Bottaro, A., Ryhming, I. L., Wehrli, M. B., Rys, F. S., and Rys, P. (1991). Laminar swirling flow and vortex breakdown in a pipe. *Computer Methods in Applied Mechanics and Engineering*, 89(1-3):41–57. 85, 87

Boysan, F., Ayers, W. H., and Swithenbank, J. (1982). A fundamental mathematical modelling approach to cyclone design. *Chemical Engineering Research and Design*, 60(a):222–230. 87

Bradley, D. (1965). *The Hydrocyclone*. Pergamon Press, Oxford. 85, 86, 91, 94, 95, 96

Bradley, D. and Pulling, D. J. (1959). Flow -atterns in the hydraulic cyclone and their interpretation in terms of performance. *Tranactions of the Institution of Chemical Engineers - Chemical Engineering Research and Design*, 37a:34–45. 85, 86, 91, 92, 93, 94, 95, 96

Bragg, S. L. and Hawthorne, W. R. (1950). Some exact solutions of the flow through annular cascade actuator discs. *Journal of Aeronautical Sciences*, 17(4):243–249. 26

Brayshaw, M. D. (1990). A numerical model for the inviscid flow of a fluid in a hydrocyclone to demonstrate the effects of changes in the vorticity function of the flow

field on particle classification. *International Journal of Mineral Processing*, 29(1-2):51–75. 87

Brücker, C. (1993). Study of vortex breakdown by particle tracking velocimetry (PTV) part 2: spiral-type vortex breakdown. *Experiments in Fluids*, 14(1-2):133–139.

Brücker, C. (2002). Some observations of vortex breakdown in a confined flow with solid body rotation. *Flow, Turbulence and Combustion*, 69(1):63–78. 87

Brücker, C. and Althaus, W. (1992). Study of vortex breakdown by particle tracking velocimetry (PTV) part I: bubble-type vortex breakdown. *Experiments in Fluids*, 13(5):339–349. 87

Brücker, C. and Althaus, W. (1995). Study of vortex breakdown by particle tracking velocimetry (PTV) Part 3: time-dependent structure and development of breakdown-modes. *Experiments in Fluids*, 18(3):174–186.

Bucher, J., Edmonds, R. G., Steele, R. C., Kendrick, D. W., Chenevert, B. C., and Malte, P. C. (2003). The development of a lean-premixed trapped vortex combustor. In *Proceedings of ASME Turbo Expo 2003 - Power for Land, Sea, and Air*. ASME Paper No. GT-2003-38263. 19

Castro, O., Concha, F., Montero, J., Miranda, J., Castro, J., and Urizar, D. (1996). Air core modelling for an industrial hydrocyclone. In Claxton, D., Svarovsky, L., and Thew, M., editors, *International Conference on Hydrocyclones '96*, pages 229–239, Cambridge, UK. MEP Ltd. 87

Cervantes, M. J. and Gustavsson, L. H. (2007). On the use of the Squire-Long equation to estimate radial velocities in swirling flows. *Journal of Fluids Engineering*, 129(2):209–217. 26

Chaplygin, S. A. (1899). On a pulsating cylindrical vortex. *Trudy otdeleniya fizicheskikh nauk imperatorskogo Moskovskogo obshchestva lyubitelei estestvoznaniya, antropologii*

i etnografii (Proceedings of the Physical Sciences Division of the Imperial Moscow Society of Naturalists, Anthropology and Ethnography), 10(1):13–22.

Chaplygin, S. A. (1903). One case of vortex motion in fluid. *Trudy otdeleniya fizicheskikh nauk imperatorskogo Moskovskogo obshchestva lyubitelei estestvoznaniya, antropologii i etnografii (Proceedings of the Physical Sciences Division of the Imperial Moscow Society of Naturalists, Anthropology and Ethnography)*, 11(2):11–14.

Chesnokov, Y. G., Bauman, A. V., and Flisyuk, O. M. (2006). Calculation of the velocity field of a fluid in a hydrocyclone. *Russian Journal of Applied Chemistry*, 79(5):774–777.

Chiné, B. and Concha, F. (2000). Flow patterns in conical and cylindrical hydrocyclones. *Chemical Engineering Journal*, 80(1-3):267–273. 87

Chow, C.-Y. (1969). Swirling flow in tubes of non-uniform cross-sections. *Journal of Fluid Mechanics*, 38(04):843–854. 87

Church, C. R., Snow, J. T., Baker, G. L., and Agee, E. M. (1979). Characteristics of tornado-like vortices as a function of swirl ratio: a laboratory investigation. *Journal of the Atmospheric Sciences*, 36(9):1755–1776.

Concha, F. (2007). Flow pattern in hydrocyclones. *KONA*, 25:97–132. 107

Cooper, A. J. and Peake, N. (2001). Propagation of unsteady disturbances in a slowly varying duct with mean swirling flow. *Journal of Fluid Mechanics*, 445:207–234. 22

Culick, F. E. C. (1966). Rotational axisymmetric mean flow and damping of acoustic waves in a solid propellant rocket. *AIAA Journal*, 4(8):1462–1464. 30

Dabir, B. and Petty, C. A. (1986). Measurements of mean velocity profiles in a hydrocyclone using laser doppler anemometry. *Chemical Engineering Communications*, 48(4):377–388. 87

Dassios, G. (2008). *Spheriodal and Spherical Green's Function for Stokes Flow*, pages 117–123. World Scientific Publishing Company, Hackensack, NJ. 125, 129

Dassios, G. and Vafeas, P. (2006). *Spheriodal Semiseparation in Stokes Flow Revisted*, pages 136–143. World Scientific Publishing Company, Singapore ; Hackensack, NJ. 125, 129

Dassios, G. and Vafeas, P. (2008). On the spheroidal semiseparation for Stokes flow. *Research Letters in Physics*. 125, 129

Delery, J. M. (1994). Aspects of vortex breakdown. *Progress in Aerospace Sciences*, 30(1):1–59. 87

Derksen, J. J. (2003). Separation performance predictions of a Stairmand high-efficiency cyclone. *AIChE Journal*, 49(6):1359–1371. 96

Derksen, J. J. and van den Akker, H. E. A. (2000). Simulation of vortex core precession in a reverse-flow cyclone. *AIChE Journal*, 46(7):1317–1331. 57

Dietz, P. W. (1981). Collection efficiency of cyclone separators. *AIChE Journal*, 27(6):888–892. 96

Donaldson, C. D. (1957). *Solutions of the Navier-Stokes equations for two and three dimensional vortices*. PhD thesis, Princeton University. 4

Donaldson, C. D. and Sullivan, R. D. (1960). Behaviour of solutions of the Navier-Stokes equations for a complete class of three-dimensional viscous vortices. In *Proceedings of the 1960 Heat Transfer Fluid Dynamics Institute*, pages 16–30. 95

Donnelly, R. J. (1991). *Quantized Vortices in Helium II*. Cambridge Studies in Low Temperature Physics. Cambridge University Press, New York. 17

Drazin, P. G. and Riley, N. (2006). *The Navier-Stokes Equations: A Classification of Flows and Exact Solutions*. Cambridge University Press, Cambridge, UK. 7, 8, 10, 11

Dryden, H. L., Murnaghan, F. D., and Bateman, H. (1932). Report of the committee on hydrodynamics. Technical Report 84. 7

Duda, J. L. and Vrentas, J. S. (1972). Inviscid flow through a sudden contraction. *Industrial & Engineering Chemistry Fundamentals*, 11(4):590–593. 82, 94

Escudier, M. P., Bornstein, J., and Zehnder, N. (1980). Observations and LDA measurements of confined turbulent vortex flow. *Journal of Fluid Mechanics*, 98(01):49–63. 85, 92

Faler, J. H. and Leibovich, S. (1977). Disrupted states of vortex flow and vortex breakdown. *Physics of Fluids*, 20(9):1385–1400. 87

Faler, J. H. and Leibovich, S. (1978). An experimental map of the internal structure of a vortex breakdown. *Journal of Fluid Mechanics*, 86(02):313–335. 87

Finch, J. M. (1885). Dust collector. 35

Fist, A. and Majdalani, J. (2014). Improved mean flow solution for solid rocket motors. In *52nd Aerospace Sciences Meeting*. American Institute of Aeronautics and Astronautics.

Fraenkel, L. E. (1956). On the flow of rotating fluid past bodies in a pipe. *Proceedings of the Royal Society of London. Series A, Mathematical and Physical Sciences*, 233(1195):506–526. 82

Gledzer, E. B. and Makarov, A. L. (1990). A class of steady axisymmetric incompressible flows. *Fluid Dynamics*, 25(6):832–838. 27

Gol'dshtik, M. A. (1966). A class of exact solutions of the Navier-Stokes equations. *Journal of Applied Mechanics and Technical Physics*, 7(2):70–72.

Gol'dshtik, M. A. (1979). On swirling jets. *Fluid Dynamics*, 14(1):19–26.

Gol'dshtik, M. A. and Hussain, F. (1998). Analysis of inviscid vortex breakdown in a semi-infinite pipe. *Fluid Dynamics Research*, 23(4):189–234. 26

Gol'dshtik, M. A. and Shtern, V. N. (1990). Collapse in conical viscous flows. *Journal of Fluid Mechanics*, 218:483–508. 26

Gore, R. W. and Ranz, W. E. (1964). Backflows in rotating fluids moving axially through expanding cross sections. *AIChE Journal*, 10(1):83–88. 85, 87, 92

Gostintsev, Y. A., Pokhil, P. F., and Uspenskii, O. A. (1971). Gromeka-Beltrami flow in a semiinfinite cylindrical pipe. *Fluid Dynamics*, 6(2):281–284. 20, 82

Graebel, W. P. (2007). *Advanced Fluid Mechanics*. Academic Press, San Diego, CA. 43

Granger, R. A. (1995). *Fluid Mechanics*. Dover Publications, New York. 20, 22

Green, S. I. (1995). *Fluid Vortices*. Kluwer Academic Publishers. 14, 16, 17

Greitzer, E. M., Tan, C. S., and Graf, M. B. (2004). *Internal Flow: Concepts and Applications*. Cambridge University Press, Cambridge, UK. 57

Griffiths, W. D. and Boysan, F. (1996). Computational fluid dynamics (CFD) and empirical modelling of the performance of a number of cyclone samplers. *Journal of Aerosol Science*, 27(2):281–304. 96

Gupta, A. K., Lilley, D. G., and Syred, N. (1984). *Swirl Flows*. Energy and Engineering Science. Taylor & Francis, Abacus Press, Tunbridge Wells, Kent. 18, 19

Guyon, E., Hulin, J.-P., Petit, L., and Mitescu, C. D. (2001). *Physical Hydrodynamics*. Oxford University Press, USA. 13

Hadamard, J. (1911). Mouvement permanent lent d'une sphère liquide et visqueuse dans un liquide visqueux (Standing slow motion of a viscous liquid sphere in a viscous liquid). *Comptes Rendus Hebdomadaires des Seances de l' Academie des Sciences*, 152:1735–1743.

Hamman, C. W., Klewicki, J. C., and Kirby, R. M. (2008). On the Lamb vector divergence in Navier-Stokes flows. *Journal of Fluid Mechanics*, 610:261–284. 22

Happel, J. and Brenner, H. (1983). *Low Reynolds Number Hydrodynamics: With Special Applications to Particulate Media*. Mechanics of Fluids and Transport Processes. Martinus Nijhoff Publishers, The Hague. 43, 126, 129

Harvey, J. K. (1962). Some observations of the vortex breakdown phenomenon. *Journal of Fluid Mechanics*, 14(04):585–592. 87

Helmholtz, H. L. F. v. (1858). Über Integrale der hydrodynamischen Gleichungen, welche den Wirbelbewegungen entsprechen. *Journal für die reine und angewandte Mathematik (Crelles Journal)*, 1858(55):25–55. 3, 13

Helmholtz, H. L. F. v. (1867). LXIII. On integrals of the hydrodynamical equations, which express vortex-motion. *Philosophical Magazine Series 4*, 33(226):485–512. 13

Hicks, W. M. (1884). On the steady motion and small vibrations of a hollow vortex. *Philosophical Transactions of the Royal Society of London*, 175:161–195. 29

Hicks, W. M. (1885). Researches on the theory of vortex rings. part II. *Philosophical Transactions of the Royal Society of London*, 176:725–780. 29

Hicks, W. M. (1899). Researches in vortex motion. part III: on spiral or gyrostatic vortex aggregates. *Philosophical Transactions of the Royal Society of London. Series A, Containing Papers of a Mathematical or Physical Character*, 192:33–99. 82

Hill, M. J. M. (1894). On a spherical vortex. *Philosophical Transactions of the Royal Society A: Mathematical, Physical and Engineering Sciences*, 185:213–245. 30, 82

Hoekstra, A. J., Derksen, J. J., and van den Akker, A. H. E. (1999). An experimental and numerical study of turbulent swirling flow in gas cyclones. *Chemical Engineering Science*, 54(13-14):2055–2065. 57, 105

Hoffmann, A. C. and Stein, L. E. (2008). *Gas Cyclones and Swirl Tubes*. Springer, Berlin, Germany, 2nd edition. 35, 43

Horlock, J. (1978). *Actuator Disk Theory: Discontinuities in Thermo-Fluid Dynamics*. McGraw-Hill Inc.,US. 26

Houghton, E. L. and Carpenter, P. W. (2003). *Aerodynamics for Engineering Students*. Butterworth-Heinemann, Burlington, MA, 5th edition.

Houghton, E. L., Carpenter, P. W., Collicott, S., and Valentine, D. T. (2012). *Aerodynamics for Engineering Students*. Butterworth-Heinemann, Waltham, MA, 6th edition.

Hsieh, K. T. and Rajamani, R. K. (1988). Phenomenological Model of the Hydrocyclone: Model Development and Verification for Single-Phase Flow. *International Journal of Mineral Processing*, 22(1-4):223–237. x, xii, xiii, 2, 105, 107, 108, 109, 110, 149, 150

Huang, S.-L., Chen, H.-C., Chu, C.-C., and Chang, C.-C. (2008). On the transition process of a swirling vortex generated in a rotating tank. *Experiments in Fluids*, 45(2):267–282. 95

Karamcheti, K. (1966). *Principles of Ideal-Fluid Aerodynamics*. John Wiley & Sons, Inc., New York, NY, 1st edition. 17

Kee, R. J., Coltrin, M. E., and Glarborg, P. (2003). *Chemically Reacting Flow: Theory and Practice*. John Wiley & Sons, Inc., Hoboken, NJ. 6, 11, 19

Kelsall, D. F. (1952). A study of the motion of solid particles in a hydraulic cyclone. *Chemical Engineering Research and Design*, 30(a):87–108. 96, 107

Kendall, W. M. (1978). Unsteady two-cell similarity solution to a convective atmospheric vortex model. *Tellus*, 30(4):376–382. 95

Kessler, M. and Leith, D. (1991). Flow measurement and efficiency modeling of cyclones for particle collection. *Aerosol Science and Technology*, 15(1):8–18. 105

Kimura, Y. and Okamoto, H. (1987). Vortex motion on a sphere. *Journal of the Physical Society of Japan*, 56(12):4203–4206. 8

King, M. K., Rothfus, R. R., and Kermode, R. I. (1969). Static pressure and velocity profiles in swirling incompressible tube flow. *AIChE Journal*, 15(6):837–842. 85, 87

Kiselev, S. P., Vorozhtsov, E. V., and Fomin, V. M. (1999). *Foundations of Fluid Mechanics with Applications: Problem Solving Using Mathematica*. Birkhäuser, Boston. 20

Knowles, S. R., Woods, D. R., and Feuerstein, I. A. (1973). The velocity distribution within a hydrocyclone operating without an air core. *The Canadian Journal of Chemical Engineering*, 51(3):263–271. 107

Koplik, J. and Levine, H. (1993). Vortex reconnection in superfluid helium. *Physical Review Letters*, 71(9):1375–1378. 18

Kreyszig, E. (1999). *Advanced Engineering Mathematics*. John Wiley & Sons, Inc., New York, 8 edition. 125

Kundu, P. K., Cohen, I. M., and Dowling, D. R. (2012). *Fluid Mechanics*. Academic Press, Waltham, MA, 5th edition.

Kuo, H. L. (1966). On the dynamics of convective atmospheric vortices. *Journal of the Atmospheric Sciences*, 23(1):25–42. 95

Lai, W. (1961). *Three studies in fluid mechanics*. Phd, University of Michigan.

Lai, W. (1964). Flow of an inviscid fluid past a sphere in a pipe. *Journal of Fluid Mechanics*, 18(04):587–594.

Lakhtakia, A. (1994). Viktor Trkal, Beltrami fields, and Trkalian flows. *Czechoslovak Journal of Physics*, 44(2):89–96. 20, 22, 27

Lamb, H. (1877). On the conditions for steady motion of a fluid. *Proceedings of the London Mathematical Society*, 1(1):91. 3, 20, 27

Lamb, H. (1879). *A Treatise on the Mathematical Theory of the Motion of Fluids*. Cambridge University Press, Cambridge, UK, 1st edition. 20, 28

Lamb, H. (1975). *Hydrodynamics*. Cambridge University Press, Cambridge, UK, 6th edition. 20, 28

Lavan, Z., Nielsen, H., and Fejer, A. A. (1969). Separation and flow reversal in swirling flows in circular Dducts. *Physics of Fluids*, 12(9):1747–1757. 85, 87

Leibovich, S. (1978). The structure of vortex breakdown. *Annual Review of Fluid Mechanics*, 10:221–246. 85

Leith, D. and Licht, W. (1972). The collection eEfficiency of cyclone type particle collectors - a new theoretical approach. In *AIChE Symposium Series*, volume 68, pages 196–206. 105

Leith, D. and Mehta, D. (1973). Cyclone performance and design. *Atmospheric Environment*, 7(5):527–549. 105

Lilley, D. G. (1977). Swirl flows in combustion: a review. *AIAA Journal*, 15(8):1063–1078. 19

Long, R. R. (1953). Steady motion around a symmetrical obstacle moving along the axis of a rotating liquid. *Journal of Meteorology*, 10(3):197–203. 26

Lugt, H. J. (1996). *Introduction to Vortex Theory*. Vortex Flow Press, Potomac, MD. 13, 22

Luniev, V. V. (2009). *Real Gas Flows with High Velocities*. CRC Press, Boca Raton, FL. 20

Luo, Q., Deng, C., Xu, J., Yu, L., and Xiong, G. (1989). Comparison of the performance of water-sealed and commercial hydrocyclones. *International Journal of Mineral Processing*, 25(3):297–310. 96

Maicke, B. A. (2006). *Compressible flow in slab rocket motors*. Thesis, University of Tennessee.

Maicke, B. A. (2012). *On compressible gaseous motions in swirl dominated combustors*. PhD, University of Tennessee. 87

Maicke, B. A. and Majdalani, J. (2008a). On the compressible bidirectional vortex. In *44th AIAA/ASME/SAE/ASEE Joint Propulsion Conference & Exhibit*. AIAA Paper No. 2008-4834. 85, 93

Maicke, B. A. and Majdalani, J. (2008b). On the rotational compressible Taylor flow in injection-driven porous chambers. *Journal of Fluid Mechanics*, 603:391–411. 82

Maicke, B. A. and Majdalani, J. (2012a). On the compressible bidirectional vortex. part 1: a Bragg-Hawthorne stream function formulation. In *50th AIAA Aerospace Sciences Meeting including the New Horizons Forum and Aerospace Exposition*. AIAA Paper No. 2012-1103. 93

Maicke, B. A. and Majdalani, J. (2012b). On the compressible bidirectional vortex. part 2: a Beltramian flowfield approximation. In *50th AIAA Aerospace Sciences Meeting including the New Horizons Forum and Aerospace Exposition*. AIAA Paper No. 2012-1104. 93

Majdalani, J. (2007). Vortex Injection Hybrid Rockets. In Chiaverini, M. J. and Kuo, K., editors, *Fundamentals of Hybrid Rocket Combustion and Propulsion*, volume 218 of *Progress in Astronautics and Aeronautics*, chapter 6, pages 247–276. AIAA (American Institute of Aeronautics and Astronautics), Reston, Virginia. 85, 87, 93

Majdalani, J. (2009). Exact Eulerian solutions of the cylindrical bidirectional vortex. In *45th AIAA/ASME/SAE/ASEE Joint Propulsion Conference & Exhibit*. AIAA. AIAA Paper No. 2009-5307. 87

Majdalani, J. (2012). Helical solutions of the bidirectional vortex in a cylindrical cyclone: Beltramian and Trkalian motions. *Fluid Dynamics Research*, 44(6):065506. 60, 82, 93, 109

Majdalani, J. and Rienstra, S. (2007). On the bidirectional vortex and other similarity solutions in spherical coordinates. *Zeitschrift für Angewandte Mathematik und Physik (ZAMP)*, 58(2):289–308. 60

Majdalani, J. and Saad, T. (2007). The Taylor-Culick profile with arbitrary headwall injection. *Physics of Fluids*, 19(9):93601 (1–10). 60

Mariotte, E. (1686). *Traité du mouvement des eaux (Treaty of the movement of water)*. Paris, France. 4

Marshall, J. S. (2001). *Inviscid Incompressible Flow*. John Wiley & Sons, Inc., New York, NY. 111

Mattner, T. W., Joubert, P. N., and Chong, M. S. (2002). Vortical flow. part 1. flow through a constant-diameter pipe. *Journal of Fluid Mechanics*, 463:259–291. 92

Matveev, I. (2006). Experimental and numerical definition of the reverse vortex combustor parameters. In *44th AIAA Aerospace Sciences Meeting and Exhibit*. AIAA Paper No. 2006-551. 93

Meissel, E. (1873). Uber den Ausfluss der Wasser aus Gefässen in zwei besonderen Fällen nach Eintritt des Beharrungszustandes (On water flow from vessels: two special steady-state cases). *Archiv der Mathematik und Physik*, 55:241–251. 3, 26

Mickel, C. E. (2000). *Donaldson-Sullivan tornado model*. Ms in math, Texas Tech University. 95

Mikhaylov, P. M. and Romenskiy, A. A. (1974). On calculation of flow dynamics in liquid cyclones. *Fluid Mechanics - Soviet Research*, 3(1):154–159. 96

Mitsuta, Y., Monji, N., and Ishikawa, H. (1987). On the multiple structure of atmospheric vortices. *Journal of Geophysical Research*, 92(D12):14827–14831. 95

Moffatt, H. K. (1969). The degree of knottedness of tangled vortex lines. *Journal of Fluid Mechanics*, 35(1):117. 82

Monredon, T. C., Hsieh, K. T., and Rajamani, R. K. (1992). Fluid flow model of the hydrocyclone: an investigation of device dimensions. *International Journal of Mineral Processing*, 35(1-2):65–83. xii, xiii, 2, 105, 107, 109, 110, 149, 150

Morton, B. R. (1966). Geophysical vortices. *Progress in Aerospace Sciences*, 7:145–194. 18

Mothes, H. and Löffler, F. (1985). Motion and deposition of particles in cyclones. *German Chemical Engineering*, 8(4):223–233. 96

Munson, B. R., Young, D. F., and Okiishi, T. H. (2002). *Fundamentals of Fluid Mechanics*. John Wiley & Sons, Inc., New York, 4 edition. 15, 16

Newton, I. (1687). On the Attrition of Liquids. In *Principia*. 4

Nissan, A. H. and Bresan, V. P. (1961). Swirling flow in cylinders. *AIChE Journal*, 7(4):543–547. 85, 87, 92

Nuttall, J. B. (1953). Axial flow in a vortex. *Nature*, 172(4378):582–583. 85, 86, 87, 90, 92

O'Brien, V. (1961). Steady spheroidal vortices - more exact solutions to the Navier-Stokes equation. *Quarterly of Applied Mathematics*, 19:163–168. 82

O'Neil, P. V. (1995). *Advanced Engineering Mathematics*. Brooks/Cole Publishing Company, Pacific Grove, California, 4 edition. 125

Panton, R. L. (2005). *Incompressible Flow*. John Wiley & Sons, Inc., Hoboken, NJ, 3 edition. 14, 15

Paterson, A. R. (1983). *A First Course in Fluid Dynamics*. Cambridge University Press, Cambridge, UK.

Peng, W., Hoffmann, A. C., Boot, P. J. A. J., Udding, A., Dries, H. W. A., Ekker, A., and Kater, J. (2002). Flow pattern in reverse-flow centrifugal separators. *Powder Technology*, 127(3):212–222. 96

Peng, W., Hoffmann, A. C., and Dries, H. (2004). Separation characteristics of swirl-tube dust separators. *AIChE Journal: Particle Technology and Fluidization*, 50(1):87–96. 105

Pericleous, K. A. (1987). Mathematical simulation of hydrocyclones. *Applied Mathematical Modelling*, 11(4):242–255. 96

Pericleous, K. A. and Rhodes, N. (1986). The hydrocyclone classifier – a numerical approach. *International Journal of Mineral Processing*, 17(1-2):23–43. 96

Pervov, A. A. (1974). Investigation of velocity and pressure zones in SDK-TsN-33 and SK-TsN-34 cyclones. *Chemical and Petroleum Engineering*, 10(10):898–900. 96

Polyanin, A. D. and Zaitsev, V. F. (2003). *Handbook of Exact Solutions for Ordinary Differential Equations*. Chapman & Hall/CRC, Boca Raton, 2 edition. 125

Pozrikidis, C. (2011). *Introduction to Theoretical and Computational Fluid Dynamics*. Oxford University Press, New York, NY, 2nd edition. 43

Richardson, S. M. and Cornish, A. R. H. (1977). Solution of three-dimensional incompressible flow problems. *Journal of Fluid Mechanics*, 82(02):309–319. 6

Rietema, K. (1961). Performance and design of hydrocyclones–I general considerations. *Chemical Engineering Science*, 15(3-4):298–302. 96

Riley, K. F., Hobson, M. P., and Bence, S. J. (2002). *Mathematical Methods of Physics and Engineering: A Comprehensive Guide*. Cambridge University Press, Cambridge, 2 edition. 125

Rotunno, R. (1979). A study in tornado-like vortex dynamics. *Journal of the Atmospheric Sciences*, 36(1):140–155. 18

Rusak, Z. (1996). Axisymmetric swirling flow around a vortex breakdown point. *Journal of Fluid Mechanics*, 323:79–105. 26

Rusak, Z. (1998). The interaction of near-critical swirling flows in a pipe with inlet azimuthal vorticity perturbations. *Physics of Fluids*, 10(7):1672–1684. 26

Rusak, Z., Wang, S., and Whiting, C. H. (1998). The evolution of a perturbed vortex in a pipe to axisymmetric vortex breakdown. *Journal of Fluid Mechanics*, 366:211–237. 26

Rybczynski, D. P. (1911). Über die fortschreitende Bewegung einer flüssigen Kugel in einem sachen Medium (About the progressive movement of a sphere in a liquid medium matters). *Bulletin International de l'Academie des Sciences de Cracovie Series A Sciences Mathematiques*, 1:40–46.

Saad, T. (2010). *Theoretical models for wall injected duct flows*. PhD, University of Tennessee. 87

Saad, T. and Majdalani, J. (2008). Energy based solutions of the bidirectional vortex. In *44th AIAA/ASME/SAE/ASEE Joint Propulsion Conference & Exhibit*. AIAA Paper No. 2008-4382. 85, 93

Saad, T., Sams IV, O. C., and Majdalani, J. (2006). Rotational flow in tapered slab rocket motors. *Physics of Fluids*, 18:103601 (1–13). 82

Saffman, P. G. (1992). *Vortex Dynamics*. Cambridge Monographs on Mechanics. Cambridge University Press, New York. 14, 26

Sarpkaya, T. (1971). Vortex breakdown in swirling conical flows. *AIAA Journal*, 9(9):1792–1799. 87

Sarpkaya, T. (1974). Effect of the adverse pressure gradient on vortex breakdown. *AIAA Journal*, 12(5):161.

Schlichting, H. (1979). *Boundary Layer Theory*. McGraw-Hill, 7th edition. 7

Schlichting, H. and Gersten, K. (2000). *Boundary-Layer Theory*. Springer, Berlin, 8th edition. 7

Scofield, D. F. and Huq, P. (2010). Evolution of helicity in fluid flows. *Journal of Mathematical Physics*, 51(3):033520. 22

Shtern, V. N. and Hussain, F. (1999). Collapse, symmetry breaking, and hysteresis in swirling flows. *Annual Review of Fluid Mechanics*, 31(1):537–566. 26

Shtern, V. N., Hussain, F., and Herrada, M. A. (2000). New features of swirling jets. *Physics of Fluids*, 12(11):2868–2877. 26

So, K. L. (1967). Vortex phenomena in a conical diffuser. *AIAA Journal*, 5(6):1072–1078. 87

Som, S. K. and Mukherjee, S. G. (1980a). Theoretical and experimental investigations on the coefficient of discharge and spray cone angle of a swirl spray atomizing nozzle. *Acta Mechanica*, 36(1-2):79–102. 88

Som, S. K. and Mukherjee, S. G. (1980b). Theoretical and experimental investigations on the formation of air core in a swirl spray atomizing nozzle. *Applied Scientific Research*, 36(3):173–196. 88

Sotiropoulos, F. and Ventikos, Y. (1998). Transition from bubble-type vortex breakdown to columnar vortex in a confined swirling flow. *International Journal of Heat and Fluid Flow*, 19(5):446–458.

Sotiropoulos, F. and Ventikos, Y. (2001). The three-dimensional structure of confined swirling flows with vortex breakdown. *Journal of Fluid Mechanics*, 426:155–175.

Spalart, P. R. (1998). Airplane trailing vortices. *Annual Review of Fluid Mechanics*, 30(1):107–138. 19

Sposito, G. (1997). On steady flows with Lamb surfaces. *International Journal of Engineering Science*, 35(3):197–209. 22

Squire, H. B. (1956). *Rotating Fluids*, pages 139–161. Monographs on Mechanics and Applied Mathematics. Cambridge University Press, New York. 26

Stokes, G. G. (1842). On the steady motion of incompressible fluids. *Transactions of the Cambridge Philosophical Society*, 7:439–453. 3, 27

Sullivan, R. D. (1959). A two-cell vortex solution of the Navier-Stokes equations. *Journal of the Aerospace Sciences*, 26(11):767–768. 95

Susan-Resiga, R. F., Avellan, F., Ciocan, G. D., Muntean, S., and Anton, J. (2005a). Mathematical and numerical modeling of swirling flow in Francis turbine draft tube cone. In *Scientific Bulletin of the Politehnica University of Timişoara Transactions on Mechanics Special Issue, Proceedings 2nd IAHR International Meeting of the Workgroup on Cavitation and Dynamic Problems in Hydraulic Machinery and Systems - Workshop on Vortex*. 26

Susan-Resiga, R. F., Ciocan, G. D., Anton, I., and Avellan, F. (2006). Analysis of the swirling flow downstream a Francis turbine runner. *Transactions of the ASME Journal of Fluids Engineering*, 128(1):177–189. 26

Susan-Resiga, R. F., Milos, T., Alexandru, B., Muntean, S., and Bernad, S. (2005b). Mathematical and numerical models for axisymmetric swirling flows for turbomachinery applications. In *Scientific Bulletin of the Politehnica University of Timişoara Transactions on Mechanics Special issue Workshop on Vortex Dominated Flows-Achievements and Open Problems*. 26

Syred, N., Gupta, A. K., and Beér, J. M. (1975). Temperature and density gradient changes arising with the precessing vortex core and vortex breakdown in swirl burners. *Symposium (International) on Combustion, Fifteenth Symposium (International) on Combustion*, 15(1):587–597. 87

Taylor, G. I. (1950). The boundary layer in the converging nozzle of a swirl atomizer. *The Quarterly Journal of Mechanics and Applied Mathematics*, 3(2):129–139. 88

Taylor, G. I. (1956). Fluid flow in regions bounded by porous surfaces. *Proceedings of the Royal Society of London. Series A. Mathematical and Physical Sciences*, 234(1199):456–475. 30

Thomson (Kelvin), W. L. (1880). Vibrations of a vortex column. *The London, Edinburgh and Dublin Philosophical Magazine and Journal of Science - Philosophical Magazine Series 5*, 10(5):155–168. 3, 13

Trkal, V. (1919). Poznámka k hydrodynamice vazkých tekutin (A note on the hydrodynamics of viscous fluids). *Časopis pro pěstování mathematiky a fysiky (Applications of Mathematics and Physics)*, 48:302–311.

Truesdell, C. A. (1954). *The Kinematics of Vorticity*. Indiana University Press, Bloomington. 3, 20, 22

Truesdell, C. A. and Rajagopal, K. R. (2009). *An Introduction to the Mechanics of Fluids*. Modern Birkhäuser Classics. Birkhäuser Boston, New York. 22

Vakili, A. D., Tennent, S. G., and Panchpakesan, N. R. (1996). An experimental study of confined multi-cell vortex flows. In *34th Aerospace Sciences Meeting & Exhibit*. AIAA Paper No. 96-0806. 85, 92, 95

Vasil'ev (Vasilyev), O. F. (1958). *Principles of the Mechanics of Helical and Circulation Flows (Osnovy mekhaniki vintovykh i tsirkulyatsionnykh potokov)*. Gosenergoizdat, Moscow. 22

Vatistas, G. H. (2008). Vortices in Homer's Odyssey - A Scientific Approach. In Paipetis, S., editor, *Science and Technology in Homeric Epics*, pages 67–75. Springer Science+Business Media B.V. 13, 18, 19

Vyas, A. B. and Majdalani, J. (2006). Exact solution of the bidirectional vortex. *AIAA Journal*, 44(10):2208. 57, 58, 59, 60, 82, 93, 109, 146

Vyas, A. B., Majdalani, J., and Chiaverini, M. J. (2003a). The bidirectional vortex. part 1: an exact inviscid solution. In *39th AIAA/ASME/SAE/ASEE Joint Propulsion Conference and Exhibit*. AIAA Paper No. 2003-5052. 57, 59, 146

Vyas, A. B., Majdalani, J., and Chiaverini, M. J. (2003b). The bidirectional vortex. part 2: viscous core corrections. In *39th AIAA/ASME/SAE/ASEE Joint Propulsion Conference and Exhibit*. AIAA Paper. AIAA Paper No. 2003-5053. 105

Vyas, A. B., Majdalani, J., and Chiaverini, M. J. (2003c). The bidirectional vortex. part 3: multiple solutions. In *39th AIAA/ASME/SAE/ASEE Joint Propulsion Conference and Exhibit*. AIAA Paper No. 2003-5054. 95

Wang, C.-Y. (1966). On a class of exact solutions of the Navier-Stokes equations. *Transactions of the ASME Journal of Applied Mechanics*, 33(3):696–698. 4, 5, 7

Wang, C.-Y. (1989). Exact solutions of the unsteady Navier-Stokes equations. *Applied Mechanics Reviews*, 42(11S):S269–S282. 4, 5, 6

Wang, C. Y. (1990). Exact solutions of the Navier-Stokes equations - the generalized Beltrami flows, review and extension. *Acta Mechanica*, 74(1-2):36–74. 4, 21, 22

Wang, C. Y. (1991). Exact solutions of the steady-state Navier-Stokes equations. *Annual Review of Fluid Mechanics*, 23(1):159–177. 3, 4, 5, 6, 7, 12, 17, 21, 22

Ward, N. B. (1972). The exploration of certain features of tornado dynamics using a laboratory model. *Journal of the Atmospheric Sciences*, 29(6):1194–1204. 95

Warsi, Z. U. A. (1999). *Fluid Dynamics: Theoretical and Computational Approaches*. CRC Press LLC, Boca Raton, FL, 2nd edition. 22

Weisstein, E. W. (2003). *CRC Concise Encyclopedia of Mathematics*. CRC Press, Boca Raton, 2 edition. 126

White, F. M. (2003). *Fluid Mechanics*. McGraw-Hill, New York, NY, 5th edition. 15, 16

Wu, J.-Z., Ma, H.-Y., and Zhou, M.-D. (2006). *Vorticity and Vortex Dynamics*. Springer, Berlin. 13, 14, 21, 22, 32, 79, 112

Wylie, C. R. and Barrett, L. C. (1995). *Advanced Engineering Mathematics*. McGraw-Hill, New York, 6 edition. 125

Xiang, R., Park, S. H., and Lee, K. W. (2001). Effects of cone dimension on cyclone performance. *Journal of Aerosol Science*, 32(4):549–561. 105

Yarmitskii, A. G. (1974a). Axisymmetric vortex source (sink). *Fluid Dynamics*, 9(5):683–690.

Yarmitskii, A. G. (1974b). Three-dimensional analog of a vortical Chaplygin column (a generalized Hill vortex). *Journal of Applied Mechanics and Technical Physics*, 15(5):698–702.

Yarmitskii, A. G. (1992). A whirlwindlike Chaplygin vortex. *Fluid Dynamics*, 27(4):489–494. 82

Yih, C.-S. (1959). Two solutions for inviscid rotational flow with corner eddies. *Journal of Fluid Mechanics*, 5(01):36–40. 82, 94

Zeytounian, R. K. (2006). *Topics in Hyposonic Flow Theory*. Lecture Notes in Physics. Springer, Berlin. 4

Zeytounian, R. K. (2012). *Navier-Stokes-Fourier Equations - A Rational Asymptotic Modelling Point of View*. Springer Berlin Heidelberg, New York.

Zhao, J. Q. and Abrahamson, J. (1999). The flow in conical cyclones. In *Second International Conference on CFD in the Minerals and Process Industries*, pages 6–8. 1, 81, 112, 113, 114, 118, 119

Zhao, J. Q. and Abrahamson, J. (2003). The flow in cylindrical cyclones. *Developments in Chemical Engineering and Mineral Processing*, 11(3-4):201–222. 118

Zhou, L. X. and Soo, S. L. (1990). Gas–solid flow and collection of solids in a cyclone separator. *Powder Technology*, 63(1):45–53. 96

Zill, D. G. (2000). *A First Course in Differential Equations*. Brooks/Cole, Pacific Grove, California, 5 edition. 125

Zill, D. G. and Cullen, M. R. (2000). *Advanced Engineering Mathematics*. Jones and Bartlett, Boston, 2 edition. 125

Appendix

Appendix A

Lamb Vector Expansion

This appendix contains detailed mathematical formulation regarding the expansion of the Lamb vector in cylindrical polar and spherical polar coordinates. The expansion of the Lamb vector in cylindrical coordinates is

$$\boldsymbol{\ell} = -\mathbf{u} \times (\nabla \times \mathbf{u}) = \begin{vmatrix} \mathbf{e}_r & \mathbf{e}_\theta & \mathbf{e}_z \\ -u_r & -u_\theta & -u_z \\ \omega_r & \omega_\theta & \omega_z \end{vmatrix} \tag{A.1}$$

$$\boldsymbol{\ell} = (u_z\omega_\theta - u_\theta\omega_z)\,\mathbf{e}_r + (u_r\omega_z - u_z\omega_r)\,\mathbf{e}_\theta + (u_\theta\omega_r - u_r\omega_\theta)\,\mathbf{e}_z \tag{A.2}$$

$$\begin{aligned} \boldsymbol{\ell} = &\left\{ u_z\left(\frac{\partial u_r}{\partial z} - \frac{\partial u_z}{\partial r}\right) - \frac{u_\theta}{r}\left[\frac{\partial}{\partial r}(u_\theta r) - \frac{\partial u_r}{\partial \theta}\right]\right\}\mathbf{e}_r \\ &+ \left\{ \frac{u_r}{r}\left[\frac{\partial}{\partial r}(u_\theta r) - \frac{\partial u_r}{\partial \theta}\right] - \frac{u_z}{r}\left[\frac{\partial u_z}{\partial \theta} - \frac{\partial}{\partial z}(u_\theta r)\right]\right\}\mathbf{e}_\theta \\ &+ \left\{ \frac{u_\theta}{r}\left[\frac{\partial u_z}{\partial \theta} - \frac{\partial}{\partial z}(u_\theta r)\right] - u_r\left(\frac{\partial u_r}{\partial z} - \frac{\partial u_z}{\partial r}\right)\right\}\mathbf{e}_z \end{aligned} \tag{A.3}$$

$$\ell_r = u_z\left(\frac{\partial u_r}{\partial z} - \frac{\partial u_z}{\partial r}\right) - \frac{u_\theta}{r}\left[\frac{\partial}{\partial r}(u_\theta r) - \frac{\partial u_r}{\partial \theta}\right] \tag{A.4}$$

$$\ell_\theta = -\frac{u_z}{r}\left[\frac{\partial u_z}{\partial \theta} - \frac{\partial}{\partial z}(u_\theta r)\right] + \frac{u_r}{r}\left[\frac{\partial}{\partial r}(u_\theta r) - \frac{\partial u_r}{\partial \theta}\right]$$
$$= \frac{u_r}{r}\left[\frac{\partial}{\partial r}(u_\theta r) - \frac{\partial u_r}{\partial \theta}\right] - \frac{u_z}{r}\left[\frac{\partial u_z}{\partial \theta} - \frac{\partial}{\partial z}(u_\theta r)\right] \tag{A.5}$$

$$\ell_z = \frac{u_\theta}{r}\left[\frac{\partial u_z}{\partial \theta} - \frac{\partial}{\partial z}(u_\theta r)\right] - u_r\left(\frac{\partial u_r}{\partial z} - \frac{\partial u_z}{\partial r}\right) \tag{A.6}$$

Expansion gives

$$\boldsymbol{\ell} = \left(u_z\frac{\partial u_r}{\partial z} - u_z\frac{\partial u_z}{\partial r} - u_\theta\frac{\partial u_\theta}{\partial r} + \frac{u_\theta^2}{r} - \frac{u_\theta}{r}\frac{\partial u_r}{\partial \theta}\right)\mathbf{e}_r$$
$$+ \left(u_r\frac{\partial u_\theta}{\partial r} + \frac{u_r u_\theta}{r} - \frac{u_r}{r}\frac{\partial u_r}{\partial \theta} - \frac{u_z}{r}\frac{\partial u_z}{\partial \theta} + u_z\frac{\partial u_\theta}{\partial z}\right)\mathbf{e}_\theta$$
$$+ \left(\frac{u_\theta}{r}\frac{\partial u_z}{\partial \theta} - u_\theta\frac{\partial u_\theta}{\partial z} - u_r\frac{\partial u_r}{\partial z} + u_r\frac{\partial u_z}{\partial r}\right)\mathbf{e}_z \tag{A.7}$$

$$\ell_r = u_z\frac{\partial u_r}{\partial z} - u_z\frac{\partial u_z}{\partial r} - u_\theta\frac{\partial u_\theta}{\partial r} + \frac{u_\theta^2}{r} - \frac{u_\theta}{r}\frac{\partial u_r}{\partial \theta} \tag{A.8}$$

$$\ell_\theta = u_r\frac{\partial u_\theta}{\partial r} + \frac{u_r u_\theta}{r} - \frac{u_r}{r}\frac{\partial u_r}{\partial \theta} - \frac{u_z}{r}\frac{\partial u_z}{\partial \theta} + u_z\frac{\partial u_\theta}{\partial z} \tag{A.9}$$

$$\ell_z = \frac{u_\theta}{r}\frac{\partial u_z}{\partial \theta} - u_\theta\frac{\partial u_\theta}{\partial z} - u_r\frac{\partial u_r}{\partial z} + u_r\frac{\partial u_z}{\partial r} \tag{A.10}$$

The expansion of the Lamb vector in spherical coordinates is

$$\boldsymbol{\ell} = -\mathbf{u}\times(\nabla\times\mathbf{u}) = \begin{vmatrix} \mathbf{e}_R & \mathbf{e}_\phi & \mathbf{e}_\theta \\ -u_R & -u_\phi & -u_\theta \\ \omega_R & \omega_\phi & \omega_\theta \end{vmatrix} \tag{A.11}$$

$$\boldsymbol{\ell} = \left(u_\theta \omega_\phi - u_\phi \omega_\theta\right) \mathbf{e}_R - \left(u_\theta \omega_R - u_R \omega_\theta\right) \mathbf{e}_\phi + \left(u_\phi \omega_R - u_R \omega_\phi\right) \mathbf{e}_\theta \tag{A.12}$$

$$\ell_R = u_\theta \omega_\phi - u_\phi \omega_\theta \tag{A.13}$$

$$\ell_\phi = u_R \omega_\theta - u_\theta \omega_R \tag{A.14}$$

$$\ell_\theta = u_\phi \omega_R - u_R \omega_\phi \tag{A.15}$$

Inserting the vorticity components produces

$$\begin{aligned}
\boldsymbol{\ell} = &\left[\frac{u_\theta}{R\sin\phi}\left(\frac{\partial u_R}{\partial \theta} - \frac{\partial R\sin\phi u_\theta}{\partial R}\right) - \frac{u_\phi}{R}\left(\frac{\partial R u_\phi}{\partial R} - \frac{\partial u_R}{\partial \phi}\right)\right]\mathbf{e}_R \\
&+ \left[\frac{u_R}{R}\left(\frac{\partial R u_\phi}{\partial R} - \frac{\partial u_R}{\partial \phi}\right) - \frac{u_\theta}{R^2\sin\phi}\left(\frac{\partial R\sin\phi u_\theta}{\partial \phi} - \frac{\partial u_\phi}{\partial \theta}\right)\right]\mathbf{e}_\phi \\
&+ \left[\frac{u_\phi}{R^2\sin\phi}\left(\frac{\partial R\sin\phi u_\theta}{\partial \phi} - \frac{\partial u_\phi}{\partial \theta}\right) - \frac{u_R}{R\sin\phi}\left(\frac{\partial u_R}{\partial \theta} - \frac{\partial R\sin\phi u_\theta}{\partial R}\right)\right]\mathbf{e}_\theta
\end{aligned} \tag{A.16}$$

$$\begin{aligned}
\boldsymbol{\ell} = &\left\{\frac{u_\theta}{R\sin\phi}\left[\frac{\partial u_R}{\partial \theta} - \frac{\partial}{\partial R}\left(u_\theta R\sin\phi\right)\right] - \frac{u_\phi}{R}\left[\frac{\partial}{\partial R}\left(u_\phi R\right) - \frac{\partial u_R}{\partial \phi}\right]\right\}\mathbf{e}_R \\
&+ \left\{\frac{u_R}{R}\left[\frac{\partial}{\partial R}\left(R u_\phi\right) - \frac{\partial u_R}{\partial \phi}\right] - \frac{u_\theta}{R^2\sin\phi}\left[\frac{\partial}{\partial \phi}\left(u_\theta R\sin\phi\right) - \frac{\partial u_\phi}{\partial \theta}\right]\right\}\mathbf{e}_\phi \\
&+ \left\{\frac{u_\phi}{R^2\sin\phi}\left[\frac{\partial}{\partial \phi}\left(u_\theta R\sin\phi\right) - \frac{\partial u_\phi}{\partial \theta}\right] - \frac{u_R}{R\sin\phi}\left[\frac{\partial u_R}{\partial \theta} - \frac{\partial}{\partial R}\left(u_\theta R\sin\phi\right)\right]\right\}\mathbf{e}_\theta
\end{aligned} \tag{A.17}$$

where each individual component

$$\ell_R = \frac{u_\theta}{R\sin\phi}\left(\frac{\partial u_R}{\partial \theta} - \frac{\partial R\sin\phi u_\theta}{\partial R}\right) - \frac{u_\phi}{R}\left(\frac{\partial R u_\phi}{\partial R} - \frac{\partial u_R}{\partial \phi}\right) \tag{A.18}$$

$$\ell_\phi = \frac{u_R}{R}\left(\frac{\partial R u_\phi}{\partial R} - \frac{\partial u_R}{\partial \phi}\right) - \frac{u_\theta}{R^2 \sin\phi}\left(\frac{\partial R \sin\phi u_\theta}{\partial \phi} - \frac{\partial u_\phi}{\partial \theta}\right) \tag{A.19}$$

$$\ell_\theta = \frac{u_\phi}{R^2 \sin\phi}\left(\frac{\partial R \sin\phi u_\theta}{\partial \phi} - \frac{\partial u_\phi}{\partial \theta}\right) - \frac{u_R}{R \sin\phi}\left(\frac{\partial u_R}{\partial \theta} - \frac{\partial R \sin\phi u_\theta}{\partial R}\right) \tag{A.20}$$

Expansion combines the Lamb vector components to

$$\ell_R = \frac{u_\theta}{R \sin\phi}\frac{\partial u_R}{\partial \theta} - u_\theta \frac{\partial u_\theta}{\partial R} - \frac{u_\theta^2}{R} - u_\phi \frac{\partial u_\phi}{\partial R} - \frac{u_\phi^2}{R} + u_\phi \frac{\partial u_R}{\partial \phi} \tag{A.21}$$

$$\ell_\phi = u_R \frac{\partial u_\phi}{\partial R} + \frac{u_R u_\phi}{R} - u_R \frac{\partial u_R}{\partial \phi} - \frac{u_\theta}{R}\frac{\partial u_\theta}{\partial \phi} - \frac{u_\theta^2 \cot\phi}{R} + \frac{u_\theta}{R^2 \sin\phi}\frac{\partial u_\phi}{\partial \theta} \tag{A.22}$$

$$\ell_\theta = \frac{u_\phi}{R}\frac{\partial u_\theta}{\partial \phi} + u_\phi u_\theta \frac{\cot\phi}{R} - \frac{u_\phi}{R^2 \sin\phi}\frac{\partial u_\phi}{\partial \theta} - \frac{u_R}{R \sin\phi}\frac{\partial u_R}{\partial \theta} + u_R \frac{\partial u_\theta}{\partial R} + \frac{u_R u_\theta}{R} \tag{A.23}$$

Rearranging organizes the components into

$$\ell_R = \frac{u_\theta}{R \sin\phi}\frac{\partial u_R}{\partial \theta} + u_\phi \frac{\partial u_R}{\partial \phi} - u_\phi \frac{\partial u_\phi}{\partial R} - u_\theta \frac{\partial u_\theta}{\partial R} - \frac{u_\phi^2 + u_\theta^2}{R} \tag{A.24}$$

$$\ell_\phi = u_R \frac{\partial u_\phi}{\partial R} - u_R \frac{\partial u_R}{\partial \phi} - \frac{u_\theta}{R}\frac{\partial u_\theta}{\partial \phi} + \frac{u_\theta}{R^2 \sin\phi}\frac{\partial u_\phi}{\partial \theta} + \frac{u_R u_\phi}{R} - \frac{u_\theta^2 \cot\phi}{R} \tag{A.25}$$

$$\ell_\theta = u_R \frac{\partial u_\theta}{\partial R} + \frac{u_\phi}{R}\frac{\partial u_\theta}{\partial \phi} - \frac{u_\phi}{R^2 \sin\phi}\frac{\partial u_\phi}{\partial \theta} - \frac{u_R}{R \sin\phi}\frac{\partial u_R}{\partial \theta} + \frac{u_R u_\theta}{R} + u_\phi u_\theta \frac{\cot\phi}{R} \tag{A.26}$$

Appendix B

Velocity Magnitude Mathematics for Beltramian Cone Solution

This appendix contains detailed mathematical formulation regarding the velocities for the Beltramian solution.

$$u_R^2 = \kappa_c^2 \left[(\lambda - \ln \Phi)\cos\phi - 1\right]^2 = \kappa_c^2 \left[(\lambda - \ln \Phi)\cos\phi - 1\right]\left[(\lambda - \ln \Phi)\cos\phi - 1\right] \tag{B.1}$$

$$u_R^2 = \kappa_c^2 \left[(\lambda - \ln \Phi)^2 \cos^2\phi - 2\,(\lambda - \ln \Phi)\cos\phi + 1\right] \tag{B.2}$$

$$u_\phi^2 = \kappa_c^2 \left[(\lambda - \ln \Phi)\sin\phi - \Phi\right]^2 = \kappa_c^2 \left[(\lambda - \ln \Phi)\sin\phi - \Phi\right]\left[(\lambda - \ln \Phi)\sin\phi - \Phi\right] \tag{B.3}$$

$$u_\phi^2 = \kappa_c^2 \left[(\lambda - \ln \Phi)^2 \sin^2\phi - 2\,(\lambda - \ln \Phi)\,\Phi \sin\phi + \Phi^2\right] \tag{B.4}$$

$$u_\phi^2 = \kappa_c^2 \left[(\lambda - \ln \Phi)^2 \sin^2\phi - 2\,(\lambda - \ln \Phi)\,(\csc\phi - \cot\phi)\sin\phi + \Phi^2\right] \tag{B.5}$$

$$u_\phi^2 = \kappa_c^2 \left[(\lambda - \ln \Phi)^2 \sin^2 \phi - 2 (\lambda - \ln \Phi) (1 - \cos \phi) + \Phi^2 \right] \tag{B.6}$$

$$u_\theta^2 = \frac{1}{R^2 \sin^2 \phi} \left[1 + (\kappa_c R \sin \phi)^2 (\lambda - \ln \Phi - \Phi \csc \phi) \right] \tag{B.7}$$

$$u_\theta^2 = \frac{1}{R^2 \sin^2 \phi} + \kappa_c^2 (\lambda - \ln \Phi - \Phi \csc \phi) \tag{B.8}$$

$$\cos^2 u = \frac{1 + \cos 2u}{2} \tag{B.9}$$

$$\sec^2 \left(\frac{\phi}{2} \right) = \frac{2}{1 + \cos \phi} = \frac{2}{1 + \cos \phi} \frac{1 - \cos \phi}{1 - \cos \phi} = \frac{2 (1 - \cos \phi)}{1 - \cos^2 \phi} \tag{B.10}$$

$$\sec^2 \left(\frac{\phi}{2} \right) = \frac{2 (1 - \cos \phi)}{\sin^2 \phi} = \frac{2}{\sin^2 \phi} - \frac{2 \cos \phi}{\sin^2 \phi} = 2 \left(\csc^2 \phi - \cot \phi \csc \phi \right) \tag{B.11}$$

$$\sec^2 \left(\frac{\phi}{2} \right) = 2 \Phi \csc \phi \tag{B.12}$$

$$\sec^2 u = 1 + \tan^2 u \tag{B.13}$$

$$\sec^2 \left(\frac{\phi}{2} \right) = 1 + \tan^2 \left(\frac{\phi}{2} \right) = 1 + \Phi^2 \tag{B.14}$$

$$1 + \Phi^2 = 2 \Phi \csc \phi \tag{B.15}$$

$$
\begin{aligned}
u_R^2 + u_\phi^2 + u_\theta^2 = \\
&\kappa_c^2 \left[(\lambda - \ln\Phi)^2 \cos^2\phi - 2\,(\lambda - \ln\Phi)\cos\phi + 1 \right] \\
&\quad + \kappa_c^2 \left[(\lambda - \ln\Phi)^2 \sin^2\phi - 2\,(\lambda - \ln\Phi)\,(1 - \cos\phi) + \Phi^2 \right] \\
&\qquad\qquad + \frac{1}{R^2 \sin^2\phi} + \kappa_c^2\,(\lambda - \ln\Phi - \Phi\csc\phi)
\end{aligned}
\tag{B.16}
$$

$$
u_R^2 + u_\phi^2 + u_\theta^2 = \frac{1}{R^2 \sin^2\phi} + \kappa_c^2 \left[(\lambda - \ln\Phi)^2 - (\lambda - \ln\Phi) + \Phi\csc\phi \right]
\tag{B.17}
$$

$$
|u| = \sqrt{\frac{1}{R^2 \sin^2\phi} + \kappa_c^2 \left[(\lambda - \ln\Phi)^2 - (\lambda - \ln\Phi) + \Phi\csc\phi \right]}
\tag{B.18}
$$

Appendix C

Vorticity Mathematics for Beltramian Cone Solution

This appendix contains detailed mathematical formulation regarding the vorticity for the Beltramian solution.

$$\omega_R = \frac{1}{R^2 \sin\phi} \frac{\partial}{\partial \phi} \left(u_\theta R \sin\phi \right)$$

$$u_\theta R \sin\phi = \sqrt{1 + (\kappa_c R \sin\phi)^2 \left(\lambda - \ln\Phi - \Phi \csc\phi \right)} \tag{C.1}$$

$$\frac{\partial}{\partial \phi} \left(u_\theta R \sin\phi \right) = \frac{\partial}{\partial \phi} \left[\sqrt{1 + (\kappa_c R \sin\phi)^2 \left(\lambda - \ln\Phi - \Phi \csc\phi \right)} \right] \tag{C.2}$$

$$\frac{\partial}{\partial \phi} \left(u^{\frac{1}{2}} \right) = \tfrac{1}{2} u^{-\frac{1}{2}} \, \mathrm{d}u \tag{C.3}$$

$$\mathrm{d}u = \frac{\partial}{\partial \phi} \left[1 + (\kappa_c R \sin\phi)^2 \left(\lambda - \ln\Phi - \Phi \csc\phi \right) \right] \tag{C.4}$$

$$\frac{\partial}{\partial\phi}\left[1+(\kappa_c R\sin\phi)^2\,(\lambda-\ln\Phi-\Phi\csc\phi)\right]$$
$$=2\kappa_c^2R^2\sin\phi\cos\phi\,(\lambda-\ln\Phi-\Phi\csc\phi)$$
$$-(\kappa_c R\sin\phi)^2\left[\frac{\mathrm{d}}{\mathrm{d}\phi}\,(-\ln\Phi-\Phi\csc\phi)\right] \tag{C.5}$$

$$\frac{\mathrm{d}}{\mathrm{d}\phi}\,(-\ln\Phi)=-\csc\phi$$

$$\frac{\mathrm{d}}{\mathrm{d}\phi}\,(\Phi)=\frac{\mathrm{d}}{\mathrm{d}\phi}\,(\csc\phi-\cot\phi)=-\csc\phi\cot\phi+\csc^2\phi=\Phi\csc\phi \tag{C.6}$$

$$\frac{\mathrm{d}}{\mathrm{d}\phi}\,(-\Phi\csc\phi)=-(\csc\phi-\cot\phi)\csc^2\phi-\Phi\,(-\csc\phi\cot\phi) \tag{C.7}$$

$$\frac{\mathrm{d}}{\mathrm{d}\phi}\,(-\Phi\csc\phi)=-(\csc\phi-\cot\phi)\csc^2\phi+(\csc\phi-\cot\phi)\csc\phi\cot\phi \tag{C.8}$$

$$\frac{\mathrm{d}}{\mathrm{d}\phi}\,(-\Phi\csc\phi)=-\csc^3\phi+\csc^2\phi\cot\phi+\csc^2\phi\cot\phi-\csc\phi\cot^2\phi \tag{C.9}$$

$$\frac{\mathrm{d}}{\mathrm{d}\phi}\,(-\Phi\csc\phi)=-\csc^3\phi+2\csc^2\phi\cot\phi-\csc\phi\cot^2\phi \tag{C.10}$$

$$\frac{\mathrm{d}}{\mathrm{d}\phi}\,(-\ln\Phi-\Phi\csc\phi)=-\csc\phi-\csc^3\phi+2\csc^2\phi\cot\phi-\csc\phi\cot^2\phi \tag{C.11}$$

$$\mathrm{d}u=(\kappa_c R\sin\phi)^2\left[2\,(\lambda-\ln\Phi)\cot\phi-2\Phi\csc\phi\cot\phi-\csc\phi\right.$$
$$\left.-\csc^3\phi+2\csc^2\phi\cot\phi-\csc\phi\cot^2\phi\right] \tag{C.12}$$

$$\mathrm{d}u = (\kappa_c R \sin\phi)^2 \left[2\left(\lambda - \ln\Phi\right)\cot\phi - 2\left(\csc\phi - \cot\phi\right)\csc\phi\cot\phi \right. \\ \left. - \csc\phi - \csc^3\phi + 2\csc^2\phi\cot\phi - \csc\phi\cot^2\phi\right] \tag{C.13}$$

$$\mathrm{d}u = (\kappa_c R \sin\phi)^2 \left[2\left(\lambda - \ln\Phi\right)\cot\phi - 2\csc^2\phi\cot\phi + 2\csc\phi\cot^2 \right. \\ \left. - \csc\phi - \csc^3\phi + 2\csc^2\phi\cot\phi - \csc\phi\cot^2\phi\right] \tag{C.14}$$

$$\mathrm{d}u = (\kappa_c R \sin\phi)^2 \left[2\left(\lambda - \ln\Phi\right)\cot\phi + \csc\phi\cot^2 - \csc\phi - \csc^3\phi\right] \tag{C.15}$$

$$\mathrm{d}u = (\kappa_c R \sin\phi)^2 \left[2\left(\lambda - \ln\Phi\right)\cot\phi + \csc\phi\left(\cot^2 - \csc^2\phi - 1\right)\right] \tag{C.16}$$

$$\mathrm{d}u = (\kappa_c R \sin\phi)^2 \left[2\left(\lambda - \ln\Phi\right)\cot\phi + \csc\phi\left(\csc^2\phi - 1 - \csc^2\phi - 1\right)\right] \tag{C.17}$$

$$\mathrm{d}u = 2\left(\kappa_c R \sin\phi\right)^2 \left[\left(\lambda - \ln\Phi\right)\cot\phi - \csc\phi\right] \tag{C.18}$$

$$\omega_R = \frac{\kappa_c^2\left[\left(\lambda - \ln\Phi\right)\cos\phi - 1\right]}{\sqrt{1 + \left(\kappa_c R \sin\phi\right)^2\left(\lambda - \ln\Phi - \Phi\csc\phi\right)}} \tag{C.19}$$

$$\omega_R = \frac{\kappa_c u_R}{\sqrt{1 + \left(\kappa_c R \sin\phi\right)^2\left(\lambda - \ln\Phi - \Phi\csc\phi\right)}} \tag{C.20}$$

$$\omega_R = \frac{\kappa_c}{R\sin\phi}\frac{u_R}{u_\theta} \tag{C.21}$$

$$\omega_R = \frac{\kappa_c^2 \left\{ \zeta \left(1+\zeta^2\right)^{-1/2} \left[\lambda - \ln\left(\sqrt{1+\zeta^2} - \zeta \right) \right] - 1 \right\}}{\sqrt{1 + (\kappa_c r)^2 \left[\lambda - \ln\left(\sqrt{1+\zeta^2} - \zeta \right) + \zeta \sqrt{1+\zeta^2} - \zeta^2 - 1 \right]}} \tag{C.22}$$

$$\omega_R = \frac{\kappa_c^2 \left\{ \zeta \left(1+\zeta^2\right)^{-1/2} \left[\lambda + \sinh^{-1}(\zeta) \right] - 1 \right\}}{\sqrt{1 + (\kappa_c r)^2 \left[\lambda + \sinh^{-1}(\zeta) + \zeta \sqrt{1+\zeta^2} - \zeta^2 - 1 \right]}} \tag{C.23}$$

$$\omega_R = \frac{\kappa_c^2 \left[\zeta \mathcal{Z}_2 \left(\lambda - \ln \mathcal{Z} \right) - 1 \right]}{\sqrt{1 + (r\kappa_c)^2 \left(\lambda - \ln \mathcal{Z} - \mathcal{Z}\mathcal{Z}_1 \right)}} \tag{C.24}$$

$$\omega_\phi = -\frac{1}{R \sin\phi} \frac{\partial}{\partial R} \left(u_\theta R \sin\phi \right)$$

$$\omega_\phi = -\frac{1}{R \sin\phi} \frac{\partial}{\partial R} \left[\sqrt{1 + (\kappa_c R \sin\phi)^2 \left(\lambda - \ln\Phi - \Phi \csc\phi \right)} \right] \tag{C.25}$$

$$\frac{\partial}{\partial \phi} \left(u^{\frac{1}{2}} \right) = \tfrac{1}{2} u^{-\frac{1}{2}} \, \mathrm{d}u$$

$$\mathrm{d}u = -2R \left(\kappa_c \sin\phi \right)^2 \left(\lambda - \ln\Phi - \Phi \csc\phi \right) \tag{C.26}$$

$$\omega_\phi = -\frac{\kappa_c^2 \left[(\lambda - \ln\Phi) \sin\phi - \Phi \right]}{\sqrt{1 + (\kappa_c R \sin\phi)^2 \left(\lambda - \ln\Phi - \Phi \csc\phi \right)}} \tag{C.27}$$

$$\omega_\phi = \frac{\kappa_c u_\phi}{\sqrt{1 + (\kappa_c R \sin\phi)^2 \left(\lambda - \ln\Phi - \Phi \csc\phi \right)}} \tag{C.28}$$

$$\omega_\phi = \frac{\kappa_c}{R \sin\phi} \frac{u_\phi}{u_\theta} \tag{C.29}$$

$$\omega_\phi = -\frac{\kappa_c^2 \left\{ \left(1+\zeta^2\right)^{-1/2} \left[\lambda - \ln\left(\sqrt{1+\zeta^2} - \zeta \right) \right] - \sqrt{1+\zeta^2} + \zeta \right\}}{\sqrt{1 + (\kappa_c r)^2 \left[\lambda - \ln\left(\sqrt{1+\zeta^2} - \zeta \right) + \zeta \sqrt{1+\zeta^2} - \zeta^2 - 1 \right]}} \tag{C.30}$$

$$\omega_\phi = -\frac{\kappa_c^2 \left\{ \left(1+\zeta^2\right)^{-1/2} \left[\lambda + \sinh^{-1}(\zeta)\right] - \sqrt{1+\zeta^2} + \zeta \right\}}{\sqrt{1+(\kappa_c r)^2 \left[\lambda - \ln\left(\sqrt{1+\zeta^2} - \zeta\right) + \zeta\sqrt{1+\zeta^2} - \zeta^2 - 1\right]}} \tag{C.31}$$

$$\omega_\phi = -\frac{\kappa_c^2 \left[\mathcal{Z}_2 (\lambda - \ln \mathcal{Z}) - \mathcal{Z}\right]}{\sqrt{1+(r\kappa_c)^2 (\lambda - \ln \mathcal{Z} - \mathcal{Z}\mathcal{Z}_1)}} \tag{C.32}$$

$$\omega_\theta = \frac{1}{R}\left[\frac{\partial}{\partial R}\left(R u_\phi\right) - \frac{\partial u_R}{\partial \phi}\right]$$

$$\frac{\partial}{\partial R}\left(R u_\phi\right) = -\kappa_c \left[(\lambda - \ln \Phi)\sin\phi - \Phi\right] \tag{C.33}$$

$$\frac{\partial u_R}{\partial \phi} = -\kappa_c \left[(\lambda - \ln \Phi)\sin\phi + \cot\phi\right] \tag{C.34}$$

$$\omega_\theta = \frac{\kappa_c}{R}(\Phi + \cot\phi) \tag{C.35}$$

$$\omega_\theta = \frac{\kappa_c}{R}(\csc\phi - \cot\phi + \cot\phi) \tag{C.36}$$

$$\omega_\theta = \frac{\kappa_c}{R\sin\phi} \tag{C.37}$$

$$\omega_\theta = \frac{\kappa_c}{r} \tag{C.38}$$

$$\omega_R = \omega_\theta \frac{u_R}{u_\theta} \tag{C.39}$$

$$\omega_R = u_R \frac{\omega_\theta}{u_\theta} \tag{C.40}$$

$$\omega_\phi = \omega_\theta \frac{u_\phi}{u_\theta} \tag{C.41}$$

$$\omega_\phi = u_\phi \frac{\omega_\theta}{u_\theta} \tag{C.42}$$

$$\omega_r = -\frac{\partial u_\theta}{\partial z}$$

$$\omega_r = -\frac{\partial}{\partial z}\left\{\frac{1}{r}\sqrt{1+(\kappa_c r)^2\left[\lambda - \ln\left(\sqrt{1+\zeta^2}-\zeta\right)+\zeta\sqrt{1+\zeta^2}-\zeta^2-1\right]}\right\} \tag{C.43}$$

$$\omega_r = -\frac{1}{r}\frac{\partial}{\partial z}\left\{\sqrt{1+(\kappa_c r)^2\left[\lambda - \ln\left(\sqrt{1+\zeta^2}-\zeta\right)+\zeta\sqrt{1+\zeta^2}-\zeta^2-1\right]}\right\} \tag{C.44}$$

$$\frac{\partial}{\partial z}\left(u^{\frac{1}{2}}\right) = \tfrac{1}{2}u^{-\frac{1}{2}}\,\mathrm{d}u$$

$$\mathrm{d}u = \frac{\partial}{\partial z}\left\{(\kappa_c r)^2\left[\lambda - \ln\left(\sqrt{1+\zeta^2}-\zeta\right)+\zeta\sqrt{1+\zeta^2}-\zeta^2-1\right]\right\} \tag{C.45}$$

$$\mathrm{d}u = (\kappa_c r)^2\frac{\partial}{\partial z}\left[\lambda - \ln\left(\sqrt{1+\zeta^2}-\zeta\right)+\zeta\sqrt{1+\zeta^2}-\zeta^2-1\right] \tag{C.46}$$

$$\frac{\partial}{\partial z}\left[-\ln\left(\sqrt{1+\zeta^2}-\zeta\right)\right] = -\frac{u'}{u} \tag{C.47}$$

$$u' = \frac{\partial}{\partial z}\left(\sqrt{1+\zeta^2}-\zeta\right) \tag{C.48}$$

$$\frac{\partial}{\partial z}\left(\sqrt{1+\frac{z^2}{r^2}}\right)=\frac{1}{2}u^{-1/2}\mathrm{d}u \tag{C.49}$$

$$\mathrm{d}u=\frac{\partial}{\partial z}\left(\frac{z^2}{r^2}\right)=2\frac{z}{r^2} \tag{C.50}$$

$$\frac{\partial}{\partial z}\left(\sqrt{1+\frac{z^2}{r^2}}\right)=\frac{1}{2}\left(1+\frac{z^2}{r^2}\right)^{-1/2}2\frac{z}{r^2}=\frac{\frac{z}{r^2}}{\sqrt{1+\frac{z^2}{r^2}}} \tag{C.51}$$

$$u'=\frac{\partial}{\partial z}\left(\sqrt{1+\zeta^2}-\zeta\right)=\frac{\frac{z}{r^2}}{\sqrt{1+\frac{z^2}{r^2}}}-\frac{1}{r} \tag{C.52}$$

$$\frac{\partial}{\partial z}\left[-\ln\left(\sqrt{1+\zeta^2}-\zeta\right)\right]=-\frac{u'}{u}=-\frac{\frac{\frac{z}{r^2}}{\sqrt{1+\frac{z^2}{r^2}}}-\frac{1}{r}}{\sqrt{1+\frac{z^2}{r^2}}-\frac{z}{r}} \tag{C.53}$$

$$\frac{\partial}{\partial z}\left[-\ln\left(\sqrt{1+\zeta^2}-\zeta\right)\right]=-\frac{u'}{u}=\frac{-z+r\sqrt{1+\frac{z^2}{r^2}}}{r^2\sqrt{1+\frac{z^2}{r^2}}\left(\sqrt{1+\frac{z^2}{r^2}}-\frac{z}{r}\right)} \tag{C.54}$$

$$\frac{\partial}{\partial z}\left[-\ln\left(\sqrt{1+\zeta^2}-\zeta\right)\right]=-\frac{u'}{u}=\frac{-z+r\sqrt{1+\frac{z^2}{r^2}}}{r\sqrt{1+\frac{z^2}{r^2}}\left(r\sqrt{1+\frac{z^2}{r^2}}-z\right)} \tag{C.55}$$

$$\frac{\partial}{\partial z}\left[-\ln\left(\sqrt{1+\zeta^2}-\zeta\right)\right]=-\frac{u'}{u}=\frac{1}{r\sqrt{1+\frac{z^2}{r^2}}} \tag{C.56}$$

$$\frac{\partial}{\partial z}\left(\zeta\sqrt{1+\zeta^2}\right)=\frac{\partial}{\partial z}\left(\frac{z}{r}\sqrt{1+\frac{z^2}{r^2}}\right) \tag{C.57}$$

$$\frac{\partial}{\partial z}\left(\frac{z}{r}\sqrt{1+\frac{z^2}{r^2}}\right) = \frac{z}{r}\frac{\frac{z}{r^2}}{\sqrt{1+\frac{z^2}{r^2}}} + \frac{1}{r}\sqrt{1+\frac{z^2}{r^2}} = \frac{z^2}{r^3\sqrt{1+\frac{z^2}{r^2}}} + \frac{1}{r}\sqrt{1+\frac{z^2}{r^2}} \tag{C.58}$$

$$\begin{aligned} \mathrm{d}u &= (\kappa_c r)^2 \frac{\partial}{\partial z}\left[\lambda - \ln\left(\sqrt{1+\zeta^2}-\zeta\right) + \zeta\sqrt{1+\zeta^2} - \zeta^2 - 1\right] \\ &= (\kappa_c r)^2 \left(\frac{1}{r\sqrt{1+\frac{z^2}{r^2}}} + \frac{z^2}{r^3\sqrt{1+\frac{z^2}{r^2}}} + \frac{1}{r}\sqrt{1+\frac{z^2}{r^2}} - 2\frac{z}{r^2}\right) \end{aligned} \tag{C.59}$$

$$\mathrm{d}u = (\kappa_c r)^2 \left[\frac{r^2+z^2+r^2\left(1+\frac{z^2}{r^2}\right) - 2zr\sqrt{1+\frac{z^2}{r^2}}}{r^3\sqrt{1+\frac{z^2}{r^2}}}\right] \tag{C.60}$$

$$\mathrm{d}u = (\kappa_c r)^2 \left(\frac{r^2+z^2+r^2+z^2-2zr\sqrt{1+\frac{z^2}{r^2}}}{r^3\sqrt{1+\frac{z^2}{r^2}}}\right) \tag{C.61}$$

$$\mathrm{d}u = (\kappa_c r)^2 \left(\frac{2r^2+2z^2-2zr\sqrt{1+\frac{z^2}{r^2}}}{r^3\sqrt{1+\frac{z^2}{r^2}}}\right) \tag{C.62}$$

$$\begin{aligned} \omega_r &= -\frac{1}{r}\frac{\partial}{\partial z}\left\{\sqrt{1+(\kappa_c r)^2\left[\lambda - \ln\left(\sqrt{1+\zeta^2}-\zeta\right) + \zeta\sqrt{1+\zeta^2} - \zeta^2 - 1\right]}\right\} \\ &= -\frac{1}{2r}\frac{(\kappa_c r)^2\left(\frac{2r^2+2z^2-2zr\sqrt{1+\frac{z^2}{r^2}}}{r^3\sqrt{1+\frac{z^2}{r^2}}}\right)}{\sqrt{1+(\kappa_c r)^2\left[\lambda - \ln\left(\sqrt{1+\zeta^2}-\zeta\right) + \zeta\sqrt{1+\zeta^2} - \zeta^2 - 1\right]}} \end{aligned} \tag{C.63}$$

$$\omega_r = -\frac{\kappa_c^2\left(r^2+z^2-zr\sqrt{1+\frac{z^2}{r^2}}\right)}{r^2\sqrt{1+\frac{z^2}{r^2}}\sqrt{1+(\kappa_c r)^2\left[\lambda-\ln\left(\sqrt{1+\zeta^2}-\zeta\right)+\zeta\sqrt{1+\zeta^2}-\zeta^2-1\right]}} \tag{C.64}$$

$$\omega_r = -\frac{\kappa_c^2\left(1+\zeta^2-\zeta\sqrt{1+\zeta^2}\right)}{\sqrt{1+\zeta^2}\sqrt{1+(\kappa_c r)^2\left[\lambda-\ln\left(\sqrt{1+\zeta^2}-\zeta\right)+\zeta\sqrt{1+\zeta^2}-\zeta^2-1\right]}} \tag{C.65}$$

$$\omega_r = -\frac{\kappa_c^2\left(1+\zeta^2\right)^{-1/2}\left(1+\zeta^2-\zeta\sqrt{1+\zeta^2}\right)}{\sqrt{1+(\kappa_c r)^2\left[\lambda-\ln\left(\sqrt{1+\zeta^2}-\zeta\right)+\zeta\sqrt{1+\zeta^2}-\zeta^2-1\right]}} \tag{C.66}$$

$$\omega_r = -\frac{\kappa_c^2\left(1+\zeta^2\right)^{-1/2}\left(1+\zeta^2-\zeta\sqrt{1+\zeta^2}\right)}{\sqrt{1+(\kappa_c r)^2\left[\lambda+\sinh^{-1}(\zeta)+\zeta\sqrt{1+\zeta^2}-\zeta^2-1\right]}} \tag{C.67}$$

$$\omega_r = -\frac{\kappa_c^2\mathcal{Z}\mathcal{Z}_1\mathcal{Z}_2}{\sqrt{1+(\kappa_c r)^2\left(\lambda-\ln\mathcal{Z}-\mathcal{Z}\mathcal{Z}_1\right)}} \tag{C.68}$$

$$\omega_r = -\frac{\kappa_c^2\left(\frac{\sqrt{1+\zeta^2}\sqrt{1+\zeta^2}-\zeta\sqrt{1+\zeta^2}}{\sqrt{1+\zeta^2}}\right)}{\sqrt{1+(\kappa_c r)^2\left[\lambda-\ln\left(\sqrt{1+\zeta^2}-\zeta\right)+\zeta\sqrt{1+\zeta^2}-\zeta^2-1\right]}} \tag{C.69}$$

$$\omega_r = -\frac{\kappa_c^2\left(\sqrt{1+\zeta^2}-\zeta\right)}{\sqrt{1+(\kappa_c r)^2\left[\lambda-\ln\left(\sqrt{1+\zeta^2}-\zeta\right)+\zeta\sqrt{1+\zeta^2}-\zeta^2-1\right]}} \tag{C.70}$$

$$\omega_r = \frac{\kappa_c}{r}\frac{u_r}{u_\theta} \tag{C.71}$$

$$\omega_r = -\frac{\kappa_c^2\Phi}{\sqrt{1+(\kappa_c R\sin\phi)^2\left(\lambda-\ln\Phi-\Phi\csc\phi\right)}} \tag{C.72}$$

$$\omega_r = \omega_\theta \frac{u_r}{u_\theta} \tag{C.73}$$

$$\omega_r = u_r \frac{\omega_\theta}{u_\theta} \tag{C.74}$$

$$\omega_z = \frac{1}{r}\left[\frac{\partial}{\partial r}\left(u_\theta r\right)\right] \tag{C.75}$$

$$\frac{\partial}{\partial r}\left(u^{\frac{1}{2}}\right) = \tfrac{1}{2}u^{-\frac{1}{2}}\,\mathrm{d}u$$

$$\mathrm{d}u = \frac{\partial}{\partial r}\left\{(\kappa_c r)^2\left[\lambda - \ln\left(\sqrt{1+\zeta^2}-\zeta\right) + \zeta\sqrt{1+\zeta^2} - \zeta^2 - 1\right]\right\} \tag{C.76}$$

$$\begin{aligned}\mathrm{d}u = {} & \left(2\kappa_c^2 r\right)\left[\lambda - \ln\left(\sqrt{1+\zeta^2}-\zeta\right) + \zeta\sqrt{1+\zeta^2} - \zeta^2 - 1\right] \\ & + (\kappa_c r)^2 \frac{\partial}{\partial r}\left[-\ln\left(\sqrt{1+\frac{z^2}{r^2}} - \frac{z}{r}\right) + \frac{z}{r}\sqrt{1+\frac{z^2}{r^2}} - \frac{z^2}{r^2}\right]\end{aligned} \tag{C.77}$$

$$\frac{\partial}{\partial r}\left[-\ln\left(\sqrt{1+\frac{z^2}{r^2}} - \frac{z}{r}\right)\right] = -\frac{u'}{u} \tag{C.78}$$

$$u = \sqrt{1+\frac{z^2}{r^2}} - \frac{z}{r} \tag{C.79}$$

$$\frac{\partial}{\partial r}\sqrt{1+\frac{z^2}{r^2}} = \frac{\partial}{\partial r}\left(u^{\frac{1}{2}}\right) = \tfrac{1}{2}u^{-\frac{1}{2}}\,\mathrm{d}u \tag{C.80}$$

$$\mathrm{d}u = \frac{1}{2}\left(1+\frac{z^2}{r^2}\right)^{-1/2}\left(-2\frac{z^2}{r^3}\right) \tag{C.81}$$

$$\mathrm{d}u = \left(1 + \frac{z^2}{r^2}\right)^{-1/2} \left(-\frac{z^2}{r^3}\right) \tag{C.82}$$

$$\frac{\partial}{\partial r}\left(-\frac{z}{r}\right) = \frac{z}{r^2} \tag{C.83}$$

$$u' = -\frac{z^2}{r^3\sqrt{1 + \frac{z^2}{r^2}}} + \frac{z}{r^2} \tag{C.84}$$

$$\frac{\partial}{\partial r}\left[-\ln\left(\sqrt{1 + \frac{z^2}{r^2}} - \frac{z}{r}\right)\right] = -\frac{u'}{u} = \frac{\frac{z^2}{r^3\sqrt{1 + \frac{z^2}{r^2}}} - \frac{z}{r^2}}{\sqrt{1 + \frac{z^2}{r^2}} - \frac{z}{r}} \tag{C.85}$$

$$\frac{\partial}{\partial r}\left[-\ln\left(\sqrt{1 + \frac{z^2}{r^2}} - \frac{z}{r}\right)\right] = -\frac{u'}{u} = \frac{z^2 - zr\sqrt{1 + \frac{z^2}{r^2}}}{r^3\sqrt{1 + \frac{z^2}{r^2}}\left(\sqrt{1 + \frac{z^2}{r^2}} - \frac{z}{r}\right)} \tag{C.86}$$

$$\frac{\partial}{\partial r}\left[-\ln\left(\sqrt{1 + \frac{z^2}{r^2}} - \frac{z}{r}\right)\right] = -\frac{u'}{u} = \frac{z^2 - zr\sqrt{1 + \frac{z^2}{r^2}}}{r^2\sqrt{1 + \frac{z^2}{r^2}}\left(r\sqrt{1 + \frac{z^2}{r^2}} - z\right)} \tag{C.87}$$

$$\frac{\partial}{\partial r}\left[-\ln\left(\sqrt{1 + \frac{z^2}{r^2}} - \frac{z}{r}\right)\right] = -\frac{u'}{u} = -\frac{z}{r^2\sqrt{1 + \frac{z^2}{r^2}}} \tag{C.88}$$

$$\frac{\partial}{\partial r}\left(\frac{z}{r}\sqrt{1 + \frac{z^2}{r^2}}\right) = -\frac{z}{r^2}\sqrt{1 + \frac{z^2}{r^2}} - \frac{z^3}{r^4\sqrt{1 + \frac{z^2}{r^2}}} \tag{C.89}$$

$$\frac{\partial}{\partial r}\left(-\frac{z^2}{r^2}\right) = \frac{2z^2}{r^3} \tag{C.90}$$

$$\frac{\partial}{\partial r}\left[-\ln\left(\sqrt{1+\frac{z^2}{r^2}}-\frac{z}{r}\right)+\frac{z}{r}\sqrt{1+\frac{z^2}{r^2}}-\frac{z^2}{r^2}\right]$$
$$=-\frac{z}{r^2\sqrt{1+\frac{z^2}{r^2}}}-\frac{z}{r^2}\sqrt{1+\frac{z^2}{r^2}}-\frac{z^3}{r^4\sqrt{1+\frac{z^2}{r^2}}}+\frac{2z^2}{r^3} \tag{C.91}$$

$$\frac{\partial}{\partial r}\left[-\ln\left(\sqrt{1+\frac{z^2}{r^2}}-\frac{z}{r}\right)+\frac{z}{r}\sqrt{1+\frac{z^2}{r^2}}-\frac{z^2}{r^2}\right]$$
$$=\frac{-zr^2-zr^2\left(1+\frac{z^2}{r^2}\right)-z^3+2z^2r\sqrt{1+\frac{z^2}{r^2}}}{r^4\sqrt{1+\frac{z^2}{r^2}}} \tag{C.92}$$

$$\frac{\partial}{\partial r}\left[-\ln\left(\sqrt{1+\frac{z^2}{r^2}}-\frac{z}{r}\right)+\frac{z}{r}\sqrt{1+\frac{z^2}{r^2}}-\frac{z^2}{r^2}\right]$$
$$=\frac{-zr^2-zr^2-z^3-z^3+2z^2r\sqrt{1+\frac{z^2}{r^2}}}{r^4\sqrt{1+\frac{z^2}{r^2}}} \tag{C.93}$$

$$\frac{\partial}{\partial r}\left[-\ln\left(\sqrt{1+\frac{z^2}{r^2}}-\frac{z}{r}\right)+\frac{z}{r}\sqrt{1+\frac{z^2}{r^2}}-\frac{z^2}{r^2}\right]$$
$$=\frac{-2\left(zr^2+z^3\right)+2z^2r\sqrt{1+\frac{z^2}{r^2}}}{r^4\sqrt{1+\frac{z^2}{r^2}}} \tag{C.94}$$

$$\frac{\partial}{\partial r}\left[-\ln\left(\sqrt{1+\frac{z^2}{r^2}}-\frac{z}{r}\right)+\frac{z}{r}\sqrt{1+\frac{z^2}{r^2}}-\frac{z^2}{r^2}\right] = \frac{-2zr^2\left(1+\frac{z^2}{r^2}\right)+2z^2r\sqrt{1+\frac{z^2}{r^2}}}{r^4\sqrt{1+\frac{z^2}{r^2}}} \tag{C.95}$$

$$\frac{\partial}{\partial r}\left[-\ln\left(\sqrt{1+\frac{z^2}{r^2}}-\frac{z}{r}\right)+\frac{z}{r}\sqrt{1+\frac{z^2}{r^2}}-\frac{z^2}{r^2}\right] = \frac{-2zr^2\sqrt{1+\frac{z^2}{r^2}}\sqrt{1+\frac{z^2}{r^2}}+2z^2r\sqrt{1+\frac{z^2}{r^2}}}{r^3r\sqrt{1+\frac{z^2}{r^2}}} \tag{C.96}$$

$$\frac{\partial}{\partial r}\left[-\ln\left(\sqrt{1+\frac{z^2}{r^2}}-\frac{z}{r}\right)+\frac{z}{r}\sqrt{1+\frac{z^2}{r^2}}-\frac{z^2}{r^2}\right] = -\frac{2}{r^3}\left(zr\sqrt{1+\frac{z^2}{r^2}}-z^2\right) \tag{C.97}$$

$$\mathrm{d}u = \left(2\kappa_c^2 r\right)\left[\lambda-\ln\left(\sqrt{1+\zeta^2}-\zeta\right)+\zeta\sqrt{1+\zeta^2}-\zeta^2-1\right] - (\kappa_c r)^2\left[\frac{2}{r^3}\left(zr\sqrt{1+\frac{z^2}{r^2}}-z^2\right)\right] \tag{C.98}$$

$$\mathrm{d}u = \left(2\kappa_c^2 r\right)\left[\lambda-\ln\left(\sqrt{1+\zeta^2}-\zeta\right)+\zeta\sqrt{1+\zeta^2}-\zeta^2-1\right] - \left(\kappa_c^2 r\right)\left[\frac{2}{r^2}\left(zr\sqrt{1+\frac{z^2}{r^2}}-z^2\right)\right] \tag{C.99}$$

$$\mathrm{d}u = \left(2\kappa_c^2 r\right)\left[\lambda - \ln\left(\sqrt{1+\zeta^2} - \zeta\right) + \zeta\sqrt{1+\zeta^2} - \zeta^2 - 1\right] - \left(2\kappa_c^2 r\right)\left(\frac{z}{r}\sqrt{1+\frac{z^2}{r^2}} - \frac{z^2}{r^2}\right) \tag{C.100}$$

$$\mathrm{d}u = \left(2\kappa_c^2 r\right)\left[\lambda - \ln\left(\sqrt{1+\zeta^2} - \zeta\right) + \zeta\sqrt{1+\zeta^2} - \zeta^2 - 1\right] - \left(2\kappa_c^2 r\right)\left(\zeta\sqrt{1+\zeta^2} - \zeta^2\right) \tag{C.101}$$

$$\mathrm{d}u = \left(2\kappa_c^2 r\right)\left[\lambda - \ln\left(\sqrt{1+\zeta^2} - \zeta\right) - 1\right] \tag{C.102}$$

$$\omega_z = \frac{\kappa_c^2\left[\lambda - \ln\left(\sqrt{1+\zeta^2} - \zeta\right) - 1\right]}{\sqrt{1 + (\kappa_c r)^2\left[\lambda - \ln\left(\sqrt{1+\zeta^2} - \zeta\right) + \zeta\sqrt{1+\zeta^2} - \zeta^2 - 1\right]}} \tag{C.103}$$

$$\omega_z = \frac{\kappa_c}{r}\frac{u_z}{u_\theta} \tag{C.104}$$

$$\omega_z = \frac{\kappa_c^2\left(\lambda - \ln\Phi - 1\right)}{\sqrt{1 + (\kappa_c R\sin\phi)^2\left(\lambda - \ln\Phi - \Phi\csc\phi\right)}} \tag{C.105}$$

$$\omega_z = \omega_\theta\frac{u_z}{u_\theta} \tag{C.106}$$

$$\omega_z = u_z\frac{\omega_\theta}{u_\theta} \tag{C.107}$$

$$\omega_z = \frac{\kappa_c^2\left[\lambda + \sinh^{-1}(\zeta) - 1\right]}{\sqrt{1 + (\kappa_c r)^2\left[\lambda + \sinh^{-1}(\zeta) + \zeta\sqrt{1+\zeta^2} - \zeta^2 - 1\right]}} \tag{C.108}$$

$$\omega_R = \frac{\kappa_c^2 \left[(\lambda - \ln\Phi)\cos\phi - 1\right]}{\sqrt{1 + (\kappa_c R \sin\phi)^2 (\lambda - \ln\Phi - \Phi\csc\phi)}} \tag{C.109}$$

$$\omega_\phi = -\frac{\kappa_c^2 \left[(\lambda - \ln\Phi)\sin\phi - \Phi\right]}{\sqrt{1 + (\kappa_c R \sin\phi)^2 (\lambda - \ln\Phi - \Phi\csc\phi)}} \tag{C.110}$$

$$\omega_\theta = \frac{\kappa_c}{R\sin\phi} \qquad \text{(slip)} \tag{C.111}$$

$$\omega_r = -\frac{\kappa_c^2 \Phi}{\sqrt{1 + (\kappa_c R \sin\phi)^2 (\lambda - \ln\Phi - \Phi\csc\phi)}} \tag{C.112}$$

$$\omega_z = \frac{\kappa_c^2 (\lambda - \ln\Phi - 1)}{\sqrt{1 + (\kappa_c R \sin\phi)^2 (\lambda - \ln\Phi - \Phi\csc\phi)}} \tag{C.113}$$

$$\omega_R = \frac{\kappa_c \left[(\lambda - \ln\Phi)\cos\phi - 1\right]}{\sqrt{\lambda - \ln\Phi - \Phi\csc\phi}} \tag{C.114}$$

$$\omega_\phi = -\frac{\kappa_c \left[(\lambda - \ln\Phi)\sin\phi - \Phi\right]}{\sqrt{\lambda - \ln\Phi - \Phi\csc\phi}} \tag{C.115}$$

$$\omega_\theta = \frac{\kappa_c}{R\sin\phi} \qquad \text{(no slip)} \tag{C.116}$$

$$\omega_r = -\frac{\kappa_c \Phi}{\sqrt{\lambda - \ln\Phi - \Phi\csc\phi}} \tag{C.117}$$

$$\omega_z = \frac{\kappa_c (\lambda - \ln\Phi - 1)}{\sqrt{\lambda - \ln\Phi - \Phi\csc\phi}} \tag{C.118}$$

$$\omega_R = \frac{\kappa_c^2 \left\{ \zeta \left(1+\zeta^2\right)^{-1/2} \left[\lambda - \ln\left(\sqrt{1+\zeta^2} - \zeta \right) \right] - 1 \right\}}{\sqrt{1 + (\kappa_c r)^2 \left[\lambda - \ln\left(\sqrt{1+\zeta^2} - \zeta \right) + \zeta \sqrt{1+\zeta^2} - \zeta^2 - 1 \right]}} \tag{C.119}$$

$$\omega_\phi = -\frac{\kappa_c^2 \left\{ \left(1+\zeta^2\right)^{-1/2} \left[\lambda - \ln\left(\sqrt{1+\zeta^2} - \zeta \right) \right] - \sqrt{1+\zeta^2} + \zeta \right\}}{\sqrt{1 + (\kappa_c r)^2 \left[\lambda - \ln\left(\sqrt{1+\zeta^2} - \zeta \right) + \zeta \sqrt{1+\zeta^2} - \zeta^2 - 1 \right]}} \tag{C.120}$$

$$\omega_\theta = \frac{\kappa_c}{r} \qquad \text{(slip)} \tag{C.121}$$

$$\omega_r = -\frac{\kappa_c^2 \left(\sqrt{1+\zeta^2} - \zeta \right)}{\sqrt{1 + (\kappa_c r)^2 \left[\lambda - \ln\left(\sqrt{1+\zeta^2} - \zeta \right) + \zeta \sqrt{1+\zeta^2} - \zeta^2 - 1 \right]}} \tag{C.122}$$

$$\omega_z = \frac{\kappa_c^2 \left[\lambda - \ln\left(\sqrt{1+\zeta^2} - \zeta \right) - 1 \right]}{\sqrt{1 + (\kappa_c r)^2 \left[\lambda - \ln\left(\sqrt{1+\zeta^2} - \zeta \right) + \zeta \sqrt{1+\zeta^2} - \zeta^2 - 1 \right]}} \tag{C.123}$$

$$\omega_R = \frac{\kappa_c \left\{ \zeta \left(1+\zeta^2\right)^{-1/2} \left[\lambda - \ln\left(\sqrt{1+\zeta^2} - \zeta \right) \right] - 1 \right\}}{\sqrt{\lambda - \ln\left(\sqrt{1+\zeta^2} - \zeta \right) + \zeta \sqrt{1+\zeta^2} - \zeta^2 - 1}} \tag{C.124}$$

$$\omega_\phi = -\frac{\kappa_c \left\{ \left(1+\zeta^2\right)^{-1/2} \left[\lambda - \ln\left(\sqrt{1+\zeta^2} - \zeta \right) \right] - \sqrt{1+\zeta^2} + \zeta \right\}}{\sqrt{\lambda - \ln\left(\sqrt{1+\zeta^2} - \zeta \right) + \zeta \sqrt{1+\zeta^2} - \zeta^2 - 1}} \tag{C.125}$$

$$\omega_\theta = \frac{\kappa_c}{r} \qquad \text{(no slip)} \tag{C.126}$$

$$\omega_r = -\frac{\kappa_c \left(\sqrt{1+\zeta^2} - \zeta \right)}{\sqrt{\lambda - \ln\left(\sqrt{1+\zeta^2} - \zeta \right) + \zeta \sqrt{1+\zeta^2} - \zeta^2 - 1}} \tag{C.127}$$

$$\omega_z = \frac{\kappa_c \left[\lambda - \ln\left(\sqrt{1+\zeta^2} - \zeta \right) - 1 \right]}{\sqrt{\lambda - \ln\left(\sqrt{1+\zeta^2} - \zeta \right) + \zeta \sqrt{1+\zeta^2} - \zeta^2 - 1}} \tag{C.128}$$

$$\omega_R = \frac{\kappa_c^2 \left\{ \zeta \left(1+\zeta^2\right)^{-1/2} \left[\lambda + \sinh^{-1}(\zeta)\right] - 1 \right\}}{\sqrt{1+(\kappa_c r)^2 \left[\lambda + \sinh^{-1}(\zeta) + \zeta\sqrt{1+\zeta^2} - \zeta^2 - 1\right]}} \tag{C.129}$$

$$\omega_\phi = -\frac{\kappa_c^2 \left\{ \left(1+\zeta^2\right)^{-1/2} \left[\lambda + \sinh^{-1}(\zeta)\right] - \sqrt{1+\zeta^2} + \zeta \right\}}{\sqrt{1+(\kappa_c r)^2 \left[\lambda + \sinh^{-1}(\zeta) + \zeta\sqrt{1+\zeta^2} - \zeta^2 - 1\right]}} \tag{C.130}$$

$$\omega_\theta = \frac{\kappa_c}{r} \qquad \text{(slip)} \tag{C.131}$$

$$\omega_r = -\frac{\kappa_c^2 \left(\sqrt{1+\zeta^2} - \zeta \right)}{\sqrt{1+(\kappa_c r)^2 \left[\lambda + \sinh^{-1}(\zeta) + \zeta\sqrt{1+\zeta^2} - \zeta^2 - 1\right]}} \tag{C.132}$$

$$\omega_z = \frac{\kappa_c^2 \left[\lambda + \sinh^{-1}(\zeta) - 1\right]}{\sqrt{1+(\kappa_c r)^2 \left[\lambda + \sinh^{-1}(\zeta) + \zeta\sqrt{1+\zeta^2} - \zeta^2 - 1\right]}} \tag{C.133}$$

$$\omega_R = \frac{\kappa_c \left\{ \zeta \left(1+\zeta^2\right)^{-1/2} \left[\lambda + \sinh^{-1}(\zeta)\right] - 1 \right\}}{\sqrt{\lambda + \sinh^{-1}(\zeta) + \zeta\sqrt{1+\zeta^2} - \zeta^2 - 1}} \tag{C.134}$$

$$\omega_\phi = -\frac{\kappa_c \left\{ \left(1+\zeta^2\right)^{-1/2} \left[\lambda + \sinh^{-1}(\zeta)\right] - \sqrt{1+\zeta^2} + \zeta \right\}}{\sqrt{\lambda + \sinh^{-1}(\zeta) + \zeta\sqrt{1+\zeta^2} - \zeta^2 - 1}} \tag{C.135}$$

$$\omega_\theta = \frac{\kappa_c}{r} \qquad \text{(no slip)} \tag{C.136}$$

$$\omega_r = -\frac{\kappa_c \left(\sqrt{1+\zeta^2} - \zeta \right)}{\sqrt{1+(\kappa_c r)^2 \left[\lambda + \sinh^{-1}(\zeta) + \zeta\sqrt{1+\zeta^2} - \zeta^2 - 1\right]}} \tag{C.137}$$

$$\omega_z = \frac{\kappa_c \left[\lambda + \sinh^{-1}(\zeta) - 1\right]}{\sqrt{\lambda + \sinh^{-1}(\zeta) + \zeta\sqrt{1+\zeta^2} - \zeta^2 - 1}} \tag{C.138}$$

$$\frac{\omega_j}{u_j} = \frac{\kappa_c}{u_\theta r} = \frac{\kappa_c}{u_\theta R \sin\phi} = \frac{\kappa_c}{B(\psi)} \tag{C.139}$$

$$\frac{\omega_j}{u_j} = \frac{\kappa_c}{\sqrt{1 + (\kappa_c R \sin\phi)^2 (\lambda - \ln\Phi - \Phi \csc\phi)}} \tag{C.140}$$

$$\frac{\omega_j}{u_j} = \frac{\kappa_c}{\sqrt{1 + (\kappa_c r)^2 \left[\lambda - \ln\left(\sqrt{1+\zeta^2} - \zeta\right) + \zeta\sqrt{1+\zeta^2} - \zeta^2 - 1\right]}} \tag{C.141}$$

$$\frac{\omega_j}{u_j} = \frac{\kappa_c}{\sqrt{1 + (\kappa_c r)^2 \left[\lambda + \sinh^{-1}(\zeta) + \zeta\sqrt{1+\zeta^2} - \zeta^2 - 1\right]}} \tag{C.142}$$

$$\begin{cases} \omega_R = \dfrac{\kappa_c^2}{B(\psi)} \left[(\lambda - \ln\Phi)\cos\phi - 1\right] \\ \omega_\phi = -\dfrac{\kappa_c^2}{B(\psi)} \left[(\lambda - \ln\Phi)\sin\phi - \Phi\right] \\ \omega_r = -\dfrac{\kappa_c^2}{B(\psi)}\Phi \\ \omega_z = \dfrac{\kappa_c^2}{B(\psi)} (\lambda - \ln\Phi - 1) \end{cases} \tag{C.143}$$

$$\begin{cases} \omega_R = \kappa_c^2 \left[\dfrac{(\lambda - \ln\Phi)\cos\phi - 1}{B(\psi)}\right] \\ \omega_\phi = -\kappa_c^2 \left[\dfrac{(\lambda - \ln\Phi)\sin\phi - \Phi}{B(\psi)}\right] \\ \omega_r = -\kappa_c^2 \left[\dfrac{\Phi}{B(\psi)}\right] \\ \omega_z = \kappa_c^2 \left[\dfrac{(\lambda - \ln\Phi - 1)}{B(\psi)}\right] \end{cases} \tag{C.144}$$

$$\begin{cases} \omega_R = \dfrac{\kappa_c^2}{B(\psi)} \left\{ \zeta \left(1+\zeta^2\right)^{-1/2} \left[\lambda - \ln\left(\sqrt{1+\zeta^2} - \zeta \right) \right] - 1 \right\} \\ \omega_\phi = -\dfrac{\kappa_c^2}{B(\psi)} \left\{ \left(1+\zeta^2\right)^{-1/2} \left[\lambda - \ln\left(\sqrt{1+\zeta^2} - \zeta \right) \right] - \sqrt{1+\zeta^2} + \zeta \right\} \\ \omega_r = -\dfrac{\kappa_c^2}{B(\psi)} \left(\sqrt{1+\zeta^2} - \zeta \right) \\ \omega_z = \dfrac{\kappa_c^2}{B(\psi)} \left[\lambda - \ln\left(\sqrt{1+\zeta^2} - \zeta \right) - 1 \right] \end{cases} \tag{C.145}$$

$$\begin{cases} \omega_R = \kappa_c^2 \left\{ \dfrac{\zeta \left(1+\zeta^2\right)^{-1/2} \left[\lambda - \ln\left(\sqrt{1+\zeta^2} - \zeta \right) \right] - 1}{B(\psi)} \right\} \\ \omega_\phi = -\kappa_c^2 \left\{ \dfrac{\left(1+\zeta^2\right)^{-1/2} \left[\lambda - \ln\left(\sqrt{1+\zeta^2} - \zeta \right) \right] - \sqrt{1+\zeta^2} + \zeta}{B(\psi)} \right\} \\ \omega_r = -\kappa_c^2 \left\{ \dfrac{\sqrt{1+\zeta^2} - \zeta}{B(\psi)} \right\} \\ \omega_z = \kappa_c^2 \left\{ \dfrac{\lambda - \ln\left(\sqrt{1+\zeta^2} - \zeta \right) - 1}{B(\psi)} \right\} \end{cases} \tag{C.146}$$

$$\begin{cases} \omega_R = \dfrac{\kappa_c^2}{B(\psi)} \left\{ \zeta \left(1+\zeta^2\right)^{-1/2} \left[\lambda + \sinh^{-1}(\zeta) \right] - 1 \right\} \\ \omega_\phi = -\dfrac{\kappa_c^2}{B(\psi)} \left\{ \left(1+\zeta^2\right)^{-1/2} \left[\lambda + \sinh^{-1}(\zeta) \right] - \sqrt{1+\zeta^2} + \zeta \right\} \\ \omega_r = -\dfrac{\kappa_c^2}{B(\psi)} \left(\sqrt{1+\zeta^2} - \zeta \right) \\ \omega_z = \dfrac{\kappa_c^2}{B(\psi)} \left[\lambda + \sinh^{-1}(\zeta) - 1 \right] \end{cases} \tag{C.147}$$

$$\begin{cases} \omega_R = \kappa_c^2 \left\{ \dfrac{\zeta \left(1+\zeta^2\right)^{-1/2} \left[\lambda + \sinh^{-1}(\zeta)\right] - 1}{B(\psi)} \right\} \\ \omega_\phi = -\kappa_c^2 \left\{ \dfrac{\left(1+\zeta^2\right)^{-1/2} \left[\lambda + \sinh^{-1}(\zeta)\right] - \sqrt{1+\zeta^2} + \zeta}{B(\psi)} \right\} \\ \omega_r = -\kappa_c^2 \left\{ \dfrac{\sqrt{1+\zeta^2} - \zeta}{B(\psi)} \right\} \\ \omega_z = \kappa_c^2 \left\{ \dfrac{\lambda + \sinh^{-1}(\zeta) - 1}{B(\psi)} \right\} \end{cases} \tag{C.148}$$

Appendix D

Pressure Mathematics for Beltramian Cone Solution

This appendix contains detailed mathematical formulation regarding the pressure for the Beltramian solution.

$$\begin{cases} u_R \dfrac{\partial u_R}{\partial R} + \dfrac{u_\phi}{R}\dfrac{\partial u_R}{\partial \phi} = -\dfrac{1}{\rho}\dfrac{\partial p}{\partial R} \\ u_R \dfrac{\partial u_\phi}{\partial R} + \dfrac{u_\phi}{R}\dfrac{\partial u_\phi}{\partial \phi} + \dfrac{u_R u_\phi}{R} - \dfrac{u_\theta^2 \cot\phi}{R} = -\dfrac{1}{\rho R}\dfrac{\partial p}{\partial \phi} \\ u_r \dfrac{\partial u_r}{\partial r} + u_z \dfrac{\partial u_r}{\partial z} - \dfrac{u_\theta^2}{r} = -\dfrac{1}{\rho}\dfrac{\partial p}{\partial r} \\ u_r \dfrac{\partial u_z}{\partial r} + u_z \dfrac{\partial u_z}{\partial z} = -\dfrac{1}{\rho}\dfrac{\partial p}{\partial z} \end{cases} \tag{D.1}$$

$$\frac{1}{\rho}\frac{\partial p}{\partial R} = -u_R \frac{\partial u_R}{\partial R} - \frac{u_\phi}{R}\frac{\partial u_R}{\partial \phi} \tag{D.2}$$

$$p = \frac{\bar{p}}{\rho U^2} \tag{D.3}$$

$$\frac{\partial p}{\partial R} = -u_R \frac{\partial u_R}{\partial R} - \frac{u_\phi}{R}\frac{\partial u_R}{\partial \phi} \tag{D.4}$$

$$\frac{\partial p}{\partial R} = -\frac{u_\phi}{R}\frac{\partial u_R}{\partial \phi} \tag{D.5}$$

$$\frac{\partial u_R}{\partial \phi} = \kappa_c \frac{\partial}{\partial \phi}\left[(\lambda - \ln \Phi)\cos\phi - 1\right] \tag{D.6}$$

from Equations (2.7.7–2.7.15)

$$\frac{\partial}{\partial \phi}(-\ln \Phi) = -\csc\phi$$

$$\frac{\partial u_R}{\partial \phi} = -\kappa_c\left[(\lambda - \ln \Phi)\sin\phi + \cot\phi\right] \tag{D.7}$$

$$u_\phi \frac{\partial u_R}{\partial \phi} = \kappa_c^2\left[(\lambda - \ln \Phi)\sin\phi + \cot\phi\right]\left[(\lambda - \ln \Phi)\sin\phi - \Phi\right] \tag{D.8}$$

$$u_\phi \frac{\partial u_R}{\partial \phi} = \kappa_c^2\Big[(\lambda - \ln \Phi)^2 \sin^2\phi + (\lambda - \ln \Phi)\cos\phi - \Phi\,(\lambda - \ln \Phi)\sin\phi - \Phi\cot\phi\Big] \tag{D.9}$$

$$-\frac{u_\phi}{R}\frac{\partial u_R}{\partial \phi} = -\frac{\kappa_c^2}{R}\Big[(\lambda - \ln \Phi)^2 \sin^2\phi + (\lambda - \ln \Phi)\cos\phi - \Phi\,(\lambda - \ln \Phi)\sin\phi - \Phi\cot\phi\Big] \tag{D.10}$$

$$\frac{\partial p}{\partial R} = \frac{\kappa_c^2}{R}\big[\Phi\,(\lambda - \ln \Phi)\sin\phi + \Phi\cot\phi - (\lambda - \ln \Phi)^2 \sin^2\phi - (\lambda - \ln \Phi)\cos\phi\big] \tag{D.11}$$

$$\frac{\partial p}{\partial R} = \frac{\kappa_c^2}{R}\Big[(\lambda - \ln\Phi) + \Phi\cot\phi - (\lambda - \ln\Phi)^2 \sin^2\phi - 2\,(\lambda - \ln\Phi)\cos\phi\Big] \tag{D.12}$$

$$\frac{\partial p}{\partial R} = \frac{\kappa_c^2}{R}\Big[(\lambda - \ln\Phi) + \Phi\cot\phi - (\lambda - \ln\Phi)^2 \left(1 - \cos^2\phi\right) - 2\,(\lambda - \ln\Phi)\cos\phi\Big] \tag{D.13}$$

$$\frac{\partial p}{\partial R} = \frac{\kappa_c^2}{R}\Big[(\lambda - \ln\Phi) + \Phi\cot\phi - (\lambda - \ln\Phi)^2 + (\lambda - \ln\Phi)^2\cos^2\phi - 2\,(\lambda - \ln\Phi)\cos\phi\Big] \tag{D.14}$$

$$\left[(\lambda - \ln\Phi)\cos\phi - 1\right]^2 = (\lambda - \ln\Phi)^2\cos^2\phi - 2\,(\lambda - \ln\Phi)\cos\phi + 1 \tag{D.15}$$

$$\frac{\partial p}{\partial R} = \frac{\kappa_c^2}{R}\Big\{ (\lambda - \ln\Phi) + \Phi\cot\phi - (\lambda - \ln\Phi)^2 + \left[(\lambda - \ln\Phi)\cos\phi - 1\right]^2 - 1\Big\} \tag{D.16}$$

$$-\left[(\lambda - \ln\Phi) - 1\right]^2 = -(\lambda - \ln\Phi)^2 + 2\,(\lambda - \ln\Phi) - 1 \tag{D.17}$$

$$\frac{\partial p}{\partial R} = \frac{\kappa_c^2}{R}\{\left[(\lambda - \ln\Phi)\cos\phi - 1\right]^2 + \Phi\cot\phi - (\lambda - \ln\Phi) - \left[(\lambda - \ln\Phi) - 1\right]^2\} \tag{D.18}$$

$$\frac{\partial p}{\partial \phi} = -u_\phi \frac{\partial u_\phi}{\partial \phi} - u_R u_\phi + u_\theta^2 \cot\phi \tag{D.19}$$

$$\frac{\partial u_\phi}{\partial \phi} = -\kappa_c \frac{\partial}{\partial \phi}\left[(\lambda - \ln\Phi)\sin\phi - \Phi\right] \tag{D.20}$$

from Equation Eq. (C.6)

$$\frac{\partial u_\phi}{\partial \phi} = -\kappa_c \left[(\lambda - \ln\Phi)\cos\phi - \Phi\csc\phi - 1\right] \tag{D.21}$$

$$u_\phi \frac{\partial u_\phi}{\partial \phi} = \kappa_c^2 \left[(\lambda - \ln\Phi)\cos\phi - \Phi\csc\phi - 1\right]\left[(\lambda - \ln\Phi)\sin\phi - \Phi\right] \tag{D.22}$$

$$u_\phi \frac{\partial u_\phi}{\partial \phi} = \kappa_c^2 \Big[(\lambda - \ln\Phi)^2 \sin\phi\cos\phi - \Phi(\lambda - \ln\Phi)\cos\phi - (\lambda - \ln\Phi)\sin\phi + \Phi - \Phi(\lambda - \ln\Phi) + \Phi^2\csc\phi\Big] \tag{D.23}$$

$$-u_\phi \frac{\partial u_\phi}{\partial \phi} = -\kappa_c^2 \Big[(\lambda - \ln\Phi)^2 \sin\phi\cos\phi - \Phi(\lambda - \ln\Phi)\cos\phi - (\lambda - \ln\Phi)\sin\phi + \Phi - \Phi(\lambda - \ln\Phi) + \Phi^2\csc\phi\Big] \tag{D.24}$$

$$u_\phi u_R = -\kappa_c^2 \left[(\lambda - \ln\Phi)\cos\phi - 1\right]\left[(\lambda - \ln\Phi)\sin\phi - \Phi\right] \tag{D.25}$$

$$u_\phi u_R = -\kappa_c^2 \Big[(\lambda - \ln\Phi)^2 \sin\phi\cos\phi \\ -\Phi\,(\lambda - \ln\Phi)\cos\phi - (\lambda - \ln\Phi)\sin\phi + \Phi\Big] \tag{D.26}$$

$$-u_\phi u_R = \kappa_c^2 \Big[(\lambda - \ln\Phi)^2 \sin\phi\cos\phi \\ -\Phi\,(\lambda - \ln\Phi)\cos\phi - (\lambda - \ln\Phi)\sin\phi + \Phi\Big] \tag{D.27}$$

$$-u_\phi u_R - u_\phi \frac{\partial u_\phi}{\partial\phi} = \kappa_c^2 \Big[(\lambda - \ln\Phi)^2 \sin\phi\cos\phi \\ -\Phi\,(\lambda - \ln\Phi)\cos\phi - (\lambda - \ln\Phi)\sin\phi + \Phi\Big] \\ -\kappa_c^2 \Big[(\lambda - \ln\Phi)^2 \sin\phi\cos\phi - \Phi\,(\lambda - \ln\Phi)\cos\phi \\ -(\lambda - \ln\Phi)\sin\phi + \Phi - \Phi\,(\lambda - \ln\Phi) + \Phi^2 \csc\phi\Big] \tag{D.28}$$

$$-u_\phi u_R - u_\phi \frac{\partial u_\phi}{\partial\phi} = \kappa_c^2 \Big[\Phi\,(\lambda - \ln\Phi) - \Phi^2 \csc\phi\Big] \tag{D.29}$$

$$u_\theta^2 = \frac{1}{R^2 \sin^2\phi}\Big[1 + (\kappa_c R \sin\phi)^2\,(\lambda - \ln\Phi - \Phi\csc\phi)\Big] \tag{D.30}$$

$$u_\theta^2 \cot\phi = \frac{\cot\phi}{R^2 \sin^2\phi} + \kappa_c^2 \cot\phi\,(\lambda - \ln\Phi - \Phi\csc\phi) \tag{D.31}$$

$$u_\theta^2 \cot\phi - u_\phi u_R - u_\phi \frac{\partial u_\phi}{\partial\phi} = \frac{\cot\phi}{R^2 \sin^2\phi} + \kappa_c^2 \Big[\Phi\,(\lambda - \ln\Phi) - \Phi^2 \csc\phi \\ +(\lambda - \ln\Phi)\cot\phi - \Phi\csc\phi\cot\phi\Big] \tag{D.32}$$

$$\frac{\partial p}{\partial \phi} = \frac{1}{R^2 \sin^2 \phi} \left\{ \cot \phi + (\kappa_c R \sin \phi)^2 \left[\Phi \left(\lambda - \ln \Phi \right) - \Phi^2 \csc \phi \right. \right.$$
$$\left. \left. + \left(\lambda - \ln \Phi \right) \cot \phi - \Phi \csc \phi \cot \phi \right] \right\} \tag{D.33}$$

$$\frac{\partial p}{\partial \phi} = \frac{1}{R^2 \sin^2 \phi} \left\{ \cot \phi + (\kappa_c R \sin \phi)^2 \left[\left(\csc \phi - \cot \phi \right) \left(\lambda - \ln \Phi \right) \right. \right.$$
$$\left. \left. - \Phi \csc \phi \left(\csc \phi - \cot \phi \right) + \left(\lambda - \ln \Phi \right) \cot \phi - \Phi \csc \phi \cot \phi \right] \right\} \tag{D.34}$$

$$\frac{\partial p}{\partial \phi} = \frac{1}{R^2 \sin^2 \phi} \left\{ \cot \phi + (\kappa_c R \sin \phi)^2 \left[\left(\lambda - \ln \Phi \right) \csc \phi - \Phi \csc^2 \phi \right] \right\} \tag{D.35}$$

$$\frac{\partial p}{\partial r} = -u_r \frac{\partial u_r}{\partial r} - u_z \frac{\partial u_r}{\partial z} + \frac{u_\theta^2}{r} \tag{D.36}$$

$$\frac{\partial u_r}{\partial r} = -\kappa_c \frac{\partial}{\partial r} \left(\sqrt{1 + \frac{z^2}{r^2}} - \frac{z}{r} \right) \tag{D.37}$$

from Equations (C.79–C.84)

$$\frac{\partial}{\partial r} \left(\sqrt{1 + \frac{z^2}{r^2}} - \frac{z}{r} \right) = - \frac{z^2}{r^3 \sqrt{1 + \frac{z^2}{r^2}}} + \frac{z}{r^2} \tag{D.38}$$

$$u_r \frac{\partial u_r}{\partial r} = \kappa_c^2 \left(- \frac{z^2}{r^3 \sqrt{1 + \frac{z^2}{r^2}}} + \frac{z}{r^2} \right) \left(\sqrt{1 + \frac{z^2}{r^2}} - \frac{z}{r} \right) \tag{D.39}$$

$$\left(-\frac{z^2}{r^3\sqrt{1+\frac{z^2}{r^2}}}+\frac{z}{r^2}\right)\left(\sqrt{1+\frac{z^2}{r^2}}-\frac{z}{r}\right)$$

$$=-\frac{z^2}{r^3}+\frac{z^3}{r^4\sqrt{1+\frac{z^2}{r^2}}}+\frac{z\sqrt{1+\frac{z^2}{r^2}}}{r^2}-\frac{z^2}{r^3} \tag{D.40}$$

$$-2\frac{z^2}{r^3}+\frac{z^3}{r^4\sqrt{1+\frac{z^2}{r^2}}}+\frac{z\sqrt{1+\frac{z^2}{r^2}}}{r^2}=\frac{-2z^2r\sqrt{1+\frac{z^2}{r^2}}+z^3+zr^2\left(1+\frac{z^2}{r^2}\right)}{r^4\sqrt{1+\frac{z^2}{r^2}}} \tag{D.41}$$

$$-u_r\frac{\partial u_r}{\partial r}=-\kappa_c^2\left[\frac{-2z^2r\sqrt{1+\frac{z^2}{r^2}}+z^3+zr^2\left(1+\frac{z^2}{r^2}\right)}{r^4\sqrt{1+\frac{z^2}{r^2}}}\right] \tag{D.42}$$

$$-u_r\frac{\partial u_r}{\partial r}=-(\kappa_c r)^2\left[\frac{-2\frac{z^2}{r}\sqrt{1+\frac{z^2}{r^2}}+\frac{z^3}{r^2}+z\left(1+\frac{z^2}{r^2}\right)}{r^4\sqrt{1+\frac{z^2}{r^2}}}\right] \tag{D.43}$$

$$-u_r\frac{\partial u_r}{\partial r}=(\kappa_c r)^2\left[\frac{2\frac{z^2}{r}\sqrt{1+\frac{z^2}{r^2}}-\frac{z^3}{r^2}-z\left(1+\frac{z^2}{r^2}\right)}{r^4\sqrt{1+\frac{z^2}{r^2}}}\right] \tag{D.44}$$

$$\frac{\partial u_r}{\partial z}=-\kappa_c\frac{\partial}{\partial z}\left(\sqrt{1+\frac{z^2}{r^2}}-\frac{z}{r}\right) \tag{D.45}$$

from Equation Eq. (C.52)

$$\frac{\partial}{\partial z}\left(\sqrt{1+\frac{z^2}{r^2}}-\frac{z}{r}\right)=\frac{\frac{z}{r^2}}{\sqrt{1+\frac{z^2}{r^2}}}-\frac{1}{r} \tag{D.46}$$

$$\frac{\frac{z}{r^2}}{\sqrt{1+\frac{z^2}{r^2}}}-\frac{1}{r}=\frac{z-r\sqrt{1+\frac{z^2}{r^2}}}{r^2\sqrt{1+\frac{z^2}{r^2}}} \tag{D.47}$$

$$-u_z\frac{\partial u_r}{\partial z}=\kappa_c^2\left[\lambda-\ln\left(\sqrt{1+\frac{z^2}{r^2}}-\frac{z}{r}\right)-1\right]\left(\frac{z-r\sqrt{1+\frac{z^2}{r^2}}}{r^2\sqrt{1+\frac{z^2}{r^2}}}\right) \tag{D.48}$$

$$-u_z\frac{\partial u_r}{\partial z}=(\kappa_c r)^2\left[\lambda-\ln\left(\sqrt{1+\frac{z^2}{r^2}}-\frac{z}{r}\right)-1\right]\left(\frac{z-r\sqrt{1+\frac{z^2}{r^2}}}{r^4\sqrt{1+\frac{z^2}{r^2}}}\right) \tag{D.49}$$

$$-u_z\frac{\partial u_r}{\partial z}=(\kappa_c r)^2\left\{\frac{z\left[\lambda-\ln\left(\sqrt{1+\frac{z^2}{r^2}}-\frac{z}{r}\right)-1\right]}{r^4\sqrt{1+\frac{z^2}{r^2}}}-\frac{r\sqrt{1+\frac{z^2}{r^2}}\left[\lambda-\ln\left(\sqrt{1+\frac{z^2}{r^2}}-\frac{z}{r}\right)\right]-r\sqrt{1+\frac{z^2}{r^2}}}{r^4\sqrt{1+\frac{z^2}{r^2}}}\right\} \tag{D.50}$$

$$\frac{u_\theta^2}{r}=\frac{1}{r^3}\left\{1+(\kappa_c r)^2\left[\lambda-\ln\left(\sqrt{1+\frac{z^2}{r^2}}-\frac{z}{r}\right)+\frac{z}{r}\sqrt{1+\frac{z^2}{r^2}}-\frac{z^2}{r^2}-1\right]\right\} \tag{D.51}$$

$$\frac{u_\theta^2}{r} = \frac{r\sqrt{1+\frac{z^2}{r^2}}\left\{1+(\kappa_c r)^2\left[\lambda - \ln\left(\sqrt{1+\frac{z^2}{r^2}} - \frac{z}{r}\right) + \frac{z}{r}\sqrt{1+\frac{z^2}{r^2}} - \frac{z^2}{r^2} - 1\right]\right\}}{r^4\sqrt{1+\frac{z^2}{r^2}}} \tag{D.52}$$

$$\frac{u_\theta^2}{r} = \frac{r\sqrt{1+\frac{z^2}{r^2}} + r\sqrt{1+\frac{z^2}{r^2}}(\kappa_c r)^2\left[\lambda - \ln\left(\sqrt{1+\frac{z^2}{r^2}} - \frac{z}{r}\right) + \frac{z}{r}\sqrt{1+\frac{z^2}{r^2}} - \frac{z^2}{r^2} - 1\right]}{r^4\sqrt{1+\frac{z^2}{r^2}}} \tag{D.53}$$

$$\begin{aligned}\frac{u_\theta^2}{r} =& \frac{r\sqrt{1+\frac{z^2}{r^2}} + (\kappa_c r)^2\left\{r\sqrt{1+\frac{z^2}{r^2}}\left[\lambda - \ln\left(\sqrt{1+\frac{z^2}{r^2}} - \frac{z}{r}\right)\right]\right.}{r^4\sqrt{1+\frac{z^2}{r^2}}} \\ & \frac{\left. + z\left(1+\frac{z^2}{r^2}\right) - \frac{z^2}{r}\sqrt{1+\frac{z^2}{r^2}} - r\sqrt{1+\frac{z^2}{r^2}}\right\}}{r^4\sqrt{1+\frac{z^2}{r^2}}}\end{aligned} \tag{D.54}$$

$$\frac{\partial p}{\partial r} = -u_r\frac{\partial u_r}{\partial r} - u_z\frac{\partial u_r}{\partial z} + \frac{u_\theta^2}{r} = (\kappa_c r)^2\left[\frac{2\frac{z^2}{r}\sqrt{1+\frac{z^2}{r^2}} - \frac{z^3}{r^2} - z\left(1+\frac{z^2}{r^2}\right)}{r^4\sqrt{1+\frac{z^2}{r^2}}}\right]$$
$$+ (\kappa_c r)^2\left\{\frac{z\left[\lambda - \ln\left(\sqrt{1+\frac{z^2}{r^2}} - \frac{z}{r}\right) - 1\right]}{r^4\sqrt{1+\frac{z^2}{r^2}}}\right.$$
$$\left. - \frac{r\sqrt{1+\frac{z^2}{r^2}}\left[\lambda - \ln\left(\sqrt{1+\frac{z^2}{r^2}} - \frac{z}{r}\right)\right] - r\sqrt{1+\frac{z^2}{r^2}}}{r^4\sqrt{1+\frac{z^2}{r^2}}}\right\}$$
$$+ \frac{r\sqrt{1+\frac{z^2}{r^2}} + (\kappa_c r)^2\left\{r\sqrt{1+\frac{z^2}{r^2}}\left[\lambda - \ln\left(\sqrt{1+\frac{z^2}{r^2}} - \frac{z}{r}\right)\right]\right.}{r^4\sqrt{1+\frac{z^2}{r^2}}}$$
$$\left. \frac{+z\left(1+\frac{z^2}{r^2}\right) - \frac{z^2}{r}\sqrt{1+\frac{z^2}{r^2}} - r\sqrt{1+\frac{z^2}{r^2}}\right\}}{r^4\sqrt{1+\frac{z^2}{r^2}}} \tag{D.55}$$

$$\frac{\partial p}{\partial r} = \frac{r\sqrt{1+\frac{z^2}{r^2}} + (\kappa_c r)^2\left\{\frac{z^2}{r}\sqrt{1+\frac{z^2}{r^2}} - \frac{z^3}{r^2}\right.}{r^4\sqrt{1+\frac{z^2}{r^2}}}$$
$$\left. + \frac{z\left[\lambda - \ln\left(\sqrt{1+\frac{z^2}{r^2}} - \frac{z}{r}\right) - 1\right]\right\}}{r^4\sqrt{1+\frac{z^2}{r^2}}} \tag{D.56}$$

$$\frac{\partial p}{\partial r} = \frac{r\sqrt{1+\frac{z^2}{r^2}} + \kappa_c^2 \left\{ z^2 r \sqrt{1+\frac{z^2}{r^2}} - z^3 \right.}{r^4 \sqrt{1+\frac{z^2}{r^2}}}$$
$$\left. + \frac{z r^2 \left[\lambda - \ln\left(\sqrt{1+\frac{z^2}{r^2}} - \frac{z}{r} \right) - 1 \right] \right\}}{r^4 \sqrt{1+\frac{z^2}{r^2}}} \tag{D.57}$$

$$\frac{\partial u_z}{\partial r} = \kappa_c \frac{\partial}{\partial r} \left[\lambda - \ln\left(\sqrt{1+\frac{z^2}{r^2}} - \frac{z}{r} \right) - 1 \right] \tag{D.58}$$

$$\frac{\partial u_z}{\partial r} = \kappa_c \frac{\partial}{\partial r} \left[- \ln\left(\sqrt{1+\frac{z^2}{r^2}} - \frac{z}{r} \right) \right] \tag{D.59}$$

see Equation Eq. (C.88)

$$\frac{\partial u_z}{\partial r} = \kappa_c \frac{\partial}{\partial r} \left[- \ln\left(\sqrt{1+\frac{z^2}{r^2}} - \frac{z}{r} \right) \right] = -\kappa_c \frac{u'}{u} = -\kappa_c \left(\frac{z}{r^2 \sqrt{1+\frac{z^2}{r^2}}} \right) \tag{D.60}$$

$$u_r \frac{\partial u_z}{\partial r} = \kappa_c^2 \left(\frac{z}{r^2 \sqrt{1+\frac{z^2}{r^2}}} \right) \left(\sqrt{1+\frac{z^2}{r^2}} - \frac{z}{r} \right) \tag{D.61}$$

$$- u_r \frac{\partial u_z}{\partial r} = -\kappa_c^2 \left(\frac{z\sqrt{1+\frac{z^2}{r^2}}}{r^2 \sqrt{1+\frac{z^2}{r^2}}} - \frac{z^2}{r^3 \sqrt{1+\frac{z^2}{r^2}}} \right) \tag{D.62}$$

$$- u_r \frac{\partial u_z}{\partial r} = -\kappa_c^2 \left(\frac{zr\sqrt{1+\frac{z^2}{r^2}} - z^2}{r^3 \sqrt{1+\frac{z^2}{r^2}}} \right) \tag{D.63}$$

$$\frac{\partial u_z}{\partial z} = \kappa_c \frac{\partial}{\partial z}\left[\lambda - \ln\left(\sqrt{1+\frac{z^2}{r^2}} - \frac{z}{r}\right) - 1\right] \tag{D.64}$$

$$\frac{\partial u_z}{\partial z} = \kappa_c \frac{\partial}{\partial z}\left[-\ln\left(\sqrt{1+\frac{z^2}{r^2}} - \frac{z}{r}\right)\right] \tag{D.65}$$

see Equation Eq. (C.56)

$$\kappa_c \frac{\partial}{\partial z}\left[-\ln\left(\sqrt{1+\frac{z^2}{r^2}} - \frac{z}{r}\right)\right] = -\kappa_c \frac{u'}{u} = \frac{\kappa_c}{r\sqrt{1+\frac{z^2}{r^2}}} \tag{D.66}$$

$$u_z \frac{\partial u_z}{\partial z} = \kappa_c^2 \frac{\lambda - \ln\left(\sqrt{1+\frac{z^2}{r^2}} - \frac{z}{r}\right) - 1}{r\sqrt{1+\frac{z^2}{r^2}}} \tag{D.67}$$

$$-u_z \frac{\partial u_z}{\partial z} = -\kappa_c^2 \left[\frac{\lambda - \ln\left(\sqrt{1+\frac{z^2}{r^2}} - \frac{z}{r}\right) - 1}{r\sqrt{1+\frac{z^2}{r^2}}}\right] \tag{D.68}$$

$$\frac{\partial p}{\partial z} = -u_r \frac{\partial u_z}{\partial r} - u_z \frac{\partial u_z}{\partial z} = -\kappa_c^2 \left(\frac{zr\sqrt{1+\frac{z^2}{r^2}} - z^2}{r^3\sqrt{1+\frac{z^2}{r^2}}}\right) - \kappa_c^2 \left[\frac{\lambda - \ln\left(\sqrt{1+\frac{z^2}{r^2}} - \frac{z}{r}\right) - 1}{r\sqrt{1+\frac{z^2}{r^2}}}\right] \tag{D.69}$$

$$\frac{\partial p}{\partial z} = -u_r \frac{\partial u_z}{\partial r} - u_z \frac{\partial u_z}{\partial z} = -\kappa_c^2 \left(\frac{zr\sqrt{1+\frac{z^2}{r^2}} - z^2}{r^3\sqrt{1+\frac{z^2}{r^2}}} \right) - \kappa_c^2 \left\{ \frac{r^2\left[\lambda - \ln\left(\sqrt{1+\frac{z^2}{r^2}} - \frac{z}{r}\right) - 1\right]}{r^3\sqrt{1+\frac{z^2}{r^2}}} \right\} \tag{D.70}$$

$$\begin{aligned} \frac{\partial p}{\partial z} &= -u_r \frac{\partial u_z}{\partial r} - u_z \frac{\partial u_z}{\partial z} \\ &= \kappa_c^2 \left\{ \frac{z^2 - zr\sqrt{1+\frac{z^2}{r^2}} - r^2\left[\lambda - \ln\left(\sqrt{1+\frac{z^2}{r^2}} - \frac{z}{r}\right) - 1\right]}{r^3\sqrt{1+\frac{z^2}{r^2}}} \right\} \end{aligned} \tag{D.71}$$

$$\frac{\partial p}{\partial z} = \kappa_c^2 \left\{ \frac{z^2 - zr\sqrt{1+\frac{z^2}{r^2}} - r^2\left[\lambda - \ln\left(\sqrt{1+\frac{z^2}{r^2}} - \frac{z}{r}\right) - 1\right]}{r^3\sqrt{1+\frac{z^2}{r^2}}} \right\} \tag{D.72}$$

$$
\begin{cases}
\dfrac{\partial p}{\partial R} = \dfrac{\kappa_c^2}{R}\left[\Phi_1 + \Phi\cot\phi - \Phi_1^2 + (\Phi_1\cos\phi - 1)^2 - 1\right] \\
\dfrac{\partial p}{\partial \phi} = \dfrac{1}{R^2\sin^2\phi}\left[\cot\phi + (\kappa_c R\sin\phi)^2\,(\Phi_1\csc\phi - \Phi_2\csc\phi)\right] \\
\dfrac{\partial p}{\partial r} = \dfrac{r\sqrt{1+\dfrac{z^2}{r^2}} + \kappa_c^2\left\{z^2 r\sqrt{1+\dfrac{z^2}{r^2}} - z^3\right.}{r^4\sqrt{1+\dfrac{z^2}{r^2}}} \\
\qquad\qquad + \dfrac{\left.zr^2\left[\lambda - \ln\left(\sqrt{1+\dfrac{z^2}{r^2}} - \dfrac{z}{r}\right) - 1\right]\right\}}{r^4\sqrt{1+\dfrac{z^2}{r^2}}} \\
\dfrac{\partial p}{\partial z} = \kappa_c^2\left\{\dfrac{z^2 - zr\sqrt{1+\dfrac{z^2}{r^2}} - r^2\left[\lambda - \ln\left(\sqrt{1+\dfrac{z^2}{r^2}} - \dfrac{z}{r}\right) - 1\right]}{r^3\sqrt{1+\dfrac{z^2}{r^2}}}\right\}
\end{cases}
\tag{D.73}
$$

Vita

Born and raised in Nashville, TN, Timothy Andrew Barber received a BS in Mechanical Engineering in May 2006 from Tennessee Technological University (TTU) located about 80 miles east of Nashville in Cookeville, TN.

In May 2012, Tim completed the requirements for a MS in Aerospace Engineering from the Department of Mechanical, Aerospace, and Biomedical Engineering (MABE) University of Tennessee Space Institute, Tullahoma, TN which is affiliated with the College of Engineering at the University of Tennessee, Knoxville, TN. His thesis and MS research consisted of reviewing and identifying hypersonic technology including past, current, and future problems. The MS is entitled "A Survey of Gaps, Obstacles, and Technical Challenges for Hypersonic Applications."

Tim received a Full Graduate Research Assistantship (2006-2011 and 2011-2012) and the William Carter Fellowship for 2006-2007 at UTSI. He is a member of ASME, AIAA, SAE, and Pi Tau Sigma. In April 2012, Tim won 1st at the 63rd Region II AIAA Student Conference in Cape Canaveral, FL in the Master Division competition for the technical paper and presentation of "Bidirectional Helical Motion in Tapered Rocket Engines."